

AD-F 500076

12

NSWC MP 91-388

AD A119965

NOTES FROM LECTURES ON DETONATION PHYSICS

BY FRANK J. ZERILLI,
TRANSCRIBER AND EDITOR

RESEARCH AND TECHNOLOGY DEPARTMENT

OCTOBER 1981

Approved for public release, distribution unlimited.

DTIC FILE COPY

DTIC
ELECTE
S OCT 6 1982 D
B



NAVAL SURFACE WEAPONS CENTER

Dahlgren, Virginia 22448 • Silver Spring, Maryland 20910

82 09 29 005

UNCLASSIFIED

SECURITY CLASSIFICATION OF THIS PAGE (When Data Entered)

REPORT DOCUMENTATION PAGE		READ INSTRUCTIONS BEFORE COMPLETING FORM
1. REPORT NUMBER NSWC MP 81-399	2. GOVY ACCESSION NO. AD-A114 965	3. RECIPIENT'S CATALOG NUMBER
4. TITLE (and Subtitle) NOTES FROM LECTURES ON DETONATION PHYSICS		5. TYPE OF REPORT & PERIOD COVERED
7. AUTHOR(s) Frank J. Zerilli, Transcriber and Editor		6. PERFORMING ORG. REPORT NUMBER
9. PERFORMING ORGANIZATION NAME AND ADDRESS Naval Surface Weapons Center White Oak Silver Spring, MD 20910		8. CONTRACT OR GRANT NUMBER(s)
11. CONTROLLING OFFICE NAME AND ADDRESS		10. PROGRAM ELEMENT PROJECT, TASK AREA & WORK UNIT NUMBERS
14. MONITORING AGENCY NAME & ADDRESS (if different from Controlling Office)		12. REPORT DATE October 1981
		13. NUMBER OF PAGES 207
		15. SECURITY CLASS. (of this report) UNCLASSIFIED
		15a. DECLASSIFICATION/DOWNGRADING SCHEDULE
16. DISTRIBUTION STATEMENT (of this Report) Approved for public release, distribution unlimited		
17. DISTRIBUTION STATEMENT (of the abstract entered in Block 20, if different from Report)		
18. SUPPLEMENTARY NOTES		
19. KEY WORDS (Continue on reverse side if necessary and identify by block number) (over)		
Detonations	Classification of Explosives	Explosive Sensitivity Tests
Detonation Physics	Detonability Curves	Gap Test
Shock Waves	Critical Diameter	Detonation Reaction Zone
Detonation Waves	Detonation Velocity	Chapman-Jouguet Pressure
Explosions	Explosive Sensitivity	Critical Initiating Pressure
20. ABSTRACT (Continue on reverse side if necessary and identify by block number)		
<p>This is a series of lecture notes on the subject of detonation physics. The topics covered include a historical summary from the perspective of the White Oak Laboratory of NSWC dating from 1940, the basic conservation equations for shock and detonation waves, the gamma law equation of state, critical diameter and critical shock initiating pressure, detonability curves and the classification of explosives, the effects of particle size, temperature, temperature cycling, chemical composition, the large scale and small scale gap tests, the wedge test, characterization of shock</p>		

DD FORM 1473
1 JAN 73EDITION OF 1 NOV 68 IS OBSOLETE
S/N 0102-LF-014-6601

UNCLASSIFIED

SECURITY CLASSIFICATION OF THIS PAGE (When Data Entered)

UNCLASSIFIED

SECURITY CLASSIFICATION OF THIS PAGE (When Data Entered)

19. (Cont.)

Electromagnetic Velocity Gage
Detonation Pressure
Critical Parameters

20. (Cont.)

sensitivity, estimating and measuring detonation pressure, the electro-
magnetic velocity measurement method, the continuous wave method, and
reaction zone lengths and reaction times.

UNCLASSIFIED

SECURITY CLASSIFICATION OF THIS PAGE (When Data Entered)

FOREWORD

The Energetic Materials Division has several senior explosives scientists that are getting close to retirement age. In order to effectively transmit their special knowledge, as well as general basic facts of explosives science to new and junior staff members of the Division, a series of lectures were arranged. This report contains a compilation of the notes from the first series of lectures on detonation physics prepared by Dr. Donna Price and Dr. Sigmund J. Jacobs. The lecture notes were written and edited by Dr. Frank J. Zerilli and reviewed by the lecturers. Presently in progress is a second series of lectures by Dr. Mortimer J. Kamlet on detonation chemistry. It is planned to publish these lecture notes in a follow-on report.

This is to acknowledge the efforts of Dr. Donna Price and Dr. Sigmund J. Jacobs in preparing and delivering a series of lectures on detonation physics. Also acknowledged are the efforts of Dr. Frank J. Zerilli who prepared and edited detailed notes from the lectures. In addition, thanks are due to the following persons who typed the notes: Barbara J. Garner, Maureen T. Hinson, Angela M. Riley, Patricia A. Leahy, Marie E. Incarnato, Catherine G. Burch, Judith J. Scully and Wanda S. Walters.

K. F. Mueller

K. F. MUELLER
By direction

Accession For	
NTIS GRA&I	<input checked="" type="checkbox"/>
DTIC TAB	<input type="checkbox"/>
Unannounced	<input type="checkbox"/>
Justification _____	
By _____	
Distribution/ _____	
Availability Codes	
Dist	Avail and/or Special
A	



PREFACE

These notes are the result of a series of lectures on the topic of detonation physics given by Drs. Donna Price and Sigmund J. Jacobs between September 1980 and April 1981. I wrote the notes from taped transcripts of the lectures and occasionally expanded some of the elementary points for the benefit of myself and readers for whom this would be the first exposure to the subject. The manuscripts were reviewed by Drs. Price and Jacobs for technical accuracy, but I must take responsibility for any errors that remain.


F. J. ZERILLI
Detonation Physics Branch

CONTENTS

	<u>Page</u>
LECTURE #1 - "Introduction" by Sigmund J. Jacobs.....	7
LECTURE #2 - "Basic Equations for Shock & Detonation Waves" by Sigmund J. Jacobs.....	19
LECTURE #3 - "Equations of State for Explosives and Deflagration Processes" by Sigmund J. Jacobs.....	35
LECTURE #4 - "Critical Diameter and Critical Shock Initiation Pressure" by Donna Price.....	53
LECTURE #5 - "Detonability Curves and Classification of Explosives" by Donna Price.....	69
LECTURE #6 - "Factors Which Affect Critical Parameters" by Donna Price.....	85
LECTURE #7 - "The Large Scale Gap Test - I" by Donna Price.....	103
LECTURE #8 - "The Large Scale Gap Test - II" by Donna Price.....	119
LECTURE #9 - "Critical Energy and Pressure for Initiation; Wedge and Gap Test" by Donna Price.....	141
LECTURE #10 - "Characterization of Shock Sensitivity" by Donna Price...	157
LECTURE #11 - "Detonation Pressure" by Sigmund J. Jacobs.....	169
LECTURE #12 - "Detonation Reaction Zone Length and Reaction Time" by Donna Price.....	191

LECTURES ON DETONATION PHYSICS

Lecture #1

Introduction

8 September 1980

by Sigmund J. Jacobs

Notes by Frank J. Zerilli

Preface

This is the first of series of seminars on detonation physics and chemistry to be given by Sigmund Jacobs, Donna Price, and Mortimer Kamlet. The seminars given by Dr. Jacobs will start with some simple mathematics of detonations in gases and will later be extended to solids. The points to be covered include: measuring detonation velocity, obtaining detonation pressures, and determining the differences between the numbers for gases and those for solids.

Introduction

This first lecture is a historical summary based on Dr. Jacobs' archive of slides dating back to 1940-41. The slides concern techniques for measuring detonation velocities and pressures.

The Smear Camera

One of the first techniques involved the smear camera built in 1941 at the Explosives Research Laboratory. In those days, very little

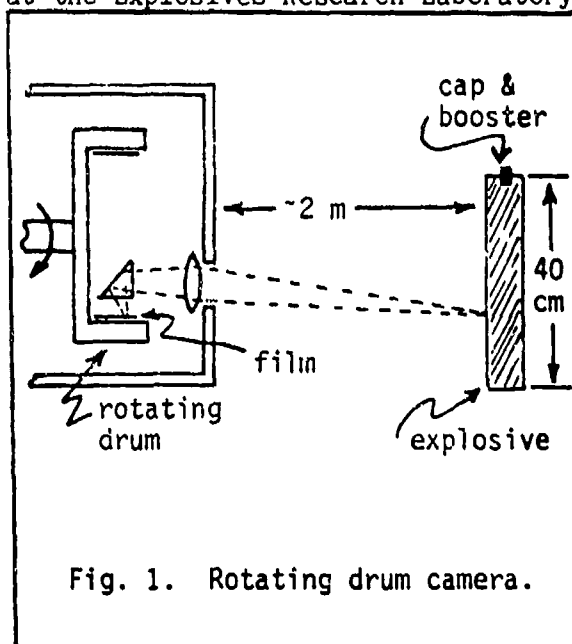


Fig. 1. Rotating drum camera.

work had been done on measurements on detonations except for gaseous systems. The rotating drum camera consisted of a drum 1 meter in circumference which rotated at 240 revolutions per second. The film was placed on the inner circumference of the drum as shown in Figure 1. A pair of razor edges 0.05 mm apart formed the slit whose image is focussed on the film by a prism and lens optical system. Thus the film moves past the slit at 0.24 mm/ μ sec. The slit width allows a time resolution of about 200 nsec. The light from the detonation wave progressing down the explosive produces an image on the film in the form of a line whose slope is proportional to the velocity of the detonation wave.

An advantage of this type of camera is that a record is produced any time the charge is fired, since the film is continuously moving past the slit. This was important at the time since synchronization of the firing to better than a few hundred microseconds was not possible. In fact, six or seven charges would normally be fired using one film, since the probability was that the random position of the film at the time of firing would not lead to overlap of the images--a typical record image might be 20 mm long out of a total 1000 mm of film length.

The detonation record appears as a line on the film, and, from the slope of the line, the detonation velocity can be calculated. A luminous area appears on the film which was called "flame". It has since been learned that this was largely due to air shock luminosity. Also appearing was a bright line due to the air shock wave coming from the end of the charge.

The brightness of the record could be improved by tightly wrapping the charge in cellulose acetate. Brightening was caused by the compression of the thin layer of air between the charge and the wrapping. In fact, the spiral structure of the wrapping was evident on the film record.

Also, black tapes would be placed on the charge, causing gaps to be left in the record. Knowing the distance between the tapes, the detonation velocity could be accurately determined by measuring the distance (along the time coordinate) between the gaps in the record.

Detonation Velocity

In several thousand of these experiments, it has been learned that detonation velocity varies almost exactly linearly with the loading density of the explosive, although the slope differs from one explosive to another.

Typical solid explosive detonation velocities are of the order of several kilometers per second. For example, TNT at a density of 1.6 g/cm^3 has a detonation velocity of about 7 km/sec while Cyclonite (Comp B) at a density of 1.7 g/cm^3 has a detonation velocity of about 8 km/sec.

The variation of detonation velocity with bulk density was one of the first keys in developing an equation of state for explosives at high density.

The detonation velocity is not only a function of density but also a function of diameter. All explosives have a critical minimum diameter below which the detonation will not propagate. This critical diameter is also a function of the charge confinement. Many explosives, for example, amatol, have larger critical diameters at high bulk density than at low so that a plot of detonation velocity vs. density at a given diameter will show a drop off from the linear behavior as the density increases. Explosives which detonate below their "infinite diameter velocity" are frequently called non-ideal but care must be taken in applying the term since all explosives can propagate below their infinite diameter velocity at small diameters.

Shock Initiation and Sensitivity

At this point an example of an experiment related to shock sensitivity of explosive materials was described. The explosive charge was interrupted at three points by gaps of inert material--sugar, in this case. The thickness of the three gaps increases from one gap to the next. The camera record shows that the shock wave weakens as it passes through the first gap, but the detonation is re-initiated as the shock passes back into explosive material. The shock again weakens as it passes

through the second gap. In this larger gap, it weakens to a greater extent, but again, the detonation is re-initiated when the shock passes back into the explosive. However, the thickness of the last gap is such that the shock weakens sufficiently so that detonation is not re-initiated after passing back into explosive material. We say that the "gap-sensitivity" is some value between the second and third thickness of inert material for this explosive. Similar results are obtained for other materials.

Detonation Build-Up

It was discovered that detonations take time to build up. In one example, we have a detonator, a booster charge, then a low density explosive, followed by a column of air. In this case, there is a "hook" in the streak record, a low velocity regime, and a build up to a high velocity regime.

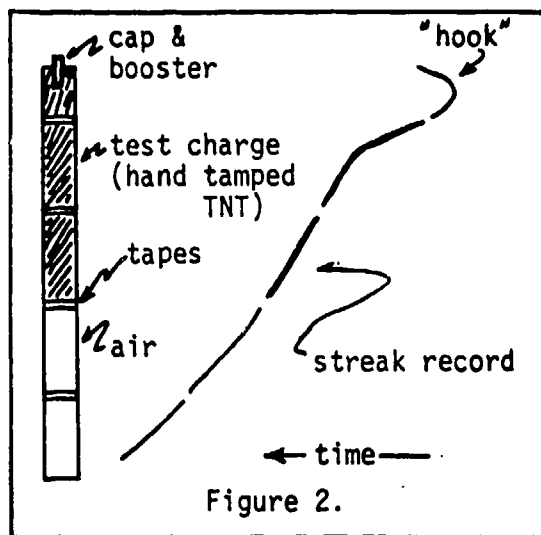


Figure 2.

Another record (Figure 2) which shows a build up was taken by Herzfeld at the University of Saskatchewan in Canada. This record, taken with a rotating mirror camera, shows a shock wave in a donor explosive charge, and, again, one sees an apparent "hook" in the detonation build up. The rotating mirror camera used allowed recording speeds ten times greater than the rotating drum camera.

Rotating Mirror Smear Camera

The demand for a higher speed camera at the Bruceton Laboratory (Pittsburgh, PA) resulted in the construction of a rotating mirror camera. In this camera, four-sided mirror spins at 600 r.p.s. The film is held in a 180° arc drum, with an external slit focussed on the drum by the mirror. This camera also provides continuous coverage in time since the next facet of the mirror takes up where the previous one left off. This avoids the problem of synchronizing the detonator--a very difficult problem in 1943! The camera was built in record time--six months. An external slit was used. This consisted of a mark 1 mm wide and about 1/2 meter long on a 35 mm photographic film. The slit outlined a line on the explosive charge (Figure 3).

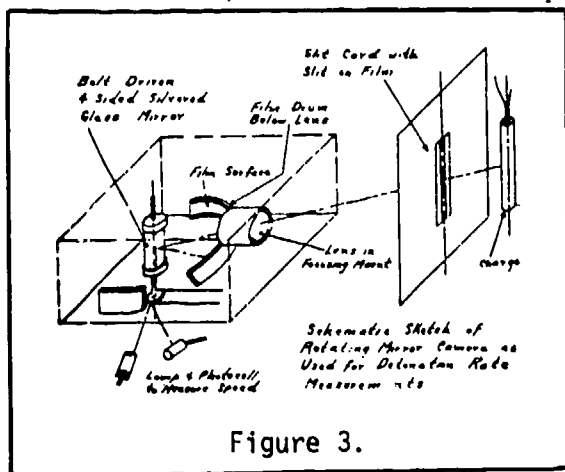


Figure 3.

A camera of the same type with an internal slit was later built at NOL. By this time it had been learned how to synchronize a commercial detonator sufficiently accurately so that continuous time access was no longer needed. Thus a single mirror face was sufficient. The synchronization was accomplished with a 50 μ sec delay with an error of $\pm 5 \mu$ sec.

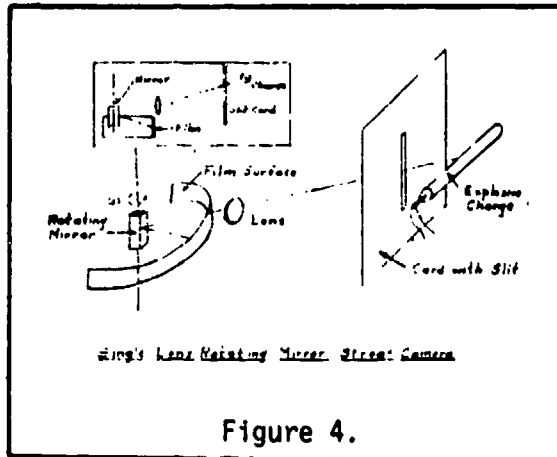


Figure 4.

Cameras of this type can also be used for measuring profiles. If one sets up the charge at right angles to the slit than the lateral spreading of the wave can be observed (Figures 4 and 5).

A photo-finish camera (first developed commercially by Beckman and Whitley) is a smear camera used to record the passage of racers (horses or men) across the finish line. The finish line is viewed through a slit in the camera and the film moves past the slit at a speed approximately that of the racers. Time marks are recorded on the edge of the film. As the racers move past the slit, they are recorded. If the film and the racer move at the same speed, there is no compression or elongation of the racer's image. This is exactly the same way that a smear camera records detonation waved profiles.

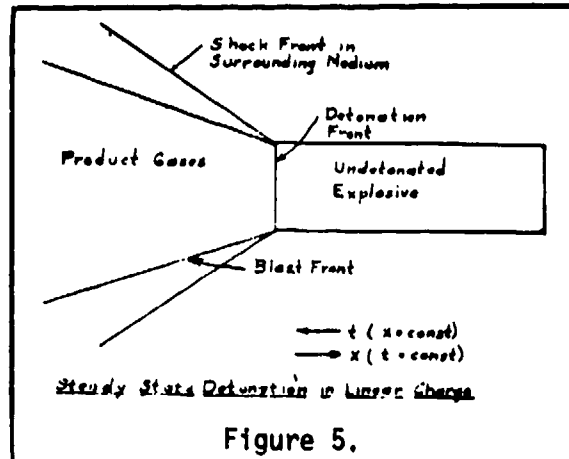


Figure 5.

Detonation Luminosity and Temperature

In studying the temperature of a detonation wave, one needs to know from what part of the material the light is coming from in order to use radiometric methods.

An experiment with nitroglycerine diluted with an organic dilutant and detonated under water showed residual luminosity in the rarefaction wave. Presumably, there is also luminosity in the interior of the charge but the surface material cools rapidly as it expands and deposited carbon prevents the light from getting through.

In order to find out where the light is coming from in a solid explosive, an experiment was performed in which a slab of explosive (Comp B) with 1% carbon black added was placed side by side with a slab of explosive with nothing added. The camera slit was opened to 2 cm

to gather as much light as possible and it was arranged for the image of the detonation wave to be moving within 1% of the velocity of the film. The blackened charge appears slightly luminous and the unblackened charge shows a greater luminosity. The additional luminosity of the unblackened charge, however, appears to the front of the detonation wave, not the rear. This shows that much of the light from the detonation is scattered out through the crystals of explosive ahead of the wave.

Case Expansion Experiments

A typical experiment in which profiles are recorded is an experiment in which a charge was surrounded by an aluminum cylinder and backlighted by an exploding wire. One sees here the air shock and the expanding case. This is a forerunner of the case expansion experiments to be done at Livermore Laboratory more than ten years later.

The Extra Shock Wave in Atomic Tests

About 1965, Liddiard did an experiment to support an explanation of an effect that was discovered in the early days of atomic bomb testing in Nevada. The testers were finding an extra shock wave! In the experiment, a detonator was placed in an aquarium (Figure 6). The lower part of the aquarium contained carbon tetrachloride, with water in the upper half. The purpose was to demonstrate that, if a shock wave moves in a medium of low propagation velocity in contact with a medium of higher propagation velocity, a second wave is established ahead of the original shock. When the shock in the low velocity medium first reaches the interface, a rarefaction is reflected back into the low velocity medium while a shock is refracted into the higher velocity medium (Figure 7). The refracted shock propagates at a higher velocity, so it moves ahead of the original shock. The refracted shock in turn, creates a second shock in the low velocity medium which moves ahead of the original shock. Gregory Hartmann, who later became director of the Naval Ordnance Laboratory (NOL, forerunner of Naval Surface Weapons Center) suggested that the second shock in the atomic tests was produced by a heated layer of air above the ground. When the atomic bomb blast wave passed through the heated layer, the faster propagating refracted shock produced the second shock.

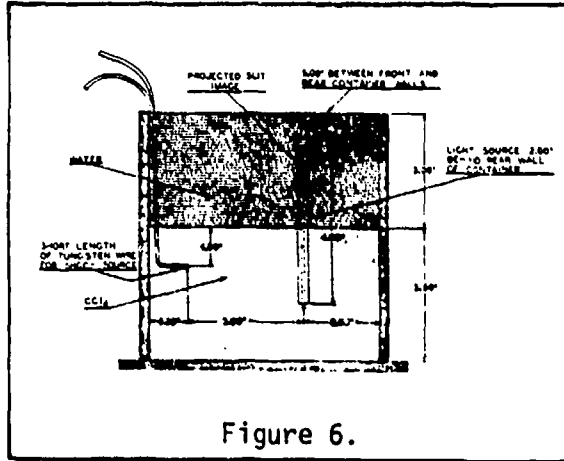


Figure 6.

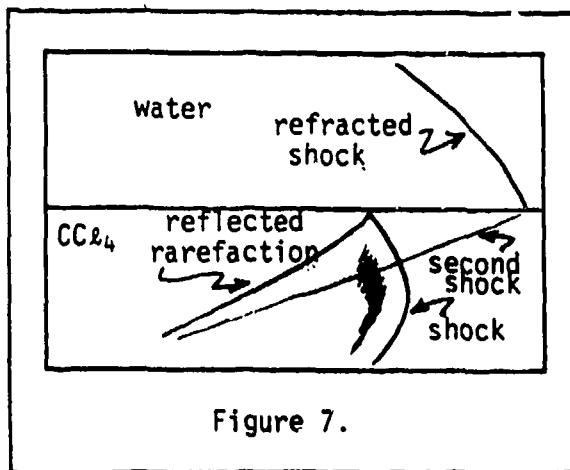


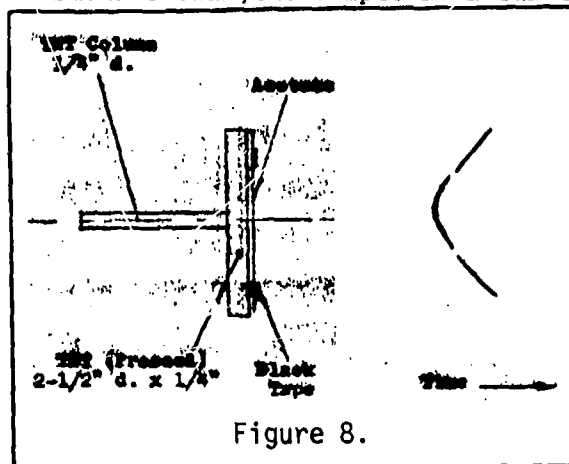
Figure 7.

The Width of the Reaction Zone

An experiment performed at Los Alamos around 1960 gives us information on the width of the reaction zone. The explosive charge was sensitized nitromethane in a glass container. Since nitromethane is transparent, we can see the wave propagating. The diameter of the glass container was such that, ordinarily, nitromethane would not detonate since rarefaction ("failure") waves propagating inward would cool the material sufficiently to stop any reaction. However, the glass container was lined up to a certain point with thin metal films of copper, tungsten, or other high impedance material. These maintain the shock amplitude in the explosive at a higher level than does glass for a time equal to the double transit time of the shock through the thickness of the liner. In the record of the experiment we can see the detonation wave propagation as a luminous area with "failure waves" (rarefactions), seen as dark zones, propagating toward the center. When the detonation got to the end of the metallic liner, the failure waves went completely to the center, and the rest of the charge did not detonate. The double transit time for waves in the liner was of the order of 50 nsec. We can infer that the reaction zone is of the order of 50 nsec long in time (or 50-250 μ wide) as an upper limit.

Shock to Detonation Transition

In an experiment done by Herzberg and Walker of the University of Saskatchewan, the sample is a bar of material initiated at the center.



The shock from the detonator builds up to a detonation faster in the forward direction than in the lateral direction thus showing a separation in the shock to detonation process in the record. It shows that the shock to detonation transition (SDT) is locally dependent on the shock amplitude. At the time the work was done, the result appeared very mysterious (Figure 8).

Figure 8.

Wedge Test

In the so called "wedge test" a smear camera is used to record the shock to detonation transition in an explosive. The arrangement is

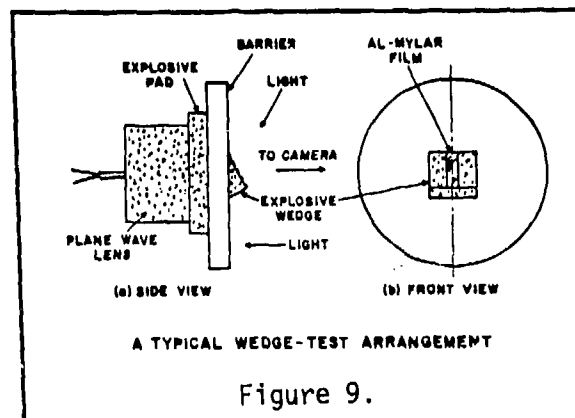


Figure 9.

a plane wave generator followed by an explosive pad (because the generator is usually made with a low energy explosive). Then there is a barrier material which transmits a shock, which, in turn, is transmitted to a wedge of explosive (Figure 9). An exploding wire is used as a light source. The progress of the shock and detonation through the explosive can be followed since the wedge shape exposes layers of explosive at various depths to view.

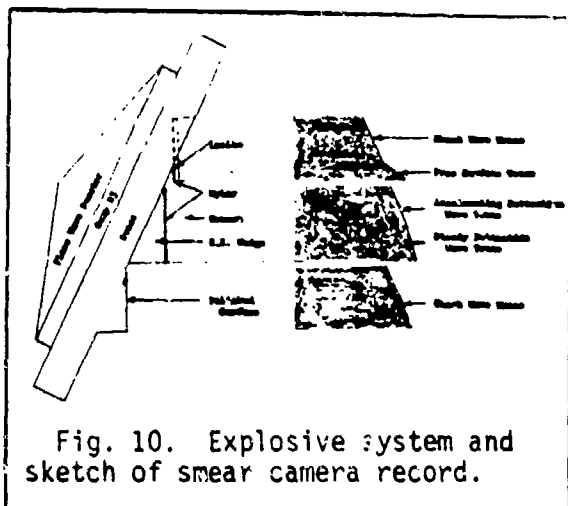


Fig. 10. Explosive system and sketch of smear camera record.

In the Walsh-Cristian technique,^{*} a similar arrangement is used to measure the shock velocity within a metal and the free surface velocity of the metal (see Figure 10). From this data, the relation between shock velocity and particle velocity in a material can be determined, and this allows the determination of the shock pressure-volume relation (Hugoniot relation).

Figure 11 shows the shock velocities and transition to detonation for three different shock amplitudes in the wedge test. Figure 12 shows pressure-volume Hugoniot's for explosive materials. We see that at pressure of around 100 kilobars, typical explosive materials are compressed to about 70-75% its their initial volume.

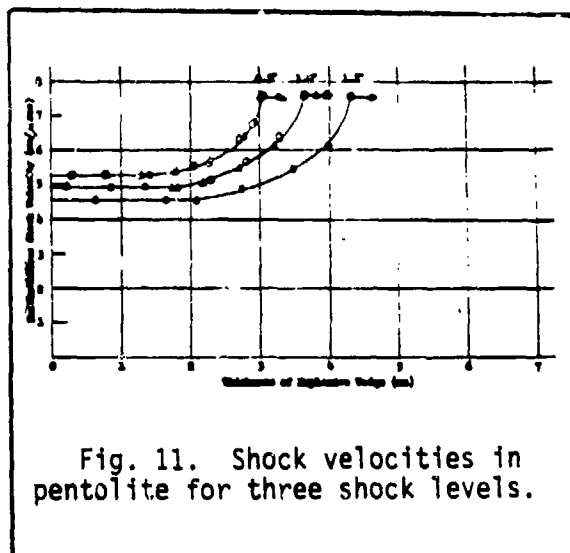


Fig. 11. Shock velocities in pentolite for three shock levels.

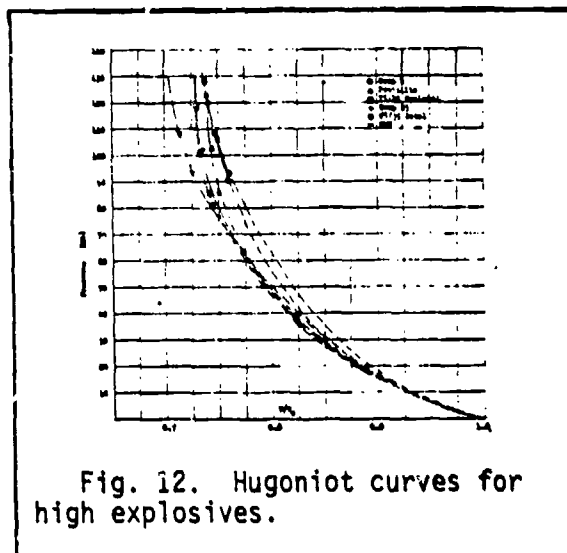
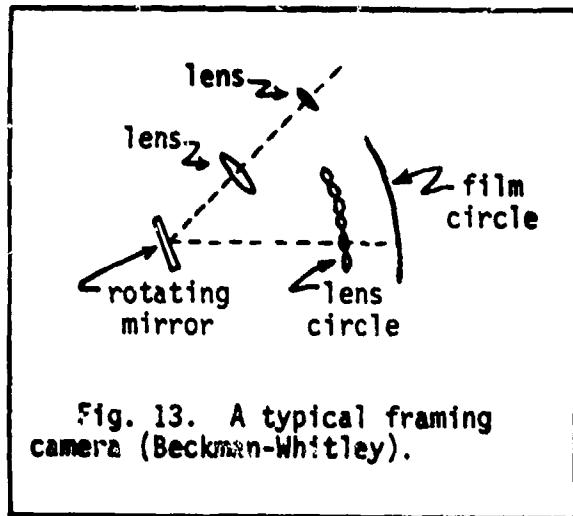


Fig. 12. Hugoniot curves for high explosives.

* John M. Walsh and Russell H. Christian, "Equation of State of Metals from Shock Wave Measurements," Phys. Rev., 97, 1554 (1955).

Framing Cameras

Framing cameras are cameras which take photographs at rates of up to ten million per second. Figure 13 shows schematically a typical early framing camera. In this camera the image of a slit is directed by a rotating mirror and viewed by a series of lenses which form images on a film.

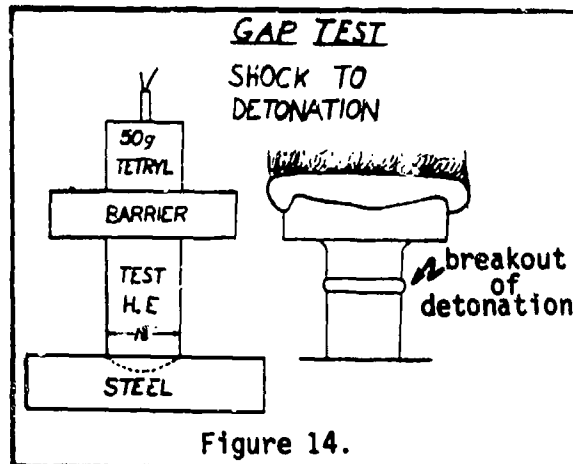


by a rotating mirror and viewed by a series of lenses which form images on a film. A given lens subtends an angle of two or three degrees. The position of the image formed on the film changes as the cosine of the change in angle of the mirror. For the two to three degree change from one lens to the next, the cosine changes by less than 0.1% so the image formed by each lens appears virtually stationary. When the mirror turns a bit further, the next lens sees the source and produces another image on the film. The number of images depends on the number of lenses in the camera. It is possible to obtain

frame rates of up to 10^7 per second, but the light gathering power goes down since small lenses are needed to achieve the highest framing rates.

Origin of the Hook in Smear Camera Records

A sequence of frames taken with a framing camera in a gap-test geometry experiment shows us clearly the origin of the "hook" that we have previously spoken of in smear camera records. The hook is produced because the detonation "breaks out" at the surface a short distance downstream from the end where the initiating shock is applied (due to the interval involved in the shock to detonation transition). The arrangement is shown in Figure 14.



the test charge to spread laterally. At the interface between the barrier and the test charge, the spreading causes a jet to be formed. In a later frame we see the first breakout of detonation as a luminous bulge a short distance down the charge from the barrier. The detonation image is smeared because the exposure time in each frame is about $1/4$ μ sec. About 1 μ sec later, we see the detonation well developed, with differences in luminosities in the regions which have and have not been passed over by the shock.

Focal Plane Shutter Framing Cameras (FPSFC)

A different type of camera, called the focal plane shutter framing camera, has advantages of both a framing camera and a smear camera.* In this camera, a rotating mirror makes an image move relative to a series of concave mirrors which focus the image onto a slit. Up to this point the operation is like that of a framing camera in which the concave mirrors take the place of the series of lenses. The image for each frame sweeps across the slit. Suitable optics are then used to pass the image back to the rotating mirror which reflects the image that has passed through the slit onto a film strip. The arrangement is such that the effect is as if the film had been moved past the slit at the same speed as the image (as occurs in a smear camera). In practice, six slits are used, giving interleaved frames, so that the effective framing rate is six times faster. The advantages are frame rates of 10^6 per second and much better resolution than a conventional framing camera. If a charge is placed so that the detonation wave moves parallel to the slit, a single frame produces a record from which an accurate velocity measurement can be made. Thus many accurate velocity measurements can be made in very short time intervals (1 μ sec).

In a typical experiment in which the FPSFC (focal plane shutter framing camera) was used, a cylindrical tetryl pellet 2" in diameter and 1" high was detonated at the center of one base. The sequence of frames shows the blow off of the luminous air shock. At first the shock is spherical, but the flat part of the outer surface of the pellet produces a different result than the cylindrical part. As time goes on, the wave separates into two pieces. The wave moving from the flat end moves faster and dissipates more slowly than the wave moving out from the sides, showing the strong influence of the geometry of the charge on the shock wave that it produces.

In order to investigate the details of the wave separation mentioned above, an experiment with backlighting was done, so that any non-luminous shocks would become visible. There was a luminosity apparent in this experiment which was believed to be due to a jetting of surface material into the shock zone--producing higher temperatures than the shock itself would produce.

* Jacobs, S. J., "Focal-Plane Shutters and the Design of High-Frame Rate Cameras", J. Soc. Motion Picture and Television Engineers, 69, 801 (1960); S. J. Jacobs, "Photographic Recording with highly Resolved Position and Time Coordinates by Means of Narrow slit Focal Plane scanning", Les Ondes de Detonation, Colloques Internationaux du Centre National de la Recherche Scientifique, No. 109, p. 197 (1962); Jacobs, McLanahan, and Whitman, "A High-Speed Focal-Plane Shutter Framing Cameras", J. Soc. MPTE, 72, 923 (1963); Liddiard, Drimmer, and Jacobs, J. Soc. MPTE 72, 927 (1963).

T. Liddiard obtained an interesting record with the FPSFC just before the Fourth Detonation Symposium. The initiating shock is seen to pass into the explosive charge and change the character of the material. Instead of showing a highly polished surface characteristic of the unshocked material, the surface becomes very diffuse. Then detonation is seen to break out a considerable distance from the end where the initial shock was applied. This is because the transition to detonation occurs largely along the central axis of the charge. At the point where the shock has transited to detonation, the detonation wave propagates to the surface. At the surface, the detonation wave propagates both forward and also rearward into shocked but yet undetonated surface material. The waves propagating forward into undisturbed material and rearward into the pre-shocked material have a different appearance, and the discontinuity remains apparent for a very long time after the initial event--shock wave effects don't have any way of ironing themselves out after they get started.

Shaped Charge Jets

A shaped charge experiment (Figure 15), in which a copper cone is collapsed by an explosive and ejects a jet of material, was done using the FPSFC to observe the jet penetrating a slab of PMMA. Flash x-rays of the

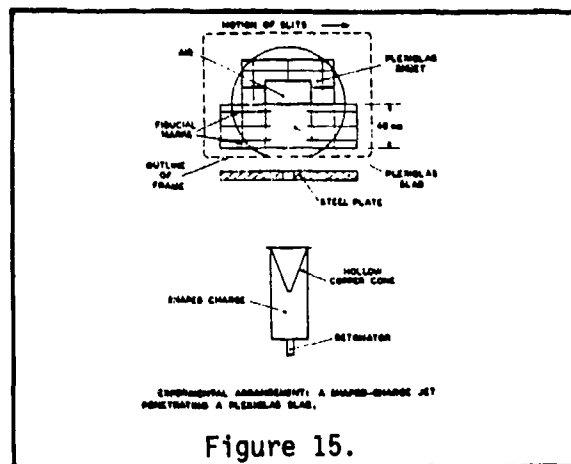


Figure 15.

jet process show the detonation and hot product gases causing collapse of the cone. A jet squirts out and a residual slug is formed (conserving momentum). Because different elements of the cone move at different velocities the jet velocity is smaller in the near region than in the far region, so that the jet elongates with time. As a result, there is an optimum stand off to achieve maximum penetration. In the record taken with the framing camera, we don't actually see the jet because of the scattering of light by the plastic PMMA, but we do see the penetration of the PMMA.*

Punching out a Metal Plate

Another example in which the FPSFC was used shows a metal plate being punched out by an explosive charge. We see the development of the push out. At 20 μ sec, the punched out plate breaks free and hot gases begin coming through. Inked grid lines on the plate become very prominent at the time that the shock hits the surface, and the grid lines stay visible throughout.

* It was only when microsecond flash x-ray photography was used that experimenters in the USA began to understand shaped charge jets.

Underwater Explosion

Finally, Goertner obtained an interesting record. An explosive charge was fired under water and the dome produced by gas expansion was photographed in a millisecond time scale. The results resemble experiments with explosive charges--although the time scales are considerably different.

LECTURES IN DETONATION PHYSICS

Lecture #2 - 22 September 1980

Basic Equations for Shock & Detonation Waves

by

SIGMUND J. JACOBS

Notes by Frank J. Zerilli

Today we will discuss the first principles for the derivation of the equations for a detonation wave. In later lectures we will introduce applications involving an equation of state, the ideal gas equation of state. We will show that the "gamma law" equation of state is essentially equivalent to the ideal gas equation of state. The gamma law equation of state is sometimes used when the ideal gas equation just doesn't work.

NOTATION:

The following notation will be used as consistently as possible. Subscripts will be used to denote quantities applying to individual components in a system. For example, ρ is density, ρ_i is the density of the i^{th} component.

v - specific volume (volume per unit mass)

ρ - density, the reciprocal of specific volume

V - volume per mole

e - specific internal energy (thermal)

E - internal energy per mole

q - specific internal energy (chemical)

Q - chemical energy per mole (comes up in Kamlet's simplified model)

T - temperature

U - shock velocity (shock waves)

D - detonation velocity (detonation waves)

u - local particle (material) velocity

c - sound speed

C_v - specific heat at constant volume

C_p - specific heat at constant pressure

$$\gamma = C_p/C_v$$

p_e - constant volume explosion pressure

p_j - C-J (Chapman-Jouget) detonation pressure

P_{Vn} , P_{Znd} - Von-Neumann pressure (or Zeldovich-Neumann-Doering pressure)

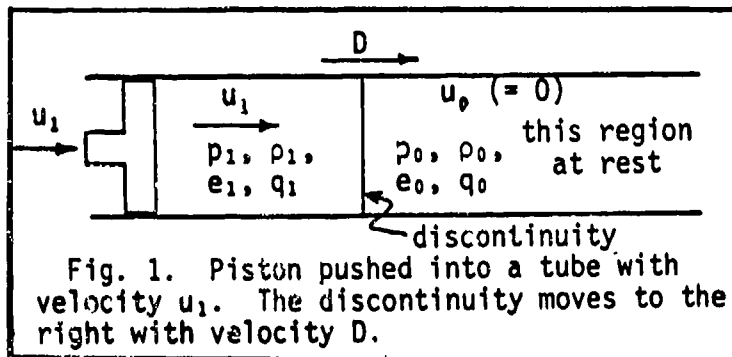
Shock Wave Problems: Assumptions

We will make some simplifying assumptions which will be found to give good approximations to real situations in spite of the simplifying assumptions.

We assume two states - an initial state preceding the detonation wave denoted by the subscript 0, and a final state denoted by the subscript 1. Both states are fixed and uniform with a constant composition and, therefore, described by an equation of state of the form $p = p(T, v)$ or $p = p(e, v)$. Viscosity and heat conduction will be neglected in the simplified model.

Application of Mass, Momentum, and Energy Conservation to Shock Wave

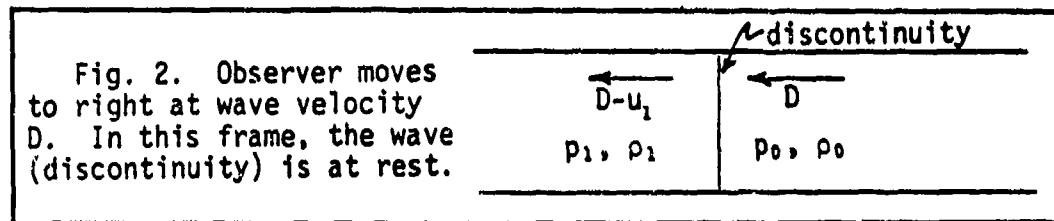
A wave moves forward (right) at velocity D (detonation) or U (shock).



The region in front of the wave is at rest, the region behind has acquired a motion (imagine that we are pushing the

piston in Figure 1 to the right with velocity u_1). The region near the piston acquires the velocity of the piston, the wave front moves with constant velocity. The wave front is a discontinuity (neglect of viscosity allows the discontinuity).

We transform the picture above into the picture in Figure 2 in which the wave front is at rest, the material on the right is flowing into the front at velocity D , the material is compressed at the front and flows out at velocity $D-u_1$.



(If this were a rarefaction wave, u_1 would be negative, and $D-u_1$ would be greater than D .)

Conservation of Mass

Mass flux, denoted by \dot{m} , is density times velocity, so the mass flowing into wave front in a unit time = $\rho_0 D$ and the mass flowing out of wave front in a unit time = $\rho_1 (D-u_1)$.

Conservation of mass requires the mass flowing in to be equal to the mass flowing out (so that no mass accumulates):

$$\rho_0 D = \rho_1 (D-u_1) \quad (1)$$

Equation (1) is the mass continuity equation and can be written also as

$$\frac{\rho_1}{\rho_0} = \frac{v_0}{v_1} = \frac{D}{D-u_1} \quad (2)$$

or

$$\frac{u_1}{D} = 1 - \frac{v_1}{v_0} \quad (3)$$

where use is made of the fact that density equals the reciprocal of specific volume.

Conservation of Momentum

We use Newton's Second Law: force = rate of change of momentum. The total force (directed to the right) on a unit area of the front is $p_1 - p_0$. This must be equal to the change in momentum in a unit time:

momentum (directed to the right) flowing into front in a unit time = $\frac{d}{dt} (-mD) = \dot{m}D$

momentum (directed to the right) flowing out in a unit time = $\frac{d}{dt} [-m(D-u_1)] =$
 $-\dot{m}(D-u_1)$

So

$$p_1 - p_0 = -\dot{m}D + \dot{m}(D-u_1)$$

or

$$p_1 + \dot{m}D = p_0 + \dot{m}(D-u_1) \quad (4)$$

But $\dot{m} = \rho_0 D$ so that

$$p_1 - p_0 = \rho_0 D u_1$$

$$p_1 - p_0 = D u_1 / v_0 \quad (5)$$

This is sometimes referred to as the shock impedance relation.

Conservation of Energy

Consider a unit mass of material. In the initial state it has a kinetic energy $\frac{1}{2}D^2$, internal thermal energy e_0 , and internal chemical energy q_0 . We must also include a term due to the work of pressure on the material, p_0v_0 . In the final state the kinetic energy is $\frac{1}{2}(D-u_1)^2$, thermal energy is e_1 , chemical energy is q_1 , and work term is p_1v_1 . Equating the total final energy to the total initial energy, we obtain

$$\frac{1}{2}D^2 + p_0v_0 + e_0 + q_0 = \frac{1}{2}(D-u_1)^2 + p_1v_1 + e_1 + q_1 \quad (6)$$

We call the difference $q_0 - q_1$ the energy of explosion and denote it by Δq :

$$\Delta q = q_0 - q_1 \quad (7)$$

Note that q_0 is normally greater than q_1 so Δq is positive.

We can rearrange Eq. (6) by collecting the internal energy terms on the left side:

$$\begin{aligned} e_1 - e_0 - \Delta q &= p_0v_0 - p_1v_1 + \frac{1}{2}[D^2 - (D-u_1)^2] \\ &= p_0v_0 - p_1v_1 + Du_1 - \frac{1}{2}u_1^2 \end{aligned} \quad (8)$$

By using the mass conservation and momentum conservation equations we can eliminate u_1 from Eq. (8).

From the impedance relation (momentum conservation)

$$Du_1 = (p_1 - p_0)v_0 \quad (5)$$

and from mass continuity

$$\frac{u_1}{D} = \frac{v_0 - v_1}{v_0} \quad (3)$$

Eliminating D from Eq. (3) and Eq. (5) we get

$$u_1^2 = (p_1 - p_0)(v_0 - v_1) \quad (9)$$

Using (5) to eliminate Du_1 and (9) to eliminate u_1^2 , Eq. (8) becomes

$$e_1 = e_0 + \Delta q + \frac{1}{2} (p_1 + p_0)(v_0 - v_1) \quad (10)$$

If we know the internal energy e as a function of p and v (i.e., if we know the equation of state), then Eq. (10) gives a relation between p and v . This is called the Hugoniot relation. If $\Delta q = 0$ this is the well-known Hugoniot shock relation.

Summary of Important Results

Conservation Equations:

Mass:
$$\frac{u_1}{D} = \frac{v_0 - v_1}{v_0} \quad (3)$$

Momentum (Impedance Relation)*:
$$p_1 - p_0 = D\rho_0 u_1 \quad (5)$$

Energy:
$$e_1 = \Delta q + e_0 + \frac{1}{2} (p_1 + p_0)(v_0 - v_1) \quad (10)$$

* If the initial medium is not at rest but has velocity u_0 , the relation is then $p_1 - p_0 = D \rho_0 (u_1 - u_0)$ where D is the shock velocity with respect to the initial medium.

Relations Obtained by Re-arranging the Conservation Relations

If we eliminate u_1 from Eqs. (3) and (5) we obtain

$$D^2 = v_0^2 \frac{p_1 - p_0}{v_0 - v_1} \quad (11)$$

For a given D , this is a straight line in the p - v plane, called the Rayleigh line. Using mass conservation in the form of Eq. (1) we also obtain

$$(D - u_1)^2 = v_1^2 \frac{p_1 - p_0}{v_0 - v_1} \quad (12)$$

$D - u_1$ is the flow velocity of the material after the passage of the wave.

Just change v_0 in Eq. (11) to v_1 to obtain (12).

Normally, v_0 , e_0 , p_0 , Δq are known from the conditions of the problem. If we know e as a function of p and v and if we can find a way to determine D , then we have sufficient information to obtain p_1 and v_1 in the final state.

Figure 3 is a plot of Hugoniot's and Rayleigh lines in the p - v plane using an equation of state similar to the ideal gas with $\gamma = 1.4$.

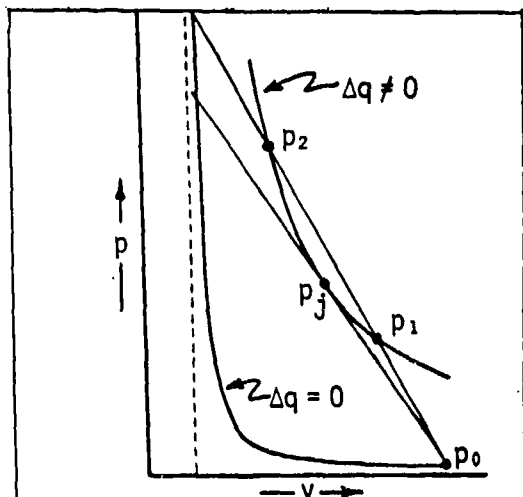


Fig. 3. Hugoniot curves. Dashed line is compressive limit, typical of most materials.

The initial pressure p_0 would be, for example, 1 atm. or .1 Megapascals. The lower curve is the Hugoniot for $\Delta q = 0$, the upper curve is the Hugoniot for some $\Delta q > 0$. The straight lines are the Rayleigh lines [Equation (11)] for various values of D . The solution involves finding the intersection of a Rayleigh line with the Hugoniot. For shocks ($\Delta q = 0$) there

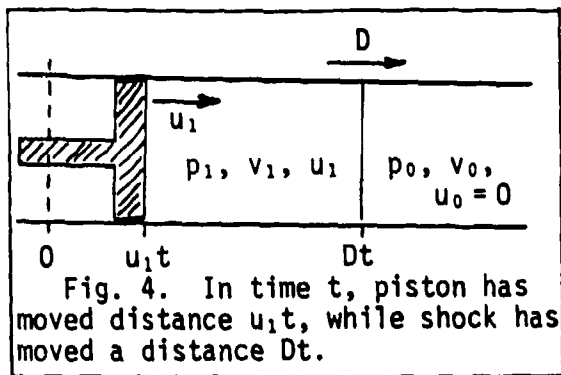
is one solution for a given value of D . In the detonation case ($\Delta q \neq 0$), we see that there are generally two solutions, labelled p_1 and p_2 in the figure.

The lower pressure solution, p_1 , is called the weak solution and does not exist as a stable solution in the idealized case and is unlikely to exist in real life. There are problems associated with the non-1-dimensionality of a real flow which might lead to a situation in which a weak solution is possible, but this is beyond scope of this series of lectures. The higher pressure solution, p_2 , is a possible solution, which we will discuss later in connection with the piston model.

The Chapman-Jouget (C-J) solution is the solution in which the Rayleigh line is tangent to the Hugoniot curve. In this solution, the flow behind the wave is sonic, that is, the flow speed is equal to the sound speed. We will show this in the following discussion of the piston model.

Piston Model

We can derive the same conservation equations using a model (Figure 4) in which a piston is driven into a gas filled tube. This model corresponds to a shock tube in which the "piston" is the expanding gas from the driving section of the shock tube which compresses the gas ahead and causes a shock wave to move down the tube.



At time $t=0$, the piston is at position $x=0$ (dotted line), the gas is at rest at pressure p_0 , density ρ_0 . The piston moves with velocity u_1 , compressing the gas ahead of it to a constant state p_1, v_1, u_1 , and the shock wave moves at velocity D . Ahead of the wave, the gas

is still in the initial state. At time t , the piston is at position $u_1 t$ and the shock wave is at position Dt .

Mass Conservation

The mass between the piston and the shock at time t is

$$m = \rho_1(Dt - u_1 t)$$

where we assume that the tube has unit cross sectional area. This is the same material that was originally between 0 and Dt at density ρ_0 , so its mass is

$$m = \rho_0 Dt$$

Thus

$$\rho_0 D = (D - u_1) \rho_1$$

as before.

Momentum Conservation

Newton's Second Law: net force = rate of change of momentum.

Again, assume unit cross sectional area, then:

net force on material between piston and shock = $p_1 - p_0$

momentum of material = $mu_1 = \rho_0 Dtu_1$

So
$$p_1 - p_0 = \frac{d}{dt} (mu_1) = \rho_0 Du_1$$

as before. This says that the wave is driven by a real force applied to back side of the piston. And the force p_1 must be greater than p_0 .

Energy Conservation

The work done by the piston must be equal to the change in energy from the initial to the final state. Consider again the material between the piston and the shock:

work done by piston in time t is the force times distance travelled by the piston = $p_1 u_1 t$

kinetic energy increase = $\frac{1}{2} m u_1^2 = \frac{1}{2} \rho_0 D t u_1^2$

initial internal energy = $(e_0 + q_0) D \rho_0 t$ (since e, q are energy per unit mass)

final internal energy = $(e_1 + q_1) D \rho_0 t$.

Thus, energy conservation requires

$$p u_1 + (D \rho_0)(e_0 + q_0) = D \rho_0 \left(\frac{1}{2} u_1^2 + e_1 + q_1 \right)$$

or

$$e_1 - e_0 - (q_0 - q_1) = \frac{p_1 u_1}{D \rho_0} - \frac{1}{2} u_1^2$$

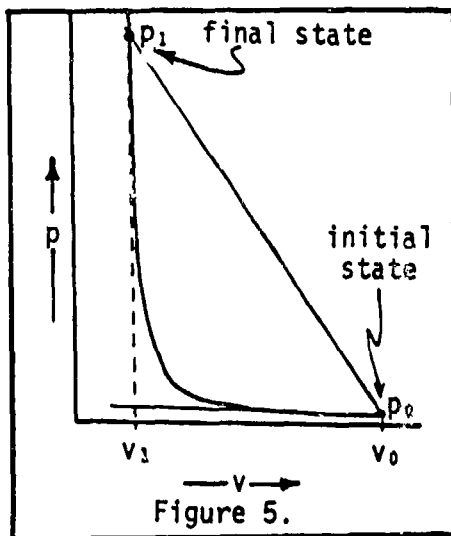
The right hand side reduces to $1/2$ the sum of the pressures times the difference in volume by using the mass and momentum conservation relations as before:

$$e_1 - e_0 - \Delta q = \frac{1}{2} (p_1 + p_0)(v_0 - v_1)$$

The piston model provides a useful first step to explain how a detonation propagates. To sustain the pressure and mass motion following the release of chemical energy we see that work must be done by an external piston pushing at the detonation pressure. You may ask, 'How, then, does a real

detonation proceed when the piston is absent and the products must be escaping from behind the zone of reaction?" The answer will be given in a later discussion. We will extend the piston model to a case where the piston is stopped after state (1) is established. In anticipation of the result we will point out that stopping the piston will cause a wave of rarefaction to move forward. This wave cannot move faster than the speed of sound in the compressed state. As a result a C-J detonation will be one in which a rarefaction can only move as fast as the detonation wave itself. The pressure formerly supplied by the piston then is maintained at the head of the rarefaction wave as a result of momentum changes in the rarefaction which keep the forces in balance. The energy previously supplied by the piston then comes from the isentropic expansion in the rarefaction wave. We will find that sound velocity plus material velocity for a strong detonation exceeds the detonation velocity. Stopping the piston then results in waves which overtake the detonation wave and weaken it until a C-J state is attained. The weak detonation case is best described after we consider the problem of deflagrations.

Properties of Shock Hugoniot and Small Amplitude Limit



The slope (or tangent) of the shock Hugoniot at the initial state is equal to the slope of the isentrope passing through the initial point. Thus, small amplitude waves (acoustic waves) are isentropic. For example, the peak pressure amplitude of human voice waves

is less than one pascal and atmospheric pressure is about 10^5 pascals so voice waves are isentropic to a very good approximation*. To show that the Hugoniot and isentrope are tangent at the initial point refer to Figure 5. The equation of the Hugoniot is

$$e_1 - e_0 = \frac{1}{2} (p+p_0)(v_0-v_1)$$

Take the limit as $v_1 \rightarrow v_0$, then the equation becomes

$$de = -p dv$$

But from the second Law of Thermodynamics, we know that

$$Tds = de + p dv$$

where s is entropy. Thus at the initial state

$$Tds = de + pdv = 0$$

or $ds = 0$ on the Hugoniot at the initial state.

The Rayleigh line determines the shock velocity:

$$U^2 = v_0^2 \frac{p_1 - p_0}{v_0 - v_1}$$

In the limit that $v_1 \rightarrow v_0$, this relation becomes

$$U^2 = -v_0^2 \frac{dp}{dv}$$

Since $ds = 0$, $\frac{dp}{dv}$ on the Hugoniot at the initial state is the isentropic (adiabatic) derivative. The definition of the isentropic sound speed is

$$c = v \sqrt{-\left(\frac{dp}{dv}\right)_s}$$

* If we ignore viscosity and heat conduction.

Thus, in the limit of small amplitude shocks, $U \rightarrow c$. The Hugoniot relation does not apply to rarefaction (that is, one should not extend the Hugoniot to the right of the initial point in the p - v plane). However, the small amplitude limit is equally valid for compressions and rarefactions. In fact, rarefactions of any amplitude are isentropic in our simplified scheme.

Small Amplitude Limit of the Mass and Momentum Conservation Equations

$$\text{Mass: } u_1 = \frac{v_0 - v_1}{v_0} U$$

In the limit $v_1 \rightarrow v_0$, we have $U \rightarrow c$ and $u_1 - 0 \rightarrow du$ so

$$du = -c \frac{dv}{v}$$

and since $\rho = \frac{1}{v}$, $-\frac{dv}{v} = \frac{d\rho}{\rho}$ so

$$du = c \frac{d\rho}{\rho}$$

$$\text{Momentum: } p_1 - p_0 = U\rho_0 u_1$$

In the limit $v_1 \rightarrow v_0$, this becomes

$$dp = \rho c du$$

If we substitute for du from the mass equation we get

$$dp = c^2 d\rho$$

which is simply the definition of the isentropic sound speed again.

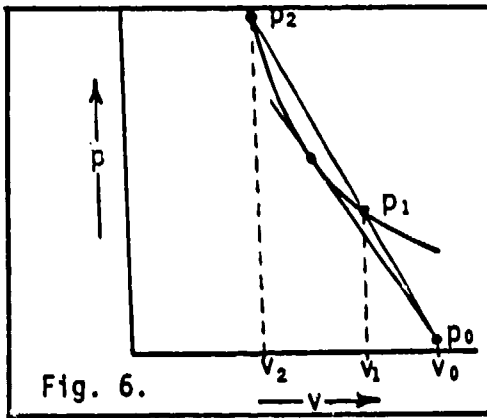
Chapman-Jouget Condition

Fig. 6.

Figure 6 shows the reaction Hugoniot-- the initial state is not on the Hugoniot since $\Delta q \neq 0$. We will show that when the Rayleigh line is tangent to the Hugoniot, the flow speed is sonic behind the wave, i.e., $D-u=c$.

First, we show that at the C-J point, the isentrope passing through that point is tangent to the reaction Hugoniot.

We can write for points p_1 and p_2 the relations

$$e_2 - e_0 = \Delta q + \frac{1}{2} (p_2 + p_0)(v_0 - v_1)$$

$$e_1 - e_0 = \Delta q + \frac{1}{2} (p_1 + p_0)(v_0 - v_1)$$

These equations, together with the fact that p_0 , p_1 , and p_2 all lie on a straight line (Rayleigh line) lead to

$$e_2 - e_1 = \frac{1}{2} (p_2 + p_1)(v_1 - v_2)$$

We can see this result without going through the calculation with the following argument:

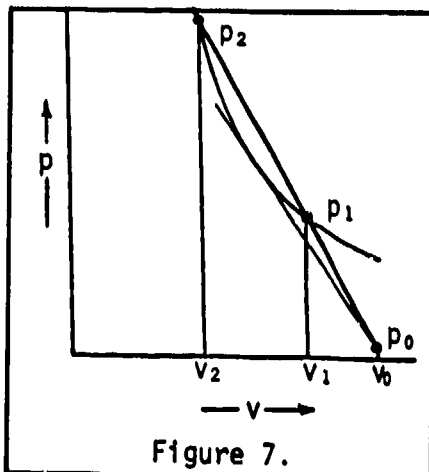


Figure 7.

$$e_2 - e_0 = \Delta q + \frac{1}{2} (p_2 + p_0)(v_0 - v_1)$$

$$= \Delta q \text{ plus area of trapezoid } \overbrace{v_0 p_0 p_2 v_2}$$

$$e_1 - e_0 = \Delta q + \frac{1}{2} (p_1 + p_0)(v_0 - v_1)$$

$$= \Delta q \text{ plus area of trapezoid } \overbrace{v_0 p_0 p_1 v_1}$$

Thus $e_2 - e_1 = (e_2 - e_0) - (e_1 - e_0) = \text{area of trapezoid } \overbrace{v_1 p_1 p_2 v_2}$

So $e_2 - e_1 = \frac{1}{2} (\text{sum of bases})(\text{altitude}) = \frac{1}{2} (p_2 + p_1)(v_1 - v_2)$

Now, in the limit that the Rayleigh line becomes tangent, we have $v_1 \rightarrow v_2$ and this expression becomes

$$de = -pdv \quad \text{or} \quad de + pdv = 0$$

Thus $ds = 0$, so at this point the Hugoniot is tangent to an isentrope.

The expression for the Rayleigh line in terms of flow speed behind the wave is

$$(D-u_2)^2 = v_2^2 \frac{p_2 - p_0}{v_0 - v_2} = v_2^2 \frac{p_1 - p_0}{v_0 - v_1} = v_2^2 \frac{p_2 - p_1}{v_1 - v_2}$$

The second and third equalities follow because, again, p_0 , p_1 , and p_2 all lie on a straight line.

Thus when the Rayleigh line becomes tangent to the Hugoniot, $p_2 \rightarrow p_1$ and

$$(D-u)^2 + -v^2 \left(\frac{dp}{dv} \right)_s = c^2$$

So

$$D - u = c.$$

Summary:

We have used the piston model to demonstrate some of the key equations for detonation and shock waves. One can infer from this model that the work that drives the wave comes from expansion of the product gas which has been formed in the reaction which creates the detonation. In the case of the ideal gas we are talking about waves reaching pressures of about 30 atm. The wave velocity is much too high to be triggered by thermal conduction processes such as occur

in flames. The initiation of the reaction must be caused by the temperature rise due to compression in the shock wave ahead of the detonation wave. If for some reason there is an insufficient reaction rate at the wave front or excessive rarefaction effects, the wave will die out.

LECTURES ON DETONATION PHYSICS

Lecture #3 -- 20 October 1980

Equations of State for Explosives and Deflagration Processes

by Sigmund J. Jacobs

Notes by Frank J. Zerilli

Dr. Donna Price will give the next lecture in this series. She will discuss critical diameter and critical shock initiating pressure.

Today we will discuss the ideal and gamma law equation of state for use in solid explosives and we will say something about deflagration processes.

REVIEW

In the last lecture we used two models to derive the equations for the conservation of mass, momentum, and energy: the steady flow and the piston model. In the steady flow model we use a coordinate system moving with the wave front so that the front appears at rest, with material flowing in from the right and flowing out to the left. In the piston model, a piston pushes material in front of it, producing a jump discontinuity (shock) separating the material in the constant initial state from the material near the piston in a constant final state. The wave front moves forward with a velocity denoted by U in the case of a shock and by D in the case of a detonation.

The important results were the equations of mass, momentum, and energy conservation.

$$\text{Mass Conservation: } \frac{u_1}{D} = \frac{v_0 - v_1}{v_0}$$

$$\text{Momentum Conservation: } p_1 - p_0 = D\rho_0 u_1$$

$$\text{Energy Conservation: } e_1 = \Delta q + e_0 + \frac{1}{2}(p_1 + p_0)(v_0 - v_1)$$

where u_1 = final particle flow velocity

v_0 = initial specific volume

v_1 = final specific volume

ρ_0 = initial density = $1/v_0$

$p_1 - p_0$ = pressure difference between initial and final states

Δq = specific chemical energy converted to mechanical energy

e_1 = final state specific internal energy

e_0 = initial state specific internal energy

In shock waves $\Delta q = 0$, while in detonation waves $\Delta q > 0$. If we know e as a function of p and v , the energy conservation equation then becomes a relation between p and v called the Hugoniot relation. The Hugoniot curve in the p - v plane is concave up and looks something like a hyperbola -- for an ideal gas, it is a hyperbola.

Eliminating u_1 from the mass and momentum equations we obtain

$$D^2 = v_0^2 \frac{p_1 - p_0}{v_0 - v_1},$$

which is a straight line (Rayleigh line) in the p - v plane:

$$p_1 - p_0 = -\frac{D^2}{v_0} (v_1 - v_0).$$

The slope of the Rayleigh line is negative, and the magnitude of the slope is proportional to the square of the detonation velocity. The intersection of a Rayleigh line with a Hugoniot determines a possible final state.

There is an interesting geometric interpretation of the energies involved in a shock or detonation wave. Refer to Figure 1. We see that area

$$A = \frac{1}{2}(p_1 + p_0)(v_0 - v_1).$$

From the energy conservation equation, therefore,

$$A = e_1 - e_0 - \Delta q.$$

Again, from the figure, area

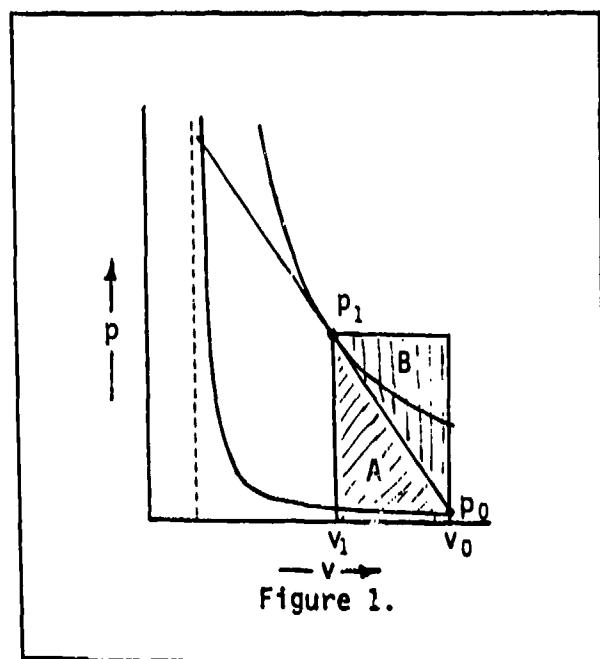
$$B = \frac{1}{2}(p_1 - p_0)(v_0 - v_1).$$

Eliminating D from the mass and momentum conservation equations, we get

$$(p_1 - p_0)(v_0 - v_1) = u_1^2.$$

Thus area $B = \frac{1}{2}u_1^2 =$ change in material kinetic energy per unit mass, area $A =$ change in total internal energy per unit mass,

and area $A + B = p_1(v_0 - v_1)$ is the work done by the "piston" per unit mass.



THE IDEAL GAS EQUATION OF STATE

The ideal gas equation of state is

$$pV = RT ,$$

where V = volume of one mole

$R = 8.3143$ joules/mole- $^{\circ}K$

T = temperature in $^{\circ}K$

The specific volume v (volume per unit mass) is the molar volume (volume per mole) divided by the mass of one mole, M , so that in terms of specific volume the equation becomes

$$pv = \frac{R}{M} T .$$

In the SI (Système Internationale) units, one mole (Avogadro's number of molecules) of C_{12} is arbitrarily fixed at 12 grams (a kilogram-mole is fixed at 12 kg). This defines the unit of mass called the atomic mass unit or a.m.u. Thus, M for any substance is simply its molecular weight in a.m.u. We will attempt to use SI units consistently. Length will be given in meters (m), mass in kilograms (kg), and time in seconds (s). In this system, the density of water is 1000 kg/m^3 . Appendix A contains a table of recommended SI units for propulsion variables which will be useful also in detonation work.

Assuming constant specific heat, the internal energy per mole of an ideal gas is

$$E = C_V T ,$$

and the specific internal energy is

$$e = \frac{C_V}{M} T = c_V T ,$$

where C_V is the molar specific heat capacity at constant volume, defined by[†]

$$C_V = \left(\frac{\partial E}{\partial T} \right)_V .$$

[†]This is consistent with the usual definition: $C_V = \left(\frac{dQ}{dT} \right)_V$ since $dQ = dE + pdV = dE$ at constant volume.

The specific heat at constant pressure is defined by[†]

$$C_p = \left(\frac{\partial H}{\partial T} \right)_p,$$

where H is the enthalpy, defined by

$$H = E + pV.$$

Thus, for the ideal gas, $H = (C_v + R)T$ so that

$$C_p = C_v + R.$$

Denoting the ratio of specific heats by γ_i we get

$$\gamma_i = \frac{C_p}{C_v} = 1 + \frac{R}{C_v}.$$

For hydrodynamic purposes, it will be convenient to write p as a function of e and v. For the ideal gas, we have

$$p = \frac{RT}{V} = \frac{R}{V} \frac{E}{C_v} = (\gamma_i - 1) \frac{E}{V}.$$

In terms of e and v, this becomes

$$p = (\gamma_i - 1) \frac{e}{v} = (\gamma_i - 1)e_p.$$

ISENTROPIC PRESSURE-VOLUME RELATION

The First Law of Thermodynamics is

$$de = Tds - pdv,$$

where s is the specific entropy. When s is a constant,

$$de = -pdv = -(\gamma_i - 1) \frac{e}{v} dv,$$

so that

$$-\frac{de}{e} = (\gamma_i - 1) \frac{dv}{v}.$$

Integrating this expression, we get

$$e = A'v^{-(\gamma_i - 1)} = A''v^{\gamma_i - 1},$$

[†]Since $dH = dE + pdV + Vdp$, we have $dQ = dE + pdV = dH - Vdp = dH$ at constant pressure.

so

$$p = (\gamma_i - 1)A\rho^{\gamma_i} = A\rho^{\gamma_i}.$$

We have been using the subscript i to emphasize the fact that we have derived these relations for an ideal gas. We will drop the subscript and consider a generalized equation of state in which γ may not be the ratio of specific heats. In the generalized case we will use a definition of γ directly related to the sound speed. The sound speed c is defined by

$$c^2 = \left(\frac{\partial p}{\partial \rho} \right)_s.$$

For the ideal gas, then,

$$c^2 = \frac{d}{d\rho} (A\rho^\gamma) = \gamma A\rho^{\gamma-1} = \frac{\gamma p}{\rho}.$$

Thus,

$$\gamma = \frac{\rho}{p} \left(\frac{\partial p}{\partial \rho} \right)_s = \left(\frac{\partial \ln p}{\partial \ln \rho} \right)_s = - \left(\frac{\partial \ln p}{\partial \ln v} \right)_s.$$

We will use this as the definition of γ . In the case of the ideal gas with constant specific heat C_v , γ is a constant and is equal to the ratio C_p/C_v . In general, γ will not be constant and/or it may not be the ratio of specific heats. We will use as our generalized equation of state the relation

$$e = \frac{pv}{\gamma - 1},$$

where γ is not necessarily the ratio of specific heats. We will refer to this as the γ -law equation of state (EOS).

SHOCKS WITH OR WITHOUT REACTION FOR THE γ -LAW EOS

We now substitute the γ -law equation of state in the energy conservation equation to obtain the Hugoniot relation. The energy conservation equation is

$$e_1 = q + e_0 + \frac{1}{2}(p_1 + p_0)(v_0 - v_1). \quad (1)$$

From the γ -law EOS we have

$$e_1 = \frac{p_1 v_1}{\gamma - 1}, \quad (2a)$$

$$e_0 = \frac{p_0 v_0}{\gamma - 1}. \quad (2b)$$

Substituting Eq. (2a) in Eq. (1) we get

$$p_1 = \frac{2(q + e_0) + p_0(v_0 - v_1)}{\frac{\gamma + 1}{\gamma - 1} v_1 - v_0}. \quad (3)$$

This is the equation of a hyperbola with a horizontal asymptote at $p_1 = -\frac{\gamma - 1}{\gamma + 1} p_0$ and a vertical asymptote at $v_1 = \frac{\gamma - 1}{\gamma + 1} v_0$. This shows that

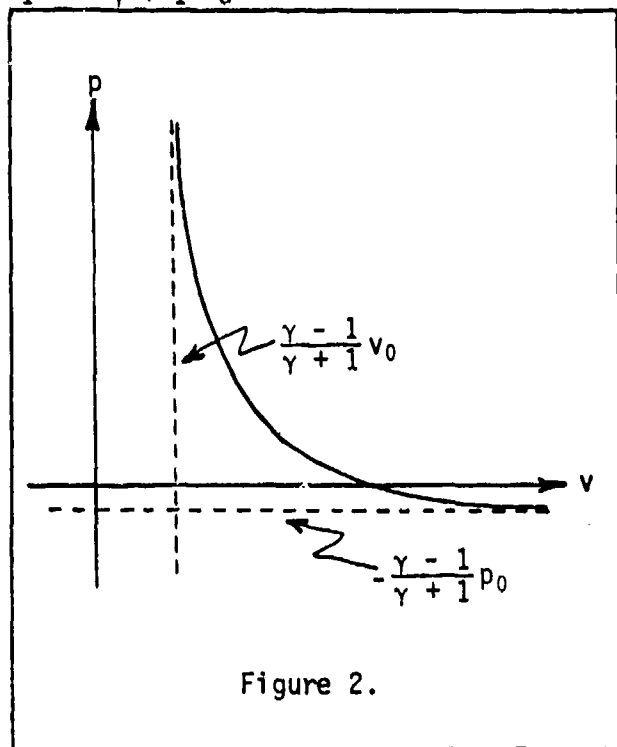


Figure 2.

there is an asymptotic limit to the amount of compression that a γ -law gas can undergo in a single shock. The limiting volume is

$$v_\infty = \frac{\gamma - 1}{\gamma + 1} v_0.$$

Thus, for example, a gas with $\gamma = 1.4$ cannot be compressed to less than 1/6 of its initial specific volume. It is convenient to write Eq. (3) in terms of the dimensionless quantities p_1/p_0 , v_1/v_0 , and q/e_0 .

$$\frac{p_1}{p_0} = \frac{2}{\gamma - 1} \left(\frac{q}{e_0} + 1 \right) + 1 - \frac{v_1}{v_0} \quad (4)$$

$$\frac{p_1}{p_0} = \frac{\frac{2}{\gamma - 1} \left(\frac{q}{e_0} + 1 \right) + 1 - \frac{v_1}{v_0}}{\frac{\gamma + 1}{\gamma - 1} \frac{v_1}{v_0} - 1}.$$

When $q = 0$, Eq. (4) is a Hugoniot for a shock. In the case of reactions, however, the value of γ for the product gases will not, in general, be the same as the value for the unreacted material.

The equation for the Rayleigh lines is

$$U^2 = v_0^2 \frac{p_1 - p_0}{v_0 - v_1} = p_0 v_0 \frac{\frac{p_1}{p_0} - 1}{1 - \frac{v_1}{v_0}} \quad (5)$$

NUMERICAL EXAMPLE: NITRIC OXIDE

We apply Eqs. (4) and (5) to nitric oxide (NO). Nitric oxide reacts to form nitrogen and oxygen:



The average molecular weight \bar{M} for both the reactants and the products is 30. The heat of reaction q (which is the same as the change in specific enthalpy Δh) is 720 cal/g or 3013 kJ/kg. We'll assume the following values:

$$\begin{aligned} p_0 &= 1 \text{ bar} = .1 \text{ MPa} = 10^5 \text{ Pa} \\ C_v &= 5R/2 \\ \gamma &= 1.4 \\ T_0 &= 300^\circ\text{K} \\ v_0 &= 831.4 \text{ cm}^3/\text{g} = 0.8314 \text{ m}^3/\text{kg} \end{aligned}$$

If we assume that C_v is constant at $5R/2$ from 0°K to 300°K , then

$$e_0 = \frac{5RT_0}{2M} = \frac{p_0 v_0}{\gamma - 1} \approx 208 \text{ kJ/kg} ,$$

so

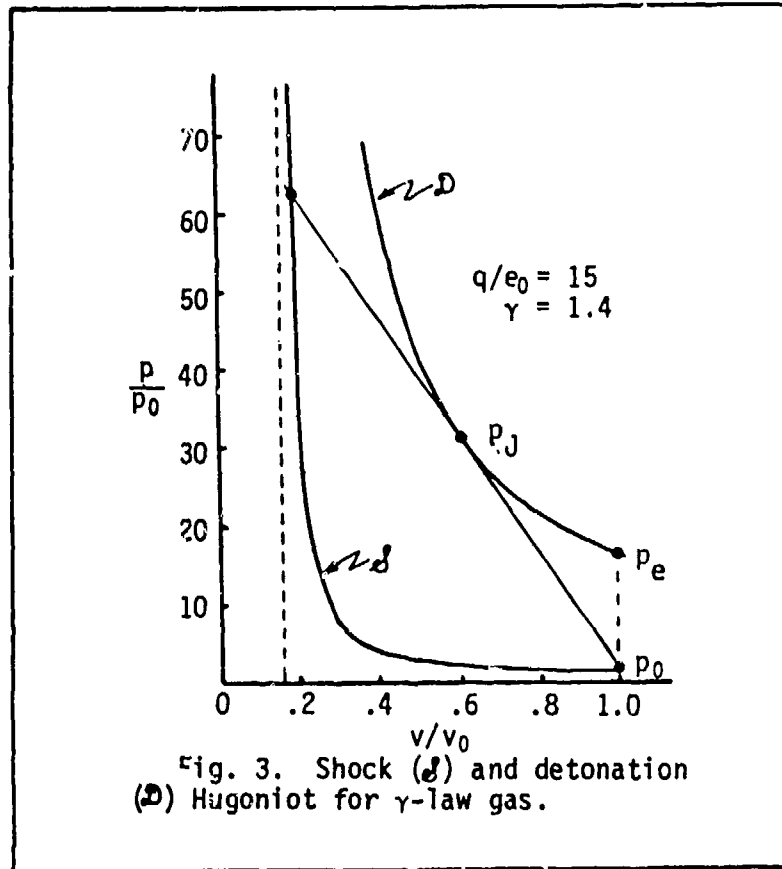
$$\frac{q}{e_0} \approx 14.5 \quad .$$

Thus, the detonation Hugoniot is

$$\frac{p_1}{p_0} = \frac{78.5 - \frac{v_1}{v_0}}{6 \frac{v_1}{v_0} - 1} \quad (7)$$

The shock Hugoniot ($q = 0$) is

$$\frac{p_1}{p_0} = \frac{6 - \frac{v_1}{v_0}}{6 \frac{v_1}{v_0} - 1} \quad (8)$$



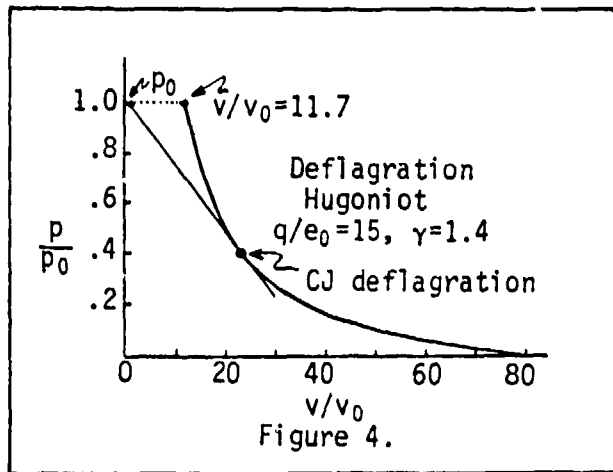
Detonation and shock Hugoniot's are plotted in Fig. 3 for $q/e_0 = 15$ and $\gamma = 1.4$. The pressure on the detonation Hugoniot corresponding to $v/v_0 = 1$ is the constant volume explosion pressure.[†] Note that it is roughly half the C-J pressure.

DEFLAGRATIONS

The relations obtained above can also be used in the case of deflagrations. Here, we use the term deflagration to indicate combustion accompanied by expansion

[†]This is the pressure that would be obtained if all the material were reacted in a sealed and thermally insulated bomb (container).

as occurs within a rocket motor. Figure 4 shows the reaction Hugoniot plotted



for pressures smaller than the initial pressure and volumes greater than the initial volume. For this particular plot, the constant pressure reaction product volume is 11.7 times the initial volume. The Rayleigh line tangent to the Hugoniot defines a "C-J deflagration" state, but this does not represent an actually occurring stable physical situation.

Figure 5 illustrates a rocket motor in which the initial pressure of the unburned propellant, p_0 , is 7 MPa (1015 psi) and the initial specific volume is $0.556 \text{ cm}^3/\text{g}$. The heat of reaction Δh is 6000 J/g, and at the high temperature which occurs in this situation, a reasonable value of γ for the product gases is about 1.2. The deflagration Hugoniot is plotted in Fig. 6. To find the state p_1, v_1 behind the burning front we draw the Rayleigh line whose slope corresponds to the velocity of the front.

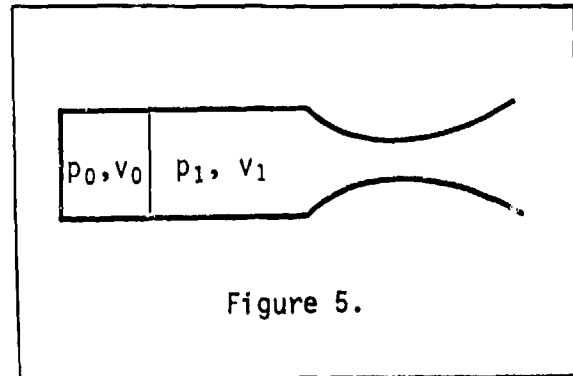
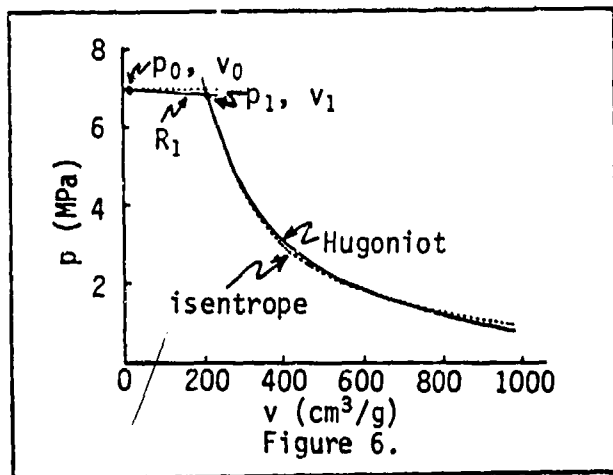


Figure 5.



The Rayleigh line whose slope corresponds to the velocity of the front. The Rayleigh line is labeled R_1 in Fig. 6. The intersection with the Hugoniot gives the state p_1, v_1 . Clearly, p_1 is only very slightly less than p_0 since the burning velocity is usually very small (of the order of a cm/sec), so the slope of the Rayleigh line is very small. Upon passing through the nozzle, the gases expand

isentropically. The isentrope passing through the point p_1, v_1 almost coincides with the Hugoniot (the coincidence is closer, in fact, than the experimental error in

measurement). As the gases expand, the flow velocity increases, becoming sonic as they pass through the throat and supersonic beyond the throat.

PRESSURE AND DENSITY IN THE CHAPMAN-JOUGET STATE

We now obtain expressions for the pressure and density in the C-J (Chapman-Jouget) state for a γ -law gas. In the C-J state, the condition

$$D - u_1 = c_1$$

is satisfied. From momentum and mass conservation we know that

$$(D - u_1)^2 = v_1^2 \frac{p_1 - p_0}{v_0 - v_1} \quad (9)$$

From the definition of sound speed we have

$$c_1^2 = -v_1^2 \left(\frac{\partial p}{\partial \rho} \right)_s = \gamma p_1 v_1 \quad (10)$$

Equating (9) and (10) we get

$$\frac{v_1}{v_0 - v_1} = \frac{\gamma p_1}{p_1 - p_0} = \frac{\gamma}{1 - \frac{p_0}{p_1}} \quad (11)$$

For detonations we can set $p_0 = 0$ since it is usually negligible compared to p_1 . Typical detonation pressures for liquid and solid explosives are of the order of several hundred kilobars, and p_0 , typically, is 1 ar (i.e., one atmosphere). Thus p_0 is about 10^5 times smaller than p_1 and can be safely ignored since the effect on accuracy is only .001% while detonation pressures can only be measured to a few percent accuracy at best. Thus, Eq. (11) becomes

$$\frac{v_0 - v_J}{v_J} = \frac{1}{\gamma} \quad (11a)$$

or

$$\frac{v_J}{v_0} = \frac{\gamma}{\gamma + 1} \quad (11b)$$

where the subscript J is now used to denote the Chapman-Jouget state. From mass conservation,

$$\frac{u_J}{D} = \frac{v_0 - v_J}{v_0} = \frac{1}{\gamma + 1}, \quad (12)$$

and from momentum conservation,

$$p_J = Du_J \rho_0 = \frac{D^2 \rho_0}{\gamma + 1}. \quad (13)$$

The approximate Hugoniot, neglecting p_0 , is

$$p_1 = \frac{2(q + e_0)}{\frac{\gamma + 1}{\gamma - 1} v_1 - v_0}. \quad (14)$$

We don't neglect e_0 since we wish to use this equation for solid explosives. For a gas, $e_0 = p_0 v_0 / (\gamma - 1)$ and we would neglect it. But for a solid, e_0 will be the internal energy of the solid material and will be a small, but not negligible, contribution (a few percent).

Setting $v_1 = v_J$ and substituting for v_J from Equation (11b), we obtain the C-J detonation pressure

$$p_J = \frac{2(\gamma - 1)(q + e_0)}{v_0}. \quad (15)$$

The contribution volume explosion pressure is the pressure obtained when the material is reacted at constant volume v_0 . Setting $v_1 = v_0$ in Eq. (14) we obtain

$$p_e = \frac{(\gamma - 1)(q + e_0)}{v_0}. \quad (16)$$

Comparing this with Eq. (15), we see that C-J pressure is twice the constant volume explosion pressure:

$$p_J = 2p_e \quad (17)$$

Finally, we may obtain an expression for the detonation velocity by eliminating p_J between Eqs. (13) and (15):

$$p_J = \frac{D^2 \rho_0}{\gamma + 1} = \frac{2(\gamma - 1)(q + e_0)}{v_0}$$

This gives

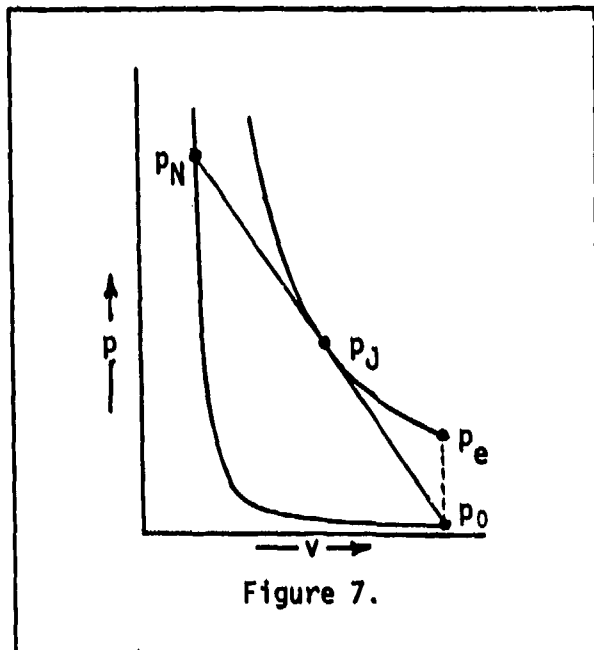
$$D^2 = 2(\gamma^2 - 1)(q + e_0) . \quad (18)$$

For more exact equations of state, the C-J value of γ is still defined by

$$\gamma_J = \left(\frac{\partial \ln p}{\partial \ln \rho} \right)_s .$$

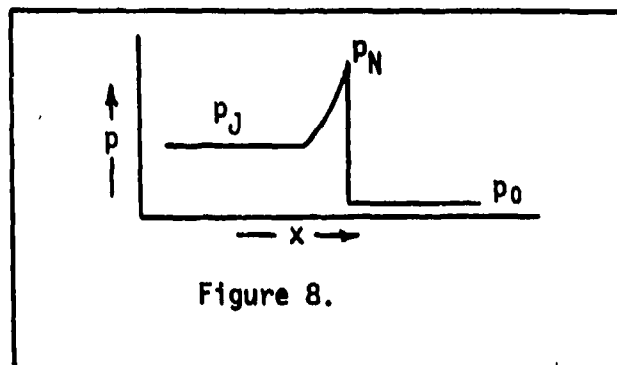
If we know D_J and $q + e_0$, we can use Eq. (18) to find an approximate value for γ_J .

The pressure of the state in which the C-J Rayleigh line intersects the unreacted Hugoniot is called the von Neumann spike (Figure 7). If we recall the



piston model and imagine a piston driven into a reactive gas, the initial piston motion creates a shock. Suppose the velocity of the piston is such that the shock velocity is the C-J detonation velocity. The pressure at the shock front will be the von Neumann pressure p_N since the Rayleigh line intersects the shock Hugoniot at this pressure. The temperature rise produced by the shock will cause the gas behind the shock to start reacting. There will be a zone of reaction behind the shock. Within the reaction zone,

the states must lie along the C-J Rayleigh line (this is required by mass and momentum conservation). At the end of the reaction zone, where the reaction has



gone to completion, the pressure will have dropped to the C-J pressure. Thus, the detonation wave will have the spatial distribution shown in Fig. 8. There is a jump from the pressure p_0 to the von Neumann pressure p_N determined by the point where the Rayleigh line intersects the unreacted

Hugoniot. Then, there is a falloff as the reaction proceeds and the states move down the Rayleigh line toward the final C-J pressure. The pressure then remains constant at the C-J value.

The degree of reaction along the Rayleigh line between p_N and p_J is undetermined until some information is given about the reaction kinetics. If we make appropriate assumptions, we can then determine (at least mathematically) the pressure versus distance and time.

THE MAGNITUDE OF THE VON NEUMANN SPIKE

It is easy to show that the ZVD (Zeldovich-von Neumann-Doering) pre-shock state pressure (i.e., von Neumann Spike) is approximately twice the C-J pressure in our γ -law model. Since detonation pressures are so high, we may approximate v_N by the asymptotic limiting volume:

$$v_N \approx \frac{\gamma - 1}{\gamma + 1} v_0 .$$

Thus, from mass conservation we obtain

$$\frac{u_N}{D} = \frac{v_0 - v_N}{v_0} = \frac{2}{\gamma + 1} .$$

From momentum conservation we get

$$p_N \approx Du_N \rho_0 = \frac{2}{\gamma + 1} D^2 \rho_0 = 2p_J = 4p_e .$$

Thus the ratio of p_e to p_J to p_N is

$$p_e : p_J : p_N = 1 : 2 : 4 .$$

In actual detonations, the pressure p_N does not satisfy this relation. However, explosion pressures do approximately satisfy the relation $p_e : p_J = 1 : 2$. The explosion pressure can be experimentally obtained by reacting the explosive in a closed bomb, waiting 100 msec or so for things to settle down, and correcting for heat losses.

Example: Gaseous and Liquid Nitric Oxide

Table 1. Measured vs. Calculated C-J Pressure and Velocity for NO.

	Gas	Liquid
T_0	300 ⁰ K	115 ⁰ K
q	3013 kJ/kg	3013 kJ/kg
e_0	208 kJ/kg	80 kJ/kg
P_0	.1 MPa	.1 MPa
γ	1.4	1.4
v_0	831.4 cm ³ /g	0.775 cm ³ /g
p_j (calculated)	3.10 MPa	3193 MPa
D_j (calculated)	2487 m/s	2437 m/s
D_j (measured)	--	5620 m/s
γ_j (from Eq. 18)	--	2.471
p_j (using γ_j)	--	11,740 MPa
p_j (measured)	--	10,000 \pm 1500 MPa

As an example, consider the gas and liquid state of NO (nitric oxide). Assume for the gaseous state that the initial temperature is 300⁰K and for the liquid state that the initial temperature is 115⁰K (the boiling point). The specific internal energy e_0 will be 208 kJ/kg for the gas and 80 kJ/kg for the liquid assuming constant specific heat.[†] The specific heat of reaction q will be the same in both cases (see the table above). The initial pressure is taken to be .1 MPa (1 atmosphere), and we'll assume γ is 1.4 since NO is a diatomic molecule.

The calculated C-J pressure for the gas is 3.10 MPa and for the liquid is 3193 MPa. The C-J pressure for the liquid is a thousand times greater than that of the gas, principally because the density of the liquid is about a thousand times greater than the density of the gas. The effect of density is evident from Eq. (15). The detonation velocity is very nearly the same in

[†] $e_0 = c_v T_0$ where $c_v = 5R/2M$ and $M = 30g$ for NO.

both cases since, according to Eq. (18), the detonation velocity depends only on γ and $q + e_0$. The slight difference is due to the difference in e_0 in each case. But e_0 is much less than q , so the effect is small.

The experimentally measured value of D_J for the gas agrees well with the calculated value as does the experimentally measured pressure (these values are not given in the table above). However, the experimentally measured value of the detonation velocity for the liquid is about twice the calculated value and, in addition, the measured pressure is three to four times the calculated pressure (see Appendix B for values reported by Ramsey and Chiles, Sixth Detonation Symposium). However, if we use Eq. (18),

$$D_J^2 = 2(\gamma^2 - 1)(q + e_0) , \quad (18)$$

and substitute the measured value of D_J along with the given values of $q + e_0$, we obtain a value for γ_J ,

$$\gamma_J = \sqrt{1 + \frac{D_J^2}{2(q + e_0)}} = 2.471 .$$

If we then use this value of γ_J in Eq. (15), we obtain a value for p_J of 11740 MPa (117.4 kbar), which is reasonably close to the measured value (see table above and Appendix B) of 110 ± 15 kbar. Compare our result with results calculated from more sophisticated equations of state (again, refer to Appendix B) and the same initial density: Smith, et al. - 105 kbar; Kamlet - 119 kbar; Mader BKW - 106 kbar; Lee - 95 kbar.

Our simple theory allows us to calculate approximately the detonation pressure if we know the detonation velocity and heat of explosion. Of course, more sophisticated models, such as Kamlet's model, allow us to calculate both the detonation velocity and pressure. Also, our simple theory does not give nearly as good an approximation to the detonation pressure for denser materials such as TNT (density 1.6 gm/cm^3).

SUMMARY

Detonation pressures for solids are much greater than those for gases. The basic reason is that solids are much denser than gases, and the C-J pressure is proportional to the initial density.

In a detonation, a chemical reaction is initiated by a compression wave and the wave, in turn, is driven by the expansion wave in the reaction products. This is in contrast to a deflagration, in which the reaction is driven by thermal conduction.

RECOMMENDED SI UNITS FOR PROPULSION VARIABLES

Variable	Basic SI Unit	Recommended Unit
1. Time, t	second (s)	s
2. Length, L, R, D	meter (m)	km, m, mm, μm
3. Mass, m	kilogram (kg)	kg
4. Temperature, T	kelvin (K)	K
5. Chemical quantity, N	mole (mol)	kmol
6. Force, F	newton (N)	N
7. Angle	radian (rad)	rad, degree
8. Area, A	m^2	m^2, cm^2
9. Volume, V	m^3	m^3, cm^3
10. Velocity, V	m/s	m/s
11. Acceleration, a	m/s^2	m/s^2
12. Mass flow rate, \dot{m}	kg/s	kg/s
13. Gas density, ρ_g	kg/m^3	kg/m^3
14. Solid or liquid density, ρ	kg/m^3	Mg/m^3
15. Energy, E	N·m (J)	kJ
16. Pressure, P	N/m^2 (Pa)	kPa, MPa
17. Stress, σ or τ	N/m^2 (Pa)	kPa, MPa
18. Gas constant, R	J/(kg·K)	KJ/(kg·K)
19. Specific heat, c_p and c_v	J/(kg·K)	kJ/(kg·K)
20. Chemical enthalpy, H	J/mol	kJ/kmol
21. Thrust, F	N	N
22. Specific impulse, I_{sp}	N·s/kg	N·s/kg
23. Total impulse, I_t	N·s	N·s
24. Temperature sensitivity, π	K^{-1}	K^{-1}
25. Burning rate, $r = cP^n$ where the units of P are	m/s N/m^2 (Pa)	mm/s MPa

Ref. CPIA Bulletin, 5, 5(1980)p 11

APPENDIX B

Summary of Experimental and Computed Detonation Properties of Liquid NO

	Density (g/cm ³)	Pressure (kbar)	Velocity (mm/μs)	Mole Fraction N ₂ in Products
EXPERIMENT				
This paper	1.294	100 ± 15	5.62 ± 0.07	—
Ribovich, et al., Ref. (4)	1.30		5.4	—
Miller, Ref. (3)	1.22		5.1	
CALCULATED				
Smith, Ref. (8)				
P = 0.2582ρ ₀ D ²	1.29	105	—	
Kamlet, Ref. (11)				
P = Kρ ₀ ² Φ	1.29	119	5.98	0.50
D = 1.01 (1 + 1.30ρ ₀)Φ ^{1/2}				
Φ = NM ^{1/2} Q ^{1/2} = 4.899				
N ≡ moles gaseous detonation products/g of explosive = 0.033				
M ≡ average molecular weight of gaseous products = 30.				
Q ≡ cal/g of detonation reaction = 720 cal/g				
K = 15.58 NM ^{0.93}				
14.65 NM > 0.93 (This value was used for the above computations)				
Mader BKW, Ref. (6)	1.30	106	5.61	0.498
Lee JCZ3, Ref. (12)	1.26 (1.30)*	88 (95)	5.38 (5.51)	0.482

*Adjusted for density, $dD/d\rho = 3.2 \text{ (mm/}\mu\text{s)}/(\text{g/cm}^3)$, $P = \rho_0 D^2 / (\gamma + 1)$

†John B. Ramsey and W. C. Chiles, "Detonation Characteristics of Liquid Nitric Oxide," Sixth Symposium on Detonation, NSWC/WO, p. 727.

Lectures On Detonation Physics

Lecture #4 - 3 November 1980

Critical Diameter and Critical Shock
Initiation Pressure

by

DONNA PRICE

Notes by Frank J. Zerilli

PREFACE

The theme of the series of lectures to be given by Dr. Price will be the description of various critical parameters for the propagation of steady state detonation and of critical initiation conditions for the shock to detonation transition. There will be a discussion of the relations which exist between these critical parameters. Critical diameter will be considered first, then critical particle size, critical temperature, critical density, and so forth.

The Two Most Common Critical Parameters

The two most common critical parameters are the critical diameter for propagation of a steady state detonation and the critical pressure for initiation of a shock to detonation transition.

Definition of Critical Diameter

The critical diameter for propagation is the minimum diameter of a cylindrical charge for which it is possible to propagate

a steady state detonation. The steady state condition is to be emphasized, since we wish to exclude situations in which, for example, detonation occurs, followed by failure, followed by re-ignition, and so forth. Although there is sustained detonation in such a situation, it does not have a "steady state" structure.

Critical Shock Initiating Pressure

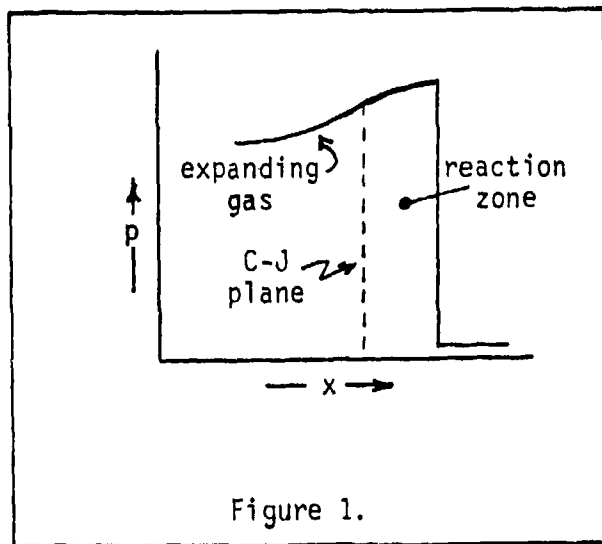
The critical pressure for initiation of a shock to detonation transition may be defined in terms of the way that it is measured by means of the gap test. In the gap test, there is a standard solid explosive "donor" followed by a solid attenuator material and followed, in turn, by the "acceptor" explosive (the material to be investigated). The thickness of the gap is varied until a thickness is found for which the test explosive detonates in fifty percent of the trials. If the donor-attenuator system is calibrated, then the thickness of the attenuator at the fifty percent point can be related to the actual pressure in the attenuator at the attenuator-test explosive interface. We call this the gap pressure P_g . If, in addition, we know the Hugoniot relation for the acceptor material, then the actual critical initiating pressure transmitted to the explosive can be determined from P_g .

The necessary and sufficient conditions for producing a steady state detonation in a cylindrical charge are that the diameter must be greater than the critical diameter and the

initiating stimulus must produce a shock in the explosive with a pressure greater than the critical initiating pressure for that specific charge.

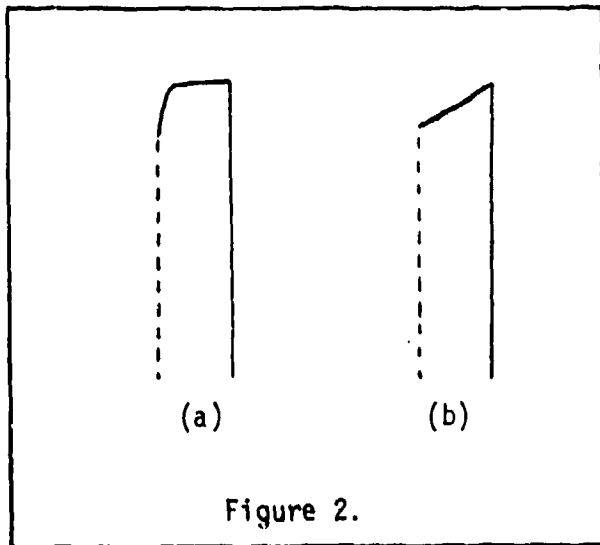
The Ideal Detonation Model

The Zeldovich-von Neumann-Doering one-dimensional plane detonation model describes a charge of "infinite diameter" and has no dissipation processes. Figure 1 shows a schematic plot



of pressure versus distance for a ZND detonation wave. The region between the von Neumann shock and the C-J plane is the reaction zone, a steady state region. The reaction is completed at the C-J plane, and following is a region of expanding

product gases. If the reaction is a homogeneous reaction of homogeneous material (such as a uni-molecular decomposition) then the drop in pressure from the von Neumann spike to the C-J pressure will take place fairly rapidly over a short distance after a long induction period (see Fig. 2a). The reaction takes place mostly near the C-J



plane. If, on the other hand, the reaction is heterogeneous (though the material may be homogeneous), as in a reaction involving hot spots, then the reaction starts sooner and the drop is more like that shown in Fig. 2b. The general case would involve some of each type of reaction. The reaction zone is a steady state region, that is, it propagates along the charge unchanged in time. The expansion wave following the C-J plane is not a steady state.

A Relation Between Critical Diameter and Critical Pressure

Although the one-dimensional model is idealized, steady state detonation also occurs in finite diameter charges. The detonation structure is comparable to the ideal case, although dissipative effects must be included so that the pressures, detonation velocities, and densities for the finite size charges will be somewhat lower than the values predicted by the idealized one dimensional model.

The first relation between critical diameter and critical initiating pressure can be inferred by considering a charge having the critical diameter, in which the detonation is at the threshold of failure. We know, then, that the structure of the wave between the von Neumann spike and the C-J plane is such that the steady state detonation barely propagates. Thus we can infer that the critical stimulus necessary to initiate detonation (in a charge of critical diameter) is described by the pressure history between the von Neumann spike and the C-J plane.

As the diameter of a charge gets smaller and approaches the critical diameter, the detonation pressure, velocity, and density will get smaller, departing more and more from their ideal values. In charges with practically no voids (less than, say, 2%), the ratio of the critical detonation velocity to the ideal velocity is not much different from unity. The ratio is .95 for TNT with an initial density of 98% of the theoretical maximum density (TMD), whether it is cast or pressed. However, for a granular charge of TNT of, say, 50% porosity, the ratio drops to 0.65. For less powerful materials, the ratio becomes even smaller. For example, for ammonium perchlorate having 25 μ particle size and 50% TMD, the ratio is 0.45.

In the following, for simplicity, we will consider only nearly voidless materials. We will use the one dimensional model to get an idea of the magnitude of the pressures involved in a solid explosive detonation, although the one dimensional model cannot tell us what the critical diameter is.

The relation between the C-J pressure and detonation velocity in the one-dimensional γ -law model is[†]

$$P_j = \frac{\rho_0 D^2}{\gamma + 1} . \quad (1)$$

We know from experiment that the ratio of critical detonation velocity to the ideal detonation velocity for TNT is

$$\frac{D_c}{D_i} \approx 0.95.$$

[†]S. J. Jacobs, Lecture 3, this series.

From Eq. (1) we see that the C-J pressure is proportional to the square of the detonation velocity so

$$\frac{(P_j)_c}{P_j} = \left(\frac{D_c}{D_i}\right)^2 \approx 0.9$$

Coleburn and Liddiard[†] measured C-J pressures for several materials. For TNT they found

$$\left. \begin{array}{l} P_j \approx 189 \text{ kbar} \\ P_{vN} \approx 1.25 P_j \end{array} \right\} \text{ (TNT)}$$

Thus we infer the critical von Neumann spike pressure to be

$$(P_{vN})_c \approx 0.9 P_{vN} \approx 213 \text{ kbar.}$$

This would be an upper limit to the critical initiating pressure for a charge of TNT at its critical diameter.

Critical Diameter and Khariton's Principle

Most of the experimental work on critical diameter has been done by Russian scientists. In the Russian literature, there are many references to Khariton's principle. The two original papers^{††} are not very accessible, and the principle is given in various forms in secondary sources.

[†]N. L. Coleburn and T. P. Liddiard, Jr., "Hugoniot Equations of State of Several Unreacted Explosives," J. Chem. Phys. 44, 1929 (1966).

^{††}Yu. B. Khariton and V. O. Rozing, Dokl. A.N. SSSR, 26, 360 (1940); Yu. B. Khariton, Collection: "Problems of the Theory of Explosives," Izd-vo A. N. SSSR, Moscow, 1947. These references are taken from: A. N. Dremin, S. D. Savrov, V. S. Trofimov, and K. K. Shvedov, "Detonation Waves in Condensed Media," Izd-vo Nauka, Moscow, 1970; A. N. Dremin and V. S. Trofimov, "Nature of Critical Detonation Diameter of Condensed Explosives," Combustion, Explosion, and Shock Waves 5 (3), 208 (1969).

There must be some sort of dissipative process which leads to the existence of a failure condition and critical diameter in explosives. The obvious process is the arrival of lateral rarefaction waves at the axis of a cylindrical charge with a consequent quenching of the reaction in the detonation reaction zone. Many others have had this idea, but Khariton was probably the first to try to give this idea a quantitative form. In order to quench the reaction, the rarefaction or relief waves must travel from the surface to the center of the charge through the dense gas products. The rarefaction waves travel at the sound velocity c and thus terminate the reaction at a time τ given by $c\tau = R$, where R is the radius of the charge. Thus Khariton's statement of the principle relates the critical diameter to the sound velocity in the reaction products and to the reaction time:

$$d_c \sim 2\tau c \quad (2)$$

where τ is the reaction time and c is the velocity of sound in the reaction products.

Another statement of Khariton's principle is

$$\frac{d_{c_1}}{d_{c_2}} \approx \frac{\tau_1}{\tau_2} \quad (3)$$

which applies for a given material under varying conditions (for instance, same charge dimensions, same porosity, but different particle size).

Another version which is more frequently quoted is

$$\frac{d_c}{D_c} = \tau_c \quad (4)$$

which can be derived from Eq. (2) by assuming a proportionality between the sound velocity and the detonation velocity. Unfortunately, the so-called "constant of proportionality" in Eq. (4) is not constant. It is a function of density and of γ , and it differs from explosive to explosive.

In fact, Eqs. (2) to (4) have been generally discredited as far as quantitative applications are concerned, ever since electromagnetic methods for measuring particle velocity and reaction times have become available.

Relation Between Detonation Velocity and Charge Diameter

Soon after Khariton's work, Jones[†] in England and Eyring^{††} in the USA developed expressions relating measured detonation velocity to the diameter of the charge. The simplest is Eyring's expression for the detonation velocity in an unconfined charge:

$$\frac{D}{D_i} = 1 - \frac{a}{d} \quad (5)$$

where d is the diameter, a is the reaction zone width and D_i is the ideal detonation velocity. Eq. (5) fits observed data well for diameters large compared to the critical diameter but poorly for diameters near the critical diameter. Jones'

[†]H. Jones, Proc. Roy. Soc. A189, 415 (1947).

^{††}H. Eyring, R. E. Powell, G. H. Duffy, and R. H. Parlin, Chem. Revs. 45, 69 (8), (1949).

relation is more complicated and fits the data slightly better, but still not very well. At the Sixth Detonation Symposium, Campbell[†] presented a relation that is a modification of Eq. (5):

$$\frac{D}{D_1} = 1 - \frac{A}{R-B} \quad (6)$$

where R is the radius of the charge and A and B are constants (for a given material). Eq. (6) fits the data very well even up to the critical diameter for about a dozen voidless explosives which Campbell examined. The relation, however, is a purely empirical fit to the data and is not based on theory.

Measuring Critical Diameter

There are three closely related ways of measuring critical diameter. In the first method, a conical charge as shown in

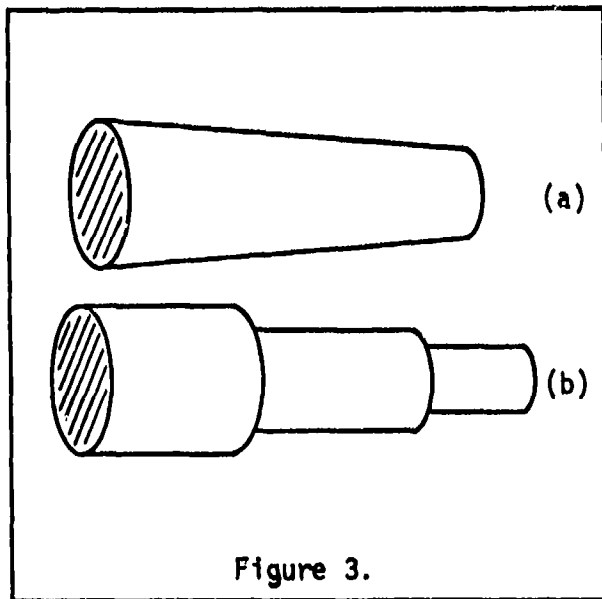


Figure 3.

Fig. 3(a) is initiated at the large face and the detonation is followed either optically or electronically until it fails. Another method is to use stepped cylinders as shown in Fig. 3(b). The detonation is initiated at the large end, and the progress of the detonation is followed through the various sections.

[†]A. W. Campbell and R. Engelke, "The Diameter Effect in High Density Heterogeneous Explosives," Sixth Symposium (International) on Detonation, ACR 221, ONR, U.S. Govt. Printing Office, Washington, DC, 1978, pp. 642-663.

In both configurations, the cone and the stepped cylinder, the detonation wave is boosted beyond the steady state since its stimulus has come from a larger diameter section. Thus, in the case of the cone, one would expect a measurement of critical diameter that is too small. So the cone angle is made as small as possible to reduce the error. In actual practice, an approximate measurement is made with a relatively large angle cone. Then when the approximate critical diameter is known, a conical section with as small an angle as possible is used to obtain a more accurate value.

In the case of the stepped cylinder, the sections must be long enough so that the detonation that is initiated in each section can achieve a steady state. If the diameter is much larger than the critical diameter, then a length to diameter ratio of about three will assure that a steady state will be reached. But if the diameter is close to the critical diameter, then l/d should be considerably larger. The Russian experimenters use an l/d of 10 to 12. There are examples of perchlorate charges that didn't fade until an l/d of eight or higher.

The third way of measuring critical diameter is, of course, to make up a number of cylindrical charges of different diameters and to map out the whole of the detonation velocity versus diameter relationship. In this method, Eq. (6) would also be used to help extrapolate to the critical diameter. But a good value of critical diameter can be obtained by simply keeping

the difference in diameter between charges small. The average of the diameters of the smallest charge that propagates steady state detonation and the largest charge that doesn't will give a very accurate value.

Continuous Wire Electronic Method of Following Detonations

The electronic method we used for following the detonation in the conical method of measuring critical diameter has other applications which we will describe in another lecture. This method, which was the inspiration of A. Amster[†], involves embedding

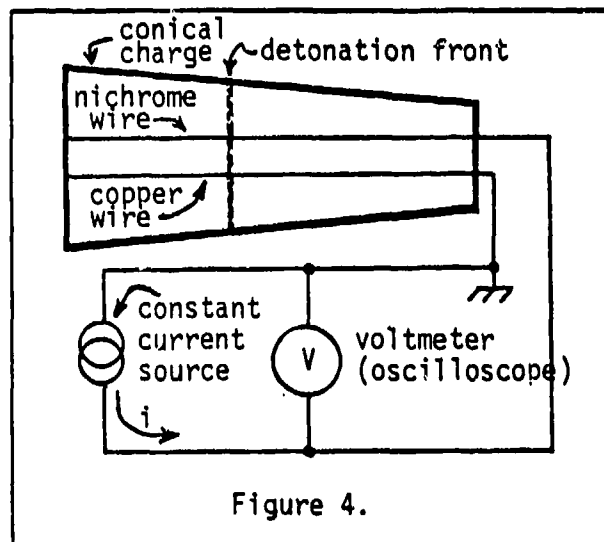


Figure 4.

continuous resistive wires in cast explosive charges as shown in Fig. 4. Amster placed a copper wire of essentially zero resistance parallel to a nichrome wire (No. 40 wire with a resistance of about 2.3 ohms/cm) of known resistance per unit

length within the cast explosive. A constant current source of about 200 mA is connected between the copper and nichrome wires and the detonation front, which has low resistance, completes the circuit. A voltmeter (oscilloscope) reads the potential difference between the copper and nichrome wires. From Ohm's Law,

$$R = \frac{V}{I} \quad (7)$$

[†]A. B. Amster, P. A. Kendall, L. J. Veillette, and B. Harrell, "Continuous Oscillographic Method for Measuring the Velocity and Conductivity of Stable and Transient Shocks in Solid Cast Explosives," *Rev. of Scientific Instruments*, 31, 188 (1960).

the resistance R of the nichrome wire remaining in the circuit is obtained. Then knowing the resistance per unit length of the nichrome wire, the distance to the detonation front can be determined.

The Bureau of Mines picked up the idea, improved on it somewhat, and published it before Amster did. The experimenters of the Bureau of Mines used Moleculoy wire with a resistance of 3.7 ohms/cm and they spiraled the wire around a central metal core to give a much improved measurement of distance. However, the large mass and size of the core (0.1" in diameter) together with the spiral wrapping produced large disturbances in the flow. Particularly in the case of liquids, reflections could produce hot spots. The 3 mil nichrome wire and the slightly thicker copper wire used by Amster also disturbed the flow, but the disturbance was negligible.

The development of the method for casting of the wires within the charges was done by Jaffe[†] and co-workers. The wires were held in a mold and the casting material poured around them. X-ray photos of the charges showed the results. In the first attempts, the wires were not molded in place very uniformly. However, with trial and error, the proper tension to place on the wires and the schedule to follow in molding was determined and good results were obtained.

[†]I. Jaffe and D. Price, "Progress Report on Adaptation of Continuous Wire Method for Measuring Transient Phenomena," NOLTR 63-136 (Sept. 1963), U.S. Naval Ordnance Laboratory, White Oak, Maryland.

From the resistance versus time record, the distance versus time data was obtained. The distance-time data is differentiated

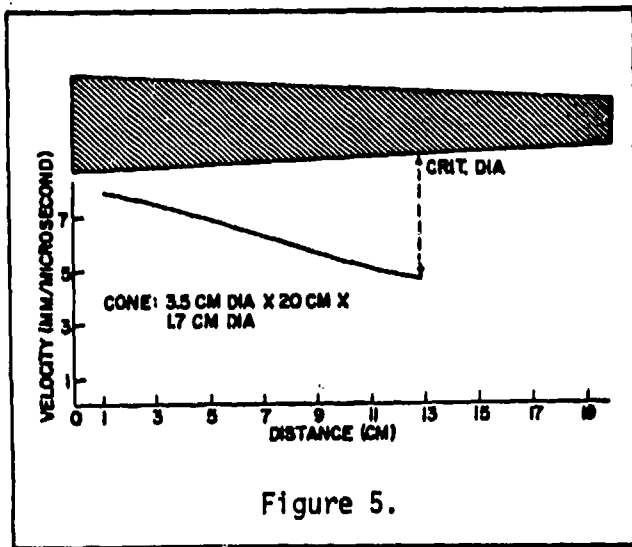


Figure 5.

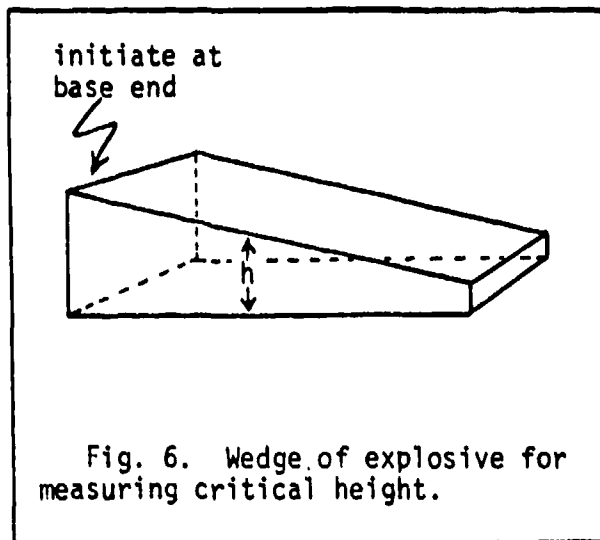
to obtain the detonation velocity. Figure 5 shows detonation velocity versus position in the cone for a particular charge. We see the decrease in detonation velocity down to the value at the critical diameter. Knowing the cone's angle, we can thus obtain the value

of the critical diameter.

The difference between critical diameter determined in this way and critical diameter determined by the use of, say, stepped cylinders is probably not any greater than the difference which will be obtained in critical diameter due to the different preparation of the same cast material at two different laboratories. Very small differences in procedures can make extraordinary differences in critical diameters. This is probably one of the reasons we have not yet a very satisfactory theoretical description of critical diameter.

Critical Height

Very sensitive and powerful explosives have very, very small critical diameters so that it is very difficult to make cylinders of sufficiently small diameter for measurement purposes.



The small cylinders will also be difficult to initiate properly. Thus, there have been attempts to measure the so-called "critical height" of a rectangular slab of explosive and to relate the critical height to critical diameter. Russian experimenters

tried this with TNT and discovered that the critical diameter was twice the value of the critical height[†]. They have used this relation for all the more sensitive explosives for which it is hard to find the critical diameter.

Relation Between Critical Height and Critical Diameter

One might expect a relation between critical height and critical diameter. However, there is nowhere any data for critical heights and critical diameters for experiments done on the same explosives in the same laboratory.

The data that is available shows no clear relation. The Los Alamos Scientific Laboratory has published a collection of data^{††} which includes critical heights determined by using

[†]A. F. Belyaev and M. K. Sukoyan, "Detonability of Some Explosives with Increase in External Pressure," *Combustion, Explosion, and Shock Waves* 3, 11-13 (1967).

^{††}M. J. Urizar, S. W. Peterson, L. C. Smith, "Detonation Sensitivity Tests," LA-7193-MS, Los Alamos Scientific Laboratory, Los Alamos, NM (April 1978).

wedges and extrapolating to zero wedge angle (Fig. 6). Like the Russians, LASL uses a bottom witness plate but unlike them, LASL has confinement on the sides as well. The following table lists critical heights extracted from the LASL report for four cast explosives and four pressed explosives for which critical diameter data is also available. The ratio of critical diameter d_c to critical height h_c is listed in the last column of the table. One sees that the ratio is not two, even for TNT. The ratio runs from 1.2 to 7.6 and it seems to make no difference whether the material is cast or pressed. If we hope to obtain a relation between critical diameter and critical height, a great deal of more careful work will have to be done.

Table 1. Critical Heights and Diameters for Various Charges

<u>Material</u>	<u>ρ_0 (g/cm³)</u>	<u>h_c (mm)</u>	<u>d_c (mm)</u>	<u>d_c/h_c</u>
50/50 Pentolite (cast)	1.70	1.39	6.7	4.8
Comp B (A) (cast)	1.71	1.42	4.3	3.0
Comp B-3 (cast)	1.73	0.82	6.2	7.6
75/25 Cyclotol (cast)	1.75	1.51	6.0-8.0	4.0-5.3
DATB (pressed)	1.72	0.73	5.3	7.3
PBX-9404 (pressed)	1.82	0.46	1.2	2.6
Comp A-3 (pressed)	1.63	0.56	<2.2	<3.9
TNT (pressed)	1.63	2.16	2.6	1.2

The next lecture will start with a discussion of "detonability curves." These are plots of critical diameter versus density or porosity.

NSWC MP 81-399
LECTURE ON DETONATION PHYSICS
LECTURE #5 - 17 NOVEMBER 1980
DETONABILITY CURVES AND CLASSIFICATION OF EXPLOSIVES
by
DONNA PRICE
Notes by Frank J. Zerilli

Introduction

The existence of a critical (failure) diameter for propagation is not unique to detonation. There is a similar failure diameter for the propagation of steady state deflagration and another failure diameter, not as well defined, for propagation of a metastable disturbance called low velocity detonation.

The reason for the existence of a failure diameter is the same in all three cases. It is that energy for propagation gained through exothermic reactions is exceeded by energy loss through dissipation mechanisms. The actual energy loss mechanisms are different in the three cases.

Factors Affecting Critical Diameter

The critical diameter for propagation of detonation is a function of many variables, and more can be named than can be measured. The variables known to affect critical diameter are: chemical composition, temperature, pressure, porosity, permeability, available reactive surface area, critical initiating pressure, and form of the material. Similarly, the critical initiating pressure can be considered to be a function of the critical diameter and all the other variables in our list.

Detonability Curves

Detonability curves are relations between critical parameters. We will use the term "detonability curve" to refer to relations plotted in the diameter versus

charge loading density plane. We will express loading density as a percent of the TMD (Theoretical Maximum Density) so that we can compare materials of different compositions. Sometimes the percent porosity ($100\% - \%TMD$) is used instead of $\%TMD$.

The most familiar detonability curve is that for pressed TNT of 200 micron initial particle size, shown in Fig. 1. The curve is a "limit line", that is,

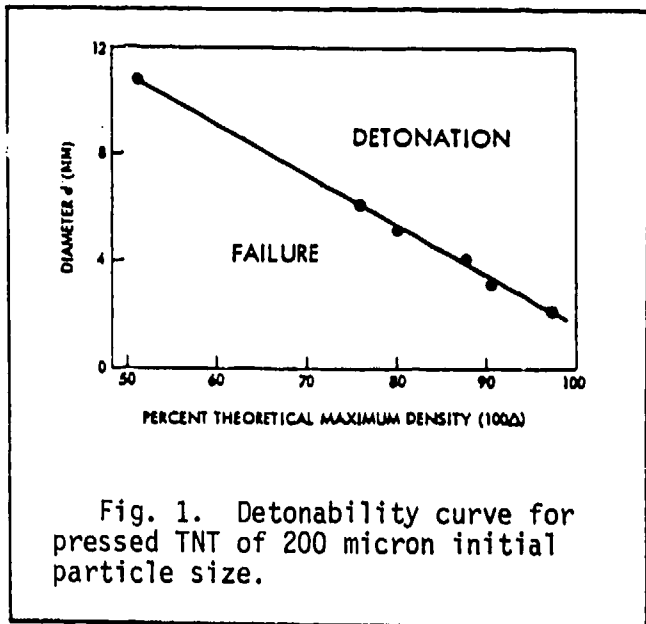


Fig. 1. Detonability curve for pressed TNT of 200 micron initial particle size.

it marks the threshold between the region where detonation can be achieved (above the line) and the region in which detonation cannot be achieved (below the line). Thus, for a fixed loading density, there exists a critical diameter, above which detonation can be achieved, and below which the detonation must fail. On the other hand, if we fix the diameter, we find that there is a critical loading

density, above which detonation can be achieved, and below which the charge must fail. Thus, we can speak of either a critical density or a critical diameter depending on which of the two parameters we wish to hold fixed.

TNT is typical of a group of materials which we will call Group 1. In these materials, the critical diameter decreases as the loading density increases. The more nearly voidless the materials, the smaller is the diameter of charges that will achieve steady state detonation. This means that the reaction zone length becomes shorter and shorter, with less and less separation between the von Neumann shock and the C-J plane as porosity decreases.

Figure 2 shows a detonability curve for ammonium perchlorate which is a typical member of the Group 2 materials. In this case, we see the opposite

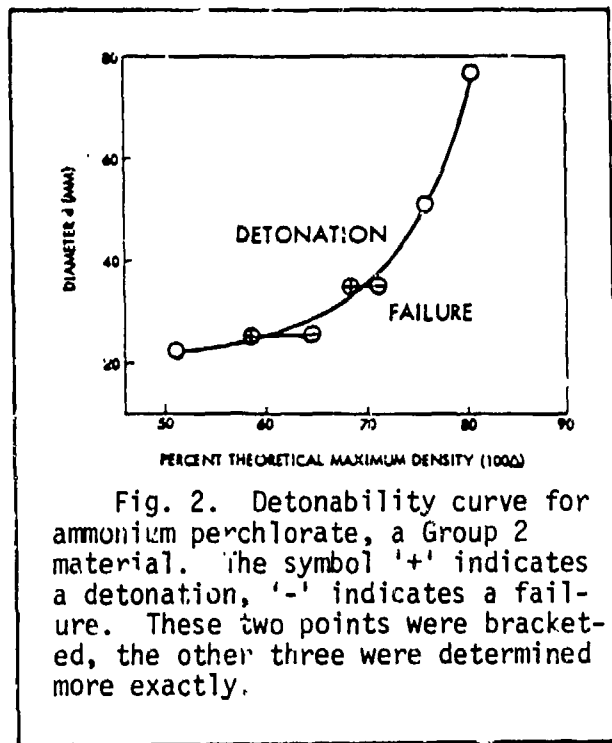


Fig. 2. Detonability curve for ammonium perchlorate, a Group 2 material. The symbol '+' indicates a detonation, '-' indicates a failure. These two points were bracketed, the other three were determined more exactly.

trend -- the critical diameter (and, therefore, the reaction zone length) increases as the material becomes denser (less porous). Thus, AP (Ammonium Perchlorate) behaves less ideally as we increase the loading density and more ideally as we decrease the loading density. So AP exhibits a detonability trend opposite to that of TNT.

When this was first discovered, it was thought that this was an unambiguous classification and that all

other materials would probably fall into one class or the other. It didn't turn out

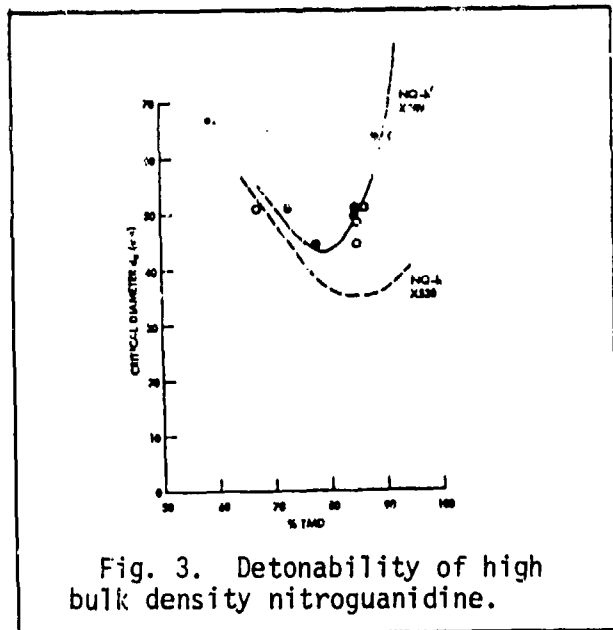


Fig. 3. Detonability of high bulk density nitroguanidine.

quite that way. It was known that nitroguanidine could be "dead pressed", that is, it could be pressed to a high density at which it would not detonate. Thus, it was thought that nitroguanidine belonged to Class 2 like ammonium perchlorate. However, this is not so. Figure 3 shows the detonability curve for high bulk density nitroguanidine (NQ-h). The curve has a minimum critical diameter at a certain value of the loading density.

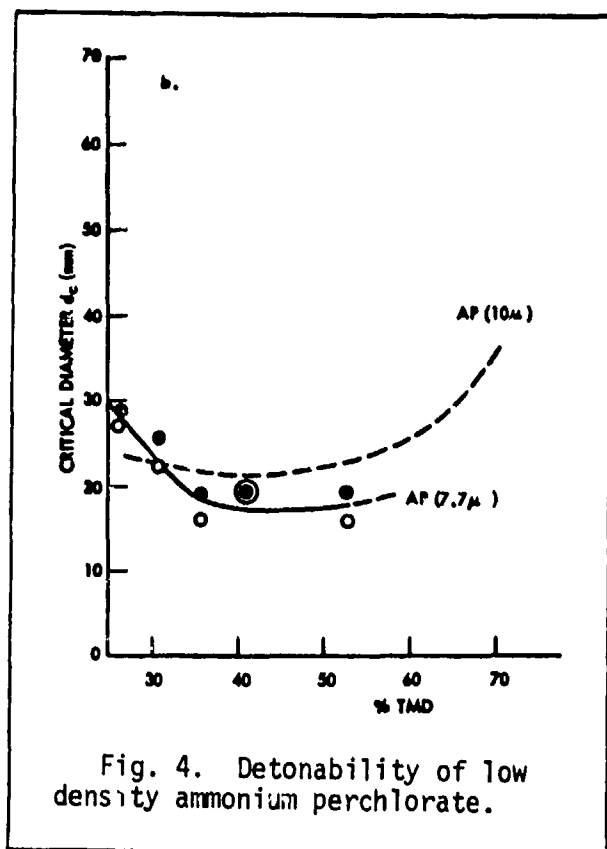


Fig. 4. Detonability of low density ammonium perchlorate.

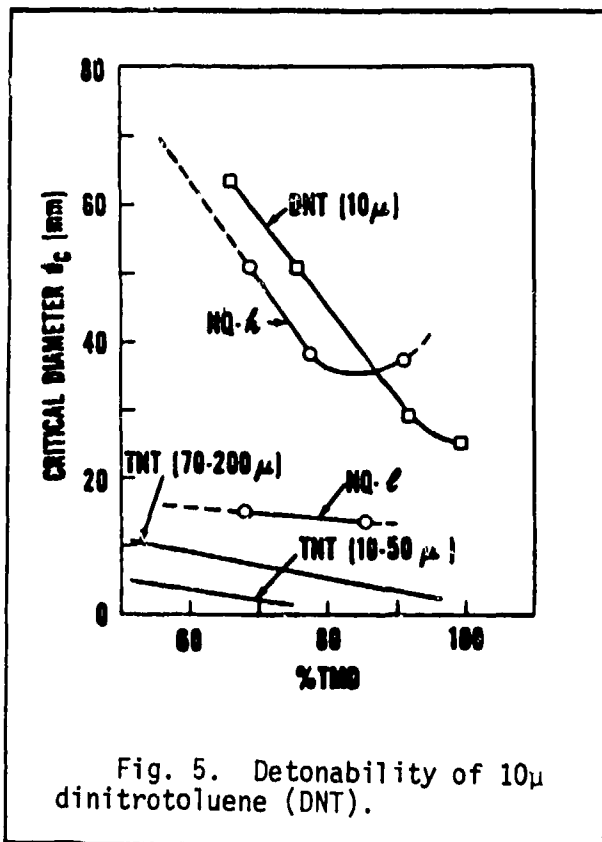


Fig. 5. Detonability of 10 μ dinitrotoluene (DNT).

At densities lower than this value, NQ-h behaves as a Group 1 material and, at higher densities, it behaves as a Group 2 material. Similarly, as Fig. 4 shows, ammonium perchlorate behaves as a Group 1 material if it is made sufficiently porous.

Thus, the general curve is U-shaped and there is no sharp division into distinct groups. This was not discovered in the case of nitroguanidine for a long time, since the commercially manufactured material is a low bulk density material consisting of small needles and is very difficult to compact to, say, 80% TMD. Similarly, it is difficult to obtain ammonium perchlorate with 70% or greater porosity, so its Group 1 behavior was not easy to discover either. In summary, nitroguanidine is chiefly a Group 1 material, but at high density, it behaves as a Group 2 material. Ammonium perchlorate is chiefly a Group 2 material, but at very low density, behaves as a Group 1 material.

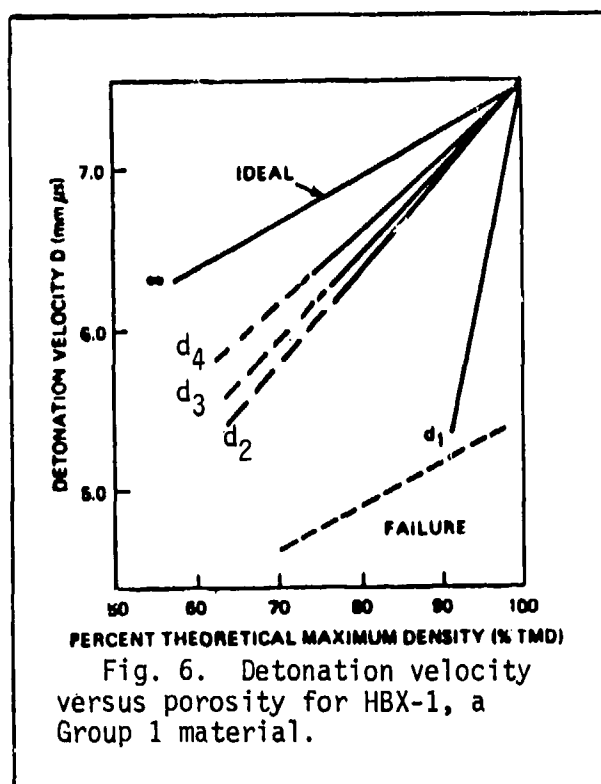
Another material that shows both Group 1 and Group 2 characteristics is dinitrotoluene (DNT). In the Russian literature, the statement was made that

dinitroaromatics behaved, in their failure phenomena, very much like ammonium nitrate which is definitely a Group 2 material. Thus, DNT, which is easy to obtain, was expected to be a Group 2 material. In fact, as seen in Fig. 5, 10 μ DNT shows chiefly Group 1 behavior. However, it appears that the minimum of the detonability curve is being approached at close to 100% TMD. This approach to Group 2 behavior was later confirmed by the discovery of a dead press region for DNT.

So, although the general curve is U-shaped, most materials will have a behavior that falls mostly in one group or the other in the normal experimental ranges of loading density.

Detonation Velocity-Loading Density Curves

Another useful type of curve is a plot of detonation velocity versus loading



density for several different charge diameters. The failure behavior of a material (that is, whether it is Group 1 or Group 2) has a marked effect on the pattern formed by these detonation velocity - density - diameter curves; their patterns can be used for classification as well as the detonability curves. This is illustrated in Figs. 6 and 7. Figure 6 shows data obtained by Coleburn and Roslund[†] for HBX-1, a typical Group 1 material. Note that the detonation velocity is not only a function of the material

composition and of the density but it is also a function of the diameter of the charge. For a given diameter, the detonation velocity versus density relation is a straight

[†]L. A. Roslund and N. L. Coleburn, "Hydrodynamic Behavior and Equation of State of Detonation Products Below the Chapman-Jouguet State," Fifth Symposium (International) on Detonation, ONR Report ACR-184, U. S. Govt. Printing Office, Washington, D. C. 1972, p. 523.

line starting from the 100% TMD point on the infinite diameter (or ideal) curve. The slopes of the lines increase as the diameter of the charge decreases. In fact, the slopes are linear functions of the reciprocal of the diameter. The behavior is most ideal near 100% TMD. As the porosity increases, the behavior becomes less ideal, departing further and further from the infinite diameter curve.

In Fig. 6, actual data are indicated by unbroken lines while the dashed lines are extrapolations. The only justification for the linear extrapolation comes from the only other explosive for which as detailed data as this exists -- TNT. There is a set of data in the Russian literature[†] and more recent data which doesn't go to as small diameters from Los Alamos^{††}. In the data for TNT, all the lines are straight and the data were taken all the way to the failure point. For HBX-1, only one critical diameter was determined and that locates one point on the failure curve -- the rest of the failure curve is estimated, and indicated by a dashed line in Fig. 6. But the smallest diameter TNT that was tested started out as a straight line and

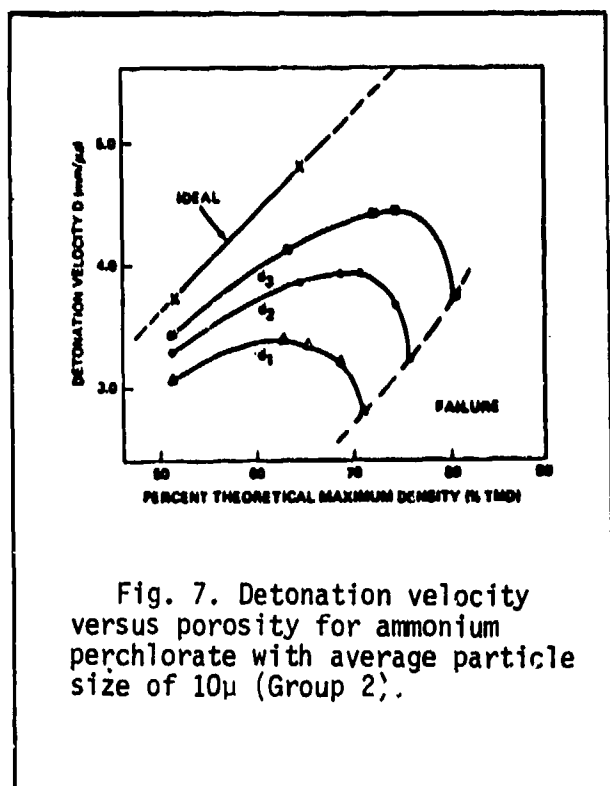


Fig. 7. Detonation velocity versus porosity for ammonium perchlorate with average particle size of 10μ (Group 2).

then showed a curved path to the failure point. Thus, the extrapolations shown as linear probably should be curved, but such curvature cannot be resolved on some of the more rapidly reacting materials such as HBX-1.

Figure 7 shows the pattern for 10μ particle size ammonium perchlorate, a typical Group 2 material. In contrast to Group 1 materials, the curves fan out from a center at somewhere between 30% and 40% TMD and are nearly linear between about 50% and 60% TMD. They fan out with slopes which decrease as the diameter gets smaller.

[†] L. N. Stesik and L. N. Akimova, "An Indirect Method of Estimating Reaction Zone Width of a Detonation Wave", *Russ. J. Phys. Chem.* 33, 148-151 (1959).

^{††} M. J. Urizar, E. James, Jr. and L. C. Smith, *Phys. Fluids* 4 (2), 262 (1961).

Group 2 materials also show a much greater tendency for the reaction to fade over a long distance than Group 1 materials. The Group 1 materials generally quench sharply. A very small change in diameter leads to either a go or no go (this is what makes possible the measurement of critical diameter by the conical method).

The Reason for Two Groups

Why do explosive materials fall into two classes? One possible reason is that two types of reaction are possible with different proportions of the two types of reaction occurring in a given material under given conditions. One type of reaction is a homogeneous reaction (especially if we have a single pure material). The homogeneous reaction is a bulk reaction. That is, the entire bulk of material in the reaction zone heats up uniformly and undergoes what we may call a "thermal" explosion. At the other extreme is the heterogeneous reaction (occurring both in pure materials and in mixtures). The heterogeneous reaction is a hot spot reaction. That is, the reaction is initially concentrated in local hot spots and not throughout the mass of the material.

It is generally agreed that heterogeneous or hot spot reactions are the important factor in the initiation of explosives to a shock-to-detonation transition -- both for Group 1 and Group 2 materials. But in Group 1 materials, after the transition to steady state has occurred, the detonation propagates with very high pressures compared to the normal initiating pressure[†]. In this case, it is conceivable that the entire bulk of material in the reaction zone is heated by a combination of compression, shear, and friction. If so, a homogeneous reaction may predominate during the propagation of steady state detonation.

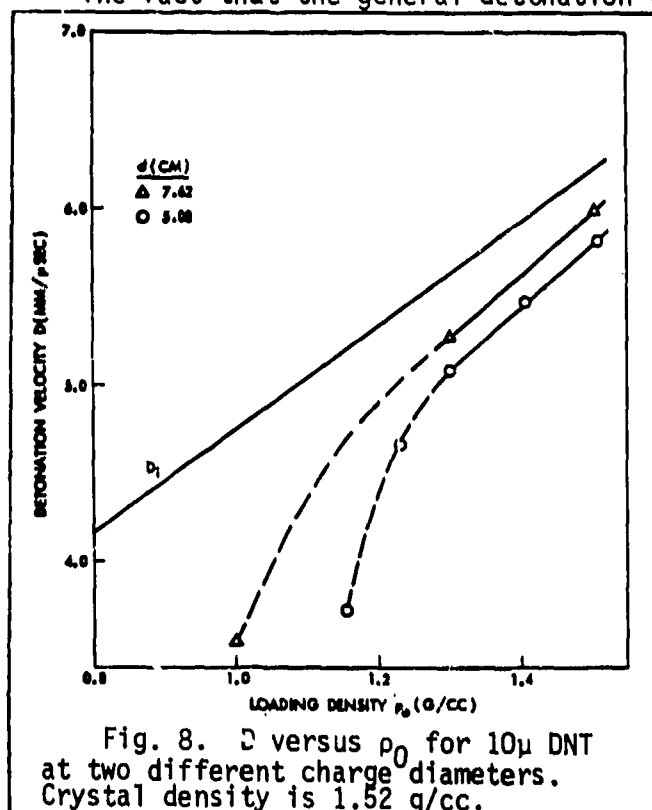
In the case of Group 2 materials, even in steady state detonation, there is still a great dependence on surface reactions. The more these materials are compressed,

[†]In the case of homogeneous materials at nearly voidless density (the least sensitive of explosive materials), the C-J pressure is roughly three times the critical initiating pressure and the von Neumann pressure is about 25 to 30 percent higher than the C-J pressure.

the less surface is available for reaction, and so they become less ideal. Thus homogeneous reactions do not dominate in the case of Group 2 materials. The fact that they tend to fail very slowly also indicates a surface reaction with a dying out of the flame rather than a bulk reaction. Abrupt failure, on the other hand, indicates a drop below the critical temperature necessary for a homogeneous reaction.

Detonation Velocity - Density Curves for Group 1 Materials, DNT and Nitroguanidine

The fact that the general detonation velocity versus density plot is curved rather



than linear as the failure line is approached is illustrated by the curves shown in Fig. 8 for DNT. The detonation velocity - loading density curves are quite linear at loading densities near the TMD but become non-linear at lower densities, even those well above the failure point. Nitroguanidine also shows the same general detonation velocity pattern.

There are two different types of nitroguanidine. One is a low bulk density material which consists of long thin needles of about 5 to 10μ diameter and

60 to 100μ length. The pour density[†] of this material is about 0.2 g/cm³, and it is very difficult to compress into a charge with any sort of structural strength. The other type of nitroguanidine is a high bulk density material which is made^{††} by precipitating the nitroguanidine in the presence of a small amount (1% or less) of a colloidal agent such as methyl cellulose. This produces a material which consists of chunky cylinders about 20μ long with a length to diameter ratio of about four. This

[†]Pour density is the density of powdered material after simply being "poured" into a container.

^{††}At the Naval Ordnance Station, Indian Head, Maryland

material is much easier to compress to high densities.

Figure 9 shows the detonation velocity versus loading density curves for the high bulk density nitroguanidine (NQ-h) at several different charge diameters.[†]

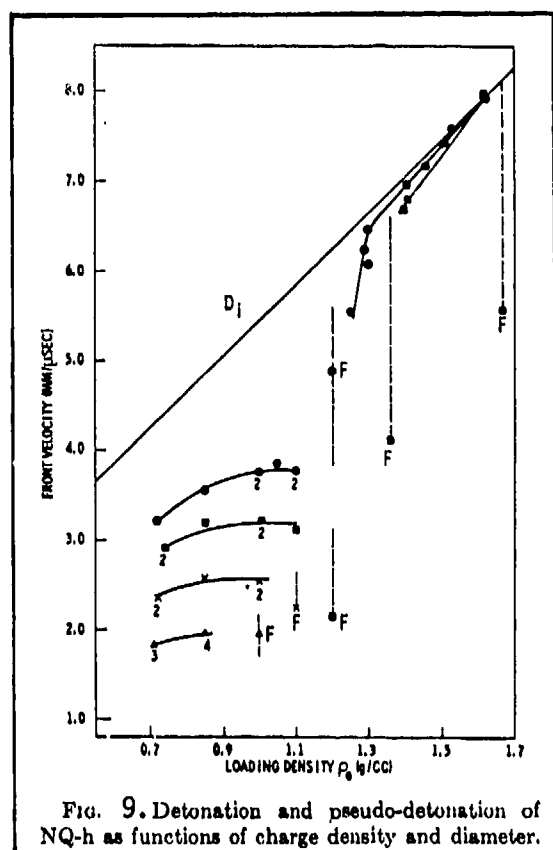


FIG. 9. Detonation and pseudo-detonation of NQ-h as functions of charge density and diameter.

The "infinite diameter" or ideal curve is the one already established using low bulk density nitroguanidine. There is no difference between the high and low bulk density nitroguanidine as far as the ideal detonation velocity - loading density curve is concerned.

Two diameters in the detonable range are shown. The smaller diameter charges, 3.8 cm, fail at both the low density end (1.36 g/cm^3) and at the high density end (1.67 g/cm^3). This indicates that at 3.8 cm diameter, we are near the valley (minimum) of the

U-shaped detonability curve for high bulk density nitroguanidine (Fig. 3). The larger diameter, 5 cm, fails at a low end density of 1.2 g/cm^3 . Except for the dead pressing effect for 3.8 cm diameter charges, both of these curves are typical of Group 1 materials. The curves are straight lines, fanning out from the upper end of the ideal curve, with smaller diameter charges having greater slopes. Just as for dinitrotoluene, the straight lines start to curve as the failure point is approached.

[†]Donna Price and A. R. Clairmont, Jr., "Explosive Behavior of Nitroguanidine", Twelfth Symposium (International) on Combustion, 1969, pp. 761-770.

Low Velocity or Pseudo-Detonation

Figure 9 also illustrates the phenomenon of low velocity detonation (LVD). The 5 cm diameter charges fail at 1.2 g/cm^3 , but when we go to lower densities we find disturbances that propagate at a constant, but much lower, velocity. The same occurs for the 3.8 cm diameter charges and even for two smaller diameters which are subcritical and hence don't show normal detonations at all. At these loading densities all the diameters are sub-critical. The type of disturbance observed in this density range is referred to as a low velocity[†] (or pseudo-) detonation.

It is possible to observe low velocity detonation also in super-critical diameter charges, if an inadequately strong booster is used. In this case, LVD often transits to steady state detonation provided it propagates far enough.

The phenomenon of low velocity detonation is only seen in granular charges when the material is very coarse. It has been seen in very coarse tetryl and it has been seen in a very small density range in large particle size RDX (as well as in NQ-H). It is also seen in non-granular charges which are gels^{††} -- nitrocellulose colloided with nitroglycerine exhibits this type of low velocity (but supersonic) disturbance. And it is also seen in many liquid explosives.

The mechanism of propagation of low velocity detonation in liquids is fairly well understood. It is not well understood in the case of coarse solids, although it is fairly certain that only a partial reaction occurs because, in some cases, unburned, unreacted material remains after the disturbance has passed. It seems to be a partial, surface reaction and the shock wave probably produces an ignition wave. The light which is detected could come from a series of hot spots (ignition spots) along the path of the shock wave.

[†]Although the velocity is still supersonic.

^{††}A gel is a dispersed system such as common jelly in which one component provides a structural framework with chain crosslinking for rigidity and the other components fill the space between structural units.

The low velocity detonation releases far less energy at the propagation front than a steady state detonation in the same material. Thus a cellulose acetate "flasher" must be used to enhance the luminosity in order to measure the velocity using a streak camera. The flasher is a wrapping which holds some air next to the charge. The shock produced in the air by the wave front makes the air luminous enough to produce a good streak record. A sensitive explosive is also used at the end of the test charge to insure that the reaction has indeed been followed. A typical streak record will then show a not too bright line with a change in slope when the LVD initiates the explosive witness at the end of the charge.

Detonation Velocity - Loading Density Curves for Group 2 Materials

We will examine some Group 2 materials. Figure 10 shows detonation velocity versus loading density[†] for several diameters of charges composed of 95% ammonium

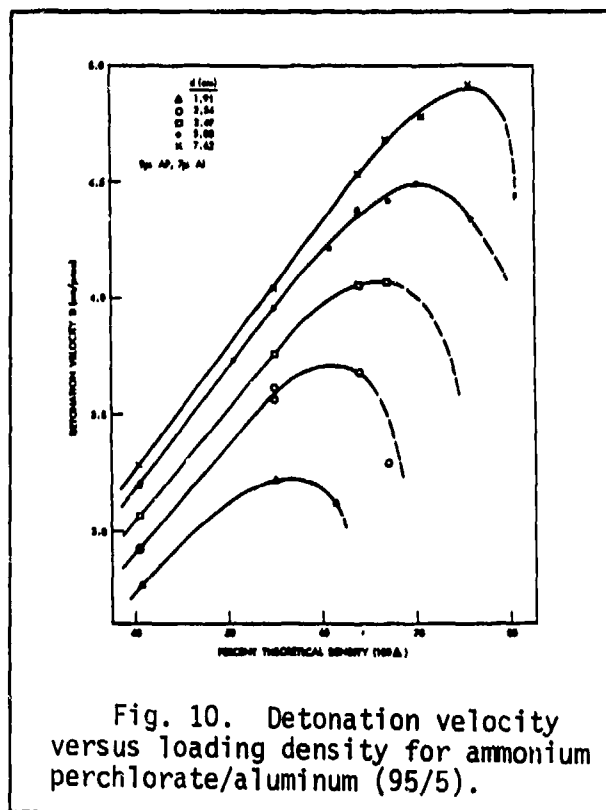


Fig. 10. Detonation velocity versus loading density for ammonium perchlorate/aluminum (95/5).

perchlorate and 5% aluminum with an AP particle size of 9 μ and aluminum particle size of 7 μ . This shows the same pattern as pure ammonium perchlorate.

Figure 11 shows detonation velocity versus loading density for hydrazine mononitrate.^{††} The data were taken in the late 40's and it was the first time anyone at NOL had seen a detonation velocity versus loading density curve with a maximum in it. The data were reported at the First Detonation Symposium

[†]D. Price, A. R. Clairmont, Jr. and J. O. Erkman, *Combust. Flame* 20, 389 (1973).

^{††}D. Price, T. P. Liddiard, Jr., and R. D. Drosd, "The Detonation Behavior of Hydrazine Mononitrate," U. S. Naval Ordnance Laboratory Report, NOLTR 66-31, 1966.

in 1951 and were then ignored until ammonium perchlorate and similar materials began to be studied.

Several charge diameters were studied from 1.27 cm up to 6.35 cm. The largest

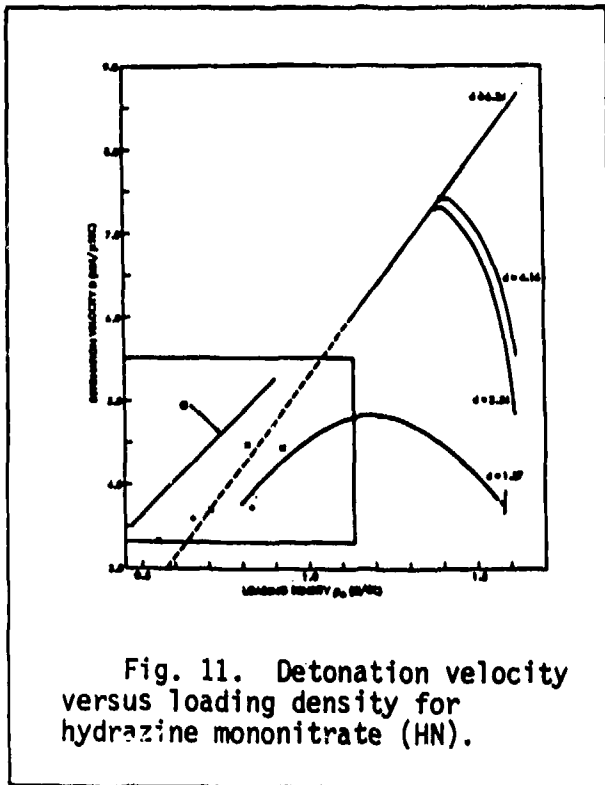


Fig. 11. Detonation velocity versus loading density for hydrazine mononitrate (HN).

diameter had a behavior almost exactly on the ideal curve. However, a difficulty appeared: the data at high densities fell on a straight line and the data at low densities fell on a straight line, but they didn't join up! The resolution of the difficulty is that hydrazine mononitrate is somewhat hygroscopic (though not as much so as ammonium nitrate) and it absorbs water. The charges were prepared and kept in dessicators, but nevertheless they had to be removed from the dessicator to be set up for firing. The crosses and pluses

in Fig. 11 in the lower density region are data obtained on very small diameter charges which were prepared in glass tubes and kept in the dessicator. These could be brought out and fired more rapidly. These data are scattered around the line extrapolated from the high density data. This supports the suggestion that water absorption was responsible for the initial discontinuity. In any case, the pattern is clearly a Group 2 pattern.

Explosives Classification Summary

In summary, Group 1 contains TNT, all of the more common, energetic explosives, all of their mixtures, and their mixtures with inerts such as wax. It may be possible to press these explosives above TMD and then find Group 2 behavior, but that has not been done as yet. In an intermediate group, we have 10 μ particle size dinitrotoluene

and high bulk density nitroguanidine. These show chiefly Group 1 behavior, but showed Group 2 behavior and the dead press phenomenon at very high densities. Finally, Group 2 contains ammonium perchlorate, ammonium nitrate, their mixtures with fuels[†], and hydrazine mononitrate. According to the Russian literature, hydrazonium azide and ammonium azide also belong to Group 2. That and the fact that lead azide dead presses indicate that lead azide is probably in Group 2 also. At this point there does not seem to exist an organic explosive which belongs entirely in Group 2.

There are not many explosives which have been examined over a large range of loading density and charge diameter. Table 1 is a summary of data for four explosives which have been studied fairly thoroughly. For each explosive (AP, NQ-h, DNT-10 μ , and TNT), the table gives the loading density (expressed in % TMD) at which the minimum in the detonability curve occurs, the loading density (in % TMD) at which dead pressing occurs, impact test ignitability (in cm), and chemical energy (cal/g). Note that the minimum in the detonability curve and the dead press location show the same trend as that

Table 1. Behavior of Four Explosives

<u>Material</u>	<u>Location of Detonability Curve Minimum (% TMD)</u>	<u>Location of Dead Press* (% TMD)</u>	<u>Impact Ignitability (cm)</u>	<u>Chemical Energy (cal/g)</u>
AP(10 μ)	44	80	100-133	405
NQ-h	84	92	>320	921
DNT (10 μ)	~100	~99	>320	1151
TNT	>100	>100	160	1297

*% TMD at which steady state detonation cannot be initiated in the largest diameter charge tested (depends on charge diameter).

of the chemical energy - these points occur at higher % TMD for the more energetic materials. The impact test ignitability, however, does not seem to correlate. The

[†]For example, wax, aluminum, fuel oil. Amatols are mixtures of ammonium nitrate with TNT -- the TNT is a fuel in this case, since TNT is oxygen deficient.

chemical energy of 405 cal/g for ammonium perchlorate (AP) is typical of most Group 2 high explosives (HE) including the azides. The value of 1300 cal/g for TNT is at the lower end of the range for Group 1 high explosives. Nitroguanidine and DNT both have intermediate chemical energies and detonability behavior.

Table 1 is meant to suggest areas of study. It is not meant to suggest that one can rely on chemical energy as the sole guide to classification. For example, hydrazine mononitrate with a chemical energy of 900 cal/g has Group 2 behavior and so is an obvious exception to the trend shown in the table.

Particle Size as a Critical Parameter

Another critical parameter is initial particle size in pressed, granular explosives. The effect of particle size on typical Group 1 and Group 2 explosives is

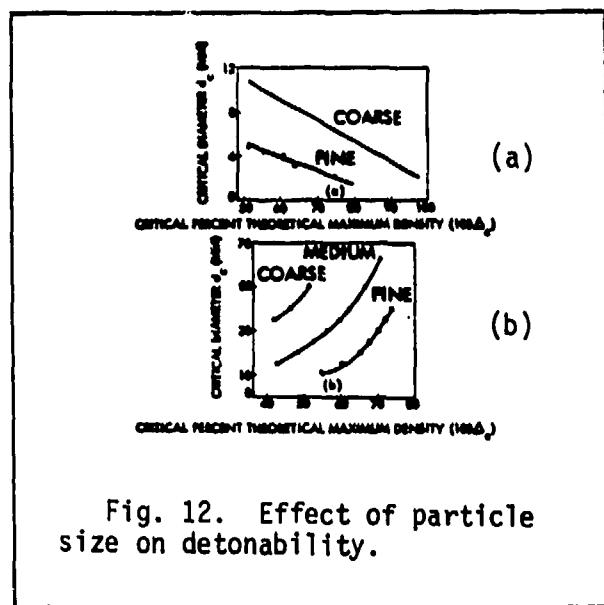


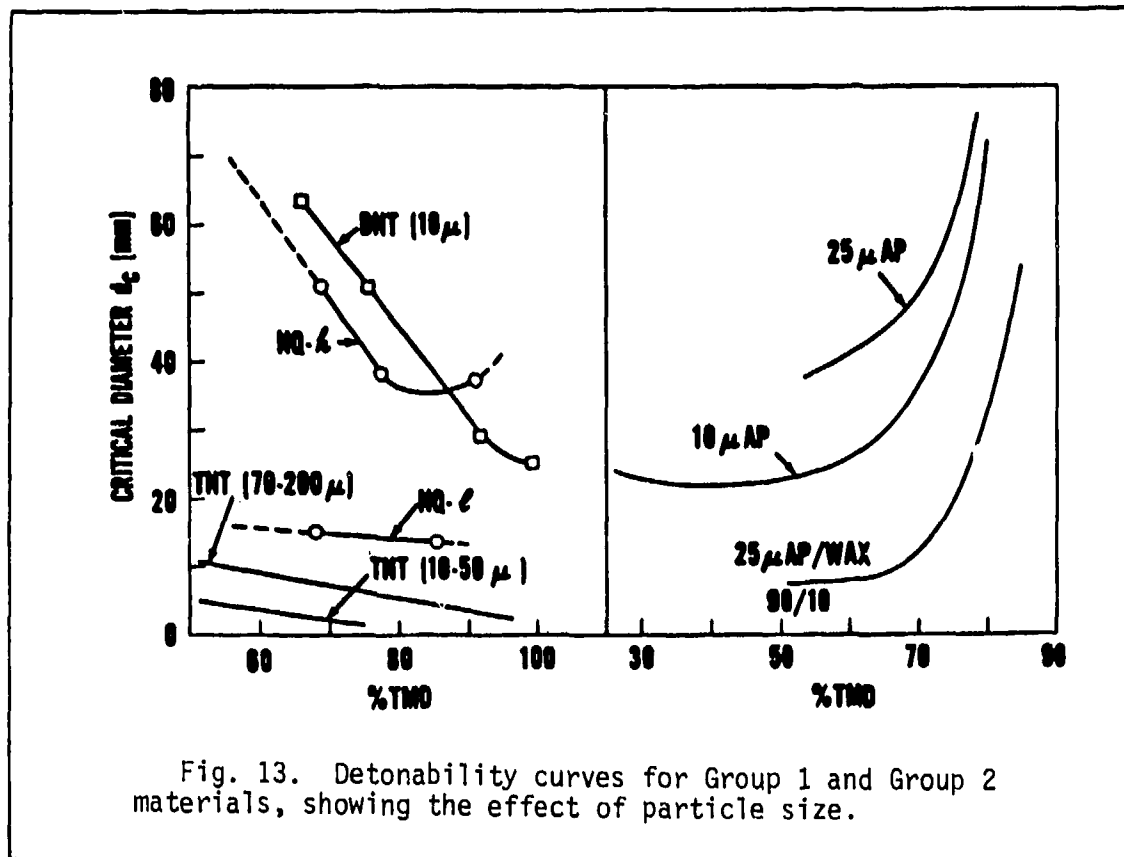
Fig. 12. Effect of particle size on detonability.

shown in Fig. 12. Figure 12a shows detonability curves for 200 μ particle size TNT and for 10 to 50 μ particle size TNT. Figure 12b shows the detonability curves for the mixture of 88% ammonium nitrate and 12% peat moss for different particle sizes.

This is a mixture consisting of a fuel (peat moss) and an oxidizer (ammonium nitrate). A more common mixture is

ammonium nitrate and fuel oil. Peat moss was used here since it can be ground to varying particle sizes which would not be possible with fuel oil. Figure 12 illustrates the same effect of particle size for both groups -- the finer the material, the lower the value of the critical diameter at any given loading density.

Figure 13, below, shows the same data that was displayed in Fig. 12a for TNT, but on a different scale. Also shown are the detonability curves for 25 μ ammonium perchlorate (AP) and 10 μ ammonium perchlorate. We should note that, in all cases, when we speak of particle size, we are referring to the initial particle



size of the material before it is compacted to a given loading density. At high compactions, the particle sizes are different from the initial size; nevertheless, the smaller the initial particle size, the smaller the failure diameter of the material.

It is clear from Fig. 13, that, for both Group 1 and Group 2 materials, if we fix the loading density, then there is a relation between critical diameter and particle size -- the smaller the particle size, the smaller the critical diameter.

Thus, just as in the case of the diameter versus loading density plane, there should be a threshold curve in the diameter versus particle size plane. The only such

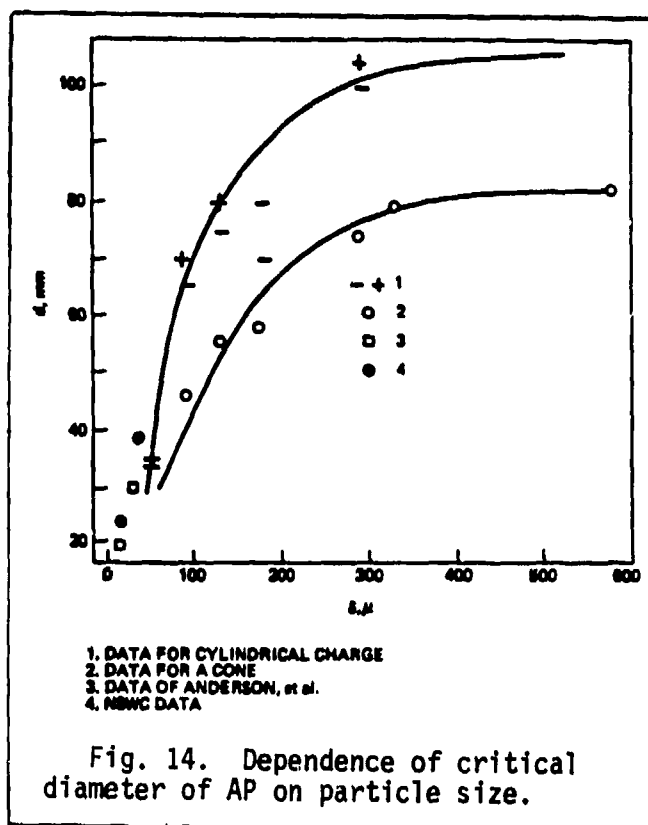


Fig. 14. Dependence of critical diameter of AP on particle size.

experimental curve is for ammonium perchlorate and comes from the Russian literature.[†] Figure 14 shows this "detonability curve" determined on cylinders and cones. In both cases the loading density was 1.1 g/cm^3 or 56.4% TMD. The symbol "plus" in the figure means a cylinder that detonated, "minus" means a cylinder that failed. The open circles are data obtained from conical charges. There is a difference in the results between cones and cylinders and this difference is fairly large in the case of AP and, in

many cases, with other low power explosives. In any case, the data are consistent with the measurements of Anderson^{††} and with the NSWC measurements for 10μ and 25μ AP. Thus, we can speak of a critical particle size for a given loading density or charge diameter.

The next lecture will finish the discussion of critical parameters for propagation and begin a discussion of the critical pressure for initiating detonation.

[†]V. A. Gor'kov and R. Kh. Kurbangalina, "Some Data Concerning the Detonation Ability of Ammonium Perchlorate," *Combust., Explosions, and Shock Waves*, 2 (2), 12 (1966).

^{††}W. H. Anderson and R. E. Pesante, *Eight Symposium (International) on Combustion*, Williams & Wilkins, Baltimore (1962): pp 705-710

Lectures on Detonation Physics

Lecture #6 - 1 December 1980

Factors Which Affect Critical Parameters

by

DONNA PRICE

Notes by Frank J. Zerilli

Effect of Particle Size -- Continued

In the preceding lecture, the effect of initial particle size of an explosive on the critical conditions for propagating steady state detonation was discussed in some detail. It should be emphasized that initial particle size (as well as initial temperature, initial pressure, and any other variable which may affect detonability) must be specified in giving a detonability curve since initial particle size has a great effect on the curve. Figure 1

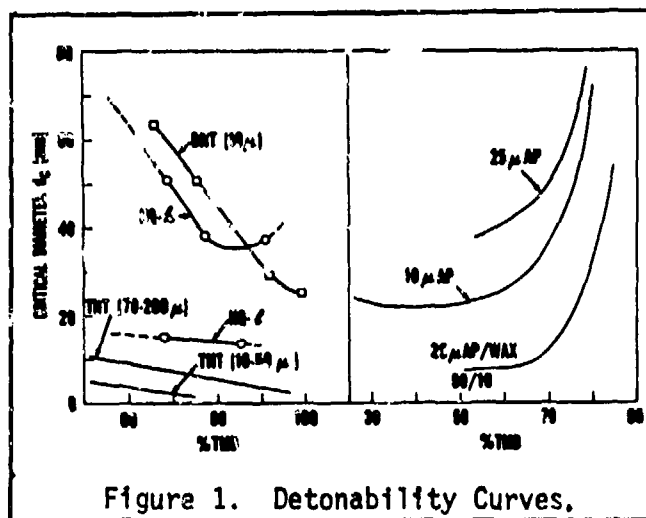


Figure 1. Detonability Curves.

shows detonability curves for ammonium perchlorate and TNT for particle sizes covering a fairly large range. Decreasing the particle size increases the detonability, that is, decreases the critical diameter.

Russian investigators reported that DNT has Group 2

behavior. It is possible that DNT with a coarser particle size (commercial samples of DNT come with particle sizes of 400μ and more) would show Group 2 behavior if the effect of particle size on its detonability curve is similar to the effect of particle size on the detonability curve of ammonium perchlorate as shown in Figure 1. With increased particle size, the U-shaped detona-

ability curve seems to be pushed up and to the left, thus exposing a greater range of Group 2 behavior.

Melt-Cast Materials

Casting is more an art than science. The method of casting and cooling will determine the particle size of the solid charge and thus its detonability. Typically, cast materials are TNT-based. For TNT and TNT-based materials, the more rapidly the melt is solidified, the smaller the particle (crystal) size, and so the smaller the critical diameter (greater detonability) of the material.

One of the earliest quantitative studies of the effect of casting procedure on particle size was made by Cybulski[†] and co-workers. They made castings of TNT with three different procedures: poured clear, creamed, and creamed plus ten percent fine solids. Table 1 summarizes the results.

Table 1. Effect of casting method on detonability of TNT.

<u>casting method</u>	<u>critical diameter d_c (cm)</u>
poured clear	$3.17 < d_c$
creamed	$2.20 < d_c < 2.54$
creamed plus 10% fines	$1.26 < d_c < 1.66$

In the first method, the TNT was poured clear, that is, the liquid was above the melting point or very slightly supercooled (melting point about 81°C) when it was poured. The casting was then maintained at room temperature, thus cooling slowly. Since the cooling is from the outside in, the cooling rate and temperature gradient will be different for different sized castings.

[†]W. B. Cybulski, W. Payman, and D. W. Woodhead, Proc. Roy. Soc. (London) 197A, 51-72 (1949).

Also, within a given casting, the cooling rate varies with distance from the surface of the casting. This is one factor which makes it difficult to reproduce melt-castings. In the second method of casting, the melt was creamed, that is, it was stirred until it turned milky due to the formation of small crystals. At this point, the melt was poured into the mold. In the final casting procedure, the melt was creamed and fine solid particles of TNT (those passing through a #300 sieve) were added to the melt in a proportion of 10% by weight.

The three methods produced castings with, respectively, finer and finer particle sizes, and, as seen in Table 1, smaller and smaller critical diameters. Procedure number one (poured clear) gives the largest crystals and the critical diameter is the largest. Procedure two, creamed cast, produced castings with a critical diameter between 2.2 and 2.5 cm. This is the method normally used at NSWC to prepare creamed cast TNT and the critical diameter agrees well with the NSWC measured value of 2.7 cm. The last method produces the smallest crystals and the smallest critical diameter.[†]

Effect of Temperature Cycling on Cast TNT

Russian investigators^{††} studied the effect of temperature cycling on cast TNT charges of two different crystal sizes -- fine crystals and coarse crystals. The results are summarized in Table 2. Since there is not much room to go to higher temperatures without melting, the castings were cooled to 77°K. Although the critical diameter at room temperature, as expected, is smaller for the finer material, when the materials were cooled to 77°K,

[†]Cybulski referred to the third type of casting as creamed cast TNT, leading to some confusion since the second method of preparation is referred to as creamed cast at NSWC.

^{††}V. V. Kravtsov and V. V. Silvestrov, "Effect of Low Temperature on Detonation Parameters of Cast Trotyl," *Combustion, Explosions and Shock Waves*, 15, 387-390 (1979).

Table 2. Effect of temperature cycling on the detonability of cast TNT.

Charge Material Crystal Size	Density (at 290 ⁰ K)	Critical Diameter (at 290 ⁰ K)	Critical Diameter (cooled to 77.4 ⁰ K)	Critical Diameter (slowly heated to 290 ⁰ K)	Critical Diameter (after a second cycle)
fine	1.62 g/cm ³	15.0 mm	9.0 mm	7.0 mm	6.5 mm
coarse	1.60 g/cm ³	27.5 mm	9.0 mm	9.0 mm	6.5 mm

the critical diameters not only became smaller, but also became identical. When slowly heated back to room temperature, there was no change for the coarse material and a slight change for the fine material. After a second complete temperature cycle, both the fine and coarse materials had the same critical diameter. The Russian investigators reported that there was no visible change in the structure of the materials due to the temperature cycling, but they did not say how the structure was examined (they did report a change of about ½% in density, however). In any case, with any casting, even with plastic binders, one must always consider the possibility of a structural change which is not very obvious, but which may affect the characteristics of the explosive.

Effect of Temperature on Detonability

It is to be expected that higher initial temperature would increase detonability since higher temperature would increase the reaction rate thus shortening the reaction zone and critical diameter. Russian investigators[†] have studied the effect of initial temperature on the critical diameter for pressed TNT at a density of 1 g/cm³ over a temperature range of -193⁰C to 75⁰C.

[†]A. F. Belyaev and R. Kh. Kurbangalina, "Effect of Initial Temperature on Critical Diameter of Nitroglycerine and Trinitrotoluene," Russian J. Phys. Chem. 34, 285-289 (1960).

Figure 2 shows the results. It is the usual type of threshold curve which divides the plane (in this case, diameter vs. temperature plane) into two regions, in one of which detonation is possible and another in which detonation is impossible. Thus, for a fixed diameter, one can speak of a critical temperature, below which detonation will not occur.

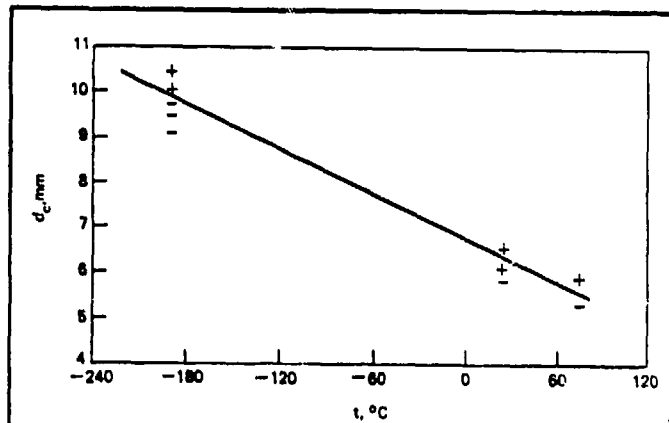
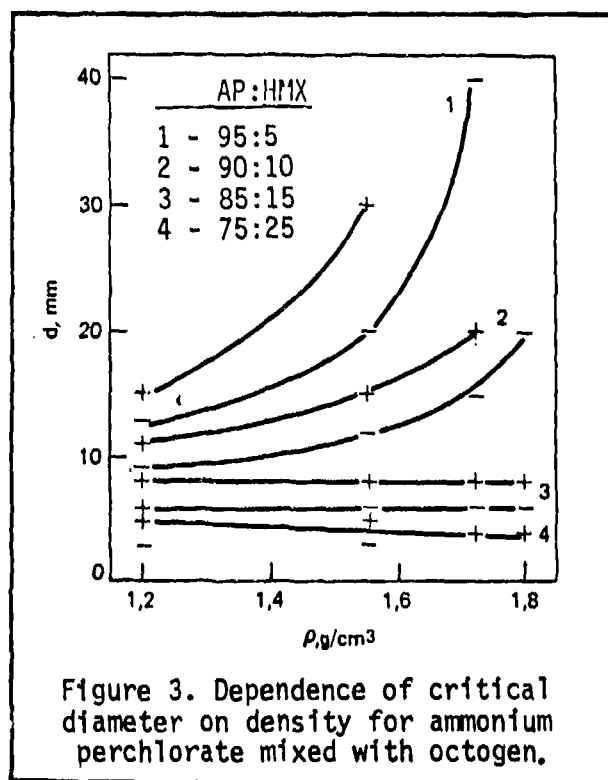


Figure 2
Critical diameter of powdered TNT as a function of initial temperature. (+ is steady detonation, - indicates failure)

The concept of critical temperature is not discussed as much as that of critical diameter. Yet it is a useful concept and it is particularly important in characterizing the lower energy materials such as ammonium nitrate and ammonium perchlorate which are frequently used as propellants. For example, ammonium nitrate (of unspecified size, but probably in the form of prills which are about 1 to 3 mm) in 1.5 inch diameter charges, highly confined in steel, will not detonate with normal boosters until the initial temperature gets beyond 140°C. Above that temperature, ammonium nitrate detonates readily. In the course of gap testing propellants, propellants have been found which would not detonate in the standard system at -60°C or -32°C, but would detonate readily at 25°C or 66°C. The effect of temperature on ammonium perchlorate's critical diameter is about five times greater than the effect on TNT's critical diameter -- the critical diameter for ammonium perchlorate decreases about 0.1 mm for every degree (centigrade) increase in initial temperature.

Effect of Chemical Composition on Detonability

One of the earliest descriptions of the effect of composition on detonability comes from Russian work in the forties.[†] The Russians describe an odd effect of mixing material from group 1 (TNT-like materials) with material from group 2 (AP-like materials). In a mixture of 50% TNT and 50% ammonium nitrate, it was observed that at low density (low % TMD), the material exhibited group 2 behavior, that is, the critical diameter increased as the density increased. Then there was an intermediate range in density in which only failure was observed, and then at higher densities, group 1 behavior was observed. Subsequent Russian work^{††} shows that mixtures of



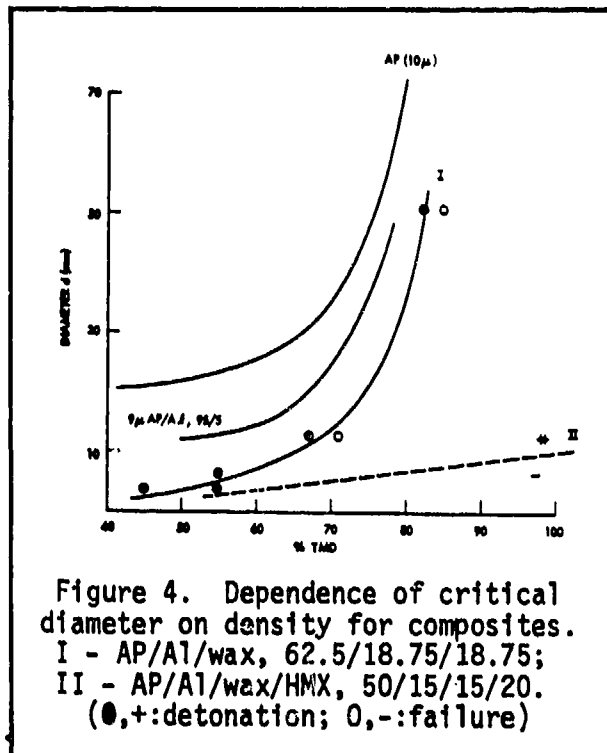
ammonium perchlorate and HMX (cyclo-tetramethylene tetranitramine, also called octogen) do not exhibit this odd pattern. Figure 3 shows the effect on the detonability curves of adding HMX to ammonium perchlorate. The top pair of curves is for 95% ammonium perchlorate and 5% HMX. The top curve (+) of the pair indicates detonations occurred, while the bottom curve (-) indicates failures; so the detonability curve lies somewhere in between. Similarly,

[†]K. K. Andreyev and A. F. Belyayev, "Theory of Explosives" (OBORONGIZ), Moscow, 1960, through a partial translation by W. A. Erwin, Jr.

^{††}L. N. Akimova and L. N. Stesik, "Detonation Capacity of Perchlorate Explosives," *Combustion, Explosions, and Shock Waves*, 12, 247-251 (1976).

the pair marked "2" delineates the detonability curve for 90% ammonium perchlorate and 10% HMX, number 3 is for 15% HMX and number 4 is for 25% HMX. There is a perfectly regular transition from group 2 behavior to group 1 behavior as the percentage of HMX is increased. At 15% HMX, the behavior changes from strongly group 2 to weakly group 1. According to more recent Russian work[†], the same is true for mixtures of ammonium perchlorate and TNT. In the case of TNT, it takes about 32% TNT for the transition to

group 1 behavior. This is more reasonable than the earlier report and agrees with a spot check study done at NOL^{††} for mixtures of propellant components. The results are shown in Figure 4. Curve I is for a mixture of ammonium perchlorate, aluminum, and wax, while curve II is for the same mixture with 20% HMX added. The behavior shown by curve II is not group 1 but it is very close to group 1 and there is no dead press phenomenon exhibited at nearly void-



less density.

If two members of the same group are mixed, the behavior of the mixture is representative of the same group. Figure 5 shows the dependence

[†]Akimova and Stesik, op. cit.

^{††}D. Price, A. R. Clairmont, Jr., and J. O. Erkman, "NOL Large Scale Gap Test III, NOLTR 74-40, 8 Mar 1974.

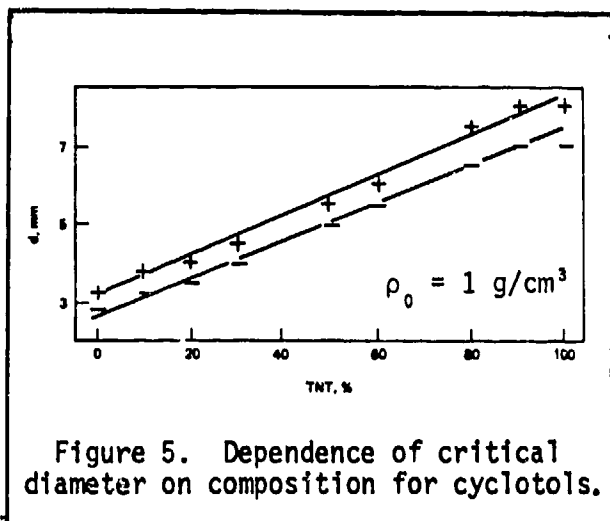


Figure 5. Dependence of critical diameter on composition for cyclotols.

of critical diameter on composition for cyclotols, which are mixtures of the group 1 explosives, TNT and RDX (cyclotrimethylene trinitramine) at a density of 1 g/cm³. The critical diameter changes uniformly from that of pure RDX at 1 g/cm³ to that of pure TNT at 1 g/cm³ as the composition varies from pure RDX to

pure TNT[†]

Effect of Non-Explosive Materials

If 5% aluminum is added to ammonium perchlorate, the detonability is increased (critical diameter decreased, see Figure 4). There is no published data for an aluminized granular group 1 explosive, but there is data for aluminized cast TNT, given in Table 3. The same effect on detonability is exhibited. As the percentage of aluminum increases from none to 20%, the

Table 3. Effect of adding aluminum to the critical diameter of cast TNT.

Percent Aluminum	Critical Diameter (cm)
0	2.69
4.8	2.26
20.0	0.70

critical diameter drops from 2.7 cm to 0.7 cm. Thus, adding aluminum to either a group 1 or group 2 explosive apparently increases the detonability. On the other hand, adding water to a member of either group lowers the detonability -- water acts as an inert diluent.

Wax has opposite effects on members of group 1 and group 2. Adding wax to a member of group 1 increases

[†]Akimova and Stesik, op. cit.

the critical diameter. In this case wax apparently acts as an inert material. But adding wax to group 2 materials (which are oxidizers) decreases the critical diameter (see Figure 1). In fact, adding any sort of easily burned fuel to ammonium perchlorate or ammonium nitrate[†] increases the detonability. Furthermore, Russian investigators^{††} have shown that, if solid fuel (e.g., polymethylmethacrylate) is added to ammonium perchlorate, the finer the fuel particles, the greater the decrease in critical diameter at a given loading density. Thus, the indications are that the fuel is taking part in an oxidation-reduction reaction with the ammonium perchlorate. The fact that the addition of these fuels to ammonium perchlorate increases the detonation velocity at constant porosity is also evidence for the presence of an oxidation-reduction reaction.

Apin and Stesik^{†††} studied the effect of adding dense inert materials such as calcium carbonate and tungsten to nearly voidless cast explosives. They found that a certain percentage of such diluents reduced the critical diameter, that is, increased the detonability. They suggested that the increase in detonability occurred because the inert materials produced focal points for the formation of hot spots by the reflection of shocks at the heterogeneity. This may be the reason for the effect that the addition of aluminum has on explosives (see Figure 4 and Table 3) since aluminum (density 2.7 g/cm³) is denser than any of the explosives with which it is mixed.

[†]Amatols are fuel-oxidizer mixtures composed of TNT and ammonium nitrate.

^{††}Akimova and Stesik, op. cit.

^{†††}Ya. A. Apin and L. N. Stesik, "On the Mechanism of the Chemical Reaction at the Detonation of Compact Explosives," Zh. prikl. Mekh. Yekh. Fiz., 2, 146 (1965).

Effect of Confinement on Detonability

It has been known for a long time that, if a heavy metal sleeve is placed around a charge, it can frequently be detonated with the same booster that failed to detonate it without the confining sleeve. The confinement adds resistance to the expansion of the gaseous detonation products, and by doing so, maintains the high pressure and high temperature a little bit longer. Thus the reaction is maintained longer before lateral rarefactions from the side quench it. Table 4 gives data[†] showing the effects of confinement on ammonium perchlorate and ammonium nitrate, two materials with relatively large critical diameters under the usual experimental conditions. The ammonium perchlorate had intermediate particle size -- it had been put through a sieve with 70 μ openings. The particle size of the ammonium nitrate was not specified, but it was probably that of prills^{††} of 1 mm diameter or less.

None of the confinements for the ammonium perchlorate were very strong. The smallest critical diameter was obtained using copper foil as the confinement. With the weaker glass confinement, the critical diameter increased by a factor of four to five. Replacing the glass with a thin cellophane sleeve again increased the critical diameter by yet another factor of four to five.

[†]V. A. Gor'kov and R. Kh. Kurbangalina, "Some Data Concerning the Detonation Ability of Ammonium Perchlorate", *Combustion, Explosions, and Shock Waves*, 2, 12 (1966); also R. Kh. Kurbangalina and L. I. Patronova, "Effect of a Steel Sheath on the Critical Detonation Diameter of Condensed Explosives," *Combustion, Explosions, and Shock Waves* 12, 587-590 (1976).

^{††}Prill is the name given to ammonium nitrate particles, as produced and sold commercially. It is now possible to produce porous or non-porous prills at specified sizes. In general, they are approximately spherical and of 1 to 3 mm diameter.

Table 4. Effect of confinement on the critical diameter of ammonium perchlorate (AP) and ammonium nitrate (AN).

<u>Material</u>	<u>Density</u>	<u>Confinement</u>	<u>Critical Diameter</u>
AP (70 μ)	1.1 g/cm ³	copper foil	b
"	"	glass	~5b
"	"	cellophane	~(5) ² b
AN	1.06 g/cm ³	steel	<3 mm
"	"	glass	80 mm
"	"	cellophane	~100 mm

The critical diameter for ammonium nitrate with the steel sleeve was less than 3 mm. Replacing the steel with glass increased the critical diameter to 80 mm, and with cellophane, the critical diameter increased to 100 mm.

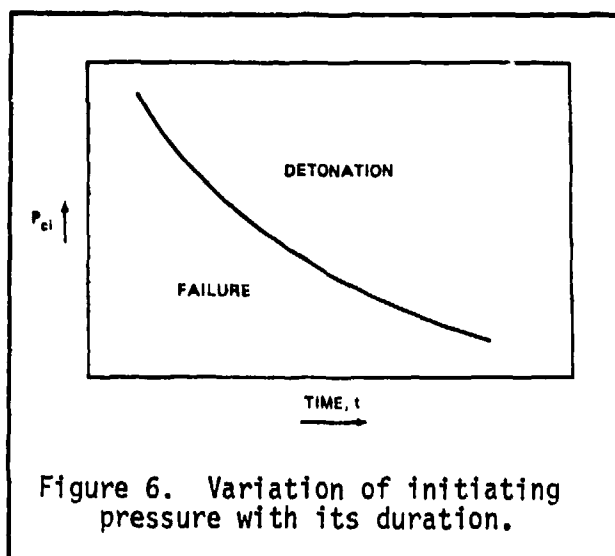
Variables Affecting Initiation of Detonation Through Shock to Detonation Transition

We have discussed above a fairly representative sample of the variables that affect the propagation of a steady state detonation and have estimated the effects by the degree to which they change the critical diameter. Now we will change our focus and examine the variables that affect the critical conditions for initiating detonation through a shock-to-detonation transition. In this case, we will estimate the effects by the effect on the critical initiating pressure.

The critical initiating pressure is that pressure just sufficient to initiate detonation (that is, produce a transition from shock to detonation) with a probability of one half. It is measured in a number of different tests, some of which will be discussed later. It is very dependent on the

test variables and it will be strongly affected by the design of the test, in particular, the physical dimensions, since the physical dimensions determine the time at which the rear and lateral rarefactions arrive to quench the reaction.

In 1959, Hubbard and Johnson[†] published a paper in which they considered a chemically and physically homogeneous material reacting homogeneously by thermal decomposition. They showed theoretically that, for a given initiating



pressure, there is a minimum duration of the initiating shock pulse below which detonation is not possible. This is illustrated graphically in Figure 6 in the form of a threshold curve in the pressure-time plane. The curve divides the plane into two regions, in one of which detonation is not possible and the other in which detonation

is possible. Three years later, Brown and Whitbread^{††} performed experiments on initiation of heterogeneous explosives by impact of cylindrical projectiles. The results showed that the critical initiating pressure must be maintained for a definite minimum time in order to effect a shock to detonation transition. Moreover, if the projectile velocity was higher than that necessary to produce the critical initiating pressure, the shock to detonation

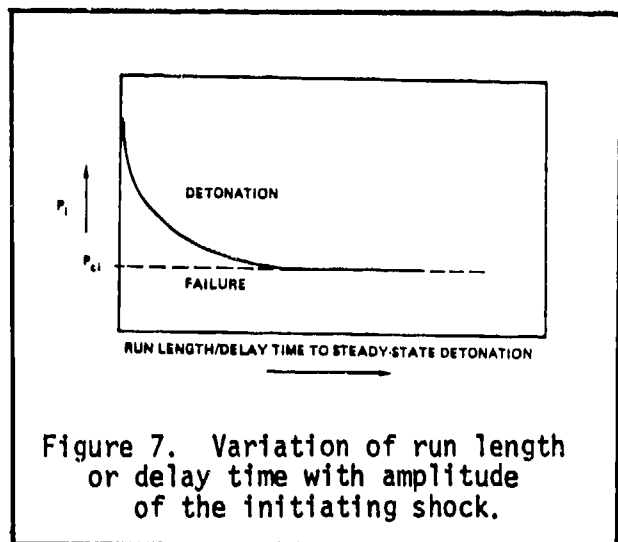
[†]H. W. Hubbard and M. H. Johnson, J. Appl. Phys. 30, 765 (1959).

^{††}S. M. Brown and E. G. Whitbread, Les Ondes de Detonation, Edition du Centre National de la Recherche Scientifique, Paris, 1962, pp. 69-80.

transition occurred in a shorter time than the time required at the critical pressure. Both these pieces of work have produced general agreement that there must be some threshold in the pressure-time plane which determines whether a shock to detonation transition can be achieved.

It is important in describing a test to state all of the conditions under which it is done so that it is repeatable and can be correlated with other tests. In many cases it is much easier to measure pressure than to measure both pressure and duration. In many tests, the duration cannot be or has not been measured. In the wedge tests done at Los Alamos Scientific Laboratory, the pressure pulses are essentially square and of infinite duration as far as the effects being studied are concerned. Just the pressure is reported. In the NOL large scale gap test, again only the pressure is determined although the duration can be estimated as will be discussed later.

The shock sensitivity behavior of all explosives exhibits a few general characteristics. First, there is a critical initiating pressure for a given



set of experimental conditions. At the critical pressure there is a definite distance between the point at which the shock enters the material and the point downstream at which detonation occurs. We refer to this distance as the run length. If the experimental conditions remain constant, but pressures higher than the

critical pressure are imposed, then the run length is reduced, as Figure 7

illustrates. Corresponding to the run length there is a total delay time which is the difference between the time of entry of the shock and the time of onset of detonation. This quantity also behaves as illustrated in Figure 7. At very high pressures, the transition is so rapid that detonation occurs nearly at the point of shock entry. At lower pressures, the run length and delay time increase and as the pressure approaches the critical pressure the run length and delay time become much greater.

This type of behavior has been observed for a number of years. Figure 8 shows an experimental curve of run length versus shock pressure obtained at the Naval Weapons Center at China Lake[†] for cast Comp B^{††} with a steel

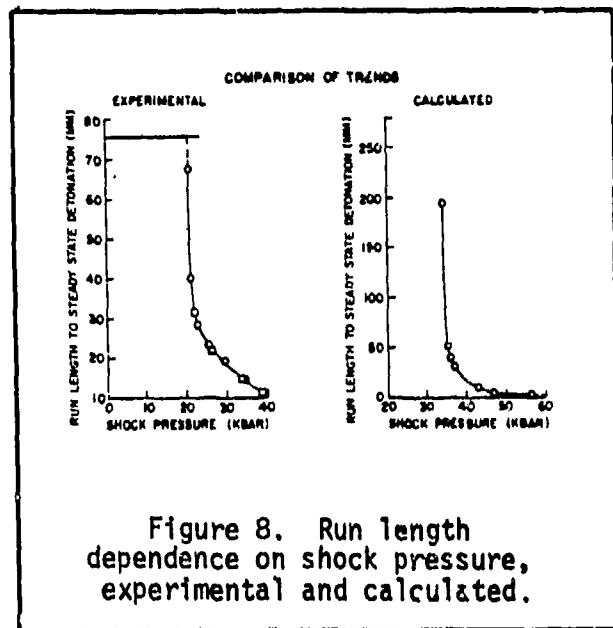


Figure 8. Run length dependence on shock pressure, experimental and calculated.

attenuator. We see the pattern described above. The higher the pressure, the shorter the run length. As the critical initiating pressure (about 20 kbar) is approached, the run length increases greatly. The longest run length shown is about 70 mm which is quite close to the end of the charge which was 75 mm long. The observations, of course, were of

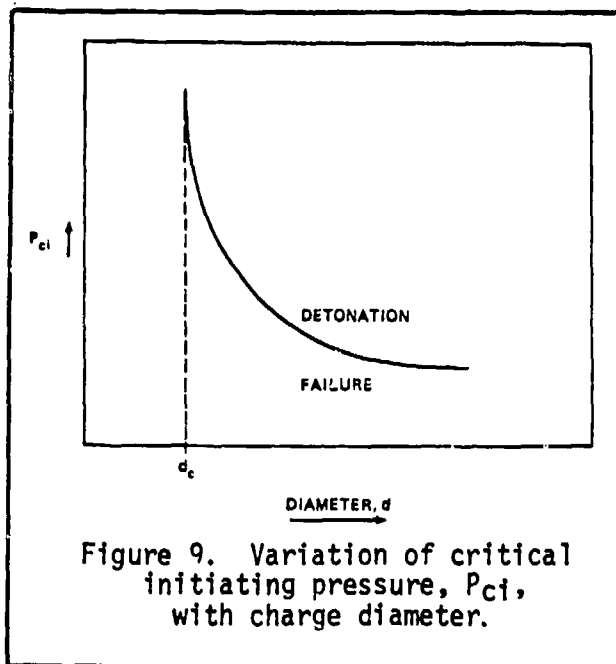
the lateral surface of the charge. The detonation transition in the interior of the charge may have occurred sooner.

[†]L. N. Cosner and R. G. S. Sewell, NavWeaps 8507 (NOTSTP 3489) Apr 1964 and Explosivestoffe Nr. 10/1969, pp. 230-238. See also D. Price and F. J. Petrone, J. Appl. Phys. 35, (3) [pt. 1], 710-714 (1964).

^{††}Comp B is a mixture of 60% RDX and 40% TNT to which 1% wax has been added.

Effect of Charge Diameter on Shock Sensitivity

One other characteristic we must consider in studying shock sensitivity is the effect of charge diameter on the critical initiating pressure. We



clearly do not expect to obtain detonation in a charge which is smaller than the critical diameter. For a charge at its critical diameter we expect the critical pressure to be of the order of the C-J pressure or von Neumann spike pressure for that particular explosive. As we increase the diameter above the critical diameter, the value of the critical initiating pressure will decrease.

Figure 9 illustrates this trend; above the curve detonation occurs, below it, only failure. As the diameter gets larger and larger, the critical initiating pressure does not get indefinitely smaller, but approaches asymptotically what we may call an "infinite diameter value". To find the value of the infinite diameter critical initiating pressure it is necessary to extrapolate the results of experiments on a series of larger and larger finite diameter charges. Unfortunately, that would require a great many experiments.

Measuring Critical Initiating Pressure

There are a variety of tests which can be used to measure critical initiating pressure. Among them are the gap test, the booster test, the wedge test, and projectile impact tests. We will discuss in detail only the gap test and the wedge test.

Figure 10 shows the experimental arrangement for the gap test. It consists of an explosive donor which produces a shock wave in an attenuator material (the "gap") which, in turn, transmits a shock into the acceptor

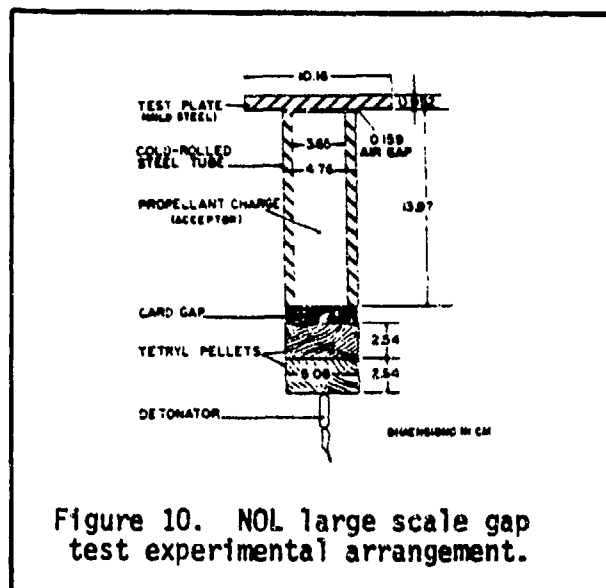


Figure 10. NOL large scale gap test experimental arrangement.

(test) explosive. The attenuator or gap is varied in thickness to adjust the amplitude of the shock transmitted into the acceptor.[†]

Tetryl (trinitrophenylmethyl nitramine) was originally used as the donor explosive because of its reproducible characteristics.

However, there is no longer a good commercial source of tetryl pellets so pressed 50/50 pentoite

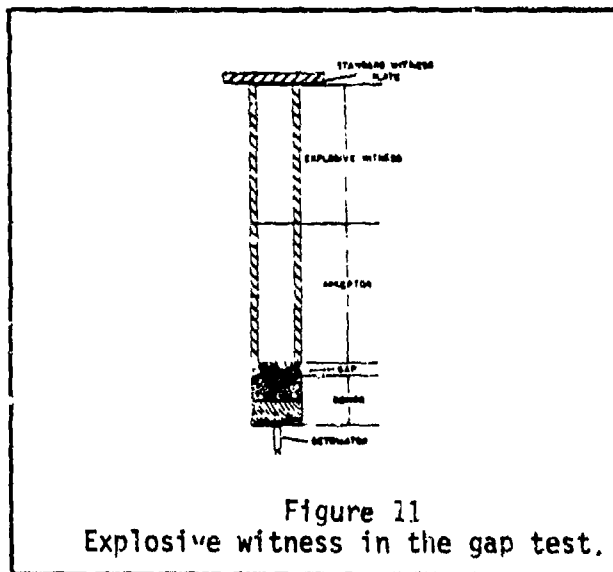
(50% TNT, 50% PETN) pellets are now used. The attenuator is PMMA (poly-methyl methacrylate, trade names Plexiglas, Lucite, and Perspex) or its equivalent.^{††} In the standard test, the acceptor is about one and a half inches in diameter and it is confined in a standard steel sleeve. The acceptor is followed by a steel witness plate which indicates whether detonation or failure occurs. There is a small air gap between the steel sleeve and the witness plate.

The detonator initiates the booster (donor) at a point, producing a spherically expanding detonation front which flattens out as it progresses.

[†]The booster test is similar to the gap test, but in the booster test, the amount of booster or donor is varied instead of the thickness of the attenuator.

^{††}The equivalent is a layer of cellulose acetate cards, each a hundredth of an inch thick.

A shock is transmitted into the attenuator which is varied in thickness until the point of 50% probability of producing detonation in the acceptor is found. If the acceptor is a fairly powerful explosive at high density, then variation of the thickness of the gap and the 50% point will produce drastic changes in the effects on the witness plate. For example, for a group I explosive at high density, the witness plate will be slightly dented for a gap thickness of one card (0.01) greater than the 50% gap, but it will be punched (clean hole) at a gap equal to the 50% gap. In this case, the witness plate gives a sharp, clear indication of detonation. However, if the explosive is of low density (porous) or if the explosive is comparatively weak (ammonium perchlorate, for example) the witness plate will not be a good indicator. Then, if from supplementary information you know that the



acceptor can detonate in the test configuration, a more sensitive witness can be used, e.g., the configuration shown in Figure 11. In place of the steel witness plate, a second tube containing an explosive with a known critical initiating pressure is placed. Then the standard witness plate is placed at the end of this

explosive witness.

Table 5 shows the results obtained by using an explosive witness to measure the critical initiating pressure (in the gap test) for ammonium perchlorate at a density of 0.85 g/cm^3 . Using a standard steel witness did

Table 5. Shock sensitivity of ammonium perchlorate at 0.85 g/cm³.

<u>Witness</u>	<u>50% gap (cards)</u>	<u>P_{c1} (kbar)</u>
steel	N<0	?
Comp B	212<N<225	~5
TNT	207	~5

not give usable results. Using Comp B and TNT as explosive witnesses gave a value of critical initiating pressure of about 5 kbar. In the table, the 50% gap is given in terms of the number of cellulose acetate cards

used, each one hundredth of an inch thick. The point to be made is that the type of witness to be used can be tailored to the type of material under study.

The next lecture will discuss the NOL large scale gap test (LSGT) and its calibration.

NSWC MP 81-399
Lectures on Detonation Physics

Lecture #7 - 12 January 1981

by

DONNA PRICE

Notes by Frank J. Zerilli

THE LARGE SCALE GAP TEST - I

Introduction

The standard large scale gap test (LSGT) arrangement is illustrated in Figure 1. It consists of a detonator, a donor explosive, an attenuator material, a confined acceptor (test) charge and a steel witness plate. The standard donor is now 50/50

pentolite[†] of density 1.56 g/cm³.

The original donor used was 1.51 g/cm³

tetryl. The detonator initiates a detonation with a spherically expanding front which, in turn, transmits a shock through the attenuator to the test explosive. The test explosive is confined within a steel sleeve. The attenuator, polymethyl methacrylate or cellulose acetate or a combination is varied in thickness until the transmitted shock is just sufficient to

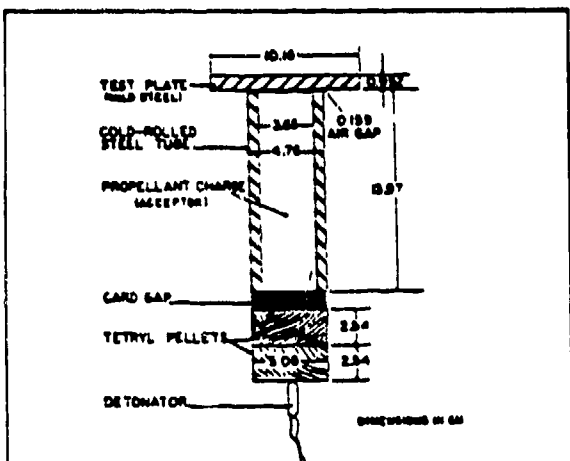


Fig. 1. Large Scale Gap Test experimental arrangement.

initiate detonation in the acceptor in

fifty percent of the trials. A steel witness plate shows whether the reaction in the acceptor is actually a detonation^{††}. The standard donor is 50.8 mm (2") in both diameter and length.

[†] Mixture of 50% TNT and 50% PETN (pentaerythritol tetranitrate).

^{††} The shock loading of the witness plate by the detonation of common explosives punches a hole through the plate.

Calibration of the System

In order to calibrate the system we must know what the pressure is in the attenuator material after the shock produced by the standard donor has traveled through a given thickness of attenuator. There are several methods of obtaining the pressure as a function of thickness.

One method is to use the relation which comes from conservation of momentum:

$$P = \rho_0 U u \quad (1)$$

In Eq. (1), P is the shock pressure, ρ_0 is the density of the unshocked material, U is the shock velocity, and u is the particle velocity in the material behind the shock. We have assumed that the initial particle velocity and initial pressure are zero. Thus we must measure the shock velocity and the particle velocity to obtain the pressure.

Another method is possible if we know the Hugoniot relation for the attenuator material. Many solid materials, to a good approximation, exhibit a linear relation between the shock velocity and the particle velocity:

$$U = a_0 + s u \quad (2)$$

where a_0 and s are constants specific to the explosive. Substituting Eq. (2) into Eq. (1), we obtain

$$P = \rho_0 (a_0 u + s u^2) \quad (3)$$

Equation (3) is a quadratic relation between the shock pressure and the particle velocity. Thus we need only measure the particle velocity to obtain the shock pressure.

Alternatively, we can solve Eq. (2) for the particle velocity, and substitute it in Eq. (1) to obtain the relation

$$P = \rho_0 (U^2 - a_0 U) / s \quad (4)$$

In this case we measure the shock velocity to obtain the pressure.

At NSWC we have used all three methods at one time or another. The method based on Eq. (4) is the one that was originally used and is perhaps the most generally used since it seems so simple in principle. Using a streak camera, a record of the distance the shock has traveled versus time is obtained. By differentiating the record, the shock velocity versus time is obtained. This gives us the shock velocity versus distance, and finally, from Eq. (4), we obtain the pressure versus distance in the attenuator.

However, the situation is not as simple in practice as it is in principle. In the first effort[†], the shock velocity was measured both with a streak camera and with pressure probes. The experimental

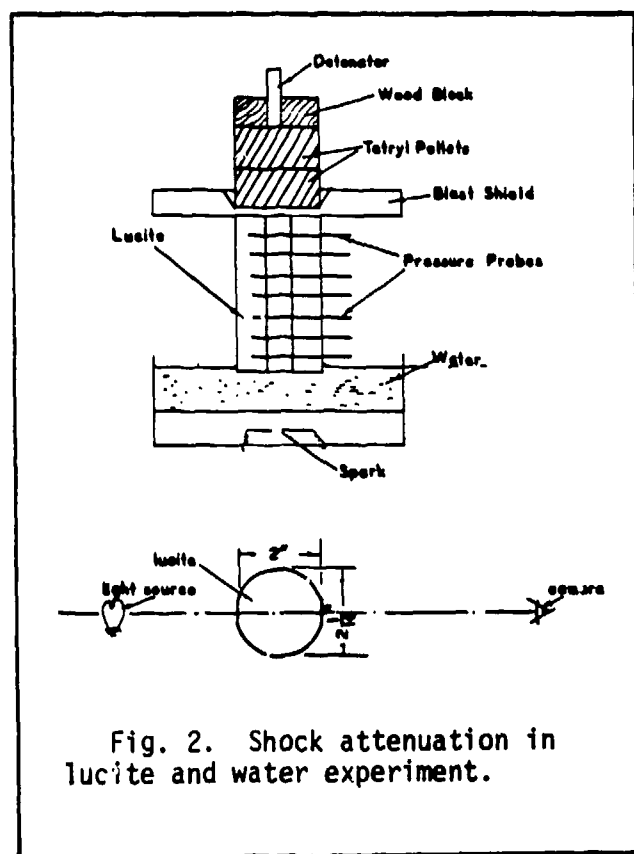


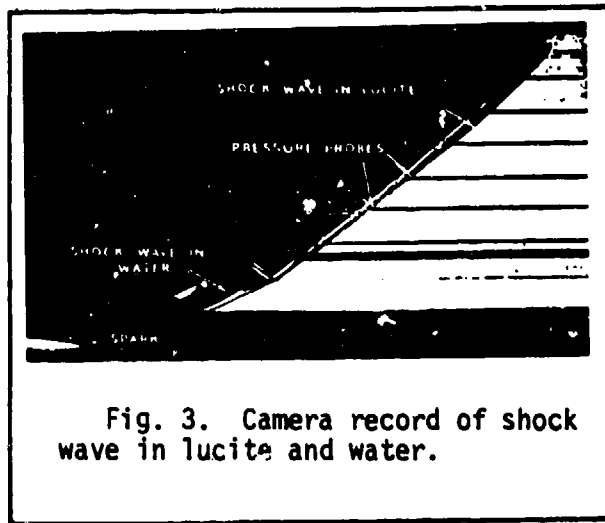
Fig. 2. Shock attenuation in lucite and water experiment.

arrangement is shown in Fig. 2a. Part of the attenuator was made into a blast shield to keep the gaseous detonation products from obscuring the view of the shock front in the PMMA. Probes were set into 0.05 inch diameter holes bored into the PMMA at half inch intervals. (The precision of the measurement of position probably did not justify that many probes, however). The PMMA cylinder ended under water so that the records showed the shock not only in the PMMA but also in the water. A

spark underneath the transparent water tank was used to provide

[†] I. Jaffe, R. L. Beauregard, and A. B. Amster, NAV ORD Rept 6876.

a fiducial point on the records. Figure 2b gives another view of the arrangement, showing the cylinder of PMMA with flats machined on two sides, a light source on one side and the camera on the other. Figure 3 shows a camera record of the shock front distance versus



time. The horizontal streaks are interruptions of the light caused by the pressure probes in the PMMA. There is a change of slope as the shock enters the water. At the bottom left is the fiducial mark produced by the spark.

In this first calibration, the difference between the probe record and the streak record of distance versus time was well within experimental error although neither was very precise. The experimental set-up for the last of a series of calibrations that were carried out was considerably better and the streak records were considerably better.

There is a great difficulty in obtaining accurate velocity data, because we must differentiate a function which is known only approximately from experimental data points subject to random errors[†]. At least an order of magnitude in precision and probably more, is lost every time we have to differentiate experimental data.

[†]See John Erkman, NOLTR 68-117, Sept 1968, and D. Tasker, "The Low Amplitude Shock Initiation Test", Seventh Symposium on Detonation (to be published) for descriptions of the difficulties involved and techniques that may be used.

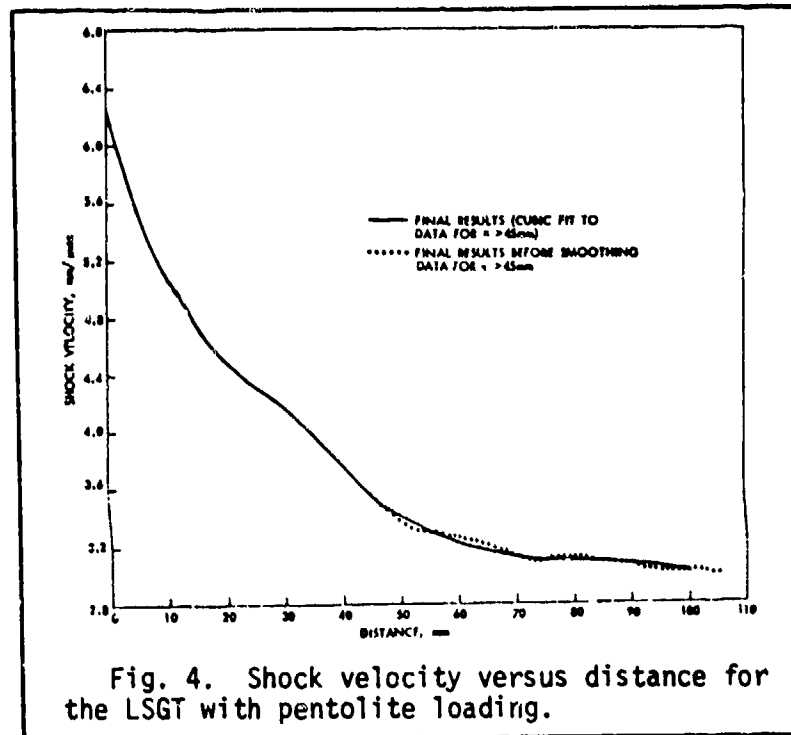


Figure 4 shows the shock velocity versus distance curve that was obtained for PMMA.[†] The dotted curve shows the final results from reading the record and the solid curve gives smoothed results which are used for the actual calibration. The curve has an obvious bulge which is real and not due to experimental error. The calibration has been repeated many times, and it is believed that the bulge is due to the arrival of the lateral rarefaction wave at the central axis of the PMMA cylinder.

If it is so hard to measure shock velocity by differentiating the distance-time curve, what other choice do we have? The other choice is to measure particle velocity directly.

MEASURING PARTICLE VELOCITY WITH THE ELECTROMAGNETIC VELOCITY GAUGE

We have used the electromagnetic velocity gauge (EMV) (sometimes called the foil gauge) to measure particle velocity. The system was developed by Russian scientists ^{††}; our system is a copy of theirs

[†] J. O. Erkman, D. J. Edwards, A. R. Clairmont, and D. Price, NOLTR 73-15, April 1973.

^{††} V. M. Zaitsev, P. F. Pokhil, and K. K. Shvedov, Dokl. Acad. Sci., U.S.S.R., 132(6), 1339, (1960).

on a smaller scale. Figure 5 shows the arrangement[†]. An aluminum

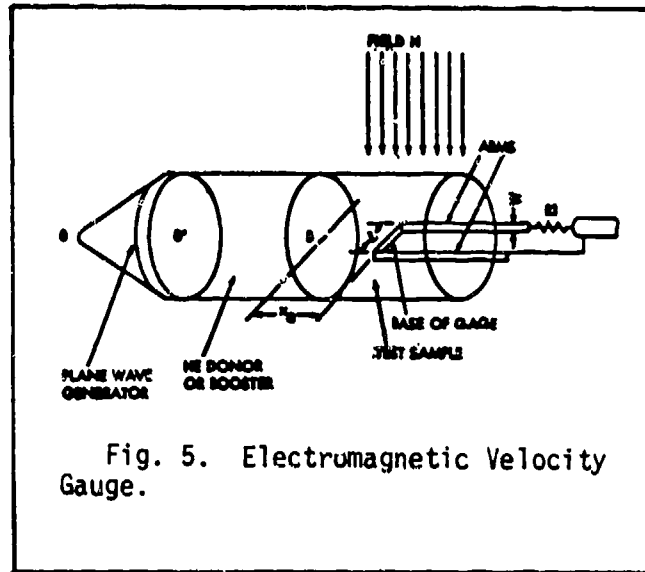


Fig. 5. Electromagnetic Velocity Gauge.

foil 0.5 mil thick, in a staple shape, is placed into the material under study, perpendicular to the expected flow. A magnetic field is imposed, perpendicular both to the expected flow and to the foil base. As the shock passes through the material, the material acquires a flow velocity and since the mass of the foil is relatively small, the foil rapidly acquires

the same velocity as the adjacent material. As the foil moves, it cuts the magnetic field lines, producing an emf V which is directly proportional to the foil velocity.

$$V = H u l \cdot 10^{-4} \quad (5)$$

In Equation (5), V is the emf in volts, H is the magnetic field strength in gauss, u is the particle velocity in millimeters per microsecond, l is the length of the portion of the foil which is perpendicular to the flow (the "base" of the staple) in millimeters. The typical base length used is 10 mm, although a 5 mm base has occasionally been used.

In the calibration study of PMMA, a plane wave generator was used only at the highest pressure loading. For all the other work the standard donor with point initiation was used as shown in Figure 6. In order to keep the metal particles out of the magnetic field, an aluminum baffle was used and, in addition, primacord was used instead of a metal cased detonator. Any metal and gas

[†] S. J. Jacobs and D. J. Edwards, "Experimental Study of the Electromagnetic Velocity Gauge Technique", Fifth symposium (International) on Detonation, ONR ACR-184, U. S. Gov't Printing Off. Washington D.C. 1972, pp 413-426.

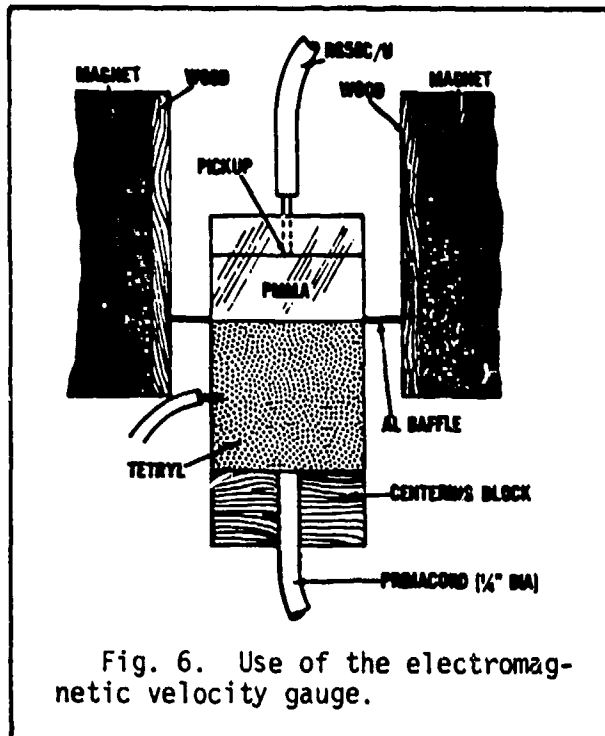


Fig. 6. Use of the electromagnetic velocity gauge.

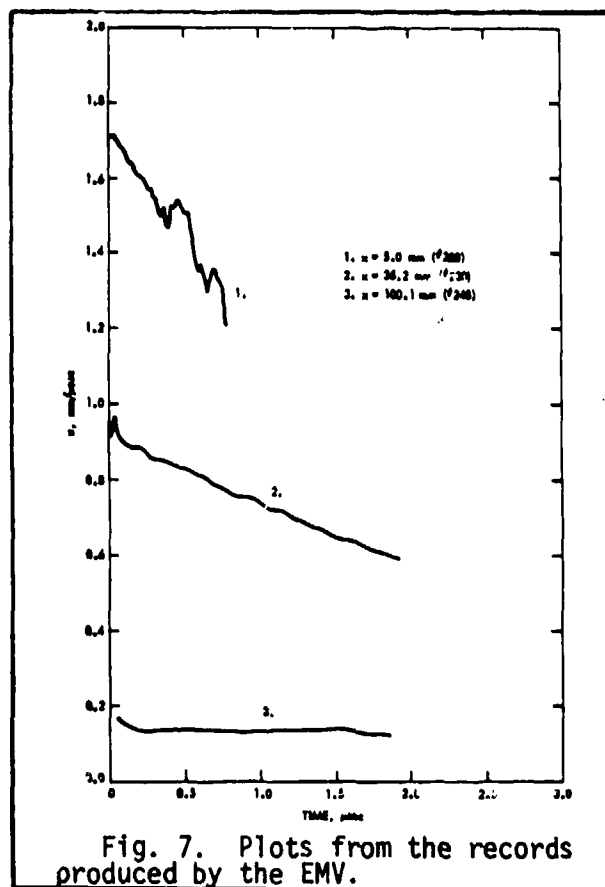


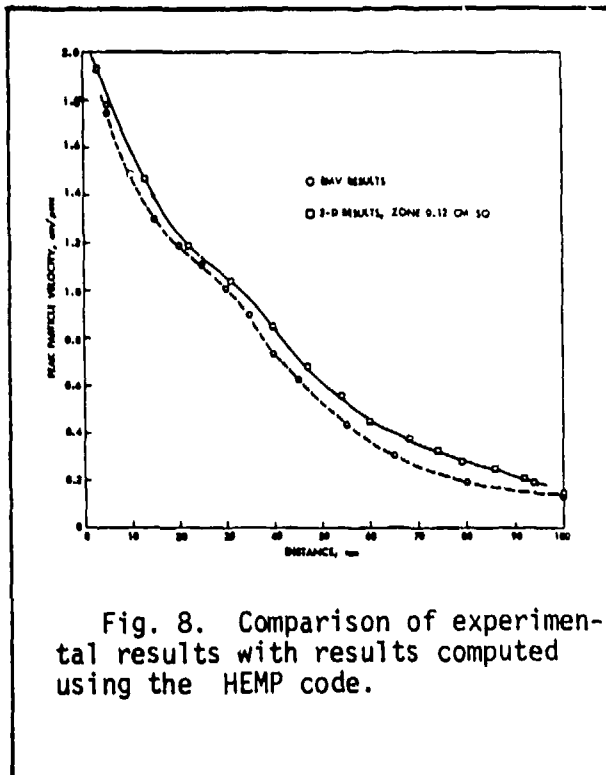
Fig. 7. Plots from the records produced by the EMV.

detonation products in the field contribute to noise on the record.

In the study of PMMA, the PMMA was cut into several pieces and the foil was folded over one piece. Then the pieces were cemented back together using chloroform as a solvent and putting the assembly under pressure. Figure 7 shows tracings from typical oscilloscope records for thicknesses of PMMA of 5, 35 and 100 mm. The records themselves show a resolvable rise time of about 25 ns. In Figure 7, voltages have been converted to velocities through Eq. (5). In each case, the particle velocity in the PMMA should be the peak velocity shown in the record. It was estimated that the values obtained for particle velocities were accurate to a $\pm 2\%$. In Figure 8 the peak particle velocities have been plotted as a function of PMMA thickness. Also plotted in Figure 8 are the results of a two dimensional hydrodynamic computer code calculation carried out by Kamegai and Erkman[†].

[†]M. Kamegai and J. Erkman, "Numerical Analysis of a Diverging Shock Wave in Plexiglass Cylinders", Fifth Symposium (International) on Detonation, ORN ACR-184, U. S. Government Printing Office, Washington DC, 1972, p.477.

Unfortunately, the value of γ used in the computation was 2.5 instead of 3.0. Since the pressure is proportional to $(\gamma+1)^{-1}$ the



computed pressure and particle velocity is too high. However, the shape of the experimental curve was reproduced and the bulge in the experimental curves appears also in the computed curve, confirming the explanation of the bulge as being due to the lateral rarefaction reaching the longitudinal axis.

Fig. 8. Comparison of experimental results with results computed using the HEMP code.

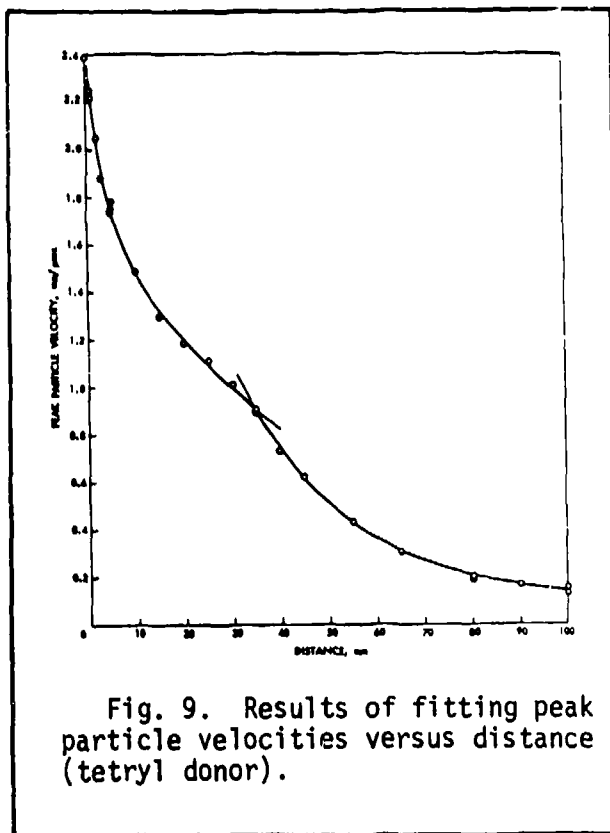


Fig. 9. Results of fitting peak particle velocities versus distance (tetryl donor).

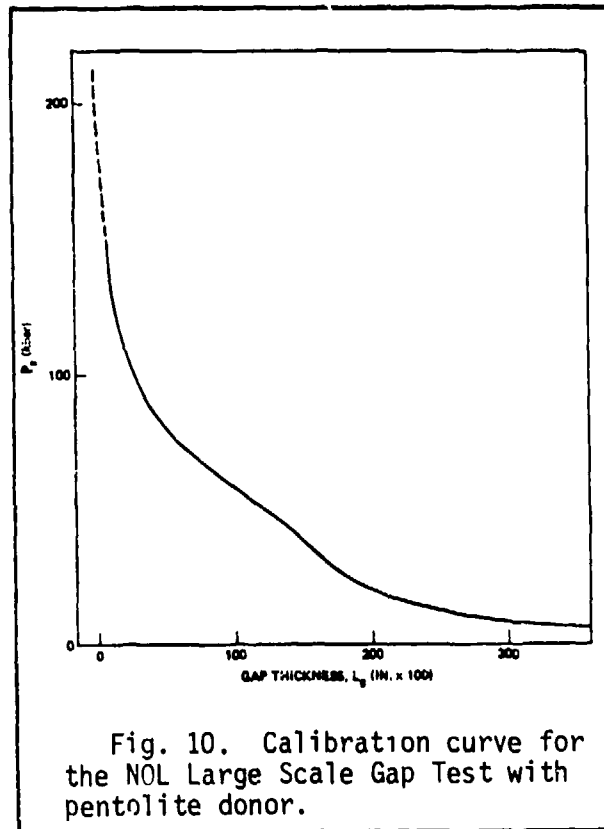


Fig. 10. Calibration curve for the NOL Large Scale Gap Test with pentolite donor.

Figure 9 shows the results of later measurements and includes a measurement in which the gap was a single card of cellulose acetate 0.01 inches thick. With the additional and more precise data, a better curve fit was obtained showing a distinct cusp at a thickness of 35 mm. This is the thickness at which the lateral rarefaction has reached the longitudinal axis. If we use Eq. (3) to convert the particle velocity to pressure, then the cusp would be reflected in the calibration curve. However, using the best measurements of shock velocity versus distance and of particle velocity versus distance, a comparatively smooth curve shown in Figure 10 is obtained. The curve, however, does show the bulge, characteristic of the lateral rarefaction reaching the central axis.

The flow in a Detonating Cylinder: Hydrodynamic Computer Calculation

We will discuss the details of the flow in a detonating cylindrical charge and follow the shock transmitted into the attenuator.

In 1966 Piacesi[†] did a hydrodynamic flow computer calculation for a detonating cylinder of explosive. The computation, using the NOL CYCLONE code for 50/50 pentolite but at a density of 1.65 g/cm^3 instead of the standard donor value of 1.56 g/cm^3 . Thus the results give us a qualitative picture of the flow when applied to the standard donor.

The geometry used in the calculation was that of a two inch diameter charge, and the computations were carried out to a length to diameter ratio of 1.7. Since the standard LSGT donor has an l over d of one, the computation goes beyond that needed to follow the flow in the donor. The computations are summarized in the chart

[†]D. Piacesi, Jr., NOLTR 66-150, Jan 1967.

shown in Figure 11, below:

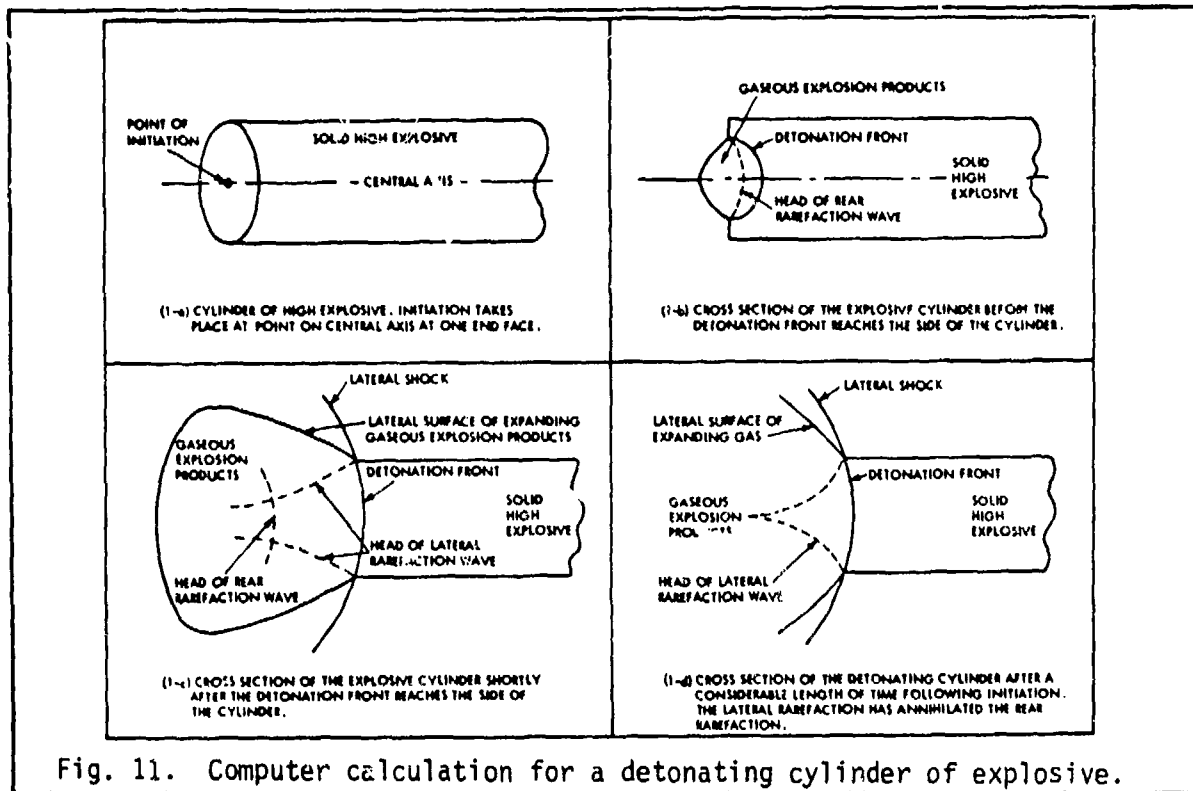


Fig. 11. Computer calculation for a detonating cylinder of explosive.

Figure 11 (1-a) shows the point of initiation on the axis of a cylinder. The initial progress of the detonation front is depicted in Figure 11 (1-b). The rear rarefaction and expansion of the detonation products is shown also. There is no lateral rarefaction yet, since the detonation front has not reached the lateral surface of the cylinder.

In Figure 11 (1-c) the detonation front has reached the lateral surface and is producing a shock in the surrounding air. The curvature of the front is decreasing[†] and a shock is being transmitted to the air while a lateral rarefaction is reflected back into the detonation products. In Figure 11 (1-d), the detonation has progressed further and the lateral rarefaction has reached the longitudinal axis and has obliterated the rear rarefaction.

[†]The detonation wave is spherical with a radius equal to the distance from the point of initiation to the front.

The spherical expansion with radius of curvature equal to the distance from the point of initiation which was calculated numerically up to an l/d of 1.7 has been checked experimentally with tetryl up to an l/d of 2. This contradicts some information found in the literature.

The summary of Figure 11 was constructed from a series of computer generated plots, examples of which are shown in Figures 12 and 13 below.

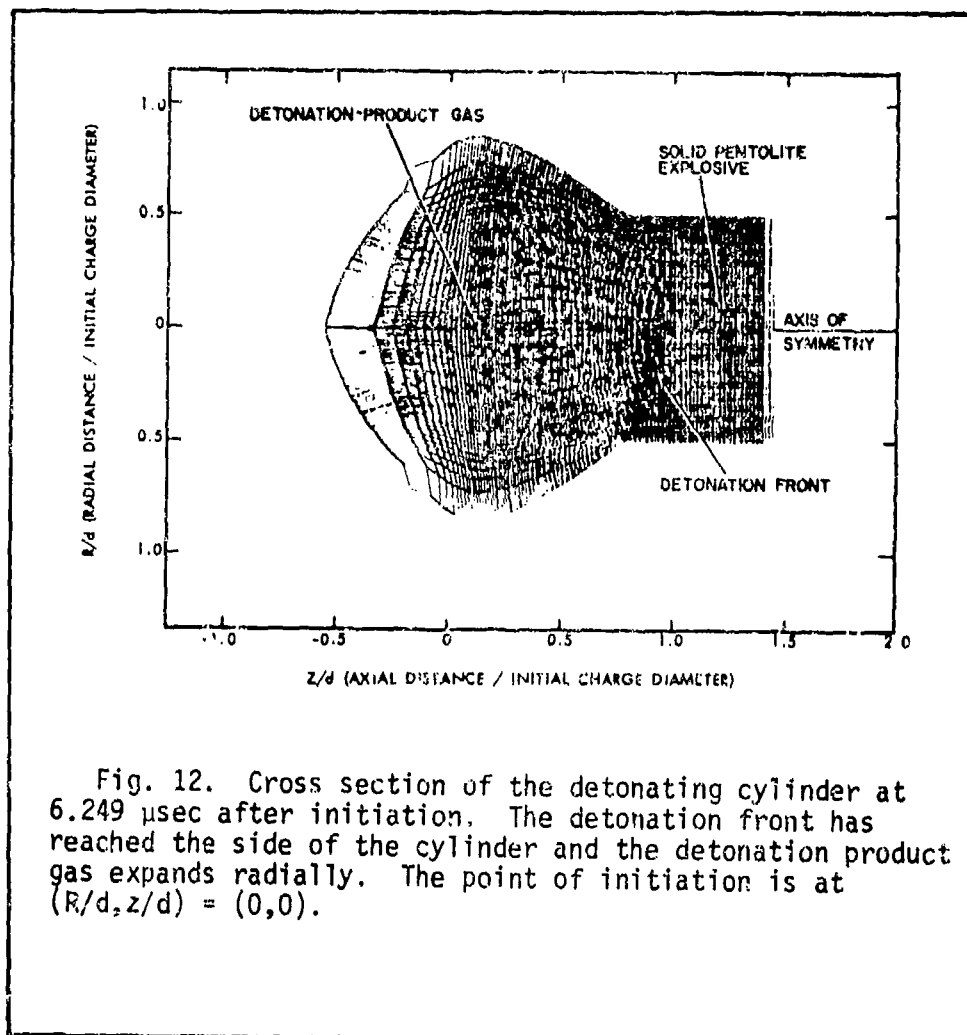


Figure 12 shows the lattice distortion at a time of 6.3 μ sec which corresponds to the detonation front reaching 48 mm (in the LSGT, this corresponds to just 2 mm short of the donor/PMMA interface).

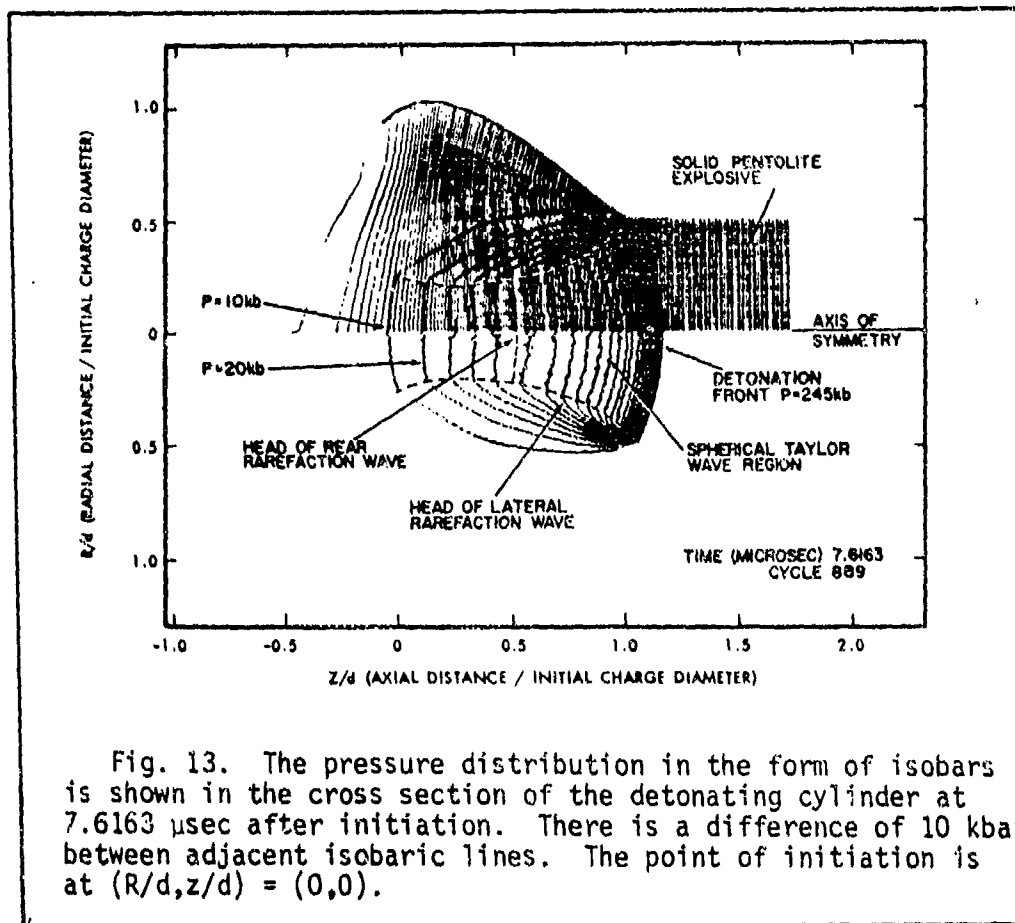


Fig. 13. The pressure distribution in the form of isobars is shown in the cross section of the detonating cylinder at 7.6163 μ sec after initiation. There is a difference of 10 kbar between adjacent isobaric lines. The point of initiation is at $(R/d, z/d) = (0, 0)$.

Figure 13 shows the isobars at a time of 7.6 μ sec which corresponds to a distance of 58 mm (this is beyond the end of the standard donor in the LSGT). The lateral rarefaction is shown and the rear rarefaction is still evident at this point.

In experiments in which a donor of twice the standard length is used it is found that the critical initiating pressure in the acceptor is the same as the critical initiating pressure found in the case of the standard donor. Since the effect of the rear rarefaction is still evident (the 50% point gap thickness is greater for the longer donor), increasing the length of the donor increases the duration of the shock. Thus the fact that this has no effect on the critical initiating pressure indicates that, for the materials under consideration, the pressure pulse produced by the standard donor is of long enough duration to be considered effectively "infinite" in duration.

Piacesi used the two dimensional CYCLONE hydrodynamic computer code to predict the pressure versus distance behind the detonation front. He compared it with the pressures in a spherical Taylor wave expansion[†]. The comparison is shown in Figure 14, below.

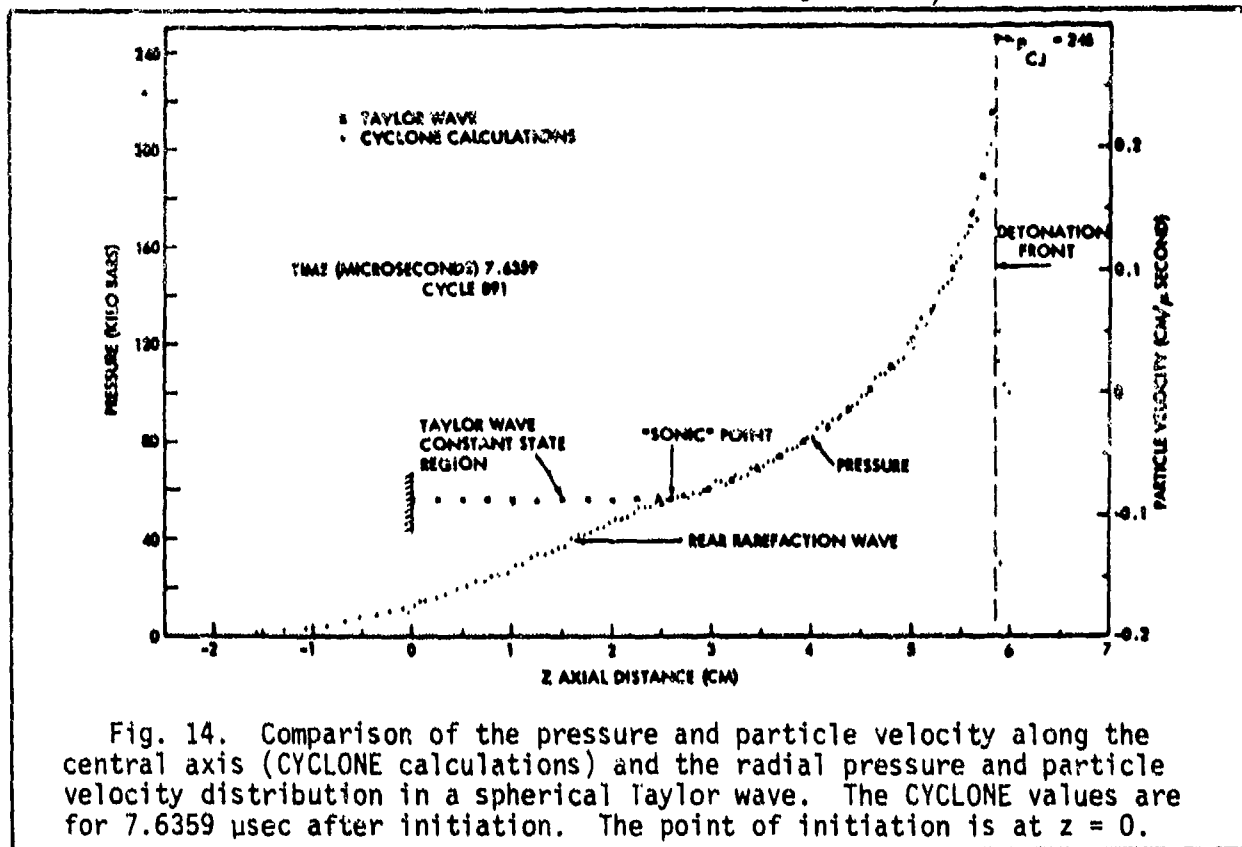


Fig. 14. Comparison of the pressure and particle velocity along the central axis (CYCLONE calculations) and the radial pressure and particle velocity distribution in a spherical Taylor wave. The CYCLONE values are for 7.6359 μ sec after initiation. The point of initiation is at $z = 0$.

The two computations coincide from the detonation front down to the sonic point (the point at which the particle velocity is zero). Thereafter, they diverge. The significant feature to note is that the pressure gradient near the detonation front is very large. Thus, it is very unlikely that it will ever be possible to measure the ideal CJ pressure^{††}. A good reason to use a plane wave generator to initiate cylindrical charges (instead of point initiation) is that

[†]G. Taylor, Proc Roy Soc. 200A, 235 (1950).

^{††}R. Cheret, "Theoretical Considerations on the Propagation of Shock and Detonation Waves," Fourth Symposium (International) on Detonation ONR, ACR-126, U. S. Govt. Printing Off., Washington, DC, 1967; pp 78-83.

this makes the shock front less curved and the gradient less steep.

How to Determine the Pressure in the Acceptor Material

We have described how the gas pressure P_g at the attenuator side of the attenuator-acceptor interface is determined. Since critical initiating pressure is the best measure we have of the shock sensitivity of a material, we wish to determine the pressure transmitted into the acceptor. To do this, we must know the unreactive Hugoniot for the acceptor material.

It is most convenient to have the Hugoniot plotted in the pressure versus particle velocity plane. This is because both pressure and particle velocity must be continuous across the boundary between the attenuator and acceptor materials—both before the shock passes and after it passes. As an example, consider the shock passing from PMMA (density 1.18 g/cm^3) into cast TNT (density 1.62 g/cm^3).

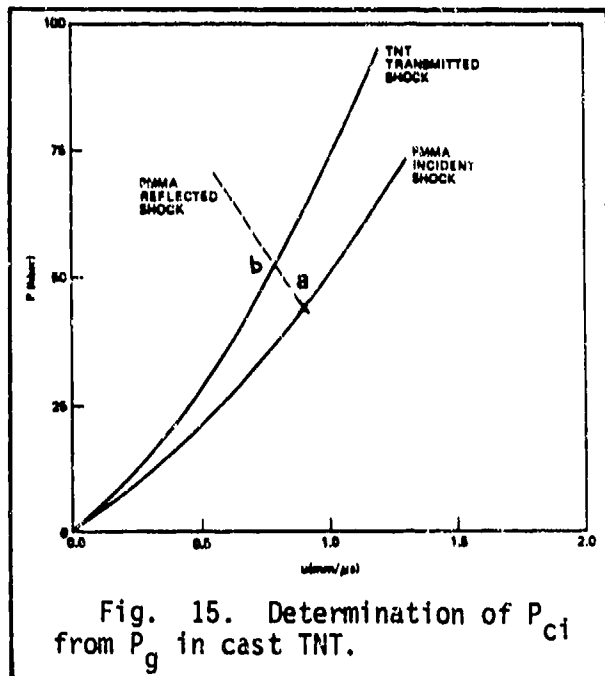


Fig. 15. Determination of P_{ci} from P_g in cast TNT.

The Hugoniots[†] are shown in Figure 15. The curve labeled "PMMA incident shock" is the PMMA Hugoniot for rightward traveling shocks which start from an initial state in which pressure and particle velocity are zero. The gap pressure P_g for a probability of one-half for the detonation is about 45 kbar. Thus the state of the shocked PMMA is represented by

the point labeled "a" on the Hugoniot. As the shock passes through the boundary, a shock is transmitted into the acceptor and a wave

[†]See, for example, High Pressure Physics and Chemistry, Vol. 2, Ed. by R. S. Bradley, Academic Press, New York, 1963, p. 222.

(which in general could be either a shock or a rarefaction; it is a shock in this case) is reflected back into the PMMA. As the reflected shock propagates back into the PMMA, there is a change of state (i.e., pressure and particle velocity) in the PMMA which is described by the PMMA Hugoniot for waves traveling to the left and starting from state "a". This Hugoniot is the dashed curve in Figure 15 and is simply the PMMA incident shock Hugoniot reflected about a vertical line through "a". The shock transmitted into the TNT produces a change of state from an initial state with zero pressure and particle velocity to some final state of, as yet unknown, pressure and particle velocity. This change of state is determined by the Hugoniot curve labeled "TNT transmitted shock" which is the non-reactive TNT Hugoniot for waves traveling to the right and passing through zero pressure and particle velocity. Since pressure and particle velocity must be continuous across the boundary, the point where this curve intersects the PMMA reflected shock Hugoniot gives the pressure and particle velocity in the transmitted and reflected waves. This point is labeled "b" in Figure 15. This gives us the pressure in the acceptor material which we call P_{ci} , or critical initiating pressure.

In the example shown in Figure 15, the acceptor Hugoniot is steeper than the attenuator Hugoniot, so the transmitted shock has a higher pressure than the incident shock (the transmitted particle velocity is lower). Also, the reflected wave is a shock since it has an increased pressure over the incident wave. If the Hugoniot for the acceptor is less steep than that of the attenuator, the transmitted shock will have a lower pressure than the incident shock and the reflected wave will be a rarefaction. Since a rarefaction wave is isentropic, we must use the isentrope for the reflected

wave in the PMMA and not the Hugoniot.

According to Eq. (1), the steepness of the Hugoniot is determined by the quantity $\rho_0 U$ which is called the shock impedance and is the product of the initial density of the material and the shock velocity. Most voidless explosives are of greater density than PMMA and so have a higher shock impedance. Thus, the transmitted shock will have a higher pressure and lower particle velocity than the incident shock. There are some porous, granular explosives with lower densities than PMMA and their Hugoniots lie well below the PMMA Hugoniot. In these cases, we have a problem since, in order to determine the transmitted pressure, we need the rarefaction isentrope for PMMA as well as the shock Hugoniot for the granular material[†].

[†]If the voidless form of the explosive has a known non-reactive Hugoniot, there are various methods to predict the non-reactive Hugoniot of the corresponding porous charge and the approximations are good as shown by checks on the inert materials. Unless the equation of state (PVT relation) for a material such as PMMA is known, there is no way to predict the isentrope. However, the denser the material, the nearer the isentrope is likely to be to the Hugoniot and the approximation of the one by the other is common in metals at pressures greater than 50 kbar.

LECTURES ON DETONATION PHYSICS

Lecture #8 - 26 January 1981

by

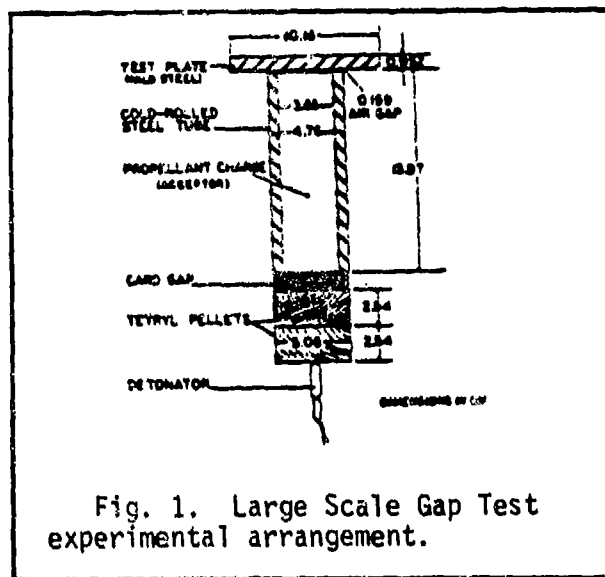
DONNA PRICE

Notes by Frank J. Zerilli

The Large Scale Gap Test - II

Introduction

In the last lecture, we examined the divergent flow produced during the detonation following the point initiation of a standard donor and the transmission



of a shock into the attenuator. The calibration of the donor-attenuator system to determine the pressure in the attenuator as a function of attenuator thickness (gap) was described. Finally, the method for determining the pressure transmitted into the attenuator was outlined. We found that, in the donor, the detonation front expanded spherically from the point of initiation so

that the radius of curvature was equal to the distance travelled by the detonation front.

What Happens When the Shock Enters the Attenuator

The amplitude of the shock decreases as it travels through the attenuator, and the curvature changes as if the PMMA were an extension of the donor for about the first 25 mm or so. Then, at about 25 mm into the PMMA, at a radius of curvature of 76 mm, there is an abrupt increase in the curvature with the radius

of curvature dropping to about 66 mm. Thereafter, the shock expands spherically again. The increase in curvature is due to the lateral rarefaction effect. There is a comparable effect on the pressure which will be discussed later.

Effect of Confinement on the Gap Test

There is another rarefaction effect that is relevant to the use of the Large Scale Gap Test to determine critical initiating pressures. This concerns the behavior of the standard test with and without the standard confining steel sleeve around the acceptor.

Effect of Confinement: Experimental Work

An experiment was done in which the progress of the detonation front in the acceptor was observed under the condition of standard confinement and under the condition of no confinement.[†] The progress of the front was followed by using the continuous wire method, described previously.^{††} The acceptor material was cast DINA (diethanol nitramine dinitrate) with a melting point of 52.5°C. DINA

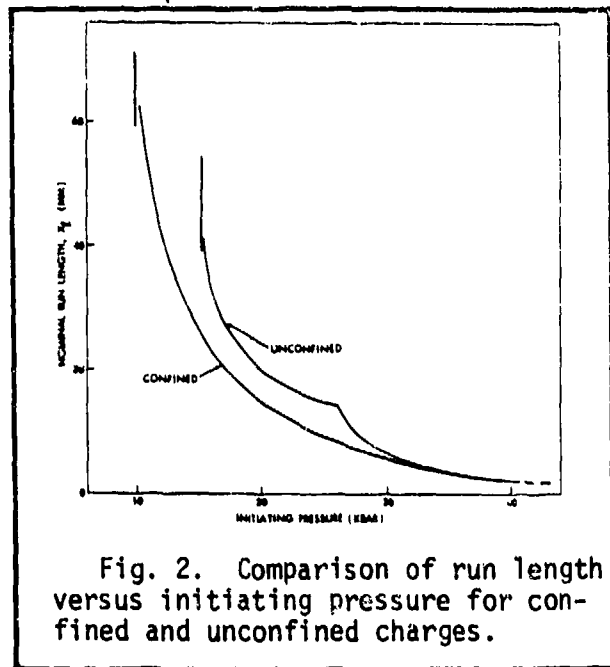


Fig. 2. Comparison of run length versus initiating pressure for confined and unconfined charges.

is very easy to cast and to work, but it is fairly shock sensitive, quite close to 50/50 pentolite (50% TNT and 50% PETN) in shock sensitivity. The distance between the point of entry of the shock into the acceptor to the onset of detonation was plotted as a function of the pressure transmitted into the acceptor. The results are shown in Fig. 2. We see that the

[†] D. Price, J. P. Toscano, and I. Jaffe, NOLTR 67-10, April 1967.

^{††} Lecture #4, this series, 3 Nov 1980.

higher the initial pressure, the shorter the run length to detonation for both the confined and unconfined situation. As the initiating pressure approaches the critical initiating pressure, the run length becomes larger and larger. For large initiating pressures, the two curves coincide. For

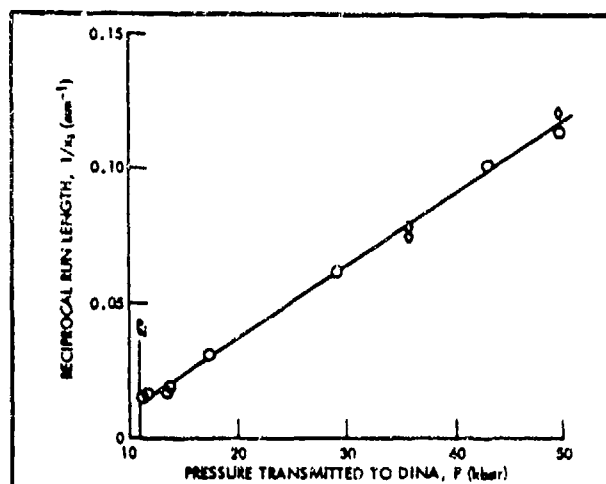


Fig. 3a. Reciprocal run length versus pressure for confined DINA.

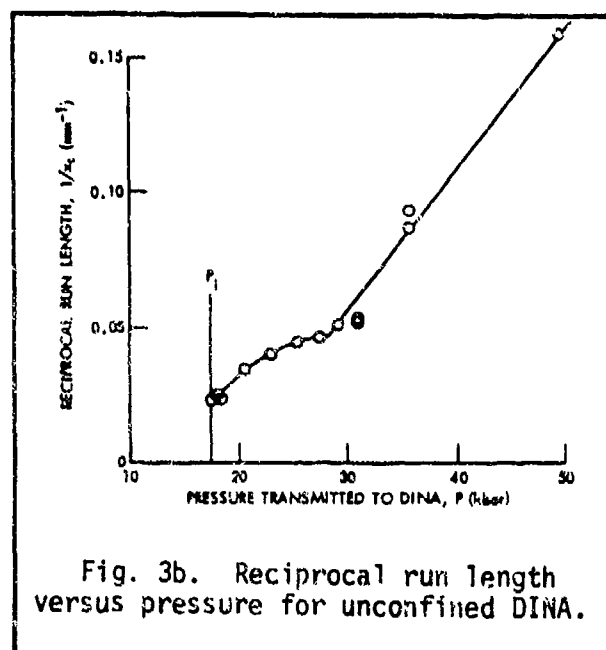


Fig. 3b. Reciprocal run length versus pressure for unconfined DINA.

smaller pressures, they diverge and approach different critical pressures. The curve for the confined explosive is smooth, but the curve for the unconfined explosive has a cusp. The cusp was located experimentally in numerous runs and exists for the same reason as the cusp in the PMMA calibration: it results from the effect of the lateral rarefaction. The same data plotted in another fashion[†] are shown in Figs. 3a and 3b. Here the reciprocal run length is plotted as a function of pressure. Figure 3a shows the data for confined DINA. The three diamond shaped points in Fig. 3a, however, are taken from the data for unconfined DINA and show the agreement in data for confined and unconfined charges for the first few millimeters of run length. Figure 3b shows the cusp in the data for unconfined DINA.

[†] D. Price, A. R. Clairmont, JR., and J. D. Erkman, NOLTR 74-40, March 1974.

We conclude from this comparison that the confinement of the acceptor in the standard large scale gap test prevents the lateral rarefaction from producing a large disturbance. The confinement gives a result which is comparable to that which would be obtained for a very much larger diameter unconfined charge. The result may even approach that which would be obtained in one dimensional flow.

Effect of Confinement: Numerical Computations at Livermore

Numerical computations done at Livermore[†] using the DYNA two dimensional hydrocode support the suggestion that the flow may approach one-dimensional flow. The available printouts are for a gap of 1.5 inches of PMMA and appear in Fig. 4, which shows the lattice distortion and isobars at times between 0.96 μ s and 18 μ s after initiation. For each time, the lattice distortion is shown in the top figure and isobaric contours in the bottom figure. Each lattice is divided into several fields. The bottom-most field is the donor, the next field is the first inch of PMMA, the next field is the other half inch of PMMA, and the last field is the acceptor and its confinement. The acceptor field is divided into sub-fields, the first subfield (the layer next to the PMMA) having a smaller cell size in the computation.

At 0.96 μ s we see the early spherical wave from the point initiation, at 2.97 μ s the wave has expanded almost to the sides, and at 6 μ s the wave has progressed through most of the donor. The numbers at the top of the isobaric contours are the pressures of the leading isobars.

[†] Unpublished.

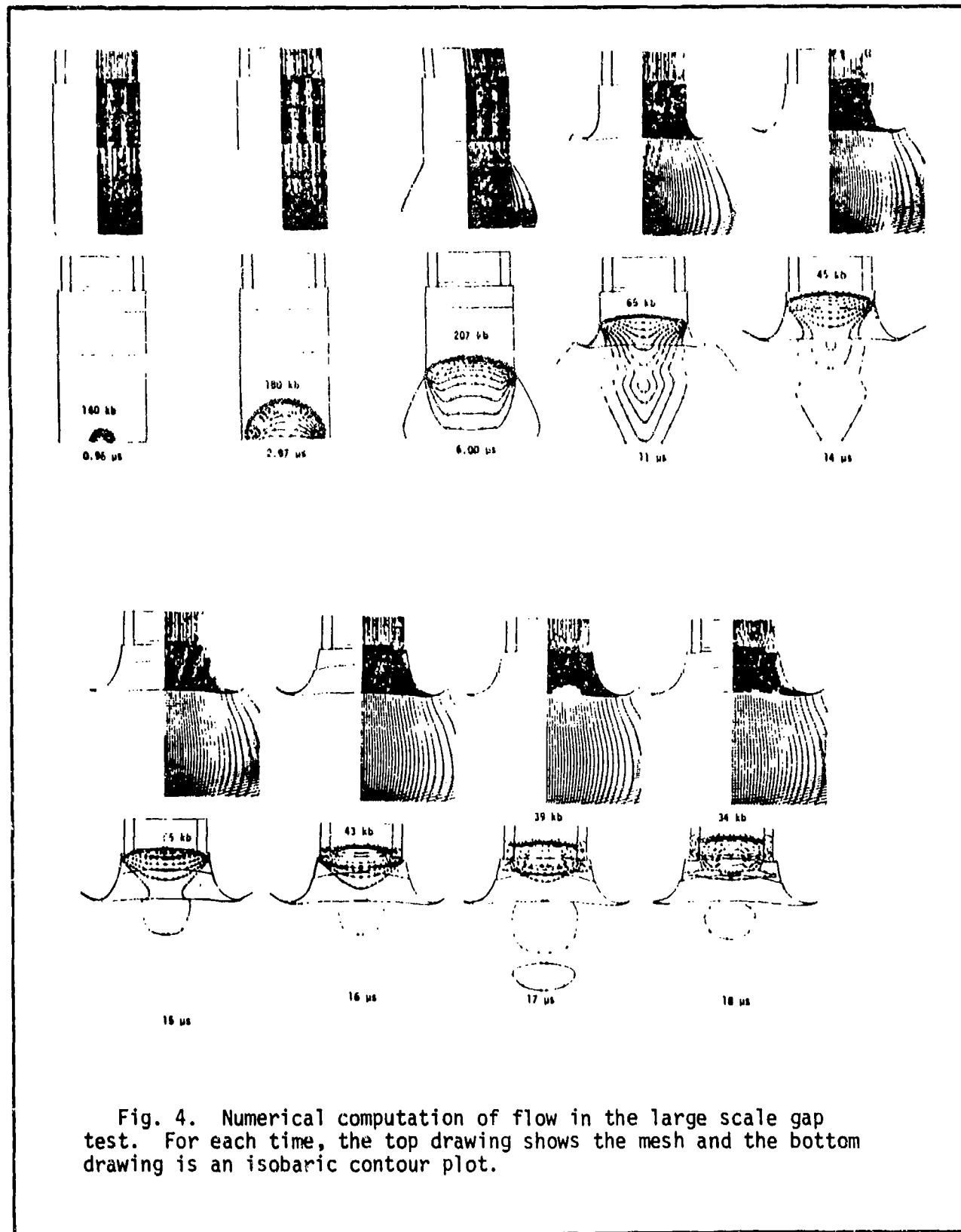


Fig. 4. Numerical computation of flow in the large scale gap test. For each time, the top drawing shows the mesh and the bottom drawing is an isobaric contour plot.

At 11 μ s, the detonation has progressed through the donor and the transmitted shock has progressed through nearly an inch of PMMA. Note that the pressure has fallen to 65 kbar at this point. At 14 μ s, the shock has progressed to the PMMA side of the interface between the attenuator and the acceptor and the pressure is down to 45 kbar.

At 15 μ s, the shock has crossed the interface into the acceptor. The acceptor is assumed to be PBX 9404 which has a density of 1.83 g/cm^3 and the unreactive Hugoniot is used in the computation so that no reaction occurs in the resulting calculation. The pressure has increased to 55 kbar as required by the conservation laws and boundary conditions when a shock moves into a material of higher shock impedance. The increase is greater than in the typical case, since PBX 9404 has higher density than most non-aluminized explosives.

The important thing to note is that the shock front has fairly low curvature when it enters the acceptor and it flattens out (as it progresses through the acceptor) somewhat more rapidly than would be expected solely from spherical expansion[†]. This appears to be a result of the steel confinement. Thus, the computation supports the hypothesis that the standard large scale gap test behaves in a manner approximating a planar (one-dimensional) system.

Figure 5 compares gap pressure vs. gap thickness obtained from the Livermore computations to the NSWC calibration for the large scale gap test. The triangles are points obtained from the computation, the circles are points from the current calibration curve. The pressures obtained from the computation are somewhat higher than the calibration curve values because a density of 1.73 g/cm^3 was used for the tetryl donor in the computation, while the density of tetryl in the standard gap test is 1.53 g/cm^3 . The shape of the computed curve compares well with the calibration curve except that the jog due to lateral rarefaction does not show up in the computed curve. However, the number of computed

[†] Also, the pressure is decreasing since the non-reactive Hugoniot has been used in the calculation so that no reaction occurs in the acceptor.

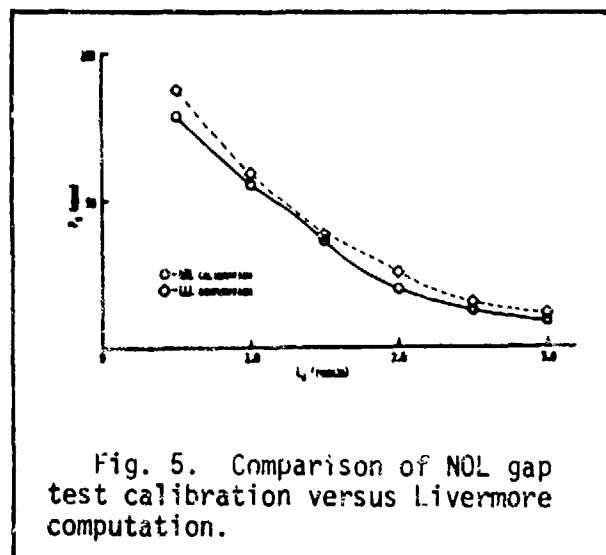


Fig. 5. Comparison of NOL gap test calibration versus Livermore computation.

points is too small to show such a jog and, in addition, the pressures were obtained from the pressure of the leading isobar. This would produce an error of the order of ten percent. Thus, considering the limitations of the calculation, the agreement is good.

Shape of the Pressure Pulse

A pressure versus time curve was also obtained from the Livermore computations.

The pulse shape is shown in Fig. 6. The pulse has a width at half amplitude of

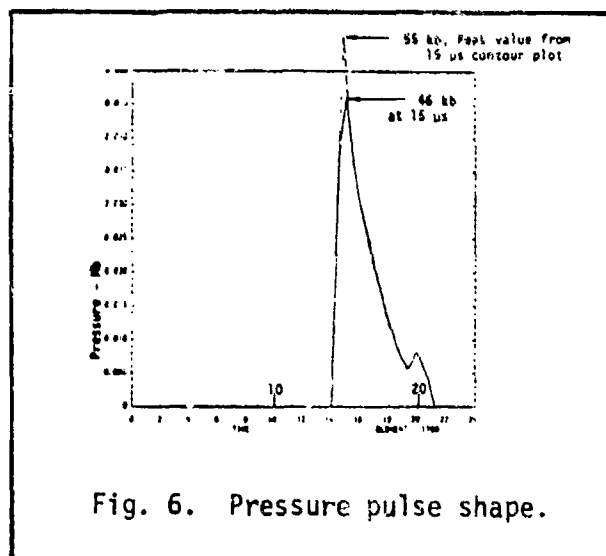


Fig. 6. Pressure pulse shape.

about 3 μ sec and a total duration of about 6 to 7 μ sec. This agrees in order of magnitude with what was determined earlier from an optical study of shocked PMMA.[†] Figure 7, taken with the Jacobs focal plane framing camera, shows the curved shock entering the PMMA. The opaque areas following the shock are due to the spalling (break up) of the PMMA

produced by the change from compression in the shock to tension induced by the arrival of following rarefaction waves. The width of the compression pulse is the distance between the shock front and the beginning of the opaque area. Knowing the writing speed of the camera and the shock speed in the PMMA, an estimate of

[†] I. Jaffe, J. Toscano, and D. Price, NOLTR 64-66, Sept. 1964.

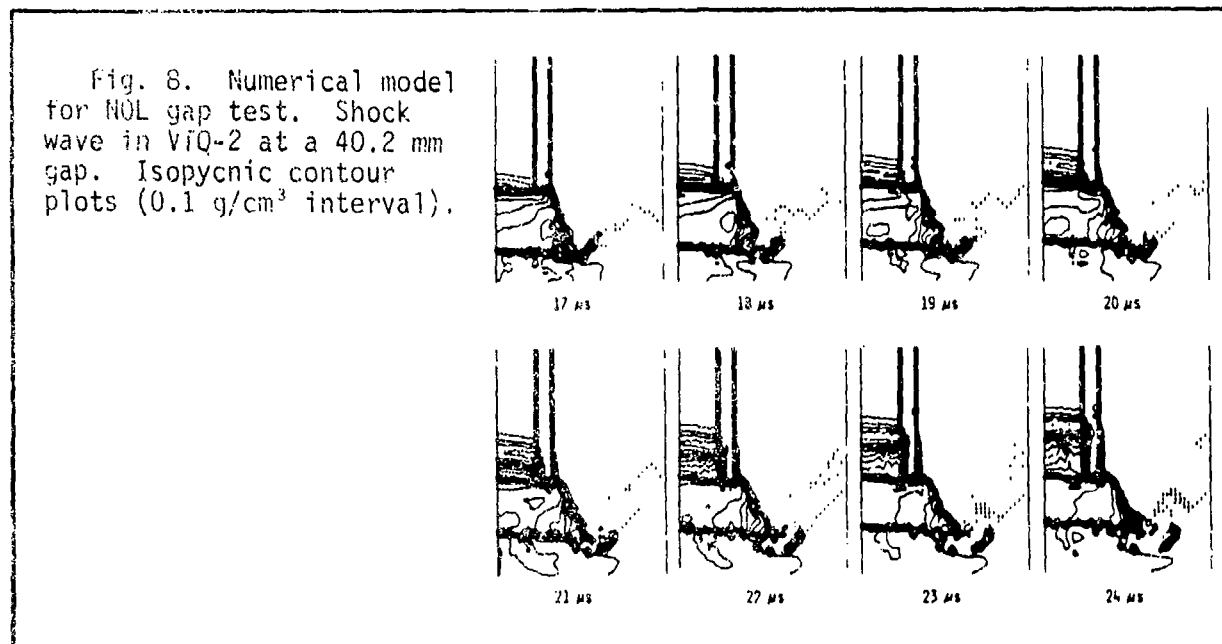


Fig. 7. Shock front after 33 mm travel in Plexiglas (Jacobs Camera).

the duration of the shock can be made. From Fig. 7, it can be estimated that the duration of the shock just as it enters the PMMA is about one or two microseconds. The width of the shock increases as it travels through the PMMA (in addition, of course, its amplitude decreases).

Effect of Confinement: Numerical Computations at LASL

Another numerical computation for the NOL gap test was done at Los Alamos Scientific Laboratory[†]. The results shown in Figure 8 are for the large scale

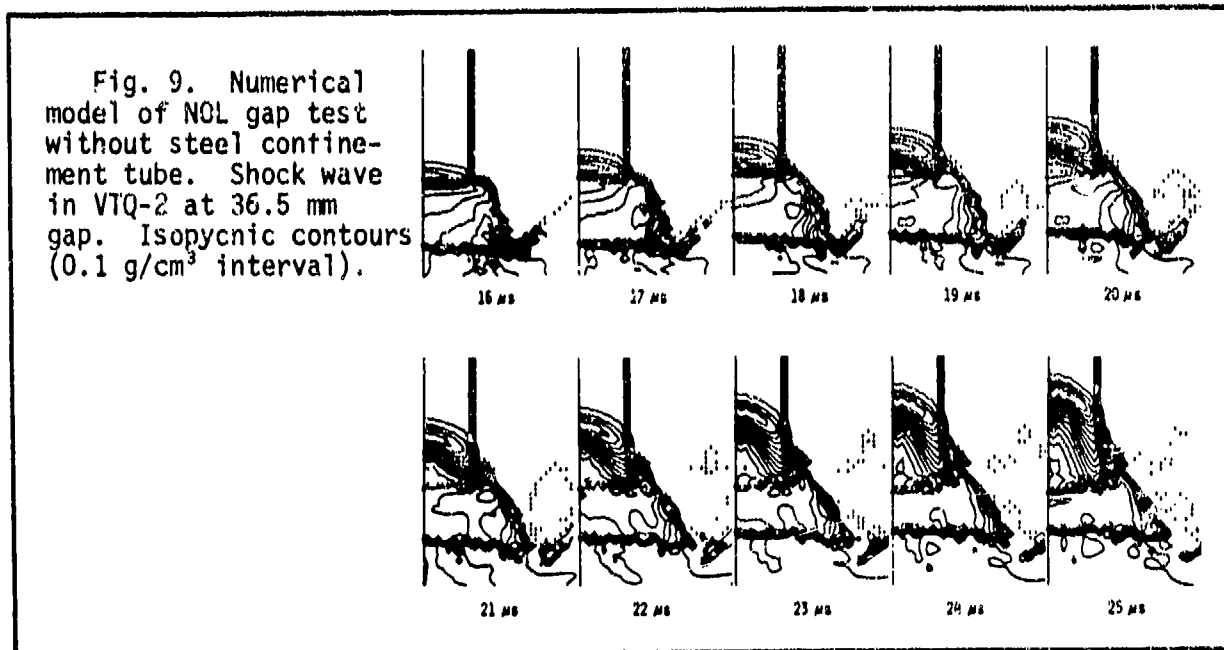


[†] A. L. Bowman, J. D. Kershner, and C. L. Mader, LA-8408, October, 1980.

gap test with confinement. A reactive code (Forest Fire) was used so that the computations follow the transition to detonation in the acceptor. Only the half of the cylinder to the right of the longitudinal axis is shown since the other half is the mirror image. The contours shown are isopycnics, that is, lines of constant density. The isopycnics will show the same general variation as the isobars.

The shock entered the acceptor at some time between 16 and 17 μsec . The first plot in Fig. 8 is for the time 17 μsec — the shock has already entered. As the shock progresses, it flattens out due to the interaction with the steel confinement. The reaction appears to start at the walls and not at the center. It is not known whether this is correct or if it is an artifact of the reaction code. The actual detonation is not shown in this series which ends at 24 μsec . The detonation occurs at about 25 μsec .

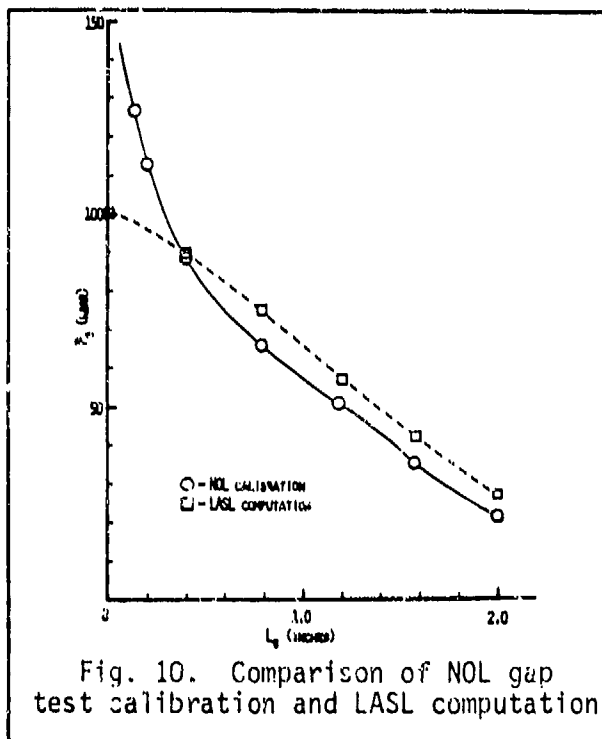
The same computation was carried out for the case of an unconfined acceptor. The results are shown in Fig. 9. Again, a curved shock front enters the



acceptor, but in this case, the curvature increases as the wave progresses. The reaction starts at the longitudinal axis, but the actual detonation occurs at about 26 μ sec, so it does not appear in the series shown in Fig. 9.

What's Wrong with the LASL Computation

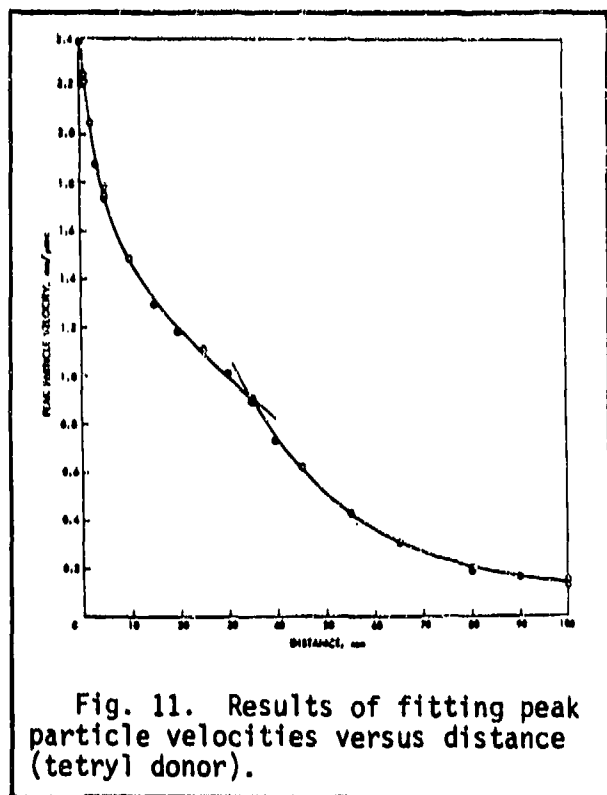
All agree that the shock transmitted into the attenuator must be less than that which would be transmitted in the case that the donor achieved the ideal C-J pressure, since the pressure gradient is so large (as we have discussed above). But the LASL investigators used what was called a "C-J volume burn" to compute the pressure achieved in the standard donor. This gave a value of 145 kilobars in the donor (compared to an ideal C-J pressure of 228 kilobars) prior to the transmission of the shock into the PMMA. It also predicted a steady pressure (with a very small gradient) transmitted from the donor to the attenuator. This is at variance with all measurements and



with the Taylor wave and CYCLONE numerical computations which indicate an extremely steep gradient. In fact, as shown in Fig. 10, the LASL computation gives results which diverge strongly from the NSWC calibration for the first 10 mm of PMMA attenuator. Beyond the first 10 mm, the LASL calculations parallel the NSWC calibration, but lie above it by an amount which is about the maximum estimated experimental error.

If we examine the results of the Taylor wave and CYCLONE code calculations (see Lecture #7, Fig. 14), it is very difficult to believe that a shock with a nearly constant pressure of 103 to 90 kbar for the first 10 mm of attenuator could be transmitted into the attenuator.

None of the experimental data supports this. We can infer the shape of the pressure distribution from the shock or particle velocity versus distance curves. The shock velocity versus distance curve has a very steep gradient for small distances into the attenuator (see Lecture #7, Fig. 4). To be fair we should note that the curve is not too accurate for distances between zero and five millimeters since streak records cannot be well resolved in that region and it is subject to differentiation errors (as discussed in Lecture #7). However, the curve of particle velocity versus distance is not



subject to differentiation errors and the particle velocity has been measured right up to nearly zero attenuator thickness. This curve (see Fig. 11) also shows a very steep gradient thus implying a very steep pressure gradient.

The particle velocities can be converted into pressure in the PMMA by using the PMMA Hugoniot. The relation between shock velocity and particle velocity for PMMA is

$$U = 2.561 + 1.595 u \quad (1)$$

where the velocities are in mm/μs.

Equation (1) is valid for $u > 0.54$ mm/ μ s. The momentum conservation (shock impedance) relation is

$$P = \rho_0 U u \quad (2)$$

Thus, the PMMA Hugoniot is

$$P = 1.185(2.561 + 1.595u)u \quad (3)$$

where P is the pressure in GPa (1 GPa = 10 kbar). Table 1, below, shows pressures calculated from Equation (3) for several small gap lengths and compares the pressures so calculated with the pressures from the standard large scale gap test calibration curve. The calibration curve pressures agree with the pressures calculated from particle velocity to within 5% for gap thicknesses of 2.5 mm or

Table 1. Gap pressure P_g calculated from particle velocity measurements and compared with calibration curve P_g .

Gap Thickness L_g (mm)	Measured Particle Velocity u (mm/ μ s)	Calculated Gap Pressure P_g (kbar)	Calibration Gap Pressure P_g (kbar)
0	2.37	178	213
2.5	1.98 (interpolated)	134.6	142
5.0	1.77	113	112
10.0	1.50	88	88.5

greater. The reason for the larger discrepancy at zero thickness is that the calibration curve was forced to have the value 213 kbar at zero thickness since that is the value which would be transmitted into the attenuator if the donor actually achieved the ideal C-J pressure. The shock velocity data also agrees with the particle velocity data. The smoothed shock velocity versus gap thickness curve extrapolates to a value of 6.25 mm/ μ s at $L_g = 0$. This gives a value of P_g of 171 kbar for $L_g = 0$. Hindsight shows us that it would have been more accurate

not to mix in this bit of theory, but to rely more heavily on the actual measurements. In any case, the steepness of the gradients in pressure, particle velocity, and shock velocity versus distance makes the results of the LASL computation of the shock loading of the PMMA questionable.

Does Gap Pressure Correlate With Critical Initiating Pressure?

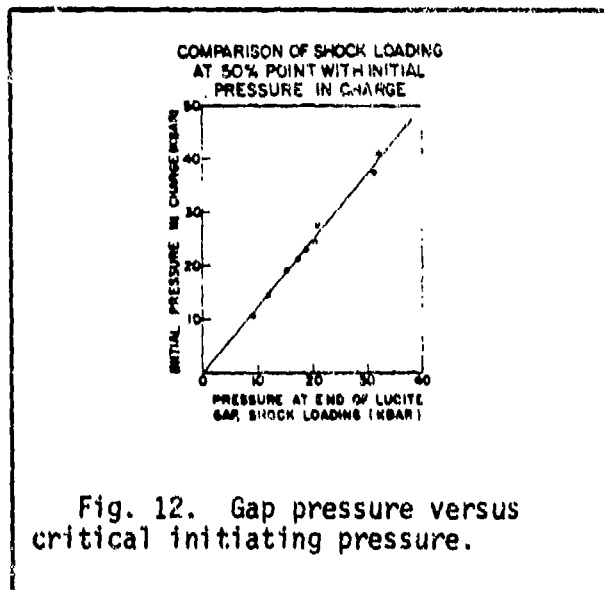


Fig. 12. Gap pressure versus critical initiating pressure.

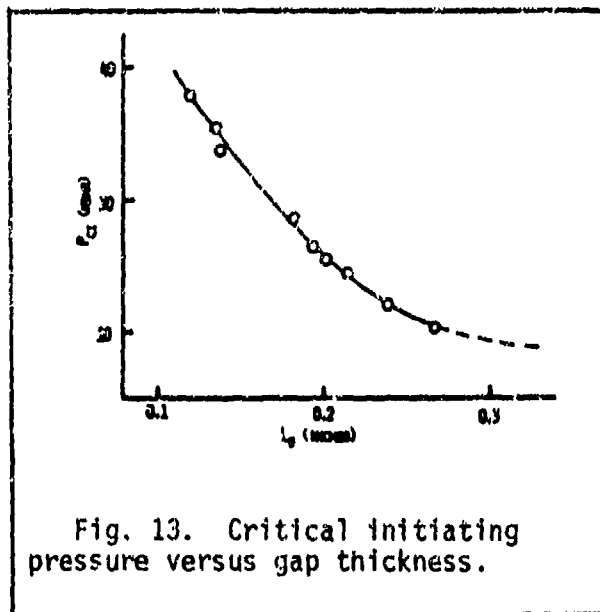


Fig. 13. Critical initiating pressure versus gap thickness.

Figure 12 compares gap pressure P_g against critical initiating pressure P_{ci} for several cast and pressed explosives which are nearly voidless[†]. The correlation is good and it is linear as far as can be determined from the precision of the data. Using P_g instead of P_{ci} merely compresses the scale, with a range of P_g of 33 kbar corresponding to a range of P_{ci} of about 42 kbar. Figure 13 compares critical pressure against gap thickness. For high sensitivity (i.e., low P_{ci}) explosives, the scale in terms of gap thickness becomes greatly expanded. A plot of P_{ci} versus the log of gap thickness would be more nearly linear, since the pressure in the attenuator decreases approximately exponentially with distance.

If we compare gap pressure for cast TNT which is nearly voidless to gap pressure for 50% TMD ammonium perchlorate

[†] D. Price and I. Jaffe, ARS Journal, 31, 595 (1961).

which is very porous we find a large compression of the sensitivity scale as can be seen in the table below.

<u>Material</u>	<u>Density (g/cm³)</u>	<u>P_g (kbar)</u>	<u>P_{ci} (kbar)</u>
cast TNT	1.61	31	37
ammonium perchlorate	0.85	15	5

Effect of Porosity on Relation Between Gap Pressure and Initiating Pressure

Porosity has a great effect on the gap pressure and critical initiating pressure. In the example above, the effect of porosity did not change the relative ordering, but, in general, it could. Figure 14 illustrates the effect of degree of compaction on ten different organic explosives[†]. The measured gap pressure is plotted against percent of theoretical maximum density.

Note that the curve for dinitrotoluene (DNT) approaches an infinite slope near 100% TMD. The curves for the nitroguanidines (NQ-1 and NQ-h) also approach infinite slopes for high density. This behavior is to be expected for group II explosives and is an indication of the approach to critical conditions for the propagation of steady state detonation. The approach to critical conditions was confirmed by making a scaled, slightly smaller version of the large scale gap test. In the smaller scale test, the dinitrotoluene and the nitroguanidine could be dead pressed and could not be initiated with a standard donor. In the standard small scale gap test^{††}, almost every explosive that has been tested shows the large increase in slope as 100% TMD is approached.

Whenever a very steep slope appears on a sensitivity curve, it is necessary to determine whether critical conditions for propagation of detonation are being approached, since approach to critical conditions increases the required

[†] D. Price, A. R. Clairmont, Jr., and J. O. Erkman, NOLTR 74-40, March 1974.

^{††} In the standard NOL small scale gap test, the acceptor is confined in a brass sleeve which has an inside diameter of 0.2" and an outside diameter of 1".

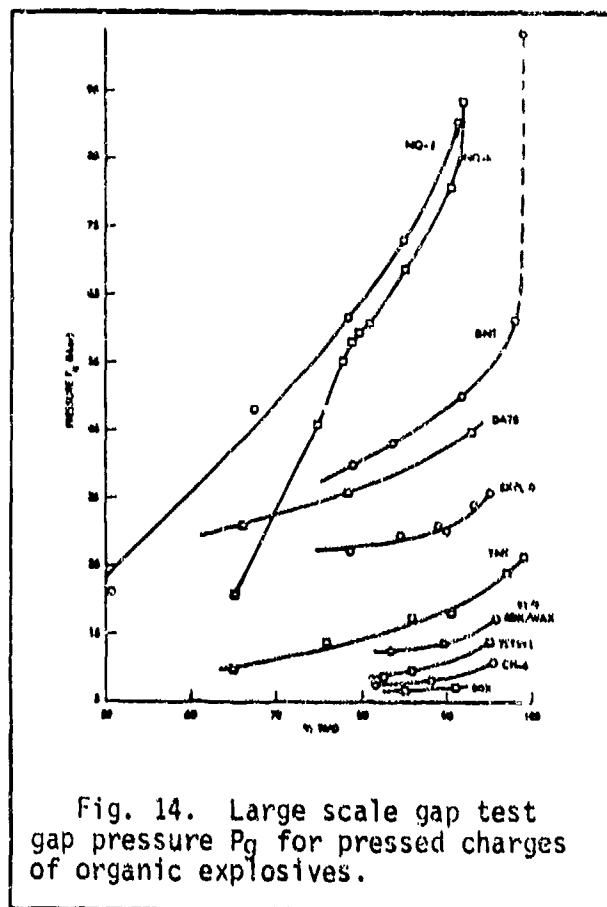


Fig. 14. Large scale gap test gap pressure P_g for pressed charges of organic explosives.

initiating pressure and so distorts the sensitivity ratings. Thus, in order to get a correlation between the NOL small scale and the large scale gap tests, the portion of the small scale gap test values where critical conditions are being approached is not considered.

The curve for high bulk density nitroguanidine (NQ-h) in Fig. 14 shows an odd change in slope at about 78% TMD. It is believed that as the loading density decreases, steady state detonation is replaced by low velocity pseudo-detonation. The low velocity detonation[†] is a metastable reaction travelling at constant

velocity. It is supersonic, with speeds as high as 4 to 5 mm/ μ s and the energy release is of the same order of magnitude as the energy released in steady state detonation (quite enough to punch a hole through the witness plate). The gap test would have to be suitably instrumented to verify that the phenomenon is, in fact, due to low-velocity detonation. A similar phenomenon has not yet been observed in low bulk density nitroguanidine.

The trends in P_g versus % TMD are the same for all porous explosives, both Group 1 and Group 2. The higher the % TMD, the higher P_g , which means the less sensitive the explosive. The more porous the explosive, the more sensitive it is.

[†] The low velocity detonation was observed in NQ-h every time the charge diameter fell below the critical diameter for a given density. See Lecture #3, this series, pp. 9-11 for a more complete description.

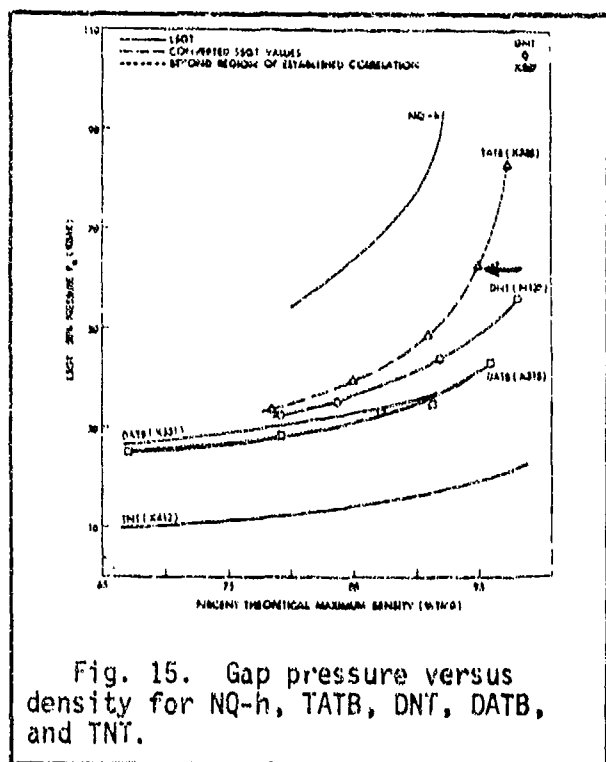


Fig. 15. Gap pressure versus density for NQ-h, TATB, DNT, DATB, and TNT.

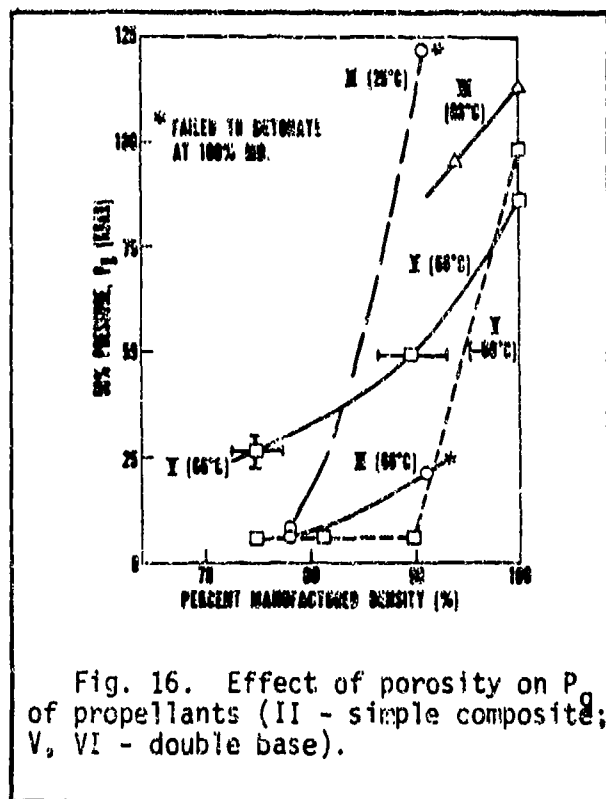


Fig. 16. Effect of porosity on P_g of propellants (II - simple composite; V, VI - double base).

The correlation between the large scale gap test and the small scale gap test was used to obtain a gap pressure versus density curve for TATB (1,3,5-triamino-2,4,6-trinitrobenzene), one of the more insensitive explosives[†]. The only point actually obtained in the large scale gap test is the one marked by the arrow in Fig. 15. The other points were obtained from the correlation between the small scale gap test and the large scale gap test because the supply of TATB was inadequate for more than one large scale gap test. Also of interest in Fig. 15 is the comparison of large scale gap test data for two different batches of DATB. The curves agree quite well.

Propellants show the same trend as explosives. Figure 16 shows data for three propellants at three different temperatures (the explosives were all shot at a conditioned temperature of 25°C)^{††}. Propellant number II is a simple composite propellant consisting of ammonium perchlorate and an organic fuel. It will not

[†] Data in NOLTR 74-40, previously cited.

^{††} D. Price, I. Jaffe, and G. E. Roberson, *Ind. Chim. Belge.*, 1967, 32 (Spec. No.), 506-510.

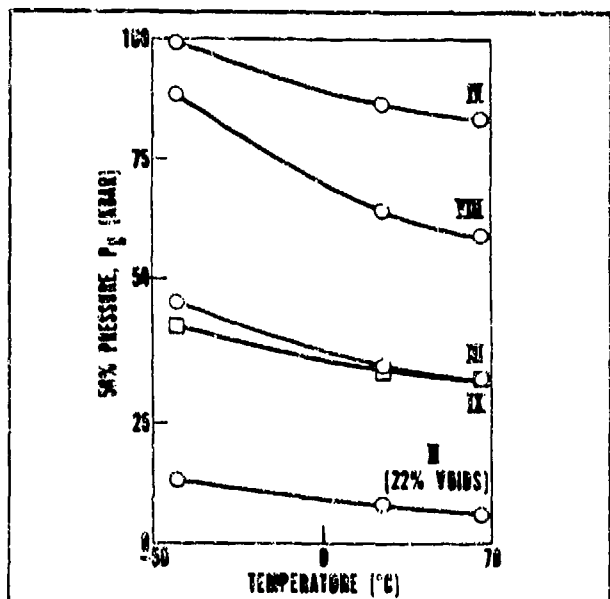


Fig. 17. Effect of temperature on P_g of explosives (II - simple composite; III - composite + HE; IV, IX - double base; VIII - double base plus AP and/or Al).

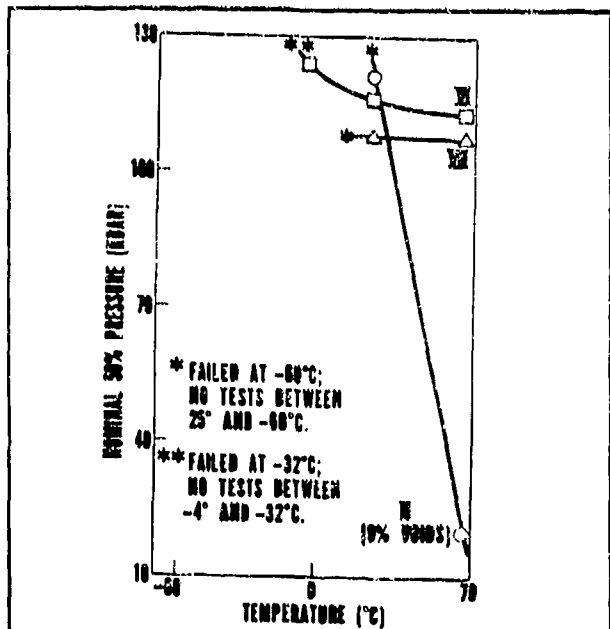


Fig. 18. Effect of temperature on P_g of explosives (II - simple composite; VI, VII - double base).

detonate in the LSGT at 100% TMD but it will detonate if there is some porosity in it. The other materials are double-base propellants consisting of nitrocellulose and nitroglycerine, both of which are explosives. These will detonate in the LSGT at 100% TMD, but colloidng of nitrocellulose with nitroglycerine makes the product somewhat less sensitive than either of the components separately.

Effect of Temperature on Gap Pressure

Figure 17 illustrates the effect of temperature on the gap pressure P_g of explosives[†]. The materials in Fig. 17 are used as propellants but the effect illustrated is the same for any material in which the reaction rate increases with increase in temperature -- the higher the temperature, the lower P_g .

Some materials that exhibit a more drastic effect with change in temperature are illustrated in Fig. 18. Materials II, IV, and VII failed at the lowest temperatures but did detonate at higher

[†] Price, Jaffe, and Roberson, op. cit.

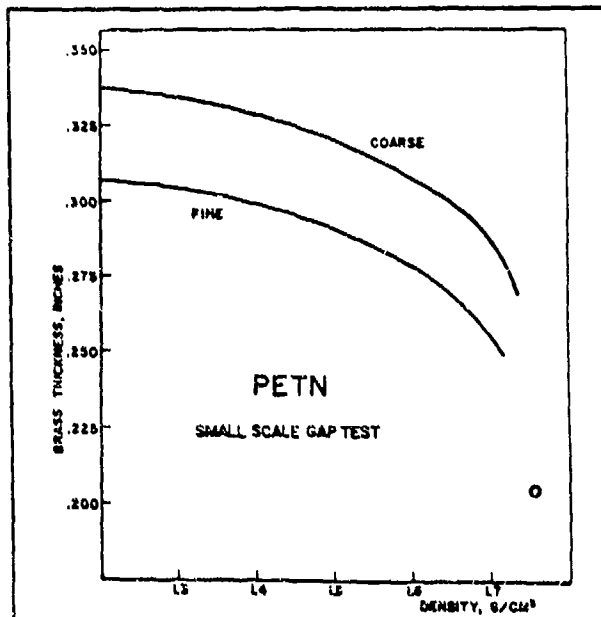


Fig. 19. Small scale gap test for two samples of PETN. Coarse material has specific surface of 3500 cm²/g, fine has specific surface of 10,000 cm²/g.

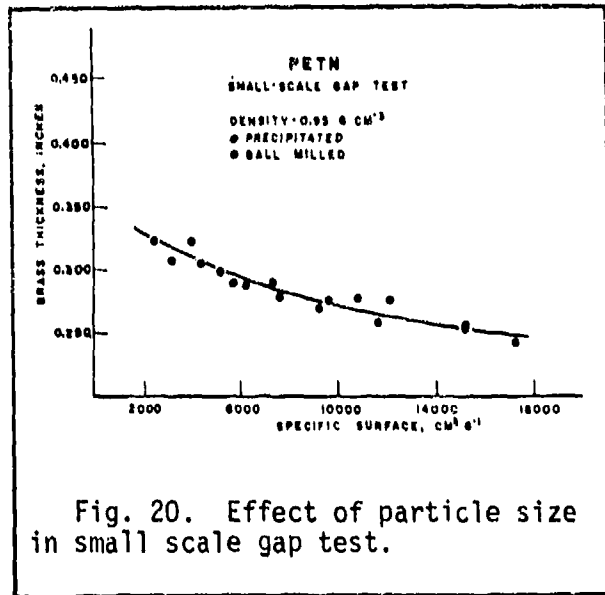


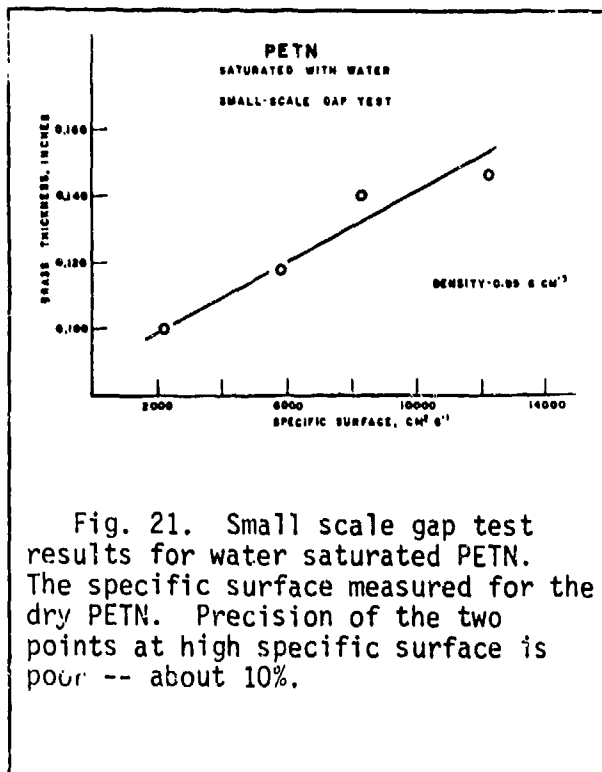
Fig. 20. Effect of particle size in small scale gap test.

temperatures. This indicates that there was a critical temperature somewhere in between the temperature at which they failed and the temperature at which they first detonated. Material II failed to detonate at 25°C, and showed a tremendous increase in sensitivity at 66°C. The very large variation is an indication of approach to a critical condition.

Effect of Particle Size on Gap Pressure

The effect of particle size is illustrated in Figs. 19, 20, and 21. The data was obtained by Seely[†] using PETN, a very sensitive explosive, in a porous form, which enhances its sensitivity, in the LASL small scale gap test. Figure 19 shows the results for fine and coarse particle size PETN at various porosities. In all cases, the coarser material is more shock sensitive (larger gap thickness or smaller gap pressure for detonation 50% of the time).

[†] L. B. Seely, "A Proposed Mechanism for Shock Initiation of Low Density Granular Explosives," Proc. 4th Elec. Initiation Symposium, Franklin Institute, Philadelphia, 1963; Paper 27 of Rept. EIS-A 2357.



In Fig. 20, the effect of particle size is shown by plotting gap thickness versus specific surface area for a given density of PETN. Specific surface is the surface area of a unit mass of particles, so the smaller the particle size, the more surface per unit mass. Again the coarser the material, the more shock sensitive it is.

The effect of particle size shown in Figs. 19 and 20 is for materials in which the pores are filled with air or a vacuum. When the air is replaced with a condensed medium such as water, the trend is reversed, as shown in Fig. 21. Here the coarse material is less sensitive than the fine material. The mechanisms by which initiation occurs must differ in the two cases.

Seely suggested that, in the case of air filled pores, hot spots can be formed by the collapse of voids (this mechanism has since been supported by numerical computations). Also large particles can spall (break up) and produce high temperatures when impacting other large particles. However, if a condensed medium such as water fills the voids, the collapse of the voids and the motion of the spalled particles is inhibited. In this case, the most important mechanisms will be shock compression, friction, and shear, all of which can create hot spots. Initiation will be enhanced by a high density of hot spots; such a high density is easier to obtain with a large number of small particles of HE (high explosive) rather than with a smaller number of large particles of the same HE. Whatever the mechanism, it is at the explosive particle that the hot spot is located.

Thus in the case of voidless charges of pure cast explosives or explosives embedded in a matrix of condensed material, the sensitivity increases with

decrease in particle size. The situation becomes more complicated, of course, in the case of composite explosives with many components.

Effect of Composition on Gap Pressure

If wax is added to TNT or to RDX, the shock sensitivity is decreased, that is, the required initiation pressure is increased. On the other hand,

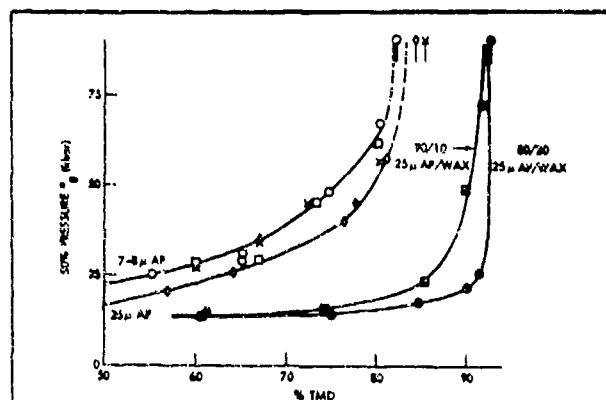


Fig. 22. Large scale gap test results for pressed charges of AP and AP/fuel (- AP 141, 7 μ ; - AP 145, 8 μ ; - AP 145/A1 95/5, 7 μ ; - AP 145/A1 90/10, 7 μ).

as illustrated in Fig. 22, if wax is added to ammonium perchlorate, its shock sensitivity is increased, that is, the required initiation pressure is lowered[†]. The decrease in required initiating pressure, the fact that the detonation velocity increases at the same time, and the nature of AP/wax as an oxidizer/fuel combination strongly suggest that an oxidation-reduction reaction is contributing to the observed behavior of AP/wax.

Adding aluminum to AP has different effects at different densities as Fig. 23 illustrates^{††}. At densities below 75% TMD, adding aluminum decreases the sensitivity (the gap is decreased so the pressure has increased), while at densities above 75% TMD, adding aluminum increases the shock sensitivity.

Adding aluminum to TNT at high compaction decreases the shock sensitivity as shown in Fig. 24^{†††}. This is true for both cast and pressed charges. Thus, the effect on TNT, a group 1 material, is opposite to that on AP, a group 2 material, at high compactions.

[†] D. Price, A. R. Clairmont, Jr., and J. O. Erkman, *Combustion and Flame*, 17, 323-336 (1971). See also NOLTR 69-16.

^{††} Data in NOLTR 74-40.

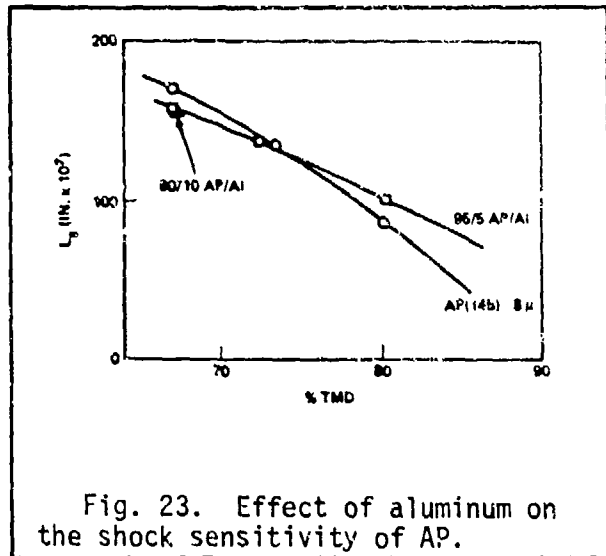


Fig. 23. Effect of aluminum on the shock sensitivity of AP.

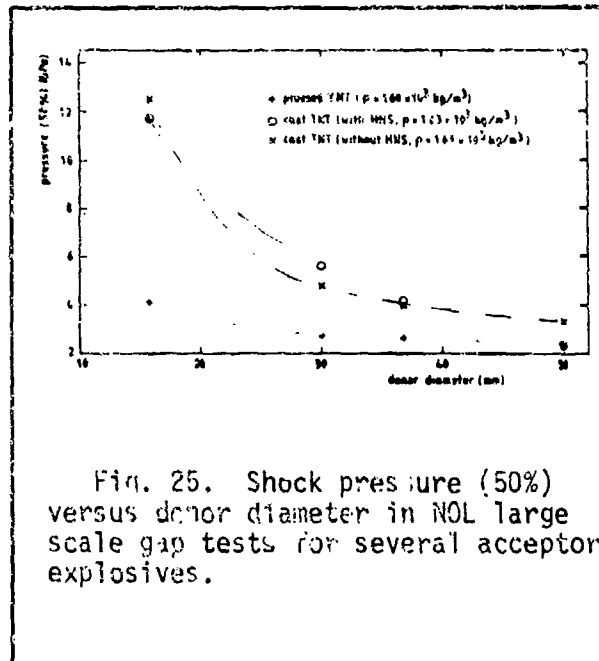


Fig. 25. Shock pressure (50%) versus donor diameter in NOL large scale gap tests for several acceptor explosives.

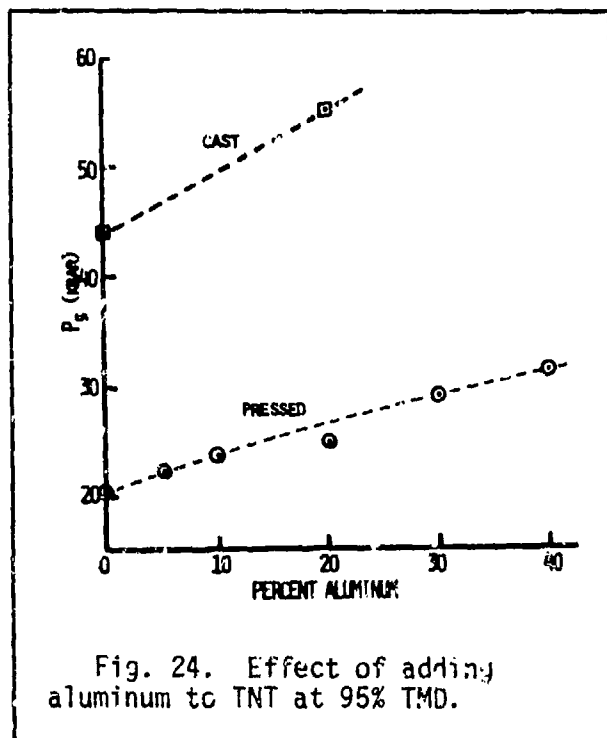


Fig. 24. Effect of adding aluminum to TNT at 95% TMD.

Effect of Donor and Attenuator Diameter

Schilperoord[†] investigated the effect on gap pressure when the diameter of the donor and attenuator was decreased below the standard size (apparently, the acceptor was maintained at the standard size). Figure 25 shows the results for cast and pressed TNT as the acceptor. The cast material is always less sensitive than the pressed material, which is to be expected. Both curves flatten out and

[†] A. A. Schilperoord, "The Effect of the Physical State of an Explosive in Shock Wave to Detonation Transition: Theory & Experiments," Presented at Internationale Jahrestagung 1979, ICT-Karlsruhe, 27-29 June 1979.

change very little as the donor diameter approaches the standard diameter (50.8 mm). Thus, we would not expect very much change in results if the diameter were increased beyond the standard size.

LECTURES ON DETONATION PHYSICS

Lecture #9 - 9 February 1981

Critical Energy and Pressure for Initiation; Wedge and Gap Test

by Donna Price

Notes by Frank J. Zerilli

Critical Energy for Initiation

The existence of a critical energy for initiation, a constant for each explosive, has been proposed a number of times in the past. Some observed effects of the duration of the shock pulse imply an effect depending on the energy of the initiating pulse. Walker and Wasley[†] made the first quantitative formulation based on the results of the initiation by projectiles of a few voidless explosives, in particular, PBX-9404^{††}. They used square pressure pulses of known amplitude and duration and arranged the experimental conditions so that multi-dimensional effects such as lateral rarefactions played no part. Under these restricted conditions, they found that there was a critical value of energy per unit area which the shock must transmit to the explosive before detonation can occur.

If the shock is a square pulse of amplitude P and duration τ , and if it produces a particle velocity u in the explosive, then the rate of work per unit area done on the explosive is Pu (rate of work is force times velocity, and pressure is force per unit area). Thus, since the pressure acts for a time τ , the total energy per unit area produced

[†] F. E. Walker and R. J. Wasley "Critical Energy for Shock Initiation of Heterogeneous Explosives", *Explosivstoffe* 17 (1969) pp. 9ff.

^{††} PBX-9404 consists of 94% HMX, 3% nitrocellulose (12% nitrogen content) and 3% Tris (β -chloroethyl)-phosphate.

in the explosive (called "fluence" by Walker and Wasley) is

$$E = P\tau t \quad (1)$$

Since $P = \rho_0 U u$ from momentum conservation (where ρ_0 is the initial density and U the shock velocity), we can also write

$$E = \frac{P^2 \tau}{\rho_0 U} \quad (2)$$

For values of E below the critical value, detonation does not occur.

The critical fluence relation has turned out to be a useful engineering development guide as long as it is applied to voidless explosives of the conventional CHNO (carbon-hydrogen-nitrogen-oxygen) composition. It is not a general relation, however. A number of investigators have studied its validity for a number of different materials. The French

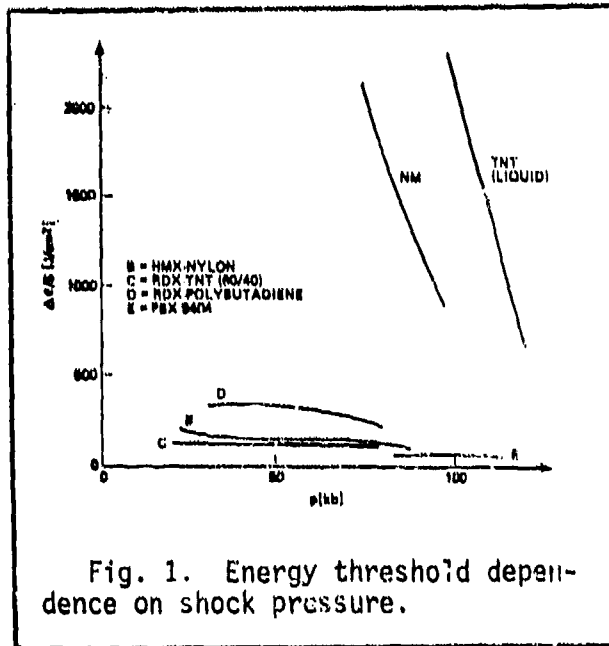


Fig. 1. Energy threshold dependence on shock pressure.

workers de Longueville and Fauquignon[†] examined a number of materials and some of their results are shown in Fig. 1, in which critical initiating energy fluence is plotted against shock amplitude. Two explosives, PBX-9404 (E in the figure) and Comp B (C in figure) show a constant critical fluence over the pressure range investigated. Plastic bonded HMX (curve B) and plastic bonded

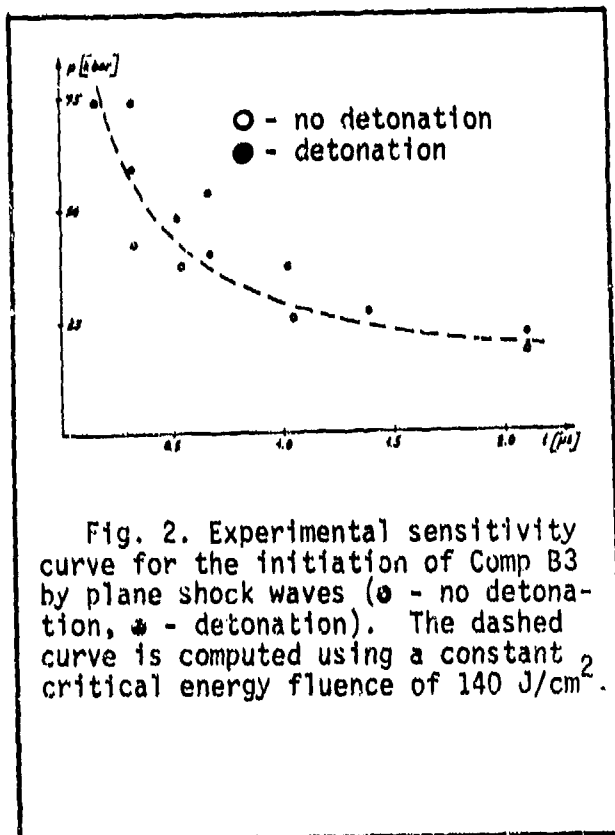
RDX (curve D) show some variation from constant fluence, and the critical fluence

[†] Y. De Longueville, C. Fauquignon, and H. Moulard, "Initiation of Several Condensed Explosives by a Given Duration Shock Wave," Sixth Symposium (International) on Detonation, ONR ACR-221, U.S. Govt. Printing Office, Washington, D.C., 1978, pp. 105-114.

for porous RDX (not shown here) varies even more. The critical fluence for the liquids, nitromethane and molten TNT varies greatly with pressure. TATB/Kel-F mixtures also show a strong pressure dependence of the critical initiating energy per unit area.

Moulard another French investigator,[†] repeated some of the work.

Figure 2 is a plot of pulse pressure against pulse duration for Comp B3



which Moulard determined had a constant critical fluence of 140 J/cm². The dashed curve in Fig. 2 was computed using this constant fluence of 140 J/cm². For points above the curve, detonation occurs and, for points below, detonation does not occur. However, the situation changes when cylindrical steel projectiles of varying diameters are used to initiate detonation in the same material. Figure 3 shows data for projectile diameters up to 15 mm. The values in parenthesis

are the values of the fluence corresponding to the projectile velocity and diameter for a given experimental point. Again, there is a threshold curve, above which detonation occurs and below which it does not. In this case, the

[†] H. Moulard, "A Critical Area Concept for the Initiation of Solid High Explosives by the Impact of Small Projectiles, presented at the Seventh International Colloquium on Gas Dynamics, Aug. 1979, and to be published in Progress in Aeronautics and Astronautics.

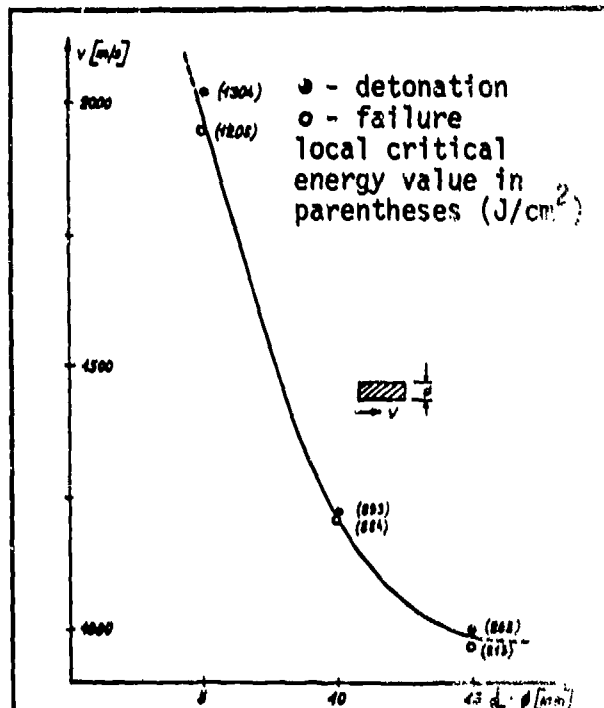


Fig. 3. Sensitivity curve for Comp B3 under the impact of cylindrical steel projectiles.

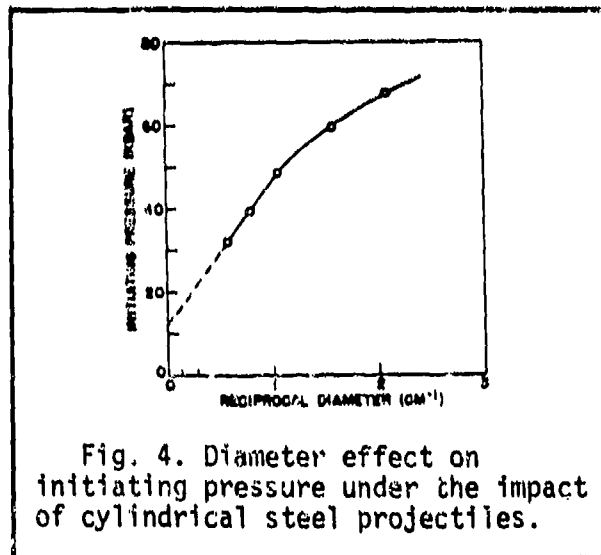


Fig. 4. Diameter effect on initiating pressure under the impact of cylindrical steel projectiles.

experimental conditions produce a two dimensional flow, and the critical fluence is significantly larger for smaller diameter projectiles. As the projectile diameter increases, the required fluence decreases and, presumably, it should approach the one dimensional critical fluence as the diameter gets larger and larger. Hence, Moulard proposed that the area of the shocked portion of the material as well as temperature, pressure, and so forth must be included in the variables that affect shock sensitivity.

The fact that the required energy, pressure, or pulse duration changes with the diameter of the projectile in initiation by projectiles has been known for a long time. Figure 4 shows critical initiating pressure as a function of reciprocal projectile diameter plotted from data obtained by Wenograd[†] some years ago.

[†] J. Wenograd and E. G. Whitbread, unpublished data, E.R.D.E. 1958-59; also, the Ballistic Research Laboratory, Aberdeen, Maryland has a large collection of data of this sort.

The Wedge Test

Critical initiating pressures are generally determined using cylindrical charges because this geometry is usually the most convenient. But in the 50's, Jacobs[†] pointed out the advantages of using a wedge geometry instead of a cylindrical geometry for studying shock initiation. Figure 5 shows the geometry of the wedge test. If the base angle of the wedge

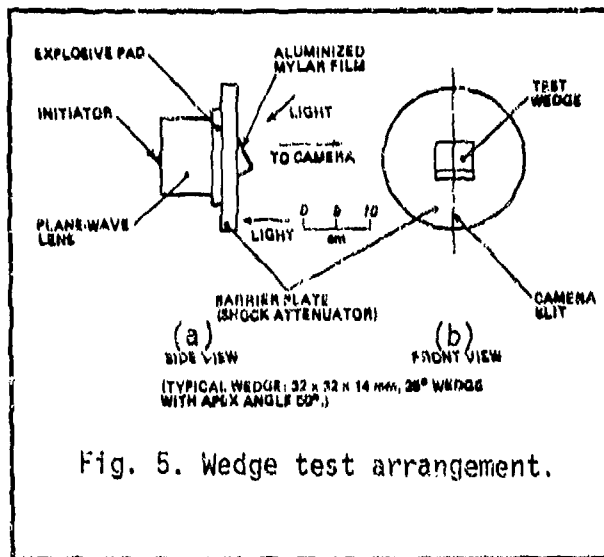


Fig. 5. Wedge test arrangement.

is sufficiently small, then the shock will reach the slant face (the face seen in the front view in Fig. 5) before lateral rarefaction waves interfere. In other words, behavior observed in the wedge is that of the interior of a cylindrical charge. Also a continuous optical record of the distance the shock front has travelled versus time can be obtained. The shock front

would appear as a horizontal line travelling downward in the front view shown in Fig. 5. This line is the intersection of the plane shock^{††} with the slant face of the wedge. Thus the distance that the line has moved down in the front view is proportional to the distance the shock has travelled through the wedge^{†††}. An aluminized mylar film covering the slant face reflects light into the camera. The shock alters the reflection, thus revealing its position to the camera. The camera is a streak camera with its slit in the vertical plane (Fig. 5b). Thus it produces the normal streak record showing position versus time.

[†] J. M. Majowicz and S. J. Jacobs, NavOrd 5710, Mar 1958; N. L. Coleburn, NavWeps Rept. 6026, Oct 1960.

^{††} Note that a plane wave lens followed by an explosive booster is used to produce a planar shock.

^{†††} Run length = $l \tan \phi$ where l is the vertical distance the line has moved and ϕ is the base angle of the wedge.

The record obtained shows the initiating shock and the onset and progress of the detonation. Although this test is much more sophisticated than the large scale gap test, it is still necessary to send in shocks of different strengths to get a complete picture. The variables usually measured in the wedge test are: run length, delay time, and initiating shock pressure. The run length, denoted by x_g , is the distance from the initially shocked surface to the plane at which detonation occurs. The delay time, denoted by τ_g , is the time interval between the time the shock enters the wedge and the time at which detonation occurs. A related quantity is the excess delay time, denoted by Δ , which is the amount by which τ_g exceeds the time which would be required for the detonation to travel a distance x_g , that is $\Delta = \tau_g - x_g/D$ where D is the detonation velocity. The initiating shock pressure, denoted by P_1 , is the pressure in the wedge material just as the shock enters the wedge. Just as in the large scale gap test, a calibration must be made to determine P_1 . Different pressures are obtained by varying the explosive booster pad and by varying the material and thickness of the attenuator.

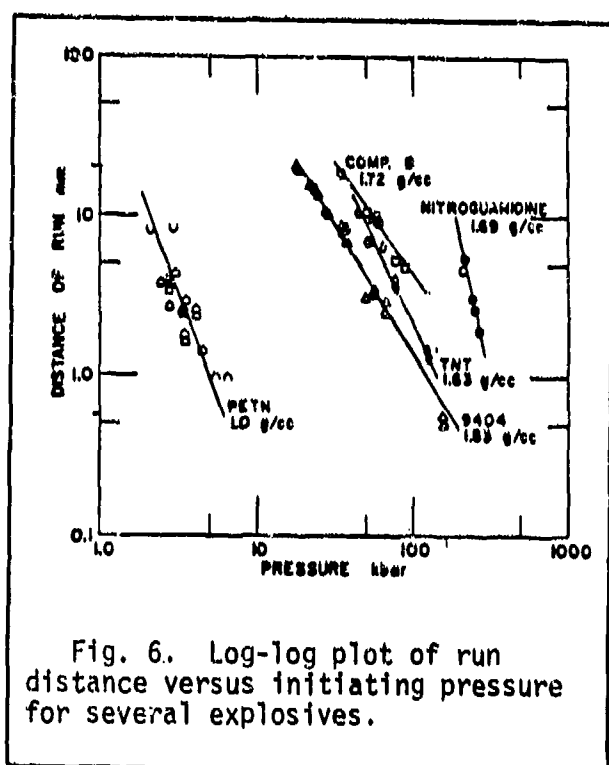
Relations Between Run Length, Delay Time, and Initiating Pressure

Study of wedge test data has led to the discovery of several relations between run length, delay time, and initiating pressure. In 1961, the sensitivity group at NOL examined wedge test data obtained in 1957 by Jacobs and Majowicz[†] using three different initiating pressures on each

[†] J. M. Majowicz and S. J. Jacobs, NavOrd 5710, Mar 1958.

of three different cast explosives. It was found that the reciprocals of run length, delay time, and excess delay time all appeared to vary linearly with initiating pressure.[†] However, since there were only three data points for each explosive, the linear variation was not certain. In 1963, Jacobs, Liddiard, and Drimmer^{††} obtained much more data on cast Comp B wedges and confirmed the linear variation of reciprocal run length with initiating pressure.

In 1965 Ramsay and Popolato^{†††} analyzed wedge test data and concluded that the dependence of $\log x_s$ on $\log P_i$ was linear over an appreciable



range for several explosives.

Since then, plots of $\log x_s$ versus $\log P_i$ have been referred to as "Pop" plots. Figure 6 shows their results. They also found that $\log x_s$ varied linearly with $\log \Delta$ for PBX-9404 as shown in Fig. 7.

These results agree with the previously observed linear dependence of reciprocal run length, reciprocal delay time, and reciprocal excess transit time on initiating pressure.

As Fig. 6. shows, each type of

[†] D. Price, "Large Scale Gap Test: Interpretation of Results for Propellants," NAVWEP 7401, 15 Mar 1961.

^{††} S. J. Jacobs, T. P. Liddiard, and B. E. Drimmer, Ninth Symposium (International) on Combustion, Academic Press, New York, 1963, pp. 517-529.

^{†††} J. B. Ramsay and A. Popolato, "Analysis of Shock Wave and Initiation Data for Solid Explosives," Fourth Symposium (International) on Detonation ONR-ACR-126, U.S. Govt. Printing Office, Washington, D.C. (1965).

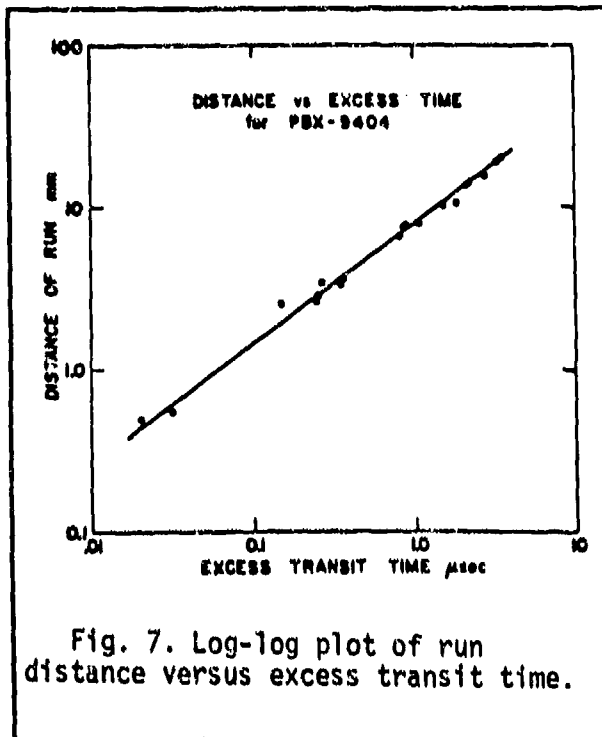


Fig. 7. Log-log plot of run distance versus excess transit time.

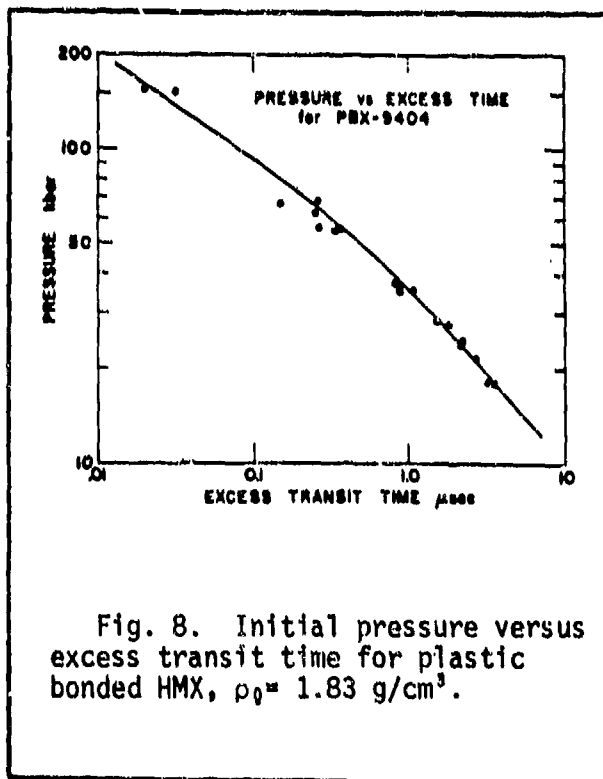


Fig. 8. Initial pressure versus excess transit time for plastic bonded HMX, $\rho_0 = 1.83 \text{ g/cm}^3$.

material has a different $x_s - P_i$ relation and the relation also depends on the density of the material and the method of preparation. Figure 8 shows Ramsay and Popolato's plot of initiating pressure versus excess transit time for PBX-9404. This log - log plot is linear for pressures below 50 kbars, agreeing with the NOL findings which were for this lower pressure region. However, for pressures greater than 50 kbar there appears to be some deviation from linearity.

Figures 9 and 10 show the Jacobs and Majowicz data with reciprocal run length plotted as a function of initial pressure. Each curve ends at the left (low pressure end) at a point which corresponds to the large scale gap test value of initial pressure and a run length of about 50 mm. Note that the position of this point on the graph is not very sensitive to the value of the run length since reciprocal run length is the quantity plotted.

The value of 50 mm is reasonable since breakout of detonation is

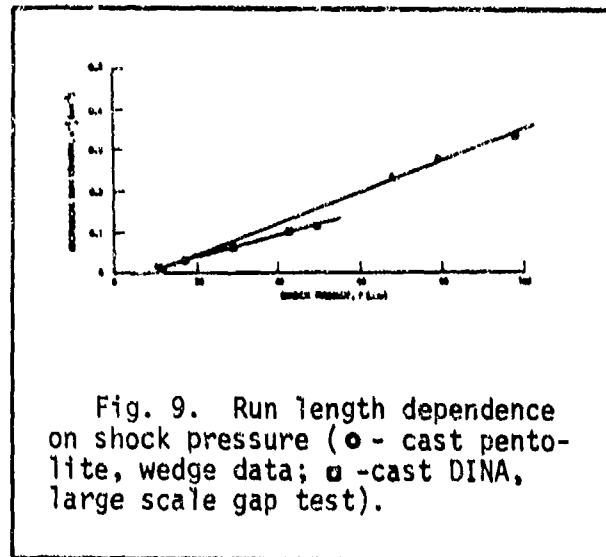


Fig. 9. Run length dependence on shock pressure (○ - cast pentolite, wedge data; □ - cast DINA, large scale gap test).

observed in unconfined charges at run distances up to two charge diameters. The LSGT charge diameter is about 35 mm and it is a confined charge. Thus a 50 mm run length would be in the appropriate range.

In Fig. 9, the upper curve represents data obtained for cast pentolite using the wedge test and the lower curve represents data for cast DINA using the instrumented

gap test (continuous wire method). There is an apparent inversion between the pentolite and DINA LSGT pressures P_{oi} but the pressures are, respectively, 11.0 and 11.9 kbar, a difference which is within the five percent precision of the LSGT calibration.

Figure 10 shows wedge test data for five more cast explosives. The curves for Comp B3 and Comp B differ significantly, although the

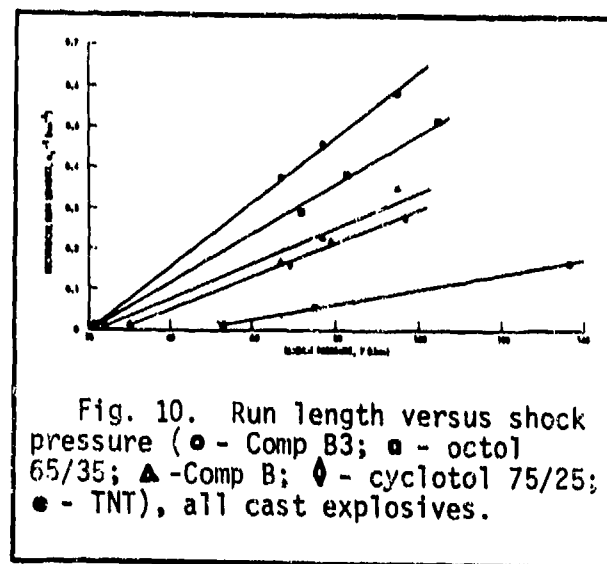


Fig. 10. Run length versus shock pressure (○ - Comp B3; □ - octol 65/35; ▲ - Comp B; ◆ - cyclotol 75/25; ● - TNT), all cast explosives.

compositions are nearly the same. Comp B3 is 60% RDX and 40% TNT, while Comp B is 60% RDX, 40% TNT with 1% wax added. The difference in sensitivities is probably due to a particle size effect and not to the composition difference. The particle size specification for the RDX[†] component of Comp B3

[†] Specifications for RDX are found in MIL-R-398C.

is strict; the average particle size is 58 μ with a very narrow distribution of sizes around the average. In Comp B, the RDX has a wide range of particle size distribution; the average size for the Comp B used to obtain this data was 130 μ . The Comp B3 which has a smaller particle size is more sensitive than Comp B with the larger particle size. (Here, sensitivity is rated by run length for a given initiating pressure -- the shorter the run length, the more sensitive the material.) Another example of the effect of particle size is illustrated by the difference between Comp B (60% RDX, 40% TNT) and cyclotol (75% RDX, 25% TNT). Although cyclotol contains a greater percentage of the more sensitive component RDX, cyclotol is less sensitive than Comp B. The average particle size of the RDX in cyclotol is about 740 μ which is much larger than the Comp B specification and the particle size effect apparently dominates the sensitivity behavior.

Wedge test data provides two measures of sensitivity: run length and delay time for a given initiating pressure. But run length and delay time alone are not dependable measures since, in the case of pressed charges, run length and delay time decrease as the porosity is decreased, yet, in terms of critical pressure, the more porous charges are easier to initiate, that is, P_{ci} is lower, despite the fact that it takes a little longer run and a little longer time to get to detonation.

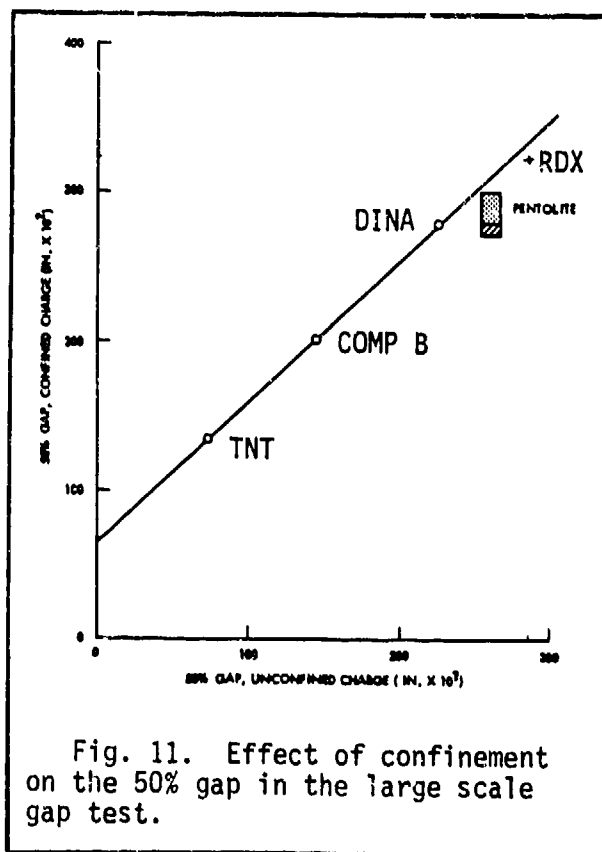
It is often not possible to compare sensitivities of explosives unless the conditions under which the comparison is made are precisely specified. For example, if the explosives, pentolite and DINA, in Fig. 9 were plotted on the same graph as those in Fig. 10, their curves would intersect some of the curves for the explosives in Fig. 10. Thus, at a low shock pressure one explosive may be more sensitive (shorter run

length) than another, but at a high shock pressure it may be less sensitive (longer run length). So a single rating point may be misleading. An explosive can only be truly characterized by a multi-variable threshold surface in a multi-dimensional space which includes all the quantities which affect shock sensitivity.

RELATIONS BETWEEN DIFFERENT GAP TESTS

Confined Versus Unconfined Charges

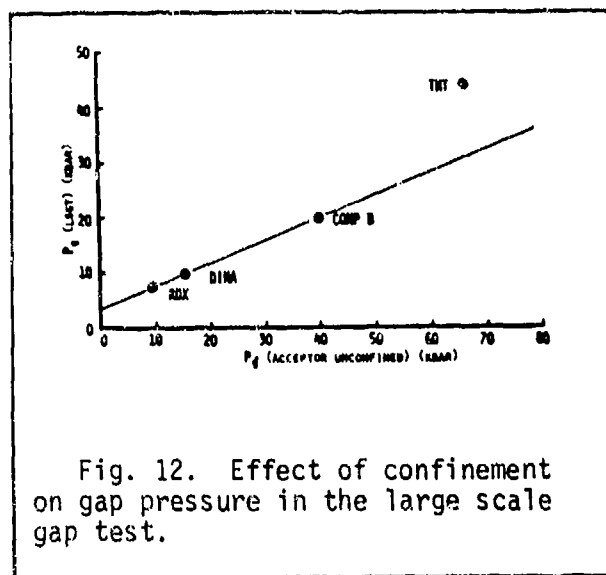
Let us consider the effect on the gap test results for confined versus unconfined charges. Figure 11 shows a comparison of the attenuator



thickness at the 50% detonation probability point in the standard large scale gap test with that in the same test after the standard confinement has been removed from the acceptor.[†] The result is surprising in view of the curves obtained from the instrumented gap test. Figure 12 shows the same data, but plotted in terms of gap pressure P_g rather than gap thickness. While Fig. 11 indicates a very good linear relation between gap thickness in the confined and unconfined tests, the point

for TNT deviates considerably from a linear relation between

[†] NOLTR 74-40



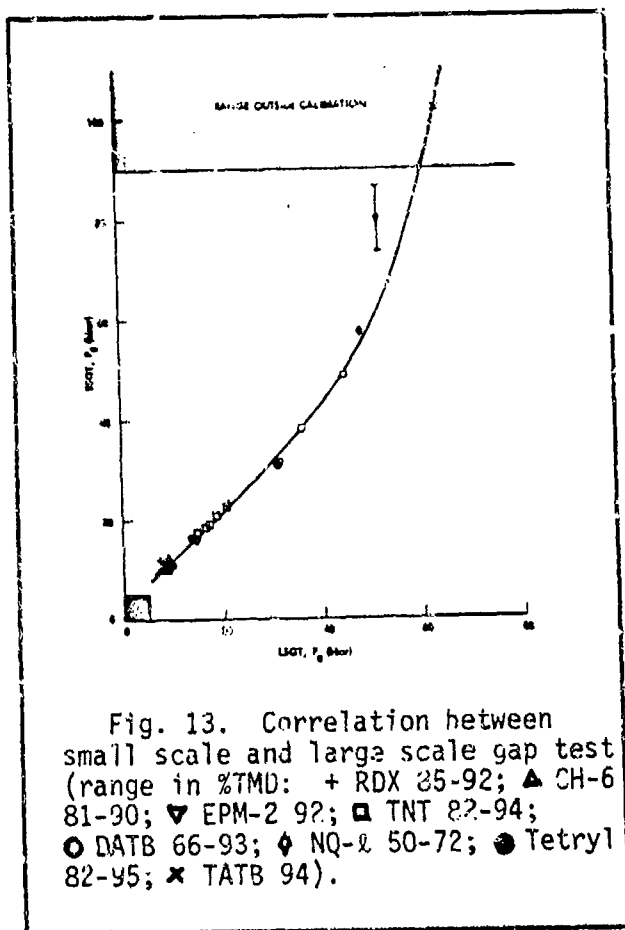
gap pressures as illustrated in Fig. 12. The reason for the difference between Fig. 11 and Fig. 12 may be that TNT is the only explosive in that particular group for which the 50% gap thickness is less than 35 mm. The gap thickness of 35 mm is the point at which the lateral rarefaction reaches the cylindrical axis of the unconfined attenuator and produces breakup of the attenuator. Thus, for

the other explosives in this group, breakup has occurred in the attenuator; that, in turn, may have some effect on the nature of the transmitted shock. This is another example which shows that it may be unwise to use gap thickness rather than critical pressures in comparing explosive shock sensitivity.

Large Scale Versus Small Scale Gap Pressures

Figure 13 shows the small scale gap test gap pressures plotted against large scale gap test gap pressures for several explosives.[†] The shaded area is a region lying beyond the original region of calibration (recall that the original calibration was done by measuring shock velocity as a function of thickness and the shock velocity could not be measured well at

[†] NOLTR 74-40



small thicknesses). Since almost all materials tested in the small scale gap test[†] show a very sharp increase in the required initiating pressure (indication of approach to critical conditions) as they approach zero porosity, only charges with 6% or greater porosity have been included in the graph of Fig. 13.

The diamond shaped data points in Fig. 13 are for two charges of low bulk density nitroguanidine (NQ-2). High bulk density nitroguanidine (NQ-h) is not detonable in the small scale gap test, nor is low bulk density nitroguanidine of porosity lower than about 28%. Hence it seems

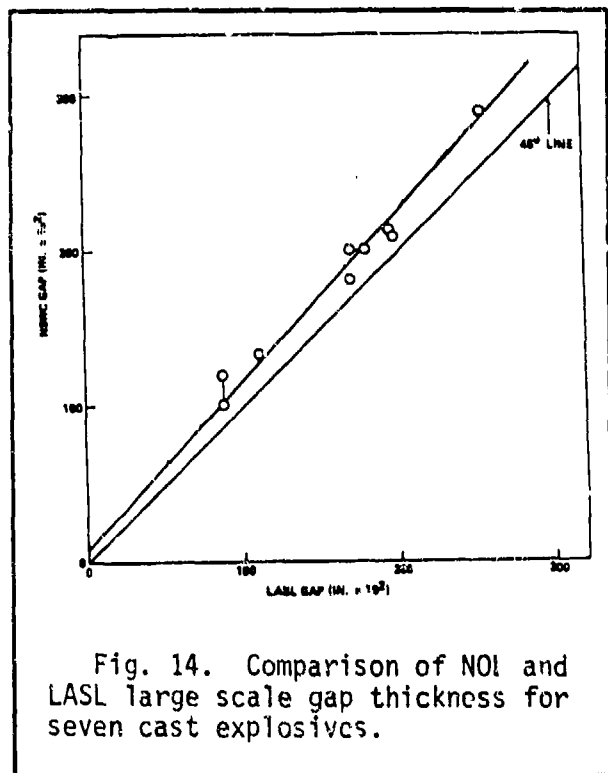
likely that the lower porosity nitroguanidine charge whose data point lies above the curve (and whose small scale gap pressure could not be very precisely determined) lies where it does because the charge is approaching critical conditions. TATB, whose data point is represented by a cross, is so insensitive that it lies beyond the calibrated range.

Comparison of NOL and LASL Gap Test Results

In order to compare the NOL large scale gap test results with gap test results from another laboratory for which calibration information is not available, the only recourse is to compare values of the attenuator thickness L_g at the 50% probability of detonation point. This is the situation with gap test results reported by Los Alamos Scientific Laboratory.

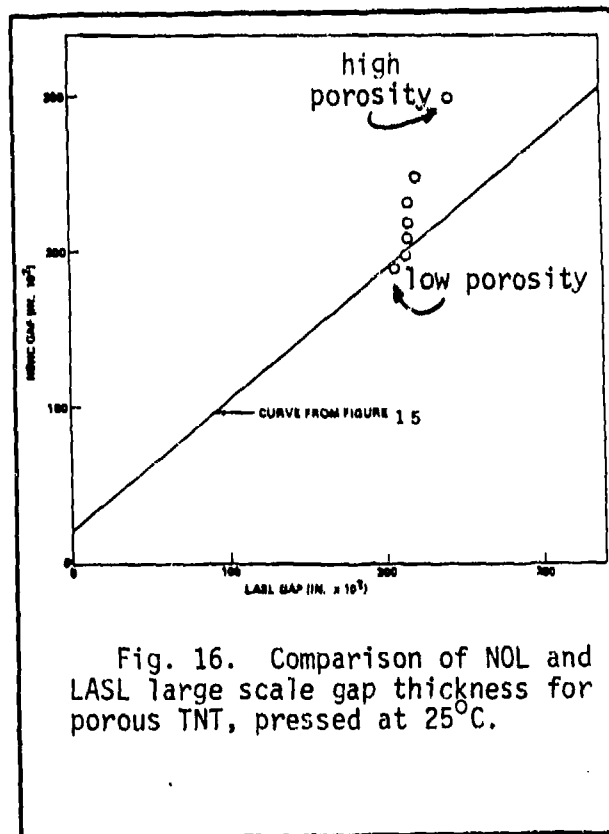
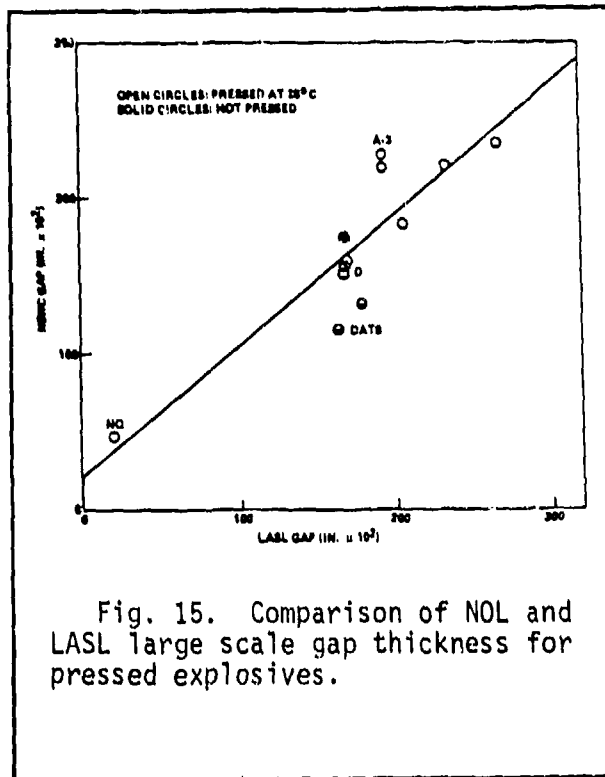
[†] Small Scale Gap Test: brass cylinder with 0.2" i.d., 1" o.d., standard RDX donor.

The LASL large scale gap test uses an unconfined acceptor with 40 mm diameter. The NOL large scale gap test without the standard sleeve uses a 38 mm diameter charge. The major differences between the LASL and NOL standard tests is the use of Dural as the attenuator in the LASL test and the confinement of the acceptor in the NOL test. Both laboratories seem to be able to reproduce their castings and the large scale gap test results on them. For example, from five different batches of 50/50 pentolite, NOL reported $L_g = 278 \pm 6$ cards, and similarly, from eight batches of cyclotol 75/25, LASL reported $L_g = 172 \pm 8$ cards[†]. However, the correlation between the results of the two laboratories varies with the nature of the charges. For cast charges it is good, for pressed charges it is poor. There are seven cast explosives common to both laboratories' data and these are compared in Fig. 14. A reasonably



good correlation is shown. The NOL gap thicknesses are consistently a little larger than the LASL gap thicknesses, but this is not surprising in view of the different attenuator materials used by NOL (PMMA) and LASL (Dural). To make a proper comparison, samples from the same batches of the same materials, prepared in the same manner, should be tested at the two laboratories, but this has not been done.

[†] M. J. Urizar, S. W. Peterson, and L. C. Smith, "Detonation Sensitivity Tests," LA-7193-MS, April 1978. See also, NOLTR 74-40.



A correlation for pressed charges is more dubious. The available data is shown in Fig. 15. At LASL, the charges are generally pressed in heated molds while at NSWC they are not. TNT is the only explosive prepared in heated molds at both laboratories. The LASL data for DATB was from a charge pressed in a heated mold, but DATB is one of the less temperature sensitive materials. There are differences in the sensitivity ratings of the two laboratories. For example, explosive D (ammonium picrate) is distinctly more sensitive than DATB according to the NOL data, while there is little difference between them according to the LASL data.

The poor correlation does not seem to be entirely due to the temperature of the mold. Figure 16 shows a comparison of data for TNT charges pressed at 25°C to varying degrees of porosity. Superimposed is the straight line fit from Fig. 15. The low porosity charges show

comparable results at both laboratories.[†] However, there is little variation in the LASL gap test results with varying porosity, while there is significant variation in the NOL results.

In the next lecture, the relationships between critical diameter and critical initiating pressure will be discussed.

[†] Note that cast explosives, which also show comparable results at both laboratories, have low porosity, typically 5% for air melt and cast and 1% for vacuum melt and cast. The cast explosives tested at NOL were air melted and cast.

LECTURES ON DETONATION PHYSICS

LECTURE #10 -- 9 MARCH 1981

CHARACTERIZATION OF SHOCK SENSITIVITY

by

DONNA PRICE

Notes by Frank J. Zerilli

Effect of Environment and Physical State on Critical Diameter and Initiating Pressure

We have seen that critical diameter and critical initiating pressure are inter-related and both are functions of many variables and, in particular, are functions of the test design. One cannot obtain the critical initiating pressure by measuring the critical diameter or vice-versa. They are both aspects of the complex

property of shock sensitivity.

Table 1. Effect of parameter change on values of critical diameter d_c and critical initiating pressure P_{ci} .

VARIABLE INCREASED	EFFECT ON		NOTES
	d_c	P_{ci}	
CONFINEMENT	-	-	
TEMPERATURE	-	-	
POROSITY	+	-	GROUP 1 GROUP 2
PARTICLE SIZE	+	-	POROUS HE VOIDLESS, GR 1
% WAX	+	+	GROUP 1 AP
% Al	-	+	CAST TNT GRANULAR TNT
	NI	+	AP AT > 80% TMD
	-	-	AP AT < 74% TMD
	-	+	

KEY

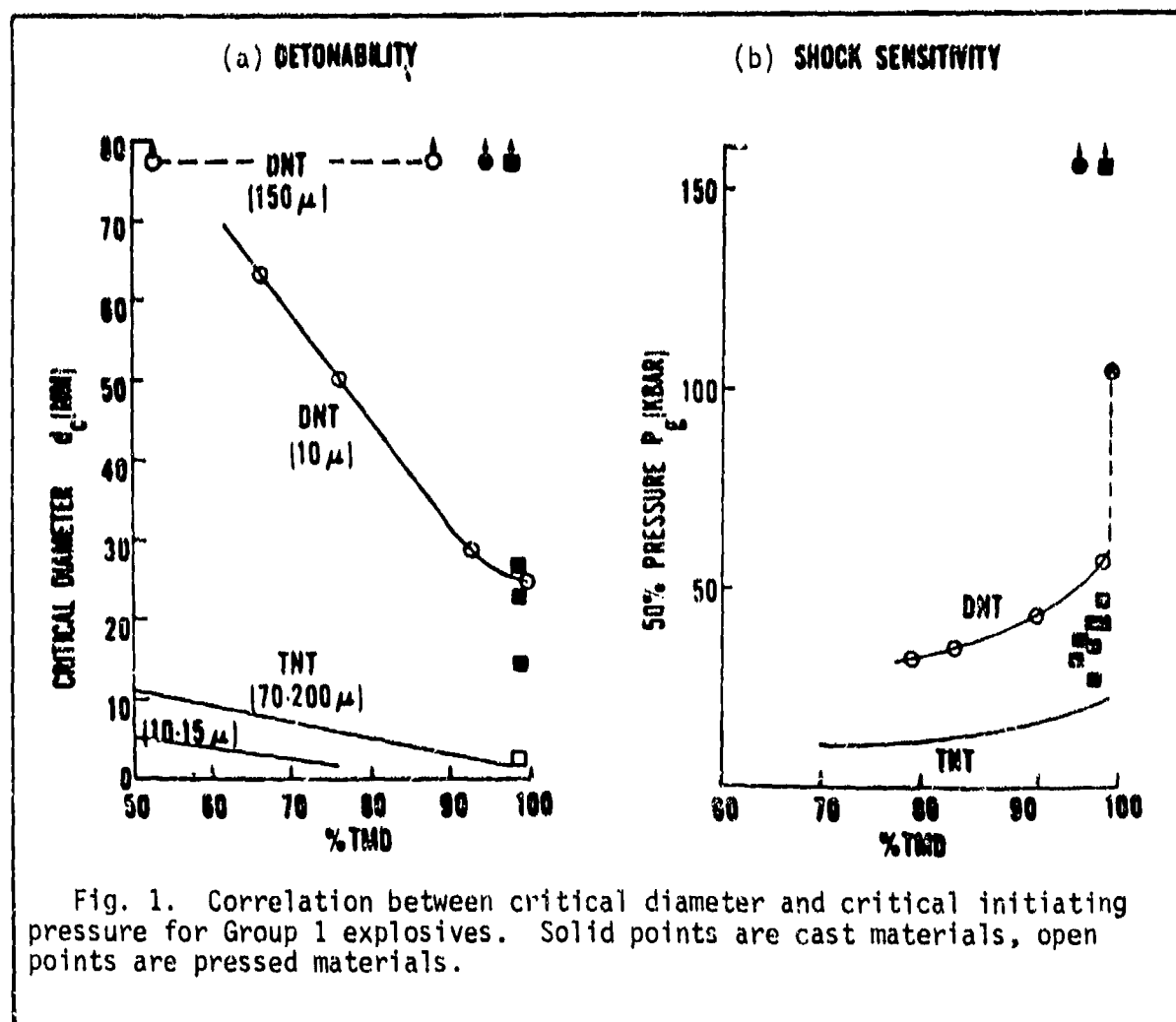
+ INCREASES
- DECREASES
NI NO INFORMATION

Table 1 summarizes the effect of two environmental, two physical state, and two compositional variables on critical diameter and pressure. Increasing the confinement decreases both critical diameter and critical initiating pressure. So does increasing the temperature. Increasing porosity decreases critical diameter and pressure for Group 2 explosives but increases critical diameter

while decreasing critical pressure for Group 1 explosives. Increasing particle size produces increases in these two critical parameters for

voidless Group 1 explosives, but produces opposite effects on the two parameters for porous explosives. Addition of wax increases both parameters for Group 1 explosives but decreases both parameters for Group 2 explosives. Thus, the results summarized in the table show that there is no generally valid relationship between critical diameter and critical initiating pressure although there are relationships in specific cases.

Figure 1 illustrates one trend of the many different relationships*. In this case, Group 1 explosives, the critical diameter



*D. Price, A. R. Clairmont, Jr., and J. O. Erkman, "NOL Large Scale Gap Test III", NOLTR 74-40, 8 Mar 1974; D. Price, J. O. Erkman, A. R. Clairmont, Jr., and D. J. Edwards, "Explosive Characterization of Dinitrotoluene", *Combustion and Flame*, 14, 145-148 (1970).

decreases and the critical initiating pressure increases as the explosive is made less porous (increasing percentage of theoretical maximum density). Figure 2 illustrates the relationships for Group 2

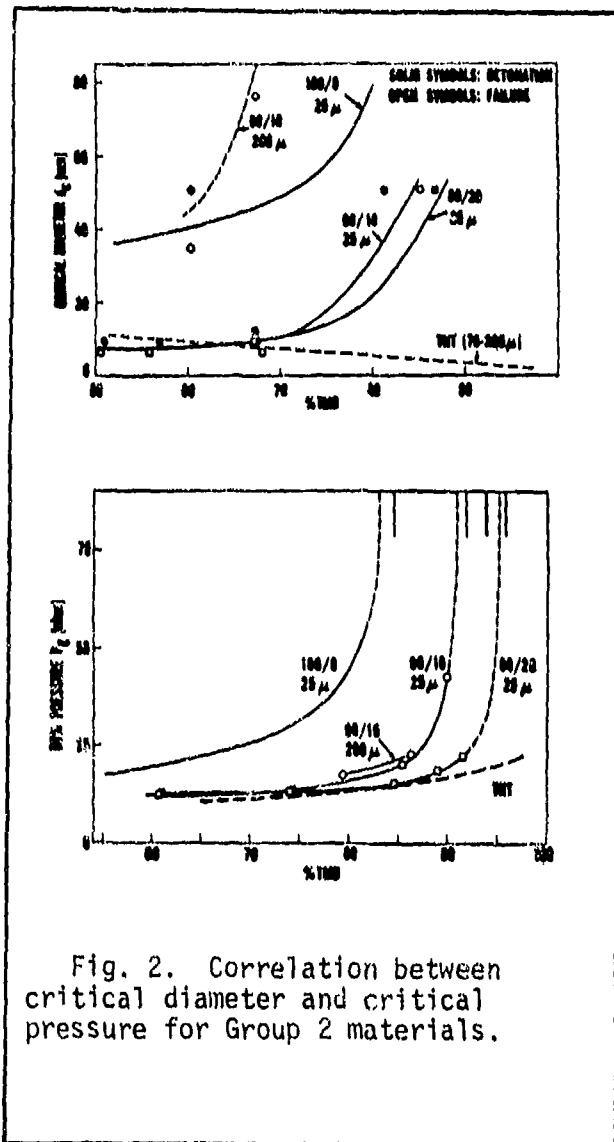


Fig. 2. Correlation between critical diameter and critical pressure for Group 2 materials.

materials*. In this case, both critical diameter and critical pressure increase with increasing percentage of theoretical maximum density. The effect in critical diameter is the opposite of the effect for Group 1 explosives.

Relation Between Critical Diameter and Critical Pressure

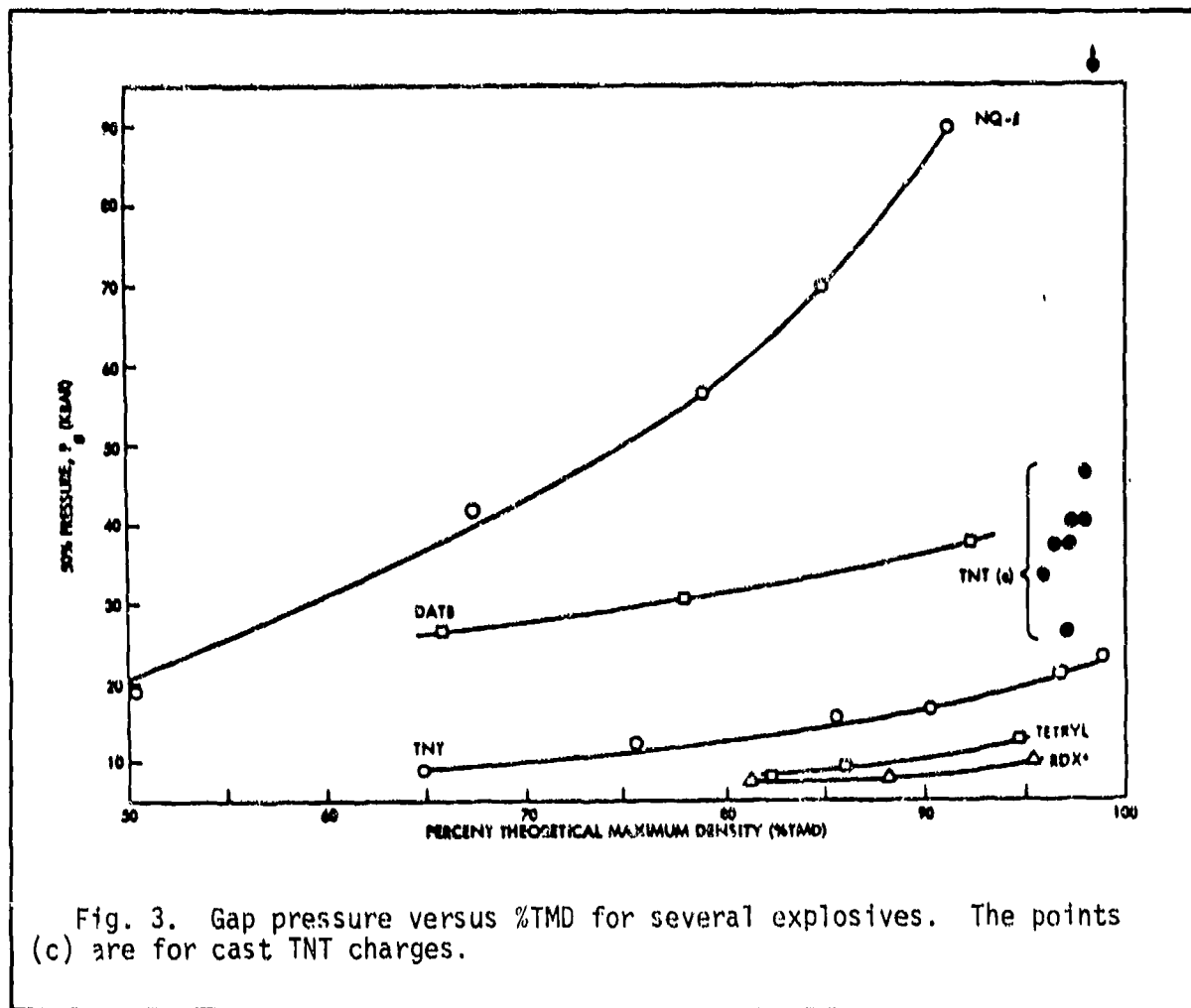
There is also a smooth relationship between critical diameter and critical pressure for a composite explosive mixture when its composition is varied continuously or for a single pure material when one of its physical parameters is varied continuously. TNT is a good example. Since it is a chemically homogeneous material, there is more data available for it than for most other explosives, and it offers as wide a range as can

be found among explosives for the different physical forms in which it can be used. It can be used in the form of porous charges of different porosities and varying initial particle sizes, in the form

*D. Price, A. R. Clairmont, Jr., and J. O. Erkman, *Combustion and Flame*, 17, 323-336 (1971).

of cast charges with several different casting methods, and also in the form of a single crystal. Few explosives offer this variety.

Figure 3 shows typical curves of gap pressure versus percent TMD, for several explosives*. Of particular interest is the curve for granular (pressed) TNT and the data points (c) for cast TNT



charges. One point, with the upward pointing arrow, is off scale and represents a casting having a very high gap pressure, approaching the single crystal initiating pressure. Except for this one, all the castings were made using the same processing schedule. Although the cast charges' range of densities overlap that of the pressed charges,

*Data from NOLTR 74-40, cited previously.

there is not a significant correlation between the initiating pressure and the density as there is for pressed charges. This is because, in pressed charges, the voids are uniformly distributed, while in cast charges, there is likely to be a concentration of large voids having little or no effect on the behavior of the adjacent condensed medium. Percent TMD is not a very useful indicator of shock sensitivity in the nearly voidless plastic bonded materials either.

The curve of gap pressure versus percent TMD for pressed TNT and the scattered data lying above the curve for TNT castings suggested a continuous variation in gap pressure with physical state. Table 2, below, contains a summary of the data available for TNT*.

Table 2. Sensitivity Data for TNT. Initiating pressure is for diameter \gt three times critical diameter.

Form of Charge	%TMD	Critical Diameter (mm)	Initiating Pressure (kbar)
Pressed at 25°C	71.5	7	11
	98.0	2	25
Pressed at 72-76°C	99.2	ca 8	--
Cast			
melt cooled rapidly	98.0	14	30
creamed cast	97.5	25.5	43
vacuum cast (Yorktown)	98.0	35	78
poured clear, cooled very slowly	97.5	\gt 38	--
Single Crystal	100	\gt 38	\gt 125

*D. Price, "Shock Sensitivity, A Property of Many Aspects," Fifth Symposium (International) on Detonation, ONR ACR-184, U.S. Govt. Printing Office, Washington, D. C., 1972, pp. 207-217.

The materials in Table 2 are arranged in order of increasing homogeneity starting from very porous charges pressed at ambient temperature, through hot pressed charges*, various types of casting**, up to the single crystal. The critical diameter at first decreases with increasing density, reaches a minimum, and then starts increasing. The hot pressed material bridges a considerable gap between the granular and the cast charges. The very slowly cooled casting was tested up to 38 mm diameter with negative results; the critical diameter for the single crystal must be greater than that for the very slowly cooled casting. Also, the single crystal presumably would require a greater critical initiating pressure than that measured for liquid TNT which is 125 kbar.

Data for hot pressed charges have been published by Rempel***.

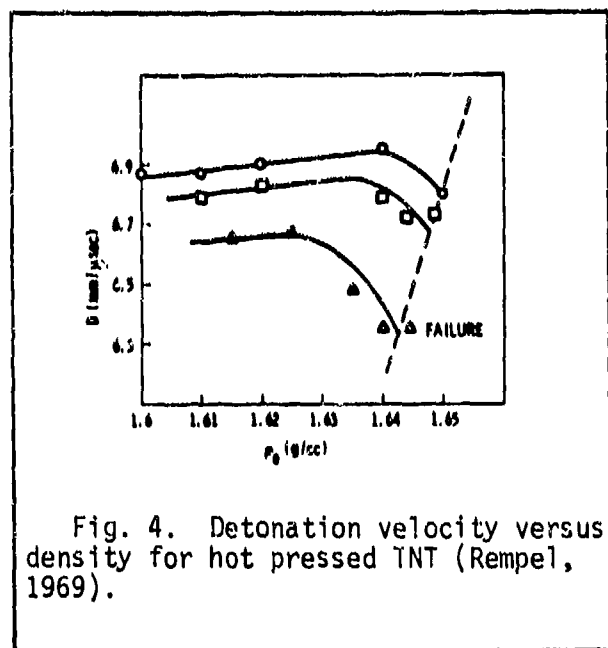


Fig. 4. Detonation velocity versus density for hot pressed TNT (Rempel, 1969).

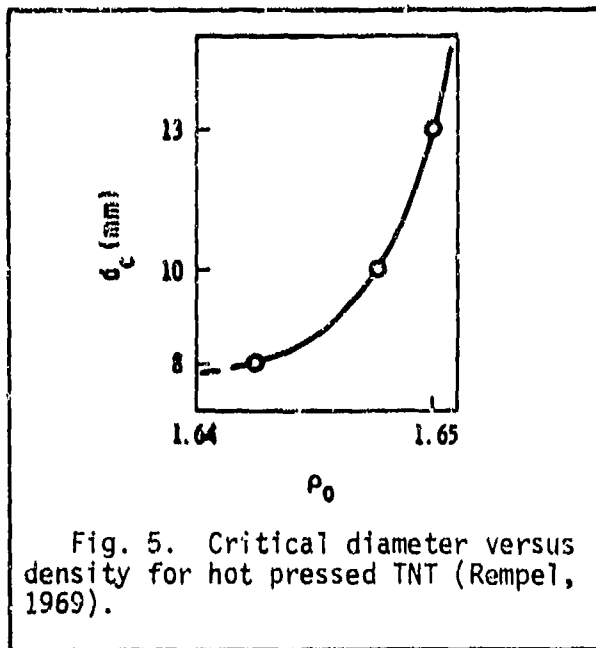


Fig. 5. Critical diameter versus density for hot pressed TNT (Rempel, 1969).

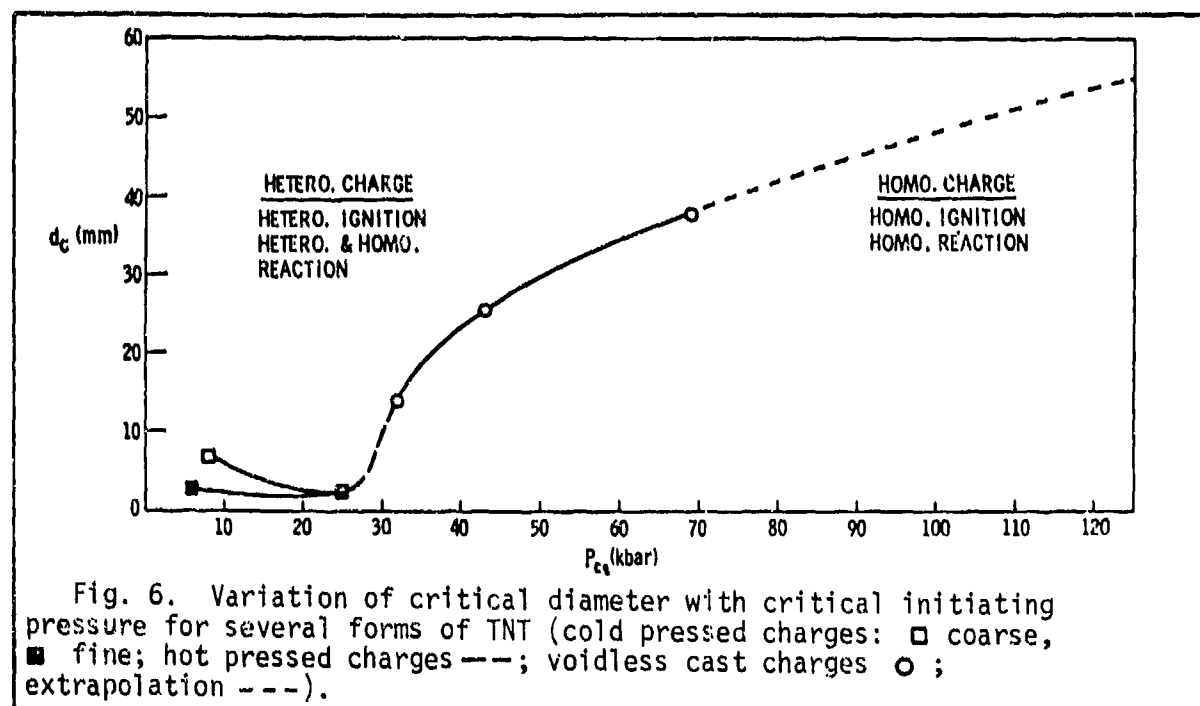
* TNT has a melting point of about 81°C and it flows easily under pressure. So pressing at a temperature of about 5°C under the melting point results in a very different charge from the cold pressed one even though there is only one percent difference in porosity.

**See Lecture #6, this series, p. 2.

***G. G. Rempel, Zh. Prikl. Mekh. Tekh. Fiz. 1969(2), 83-86, through translation journal.

He studied the range of densities close to theoretical maximum density of 1.654 g/cm^3 . As Fig. 4 shows, there is a normal trend of increasing detonation velocity D with increasing density until critical conditions are approached and then D decreases. Figure 5 shows the critical diameter versus density in this range. The data joined smoothly to the data for pressed charges and castings given in Table 2.

As a result, it was proposed* that there is a continuous relationship between critical diameter and critical initiating pressure, as depicted in Fig. 6, below. The porous charges have many branches



depending on the particle size. Two branches are shown in Fig. 6, the lower for fine TNT and the upper for coarse TNT. The branches coalesce at the point where Rempel's data for hot pressed charges begin (the dashed portion of the curve). Following Rempel's data are the data for cast TNT and the extrapolation toward single crystal values.

*D. Price, "Shock Sensitivity, A Property of Many Aspects", op. cit.

Gap test data published by LASL* shows a continuous variation in gap thickness with variation in the pressing temperature of TNT.

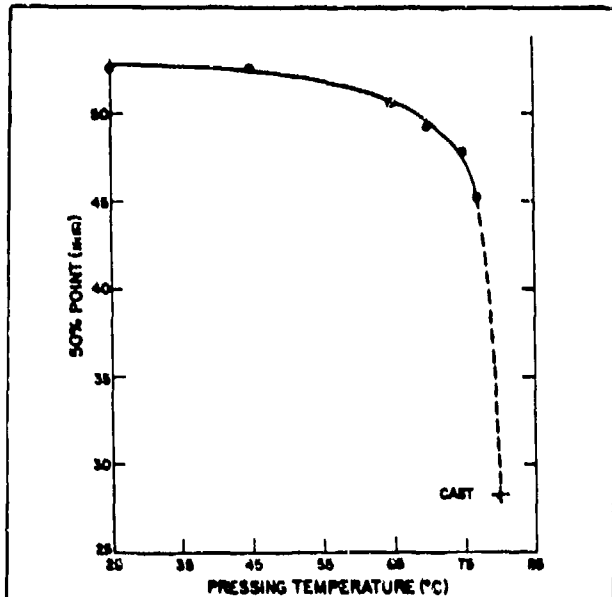


Fig. 7. Gap sensitivity versus pressing temperature for TNT at 1.595 g/cm^3 .

The data, shown in Fig. 7, extrapolated smoothly to the data for cast TNT.

There seems to be no question that there exists a smooth continuous critical pressure versus critical diameter curve as long as one deals with a single material in different physical forms. Systematic changes in composition of one component of a mixture also produce a smooth, continuous critical pressure

- critical diameter curve. But, in general, the curves obtained for one material do not give useful information about comparable curves for a different material.

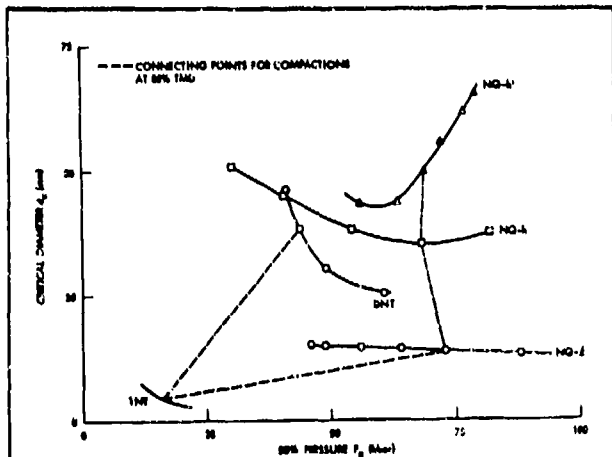


Fig. 8. Critical diameter versus gap pressure for Group 1 explosives.

Figure 8 shows a set of curves of critical diameter versus 50% gap pressure for Group 1 materials (TNT and low bulk density nitroguanidine) and materials that are predominantly Group 1 (dinitrotoluene and high bulk density nitroguanidine)**. The individual curves were obtained by pressing porous charges to differing

densities. The dotted line connects the data on each curve corresponding

* M. J. Urizar, S. W. Peterson, and L. C. Smith, "Detonation Sensitivity Tests", LA-7193-MS, Apr 1978.

** Data from NOLTR 74-40.

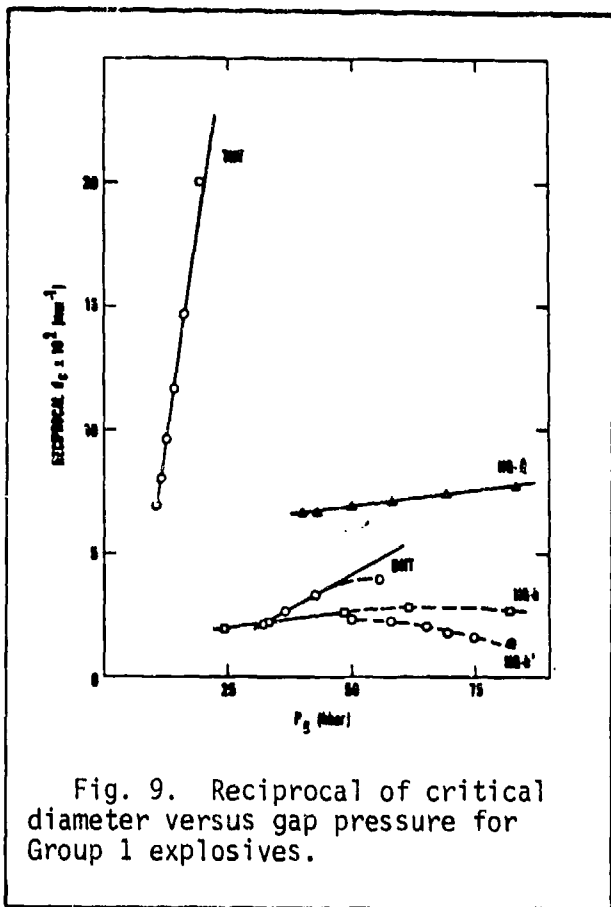


Fig. 9. Reciprocal of critical diameter versus gap pressure for Group 1 explosives.

to 85% TMD. As Fig. 8 shows, there is no evident critical diameter versus 50% point gap pressure correlation at constant % TMD. If the reciprocal of critical diameter is plotted versus gap pressure, as Fig. 9 illustrates, Group 1 materials produce straight lines and partly Group 1 materials produce straight lines in their Group 1 behavior region.

Figure 10 shows critical diameter versus 50% point gap pressure curves for Group 2 explosives: ammonium perchlorate at two different particle sizes, ammonium perchlorate and wax with two different compositions, high bulk density nitroguanidine, and two propellants containing ammonium perchlorate and aluminum*. The data for a constant 80% TMD are indicated by an arrow. Again, these data do not have a smooth relationship from explosive to explosive.

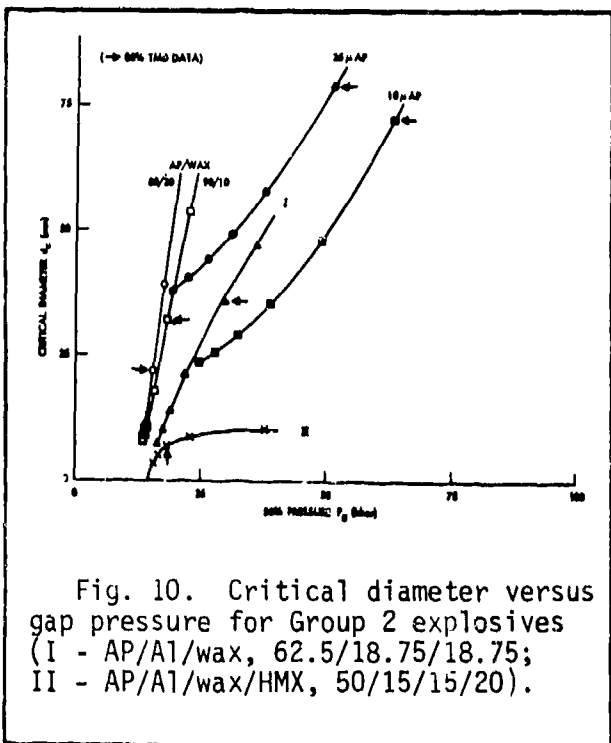


Fig. 10. Critical diameter versus gap pressure for Group 2 explosives (I - AP/A1/wax, 62.5/18.75/18.75; II - AP/A1/wax/HMX, 50/15/15/20).

In one more attempt to find a relation between critical diameter and initiating pressure, the log of critical diameter versus gap thickness was plotted for two sets of data: one

*NOLTR74-40, previously cited. 155

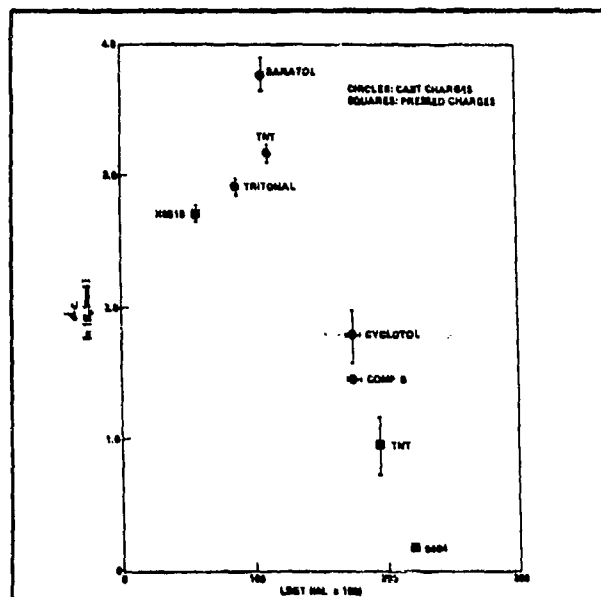


Fig. 11. Log critical diameter versus gap thickness, LASL large scale gap test data.

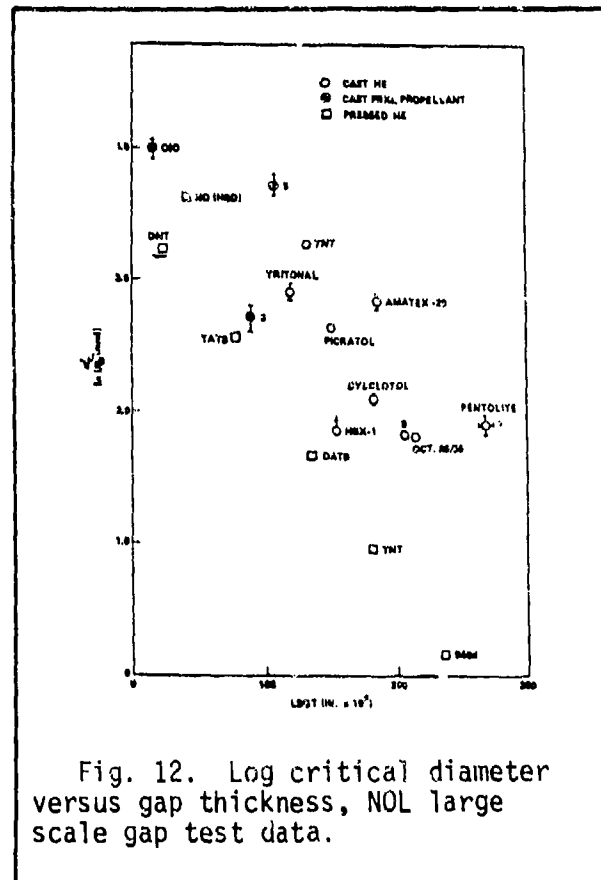


Fig. 12. Log critical diameter versus gap thickness, NOL large scale gap test data.

obtained from the LASL large scale gap test plus critical diameters which had been measured separately and on different batches of explosives, the other set of data obtained from the NOL large scale gap test*. The LASL data are shown in Fig. 11 and NOL data are shown in Fig. 12. The squares represent pressed charges and the circles represent cast charges. The LASL data for the pressed charges lie very approximately on a straight line but none of the cast charges do. In the NOL data, the pressed charges excluding NQ(HBD) lie pretty well on a straight line, but again, none of the cast charges come even close to any sort of smooth curve.

A number of investigators are beginning to consider the ignition process as a separate step from the subsequent build up and propagation of reaction. Frey** has studied the projectile initiation of explosives by means of pressure-time records obtained from pressure gauges and velocity-time records obtained optically.

*LASL data from LA-7193, previously cited, NOL data from NOLTR 74-40.

** R. Frey, P. Howe, J. Trimble, and G. Melani, Tech. Report ARBRL-TR-02176, Jun 1979.

He found that initial particle size had a different effect on the two processes of ignition and build-up. The larger particle sizes favored ignition but not the build-up phase whereas the smaller particle sizes favored the build-up process. Lee* and associates, now studying numerical modeling of the deflagration to detonation transition, have also used a separate criterion for ignition and reaction build-up. They have succeeded, in the case of PBX-9404, in reproducing quantitatively the transient pressure and particle velocity versus time dependence that they measured experimentally. The NOL gap test, at an effective diameter that is greater than or equal to three times the critical diameter, provides conditions that are extremely favorable to reaction build-up, once the reaction has started. In that sense, the gap test can be regarded as a test of ease of ignition under shock. Similarly, in measuring critical diameter, a powerful booster is used. Consequently, the testing conditions are extremely favorable for ignition so that the critical diameter measurement can be regarded as a measure of the ease of build-up and propagation.

Retrospective and Summary

The critical diameter is a function of temperature, initial particle size, loading density, confinement, composition, nature of explosive, and critical initiating pressure, as well as a number of other variables that we may not have recognized. The critical initiating pressure is a function of temperature, particle size, loading density, test dimensions, confinement, composition, nature of explosive, and the ratio of test diameter to critical diameter. Both are

*L. Green, E. Nedick, E. Lee, and C. Tarver, Proceedings of International Symposium on Behavior of Dense Media under High Dynamic Pressures, CEA, Paris, 1978, pp. 115-126

manifestations of the shock sensitivity of the explosive. Shock sensitivity is an extremely complex characteristic of explosive materials such that no single test value can represent it adequately*. A complete characterization would require a multi-variable surface since we must allow for all types of chemical reactions induced by shocks of all strengths and all possible pressure time profiles. All of the shock sensitivity tests we have examined are related and there is definitely a relationship between the large scale gap test, the wedge test, and the instrumented large scale gap test. Finally, there has been so much emphasis on critical diameter and critical initiating pressure that the other critical parameters such as density, temperature, and particle size are apt to be neglected until it is necessary to explain an accident or an odd experimental result.

*Data for comparison of shock sensitivity of various explosives may be found in NOLTR 74-40, cited previously.

LECTURES ON DETONATION PHYSICS

Lecture #11 -- 23 March 1981

by

SIGMUND J. JACOBS

Notes by Frank J. Zerilli

Detonation Pressure

Estimating Detonation Pressures

In the period 1942-1944 detonation pressures were calculated by means of the Halford-Kistiakowsky-Wilson equation of state.[†] In the work of Brinkley the calculated pressure

for cast TNT was about 170 kbar, and the question was, how accurate is this value?

If the detonation velocity is known, one can put an upper limit to the detonation pressure by using conservation of mass and momentum.

Figure 1 shows the Rayleigh line

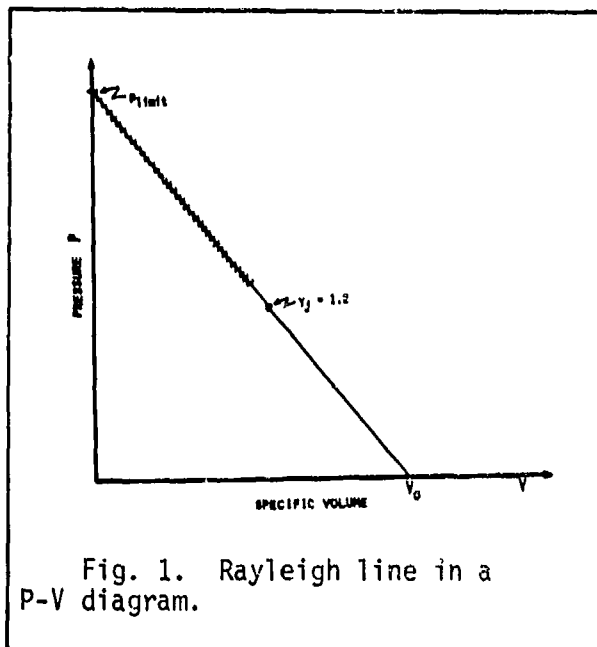


Fig. 1. Rayleigh line in a P-V diagram.

$$\frac{p}{V_0 - V} = \left(\frac{D}{V_0} \right)^2 \quad (1)$$

plotted in the p-V plane. D is the detonation velocity and V_0 is the initial specific volume. The intersection

[†] See "Principles of Explosive Behavior," Engineering Design Handbook, AMCP 706-180, U. S. Army Materiel Command (1972) p. 7-18.

of the Rayleigh line with the pressure axis (infinite compression) gives an upper limit to the detonation pressure:

$$p = \frac{D^2}{V_0} \quad (2)$$

For cast TNT with a density of 1.6 g/cm^3 and a detonation velocity of 7 km/sec the limiting pressure is 78.4 GPa (784 kbar).

The Chapman-Jouguet condition -- that the flow at the end of the reaction zone must be sonic -- leads to a further restriction. The relation

$$\frac{V}{V_0} = \frac{\gamma}{\gamma+1} \quad (3)$$

follows from the C-J condition where γ is the slope of the isentrope passing through the C-J state. For any material $\gamma > 1$ ($\gamma \sim 1.2$ for ideal gases at high temperatures). Thus $V/V_0 < 0.5$ and hence the limiting pressure must be half the p-intercept pressure:

$$P_{\text{limit}} = \frac{1}{2} \frac{D^2}{V_0} \quad (4)$$

This is 39.2 GPa for TNT and if we use a value of 1.2 for γ we get a C-J pressure of about 36 GPa . The measured detonation pressure is about half of this (20 GPa).

Measurement of Detonation Pressure

Since 1943 several methods of obtaining detonation pressures directly or indirectly have been developed. One method infers detonation pressure from the surface velocity imparted to a metal plate impacted by a plane detonation wave. Still later, in the early 50's, the magnetic velocity measurement method utilizing the Faraday effect was introduced by Russian scientists. Another method utilizes the shock

transmitted into PMMA or water -- of course one must know how to measure the pressure in the shocked material before being able to infer the pressure in the explosive. An old method, tried during World War II, was the measurement of the density of the compressed state by the use of X-ray absorption. The practicality of the method depended on the use of flash X-ray techniques which had been developed much further in Germany than in the USA. The Germans could produce a flash X-ray of about 0.1 μ sec duration. R. Schall[†] measured the density photographically and used this to estimate the detonation pressure, but since the density change in a detonation wave is not very large the method was extremely inaccurate. Thus, this approach was soon dropped as a way to obtain detonation parameters. Another method uses the shock generated in air by the detonation wave. When the detonation reaches the air boundary the velocity of the shock generated in the air is related to the properties of the isentropically expanding detonation products and one can obtain a crude estimate of the detonation pressure from that velocity. However, it is not an exact method and we will not discuss it further here.

Free Surface Velocity Method

In the free surface velocity method, a plane shock wave is produced in a metal plate by the plane detonation wave and when the shock reaches the free surface of the plate a velocity is imparted to the surface. Both the shock

[†]Information obtained from a German report dating about 1942.

velocity through the plate and the surface velocity are measured. Then two simple approximations are made to enable a calculation of the pressure in the plate and in the explosive.

The first approximation is that the particle velocity in the plate is one half the free surface velocity.[†] Then, from the impedance equation (conservation of momentum), the shock pressure in the plate can be calculated:

$$p = \rho_0 Uu \quad (5)$$

where ρ_0 is the initial density of the plate, U is the shock velocity, and u is the particle velocity.

To calculate the pressure in the explosive, the impedance of the explosive must be known. The other approximation is to assume that the impedance of the explosive is ρc where ρ is the density and c is the sound speed in the detonation state. But ρc also happens to be equal to $\rho_0 D$ where ρ_0 is the initial density and D is the detonation velocity. The approximation is good if the explosive impedance is less than that of the metal so that the reflected wave in the explosive is also a shock and if the reflected shock is not too strong so that its velocity is approximately c .

The first experiments to use this method to measure detonation pressures were done by Goranson and Houston^{††} at the Los Alamos Scientific Laboratory around 1944-45. The data obtained also provided information on the equation

[†] This is equivalent to the assumption that the release isentropes in the p - u plane can be approximated by a Hugoniot relation.

^{††} R. W. Goranson, D. Bancroft, B. L. Burton, T. Blecher, and E. E. Houston, J. Appl. Phys. 26, pp. 1472-1479 (1955).

of state of the various solids impacted by explosives. With the support of Goranson, investigators[†] at the Naval Ordnance Laboratory started experiments on measuring detonation pressures.

Figure 2 shows the manner in which the experiments at LASL and NOL were set up. A plane wave lens^{††} produces a

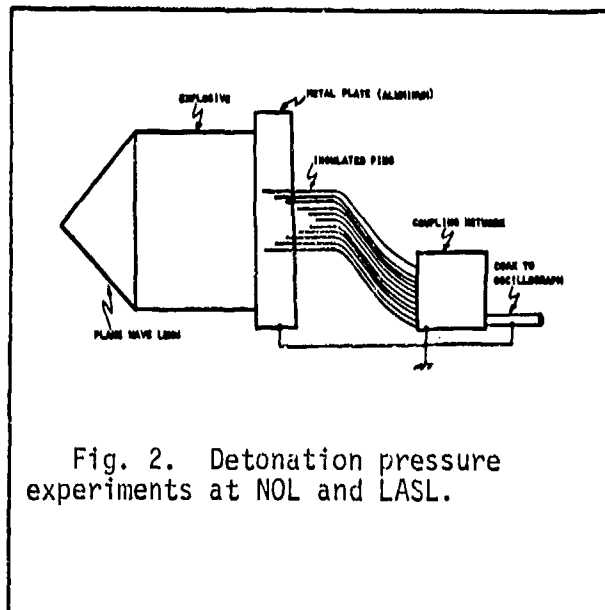


Fig. 2. Detonation pressure experiments at NOL and LASL.

plane detonation wave in the high explosive sample which, in turn, produces a shock wave in the metal plate. Pins, insulated from the plate, are embedded in the plate, and, as the shock wave reaches a particular pin, the motion of the material

next to the pin closes an electrical circuit and a signal is recorded on an oscillograph. Typically, there would be eight pins inside the metal and the same number of pins outside the metal. From the interior pins, the shock velocity would be obtained and from the exterior pins, the free surface velocity would be obtained.

Another method which used smear camera optics instead of electronics was introduced by Walsh and Christian^{†††} at

[†] Including D. Mallory, J. Ablard, S. J. Jacobs; see Conference on the Physics and Chemistry of Detonation, ONR (1951) p. 82.

^{††} See Appendix A for a description of two types of plane wave lenses.

^{†††} J. M. Walsh and R. H. Christian, Phys. Rev. 97, pp. 1544-1556 (1955).

LASL. The primary purpose was to obtain equation of state information for the metal rather than obtaining data on

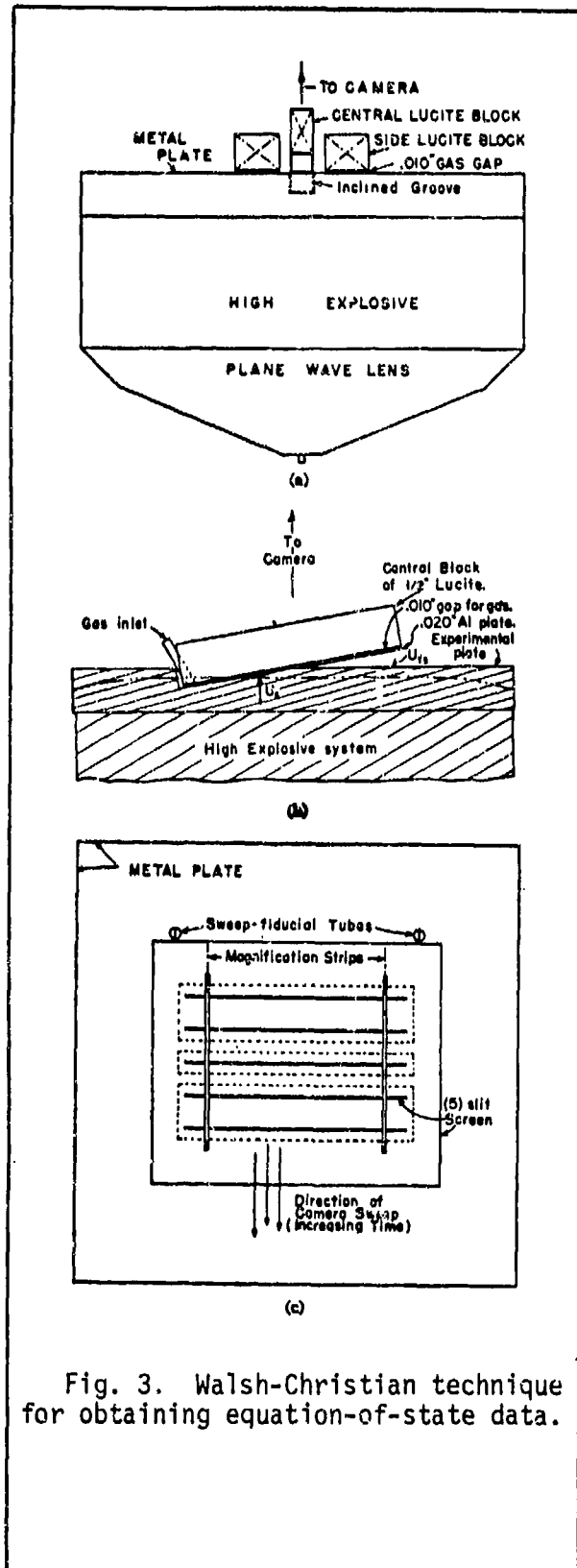


Fig. 3. Walsh-Christian technique for obtaining equation-of-state data.

the explosives. The arrangement is depicted in Fig. 3. A lot of explosive is used. The plane wave lens is eight inches in diameter and the explosive is four inches thick. There is an inclined groove cut in the metal plate and a lucite block faced with a thin metal shim with a 10 mil gap between. The gap is filled with argon and produces a flash to record the arrival of the shock. The half of the central slit of the multiple slit camera system which corresponds to the groove in the plate produces a record of shock velocity. The other half produces a trace caused by the collision of the plate with the lucite protruding

from the groove and thus produces a record of free surface velocity. The other slits record the time of arrival of the shock wave at various positions on the free surface of the plate. This information is used to correct for any curvature in the "plane" shock. A typical record would look like the diagram in Fig. 4. In order to obtain data at different pressures, the thickness of the plate would be varied.

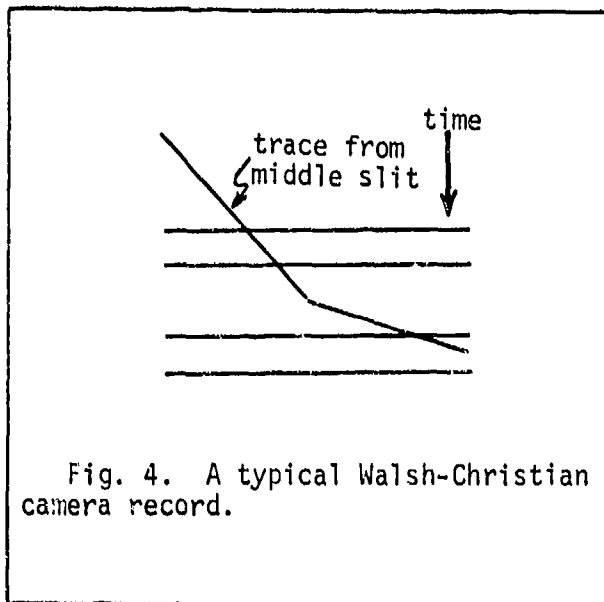


Fig. 4. A typical Walsh-Christian camera record.

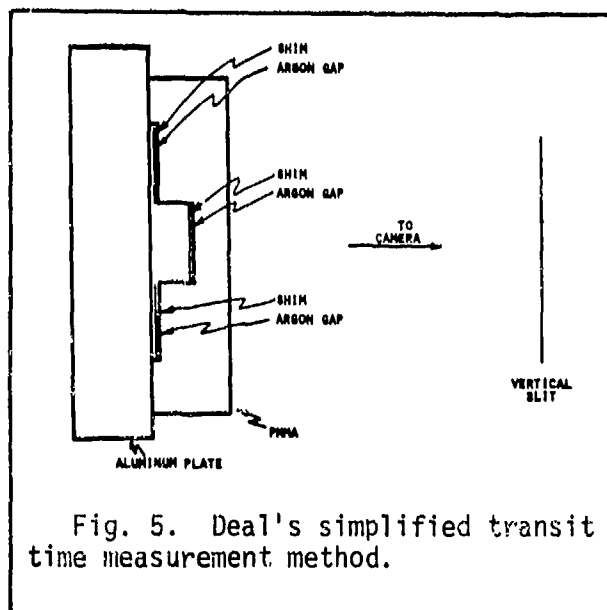


Fig. 5. Deal's simplified transit time measurement method.

Deal[†] simplified the process for obtaining equation of state data for explosives by using only transit time measurements. Figure 5 illustrates Deal's method. The camera record would show both the time of arrival of the shock and the later time of arrival of the free surface at the displaced central gap, allowing the free surface velocity to be determined. In this case, the thickness of the plate was varied to obtain information about the explosive rather than the plate itself.

[†]Second ONR Symposium on Detonation, ONR (1955) p. 209.

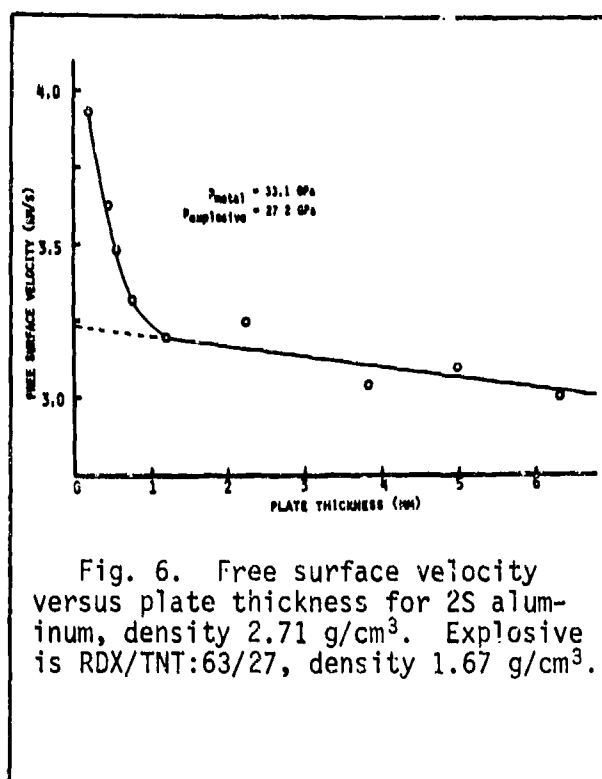


Figure 6 shows free surface velocity versus plate thickness for 2S aluminum measured by Duff and Houston.[†] The explosive was essentially Comp B -- a mixture of 63% RDX and 27% TNT. Each data point on the graph is the result of between four and fifteen experiments. The graph is the result of a total of 87 experiments

at a cost of about \$1500 per shot. The free surface velocity drops rapidly with increasing plate thickness until a plate thickness of about 1 mm at which point there is a sharp change in slope to a much less rapid, approximately linear decrease. The velocity measurements must be made before reflected waves from the boundaries have a chance to reach the surface. This allows about 300 nsec at the smaller plate thicknesses and about 2 μ sec at the larger thicknesses. The result of the work is that at the inflexion point pressure in the metal was 33.1 GPa and the CJ detonation pressure in the explosive was 27.2 GPa. To obtain these values, the shock velocity in the aluminum would have to be known, either from measurement or inferred from the free surface velocity using the equation of state data of Walsh and Christian.

[†] Second ONR Symposium on Detonation (1955) p. 225.

Determining the Detonation Pressure from the Metal Free Surface Velocity

To determine the detonation pressure in the explosive from the free surface velocity of the metal we must know the Hugoniot's for the explosive and for the metal. Figure 7 illustrates the sequence of steps. The detonation wave

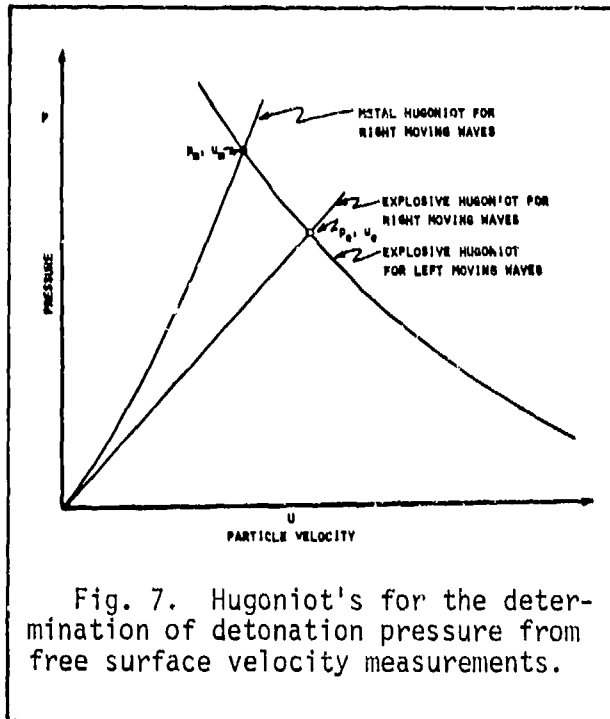


Fig. 7. Hugoniot's for the determination of detonation pressure from free surface velocity measurements.

in the explosive has some pressure p_e and some particle velocity u_e and this state must lie on the explosive Hugoniot for right moving waves which passes through the state $p=0, u=0$ (since the detonation wave represents a transition from the state of essentially zero pressure and particle

velocity to the state p_e, u_e). When the wave reaches the explosive-metal interface, a reflected wave is produced in the explosive and a transmitted shock enters the metal. The shock state p_m, u_m must lie on the metal Hugoniot for right moving waves which also passes through the state $p=0, u=0$. If the impedance of the explosive is less than that of the metal, the reflected wave in the explosive is also a shock, so the state of the reflected wave must lie on an explosive Hugoniot for left moving waves which passes through the state p_e, u_e (since the reflected shock represents a transition from the state p_e, u_e). Since pressure and particle velocity

must be continuous across the explosive-metal boundary, the pressure and particle velocity in the reflected shock must also have the values p_m and u_m , respectively. Thus, knowing u_m and the Hugoniot's, we can determine p_e and u_e from the construction in Fig. 7.

The construction in Fig. 8 shows the relation between free surface velocity and particle velocity in the metal. When the shock reaches the free surface of the metal, there is a reflected rarefaction (i.e., an unloading) described by an isentrope. If the isentrope can be approximated by

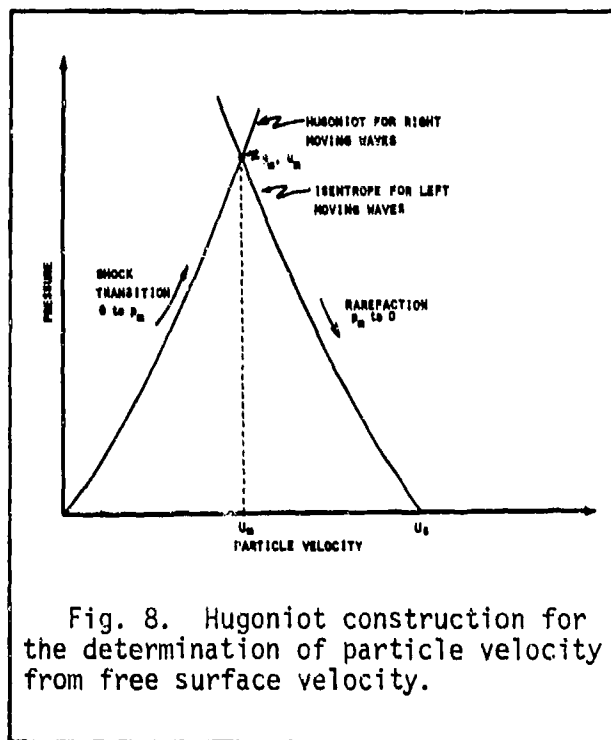


Fig. 8. Hugoniot construction for the determination of particle velocity from free surface velocity.

the Hugoniot then it is clear from the construction that $u_m = u_{fs}/2$ since the left moving wave Hugoniot is the reflection about $u = u_m$ of the right moving wave Hugoniot. The approximation turns out to be a good one because the metal remains in the solid state with little difference in density before and after shocking.

Linearized Solution for the Detonation Pressure

The conservation of momentum tells us that, whatever p_e and u_e , they are related by

$$p_e = \rho_0 D u_e \quad (6)$$

where ρ_0 is the initial density of the explosive and D is

the measured detonation velocity. Similarly, for the metal, we have

$$p_m = \rho_{om} U_m u_m \quad (7)$$

where ρ_{om} is the initial density of the metal and U_m is the measured (or inferred from Hugoniot data) shock velocity.

The approximation made by Goranson was that the Hugoniot for the explosive could be assumed to be a straight line with slope (shock impedance) ρc ($-\rho c$ for the left moving wave) where ρ is the density of the detonation products and c is the sound velocity in the products. From the conservation of mass equation, at the Chapman-Jouguet point,

$$\rho_o D = \rho c \quad (8)$$

Thus we may approximate the left moving wave Hugoniot by the straight line passing through the point p_m, u_m and having slope $-\rho_o D$:

$$p_e \doteq p_m - \rho_o D (u_e - u_m) \quad (9)$$

Solving (6) and (9) simultaneously we obtain:

$$p_e \doteq \frac{1}{2} (p_m + \rho_o D u_m) \quad (10a)$$

$$u_e \doteq \frac{p_m + \rho_o D u_m}{2 \rho_o D} \quad (10b)$$

Substituting (7) in (10) we get

$$p_e \doteq \frac{1}{2} (\rho_{om} U_m + \rho_o D) u_m \quad (11a)$$

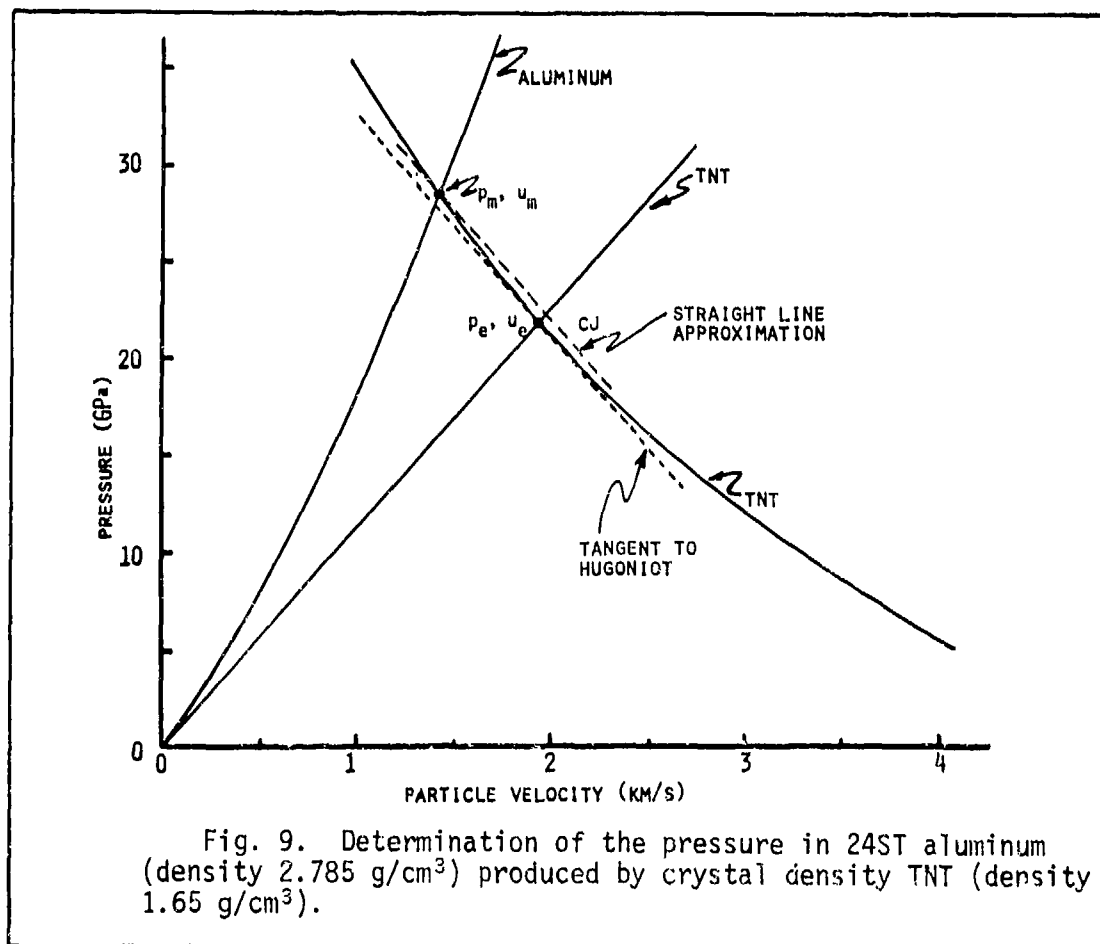
$$u_e \doteq \frac{\rho_{om} U_m + \rho_o D}{2 \rho_o D} u_m \quad (11b)$$

The particle velocity u_m is determined from the free surface velocity u_{fs} by

$$u_m \doteq \frac{1}{2} u_{fs} \quad (12)$$

Accuracy of the Approximation

The accuracy of the approximations can be judged by looking at some real curves for pressure versus particle velocity. Appendix B contains such curves, produced by H. Sternberg's group, for several explosives and metals (TNT, Comp B, tetrytol, aluminum, cadmium, nickel, zinc, and magnesium). Figure 9, below, shows the construction to obtain the relation between the pressure in the explosive and the pressure in the metal using the Hugoniot's for crystal density TNT and 24ST aluminum. The slope of the



explosive Hugoniot at the C-J point is c so that in the linear approximation we used, the straight line is parallel to the tangent to the Hugoniot at the C-J point (the dashed

line in Fig. 9). It is apparent from the figure that the straight line will produce an overestimate of the detonation pressure. It is possible to get a better estimate by using this first approximation to the detonation pressure to determine a value of $\gamma (= d \ln p / d \ln \rho)$. Then, using an approximate equation of state for the explosive, a better value of the detonation pressure can be calculated. This process can be iterated and it is possible to obtain a value of pressure with an error of about 1% which is at least as good as the accuracy of the experiment. Table 1 shows results obtained by several investigators.

Table 1. Detonation Pressures for Mixtures of RDX and TNT.

<u>Investigator</u>	<u>%RDX</u>	<u>%TNT</u>	<u>Density (Mg/m³)</u>	<u>Detonation Velocity (m/s)</u>	<u>Detonation Pressure (GPa)</u>
Ablard/Mallory ¹	60	40	1.70	7850	28.3
Ablard/Mallory ¹	0	100	1.58	6880	18.4
Duff/Houston ²	63	37	1.67	7868	27.2
Deal ³	0	100	1.64	6951	17.8
Deal ³	65	35	1.71	8022	29.3

¹ONR Conference on Detonation (1951)

²Second ONR Symposium on Detonation (1955)

³Second ONR Symposium on Detonation (1955)

The two TNT measurements show agreement to about 4% although Mallory's density was 1.58 g/cm³ and Deal's density was

1.64 g/cm³. The three measurements on Comp B were also in good agreement although the compositions and densities were slightly different.

A look at the detonation pressure data which has been published will disclose disagreement in numbers by five to ten percent. A careful critic might rule out certain data on the basis of the quality of the experimental work. One could select the best experiments of the past and possibly get values within one or two percent for a few selected materials.

A study of Appendix B would disclose that magnesium has an impedance close to that of cast TNT or Comp B. So if magnesium were used for the metal plate, corrections would be unnecessary. However, since the error in using aluminum amounts to only a percent or so, the need for the use of magnesium is an academic question.

The Magnetic Method and the Use of Small Charges

In the early work of Goranson, Duff, and Houston as many as a hundred experiments, involving explosive lenses of the order of eight inches in diameter, explosive charges four inches thick, and perhaps six to ten thicknesses of metal plate, were performed to get data for one material. At the Naval Ordnance Laboratory, field experiments were limited to ten to fifteen pounds of explosive and later to five pounds in the bombproofs. The result was that four inch plane wave generators and two inch thickness of explosive were used to obtain the data that Mallory reported. There was criticism that four inch lenses and two inch thicknesses of explosive were not sufficient to produce

accurate data. However, using the magnetic velocity method, Dremin and co-workers in Russia have been working with charges two to three inches in diameter and four to six inches long. With the magnetic method, the particle velocity as a function of time for a point in the explosive moving with the flow can be mapped out in a single experiment.[†]

Hayes^{††} has used the magnetic method to obtain detonation pressure measurements in a bombproof at LLNL which is limited to 1 kg of explosive. He has found that conduction in the explosive produced noise which made it impossible to obtain as good a rise time on the particle velocity versus distance curve as is theoretically expected. By putting a small antenna on the grounded end of the magnetic probe, he found that he could obtain a much cleaner signal. Figure 10 is

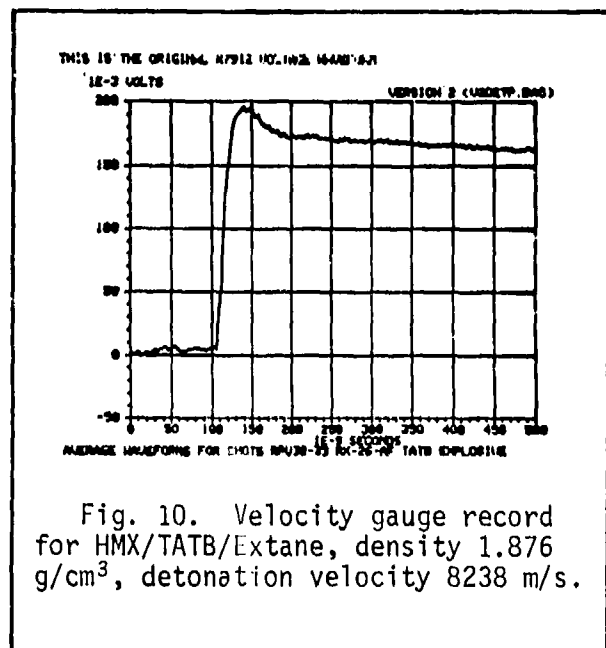


Fig. 10. Velocity gauge record for HMX/TATB/Extane, density 1.876 g/cm³, detonation velocity 8238 m/s.

an example of a magnetic velocity record obtained by Hayes. The rise time in the record is a little larger than the intrinsic gauge rise time so the excess rise time is considered to be a measure of the detonation front rise time (about 35 ns in this example).

[†] S. J. Jacobs and D. J. Edwards, "Experimental Study of the Electromagnetic Velocity-Gage Technique," Fifth Symposium (International) on Detonation, ONR ACR-184 (Aug. 1970).

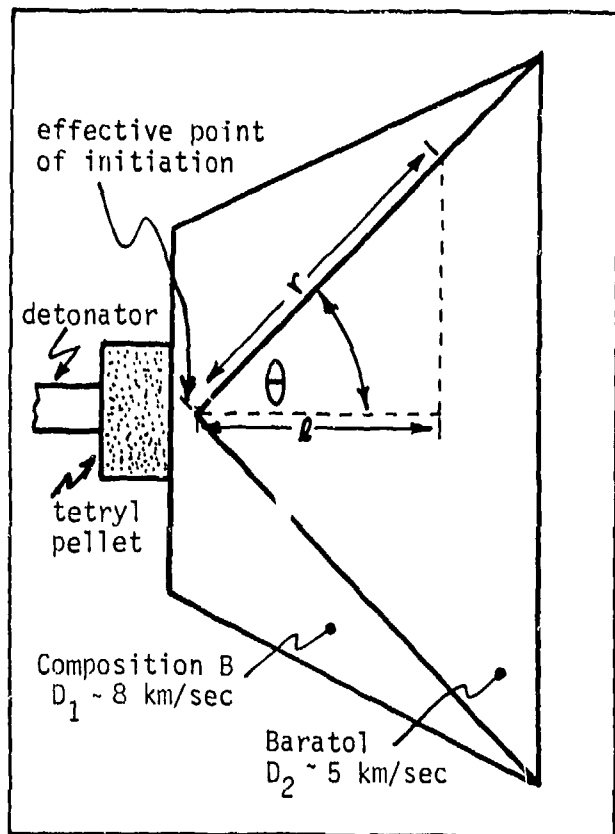
^{††} To be reported at the Seventh Symposium on Detonation, Annapolis, June 16-19, 1981.

Appendix A

Plane Wave Lenses

I. Early Type Lens

This lens consists of two explosives with different detonation velocities D_1 and D_2 where D_1 is greater than D_2 . The detonation wave produced by the detonation in the outer explosive initiates the inner explosive at the interface

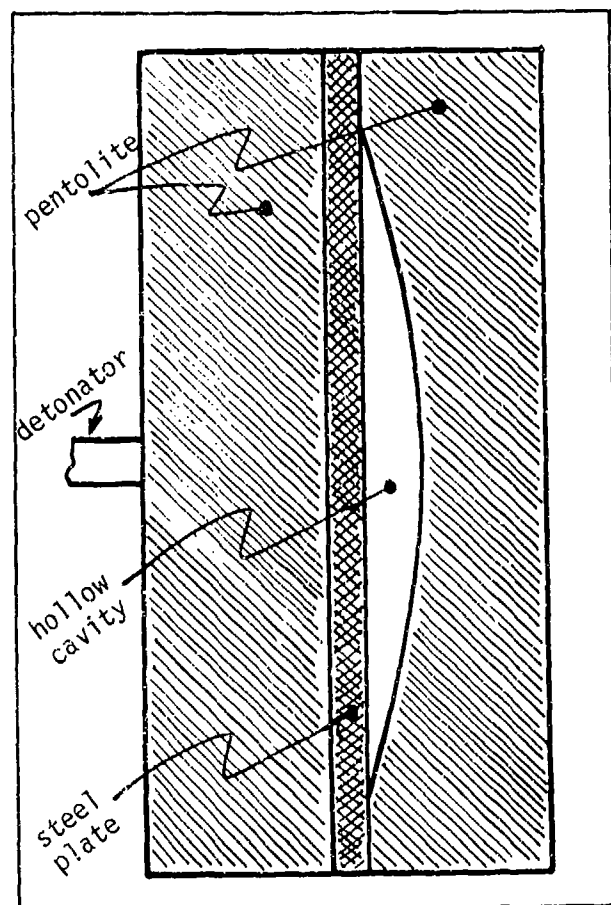


between the two. When the point of initiation of the inner explosive has travelled a distance $r = D_1 t$, the wave initiated at the apex of the inner cone has travelled a distance $l = D_2 t$. If the cone half-angle θ is such that $r \cos \theta = l$, then the wave in the inner cone will be plane.

Appendix A (Cont)

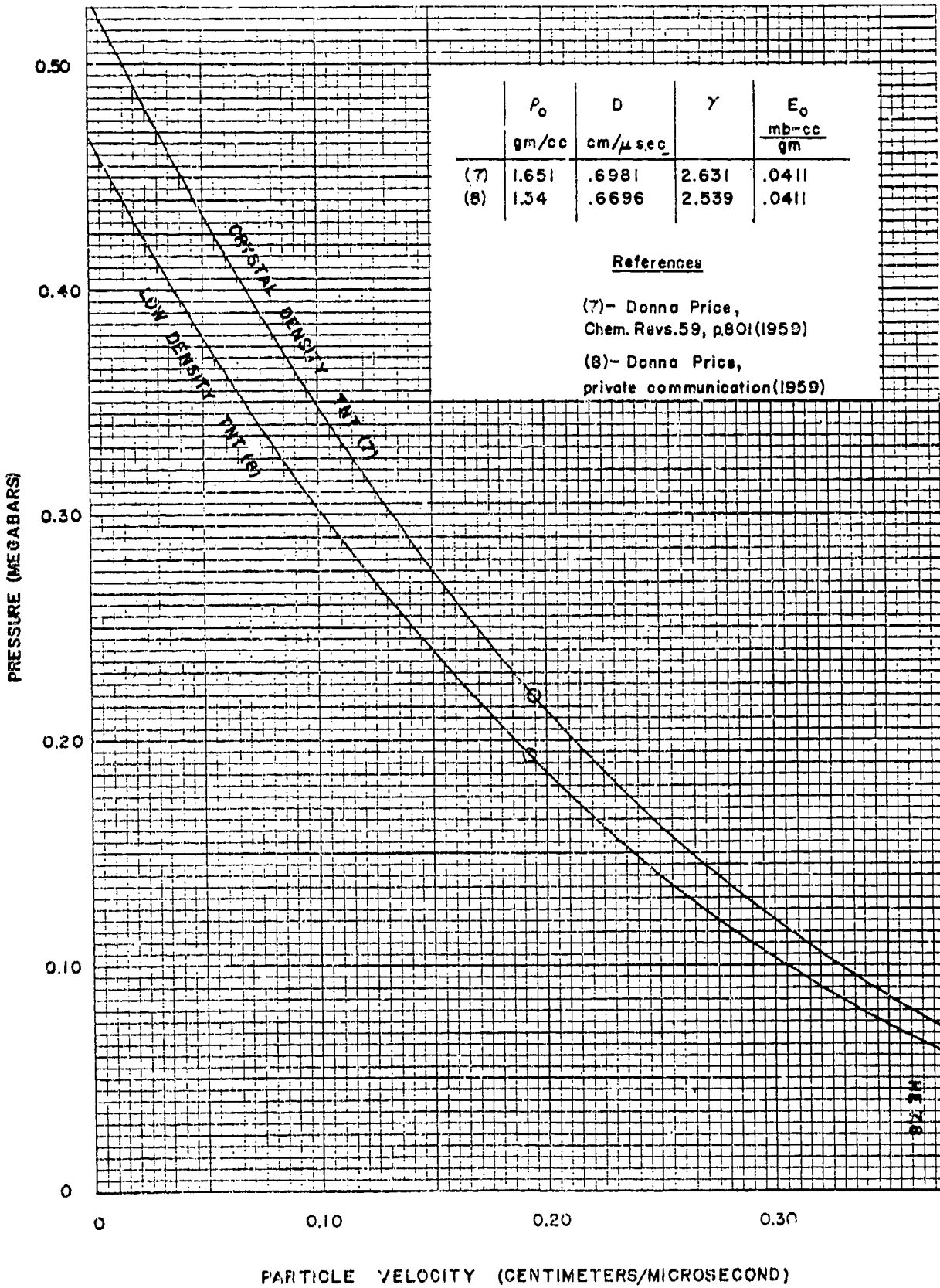
II. NOL "Air" Lens

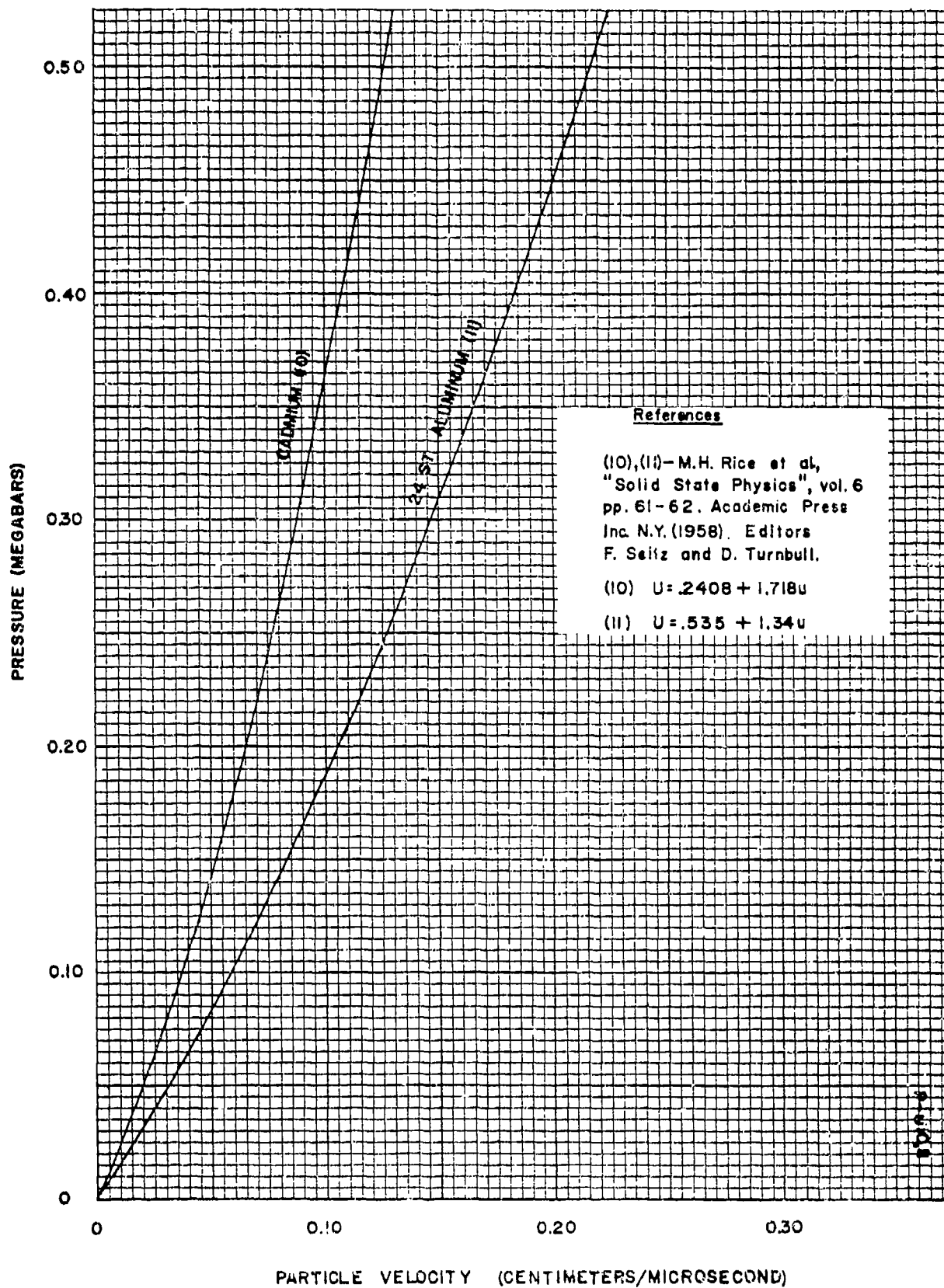
The detonator initiates a diverging wave in the first slab of explosive. This bulges the steel plate which then



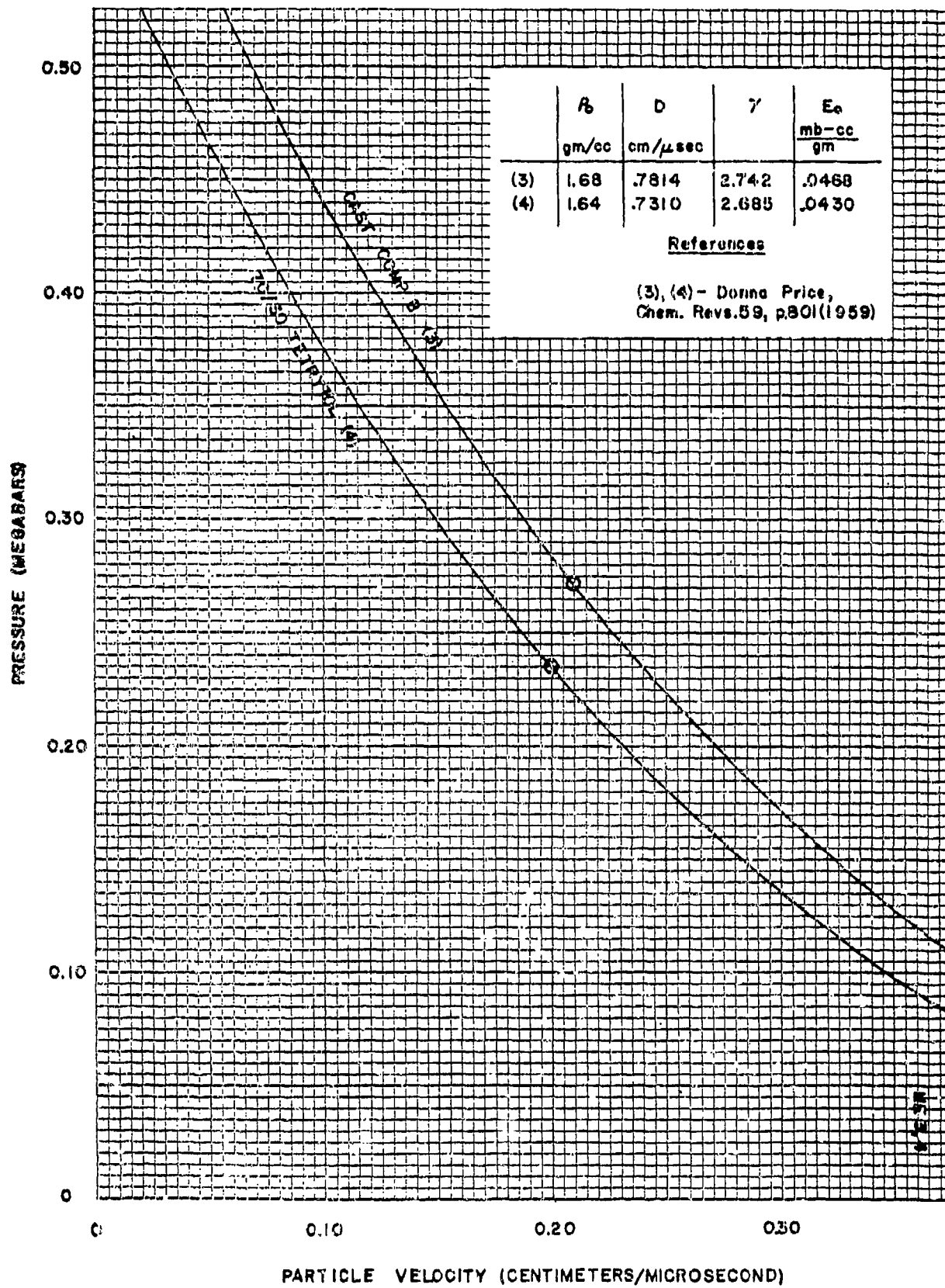
initiates a detonation on the curved face of the second explosive slab. If the curvature is chosen properly, the wave produced in the second slab will be plane. A more complete description of this and related types of plane wave lenses may be found in NAVORD Report 3620.

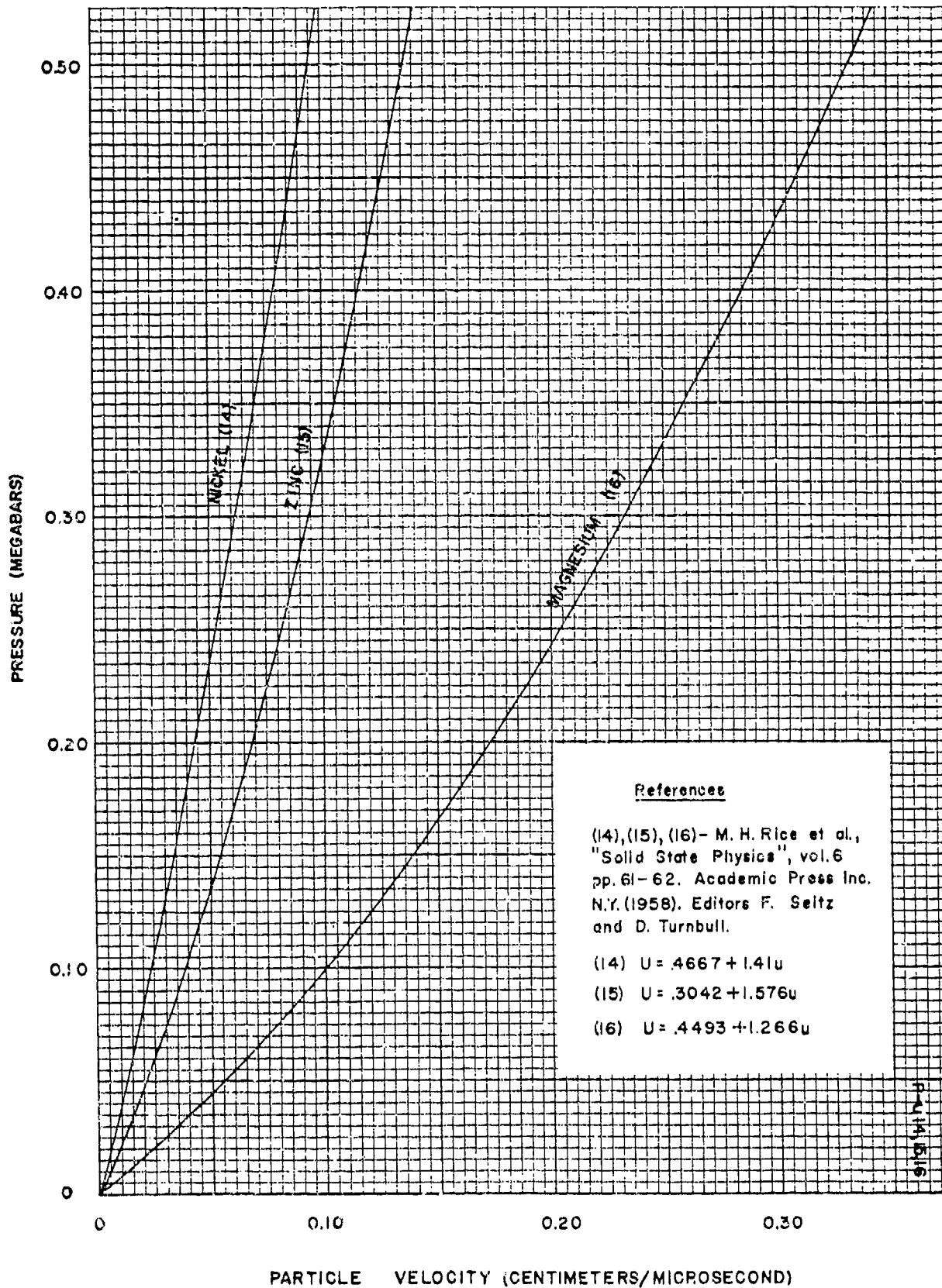
Appendix B





NSWC MP 81-399
Appendix B





LECTURES ON DETONATION PHYSICS

Lecture #12 - 6 April 1981

Detonation Reaction Zone Length and Reaction Time

By

DONNA PRICE

Notes by Frank J. Zerilli

Early Estimates of Reaction Zone Length

Eyring's equation is representative of several early attempts around the year 1946 to estimate reaction zone length.

$$a = d \left(1 - \frac{D}{D_i} \right) \quad (1)$$

In Eyring's[†] equation (1), D is the detonation velocity, D_i is the ideal detonation velocity (the detonation velocity for an infinite diameter charge), d is the charge diameter, and a is the reaction zone length. About 1954, Wood and Kirkwood^{††} presented a modified relation, given in Eq. (2).

$$Z = \frac{R_c}{3.5} \left(1 - \frac{D}{D_i} \right) \quad (2)$$

In Eq. (2), Z is the reaction zone length and R_c is the radius of curvature of the detonation front. Although the radius of curvature is not often measured, it is a relatively easy measurement to make so that, if Eq. 2 were established as a valid relationship, it would be comparatively easy to apply in practice.

[†]H. Eyring, R. E. Powell, G. H. Duffey, and R. H. Parlin, Chem. Revs. 45, 69 (1949).

^{††}W. W. Wood and J. G. Kirkwood, J. Chem. Phys. 22, 1920 (1954).

About 1965, Green and James[†] at Livermore measured the curvature of the detonation front and the detonation velocity - charge diameter relationship for a number of plastic-bonded HMX's and they found that the reaction zone length \bar{z} computed from Wood and Kirkwood's formula was approximately one seventh the reaction zone length a computed from Eyring's formula. Thus, since both cannot be correct, the question is whether either or neither is valid.

About 1975 Mader and Forest^{††} did a series of numerical computations from which they concluded that the homogeneous reactions in detonating homogeneous explosives can be represented by simple Arrhenius kinetics, shown in Eq. (3).

$$\frac{d\epsilon}{dt} = \bar{z} (1 - \epsilon) \exp(-E_a/kT) \quad (3)$$

In Eq. (3), ϵ is the fraction of material reacted, at time t , T is temperature, k is Boltzmann's constant, E_a is the activation energy, and \bar{z} is the frequency factor. Using Arrhenius kinetics they could reproduce the detonation velocity and pressure for one-dimensional steady state detonation in liquid nitromethane. The numerical computations showed that the detonation wave curvature decreased with decreasing reaction zone length which is consistent with the Wood-Kirkwood formula. In both the numerical computations and in experiments, the curvature of the detonation wave depends on the distance the exterior surface of the explosive moves during the passage of the reaction zone. For a given confinement, the thinner the reaction zone, the smaller the motion of the exterior surface and the smaller the wave curvature.

Heterogeneous detonation behavior, which is the more common situation, cannot be reproduced by using Arrhenius kinetics. For this situation, Mader and Forest developed a code, Forest Fire, in which a distribution of hot spots is assumed and

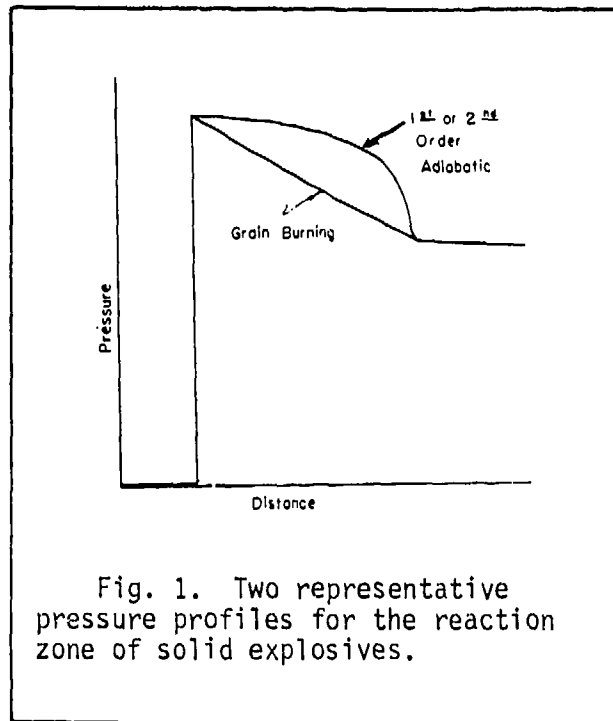
[†]L.G.Green and E. J. James, Jr., "Radius of Curvature Effect on Detonation Velocity", Fourth Symposium on Detonation, ONR, ACR-126, U.S. Gov. Printing Office, Washington, DC, 1965; pp 86-91.

^{††}C.L. Mader and C.A. Forest, "Two Dimensional Homogeneous and Heterogeneous Detonation Wave Propagation", LA-6259, June 1976.

in which experimental data on initiating pressure versus run length are used to get an approximation for the reaction kinetics.

Reaction Zone Length Inferred From Experiments

Reaction zone lengths and reaction times can be inferred from the free surface velocity measurements[†] which are made to determine the pressures in



detonation waves. Some of the earliest work on this type of measurement was published by Duff and Houston^{††} in 1955. Figure 1, reproduced from Duff and Houston's paper, shows the pressure versus distance structure of a plane detonation wave traveling to the left. The leading plane is the von Neumann plane with a pressure somewhat higher than the CJ pressure. The CJ plane is the plane defined by the completion of the reaction. The distance between is the reaction zone length and the

time the material in that zone takes to react is the reaction time. The upper curve in Fig. 1 is for a homogeneous reaction which has a long induction period. The lower curve is for a "hot spot" or heterogeneous reaction which starts at the front and proceeds more or less uniformly to the CJ plane. Figure 2 shows the results reported by Duff and Houston using aluminum plates. Shocks were produced in plates of thickness up to 0.3 inches (7 mm) by contact charges of Comp B, and the free surface velocity was measured. Duff and Houston pointed out that the curve of Figure 2 was a reflection of the detonation wave structure and that the

[†]See S. Jacobs, Lecture #11, this series.

^{††}R. E. Duff and E. Houston, J. Chem. Phys. 23, 1268 (1955). Also in Second ONR Symposium on Detonation of 1955.

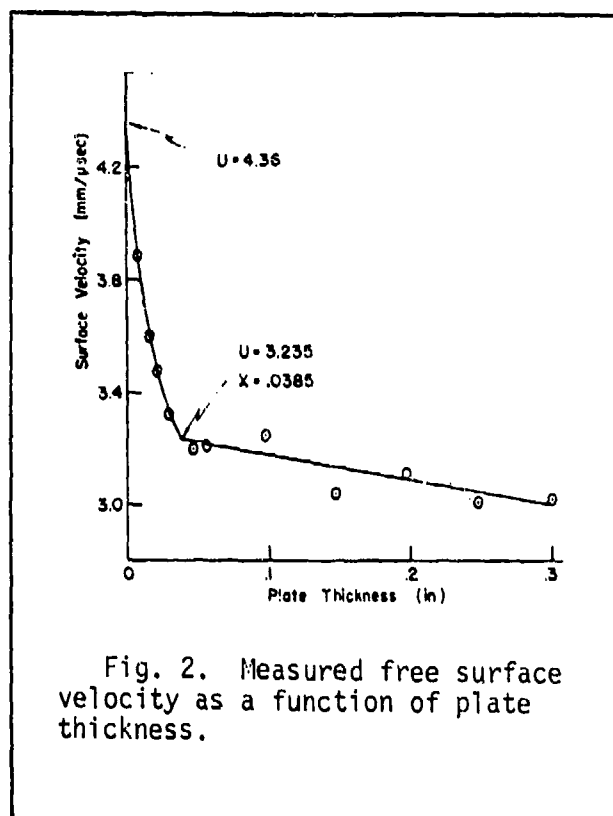


Fig. 2. Measured free surface velocity as a function of plate thickness.

break in the curve (at 0.0385 in.) should correspond to the CJ point in the detonation wave. Thus, it should be possible to determine the reaction zone thickness from the position of the break combined with a knowledge of the relevant velocities and Hugoniot relations. They arrived at a value of 0.13 mm for the reaction zone thickness of Comp B and a corresponding reaction time of 25 nsec. At about the same time Deal[†] published the results of similar measurements on several different explosives using plate thicknesses up to 20 mm.

For a steady one dimensional detonation wave, the reaction zone width is simply the distance travelled by the material in the reaction zone in a time equal to the reaction time in a reference frame moving with the wave. So

$$a = \bar{v} \tau \quad (4)$$

where a is the zone width, τ is the reaction time, and \bar{v} is the average material velocity in the zone in in co-moving frame. Transforming \bar{v} to the laboratory reference frame, $\bar{v} = D - \bar{u}$ where \bar{u} is the average material velocity in the laboratory frame. So

$$a = (D - \bar{u})\tau \quad (5)$$

The material in the reaction zone has a velocity directed toward the detonation front and, like the pressure, the material velocity decreases from the value

[†]W.E. Deal, Jr., J. Chem. Phys. 27, 796 (1957). Also Second ONR Symposium on Detonation of 1955.

at the von Neumann shock to a smaller value at the CJ plane. From the measurements of Coleburn and Liddiard[†] we estimate that the average particle velocity will be about 20% higher than the CJ value.^{††} Assuming a γ -law gas equation of state we therefore obtain

$$\bar{u} \approx 1.2u_j = \frac{1.2D}{\gamma + 1} \quad (6)$$

Substituting (6) in (5) we get

$$a \approx \frac{\gamma - 0.2}{\gamma + 1} D\tau \quad (7)$$

Thus, the reaction zone length is proportional to the detonation velocity times the reaction time with a proportionality factor which is a very slowly changing function of γ . For most voidless explosives, a value of γ equal to 3 is a good approximation, so

$$a \approx 0.7 D\tau \quad (8)$$

For $\gamma = 4$, $a \approx 0.76 D\tau$ and for $\gamma = 2$, $a \approx 0.6 D\tau$. Thus, the factor 0.7 is a reasonable approximation for a wide range of γ .

In 1959, Stesik and Akimova^{†††} published a relation between detonation velocity and charge diameter using a method that could be calibrated with the reaction zone length measurement of Duff and Houston. They tested the relation experimentally and found that it agreed well with the results for TNT and RDX and their mixtures (they did not test other materials). Table I, below, lists the reaction zone widths obtained by Duff and Houston and Stesik and Akimova, and also zone widths obtained by Dremin^{††††} using the electromagnetic velocity gauge.

[†]N.L. Coleburn and T.P. Liddiard, Jr., "Hugoniot Equations of State of Several Unreacted Explosives," J. Chem. Phys. 44, 1929-1936 (1966).

^{††}Russian investigators tend to use a slightly higher factor of about 1.25 to 1.3.

^{†††}L.N. Stesik and L.N. Akimova, Russian J. Phys. Chem. 33(8), 148-151 (1959).

^{††††}A.N. Dremin, S.D. Savrov, V.S. Trofimov, and K.K. Svedov, "Detonation Waves in Condensed Media", Izd - vo Nauka, Moscow, 1970; English translation (AD751417).

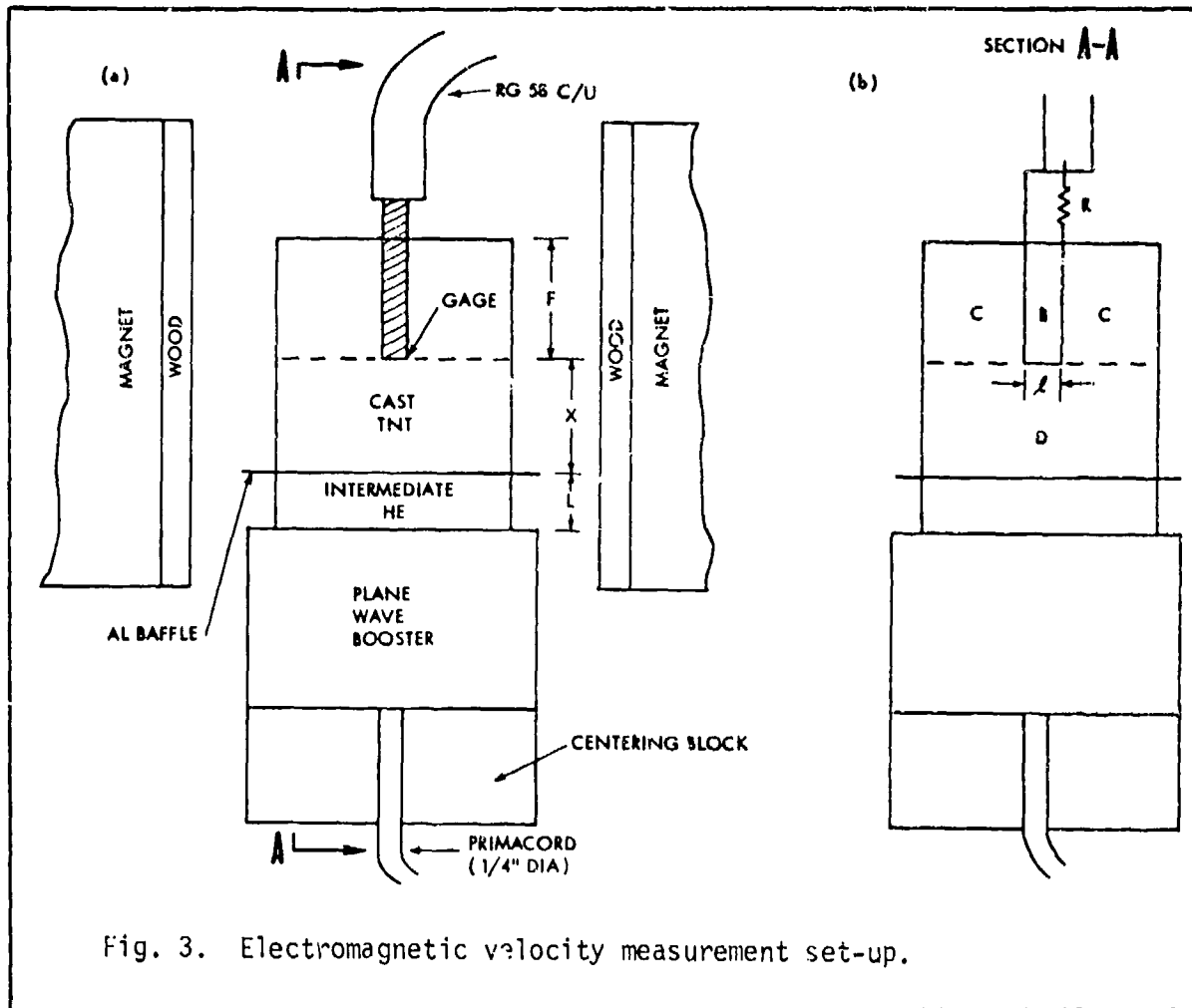
Table 1. Reaction zone widths measured experimentally.

<u>Material</u>	<u>Reference</u>	<u>Reaction Zone Width (mm)</u>	<u>Reaction Time (μ sec)</u>
cast Comp b	Duff and Houston	0.13	0.025
cast TNT (1.62 g/cm ³)	Stesik and Akimova	0.64	0.15
pressed TNT (1.62 g/cm ³)	Stesik and Akimova	0.15	0.034
cast TNT	Dremin (EMV)	1.41	0.3
cast Comp B	Dremin (EMV)	1.76	0.32

The two results for cast TNT differ by a factor of two which might not be considered bad agreement since the EMV method was in the first stages of development at the time. However, the results for cast Comp B differ by an order of magnitude and the discrepancy is still unresolved. The discussion of EMV particle velocity measurements which follows may provide some illumination of the issue, however.

Particle Velocity Measurements in Explosives

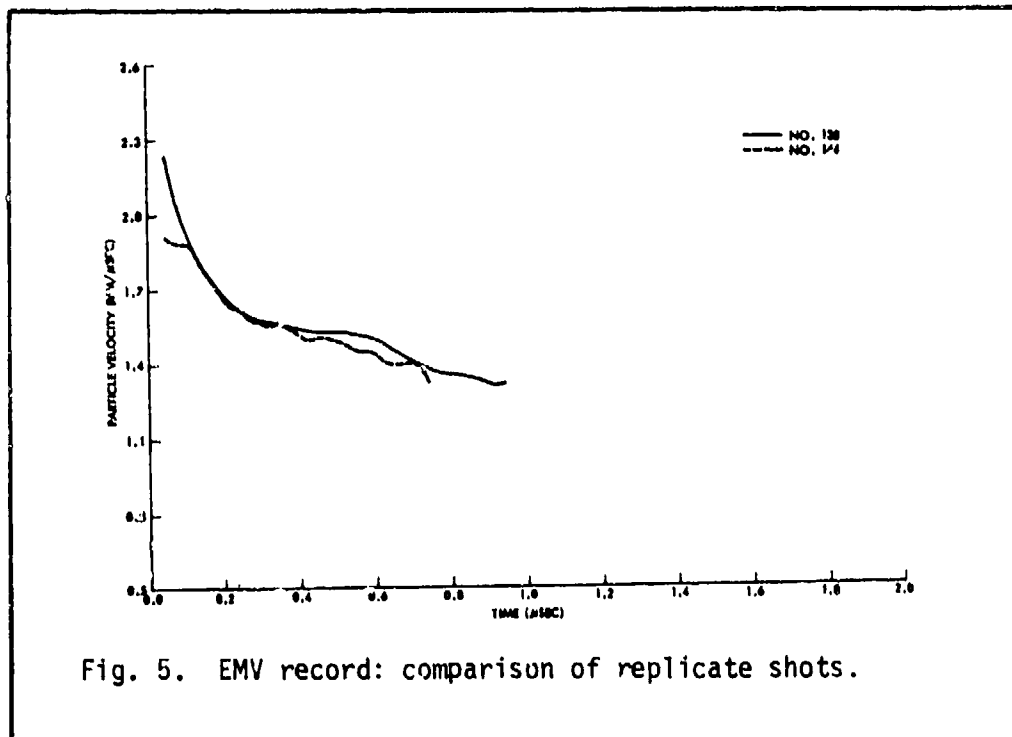
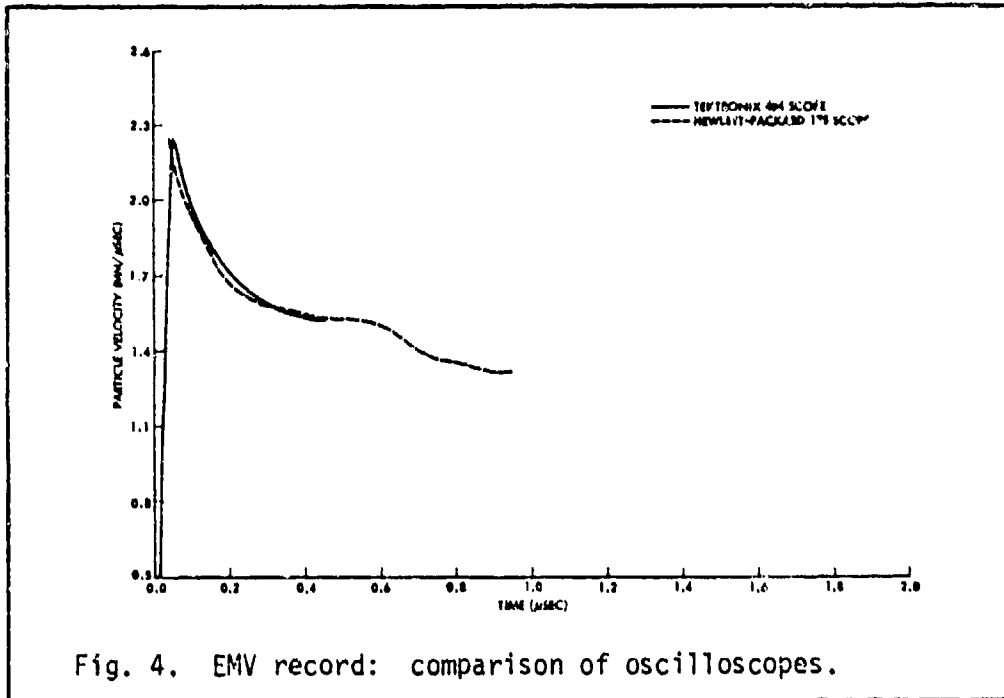
The arrangement used at NOL for the electromagnetic gauge measurement of particle velocity in detonation waves is shown in Figure 3, below. A plane wave booster was always used for initiation when measuring particle velocities in explosives. Primacord was used to initiate the booster so that no metal would be introduced into the magnetic field region to produce noise on the record. Cast TNT is relatively shock-insensitive, so the plane wave booster was followed by a second booster of pressed TNT or pressed pentolite. The purpose of the aluminum baffle was to keep the detonation products from the boosters out of the magnetic field since they also would produce noise on the records. The cross section A-A in Figure 3 shows the location of the staple shaped foil whose motion produces the record. As in the case of PMMA, the TNT was cut into suitable pieces, the foil was placed in position and the TNT was cemented together around the foil with a little adhesive and pressure. The first measurements were made on cast TNT and



later measurements were made on pressed explosives.

Figure 4 shows records obtained for the same shot with two different oscilloscopes. The duplication is reasonably good. The EMV system rise time for this set-up with TNT is about 125 ns (compared with 25 ns for PMMA or other inert material). Similar rise times were found in pressed TNT and other explosives also. The long rise times are a serious handicap in that they prevent measuring reaction times of the same order of magnitude or less than 125 ns.

A point that should be made about the Russian reaction time measurements is that in their publications, the records were reproduced with a height of about an inch so that the velocity curves showed a sharp break defining the CJ point. However, when such a record is seen in a larger scale, the sharp break becomes



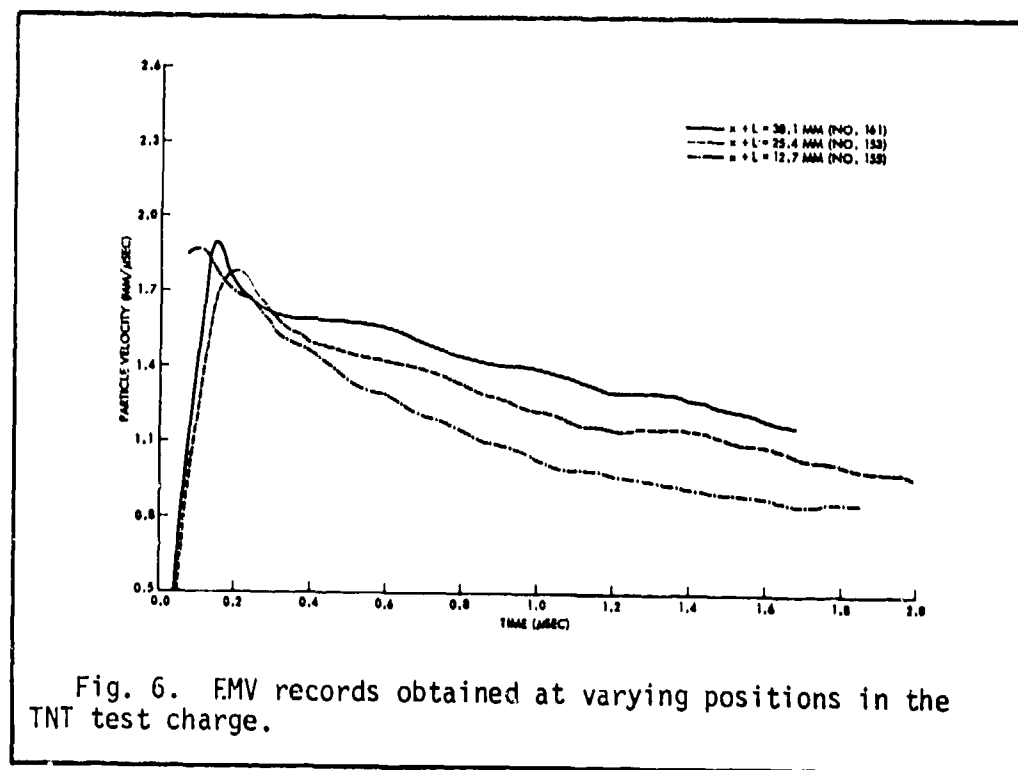
a gradual change in slope, as in Figure 4. Thus the problem is to determine the CJ point since the reaction time can then be read from the record at that point.

Figure 5 shows records from two different charges prepared identically. Except for greater noise on one of the records (shot 144), the portions of the records that are thought to be important agree fairly well.

Determining the CJ Point on the EMV Record

There are several ways to determine the CJ point. One method makes use of the fact that the ZND (Zel'dovich-von Neumann-Doering) portion of the detonation wave (the reaction zone) is a steady state flow. Thus records obtained from foils placed in the charge at different distances from the plane wave booster should be the same in the ZND portion and differ in the expansion wave portion with the difference in the detonation run length.

Figure 6 shows records obtained at several different values of distance in the charge. There is an uncertainty in the time zero point of each record which has several causes including effects of optics and film sensitivity. But by shifting the curves of Figure 6 within a reasonable time uncertainty we can superimpose the early portions to obtain an intersection of the three curves shown, and that intersection should be the Chapman-Jouquet point.



Examination of Figure 6 suggests another method of finding the CJ point. The slope of the expansion portion of the curves decreases with increasing length of detonation run as long as the flow is one dimensional at the axis (where the foil gauge is located). Numerical computations, as well as the experiments themselves, indicate that the flow at the axis will be one-dimensional for run distances up to about one half to two thirds the charge diameter since up to this point lateral rarefactions will not have penetrated to the axis. For larger run distances, the flow is no longer one-dimensional and the slope of the expansion portion begins to increase with increasing run distance. The mathematical solution for the one-dimensional expansion has been given by Taylor[†] and may be fitted to the expansion part of the EMV record in order to determine the CJ point. Figure 7 shows an example of the fitting of a Taylor expansion wave to an experimental EMV gage record.

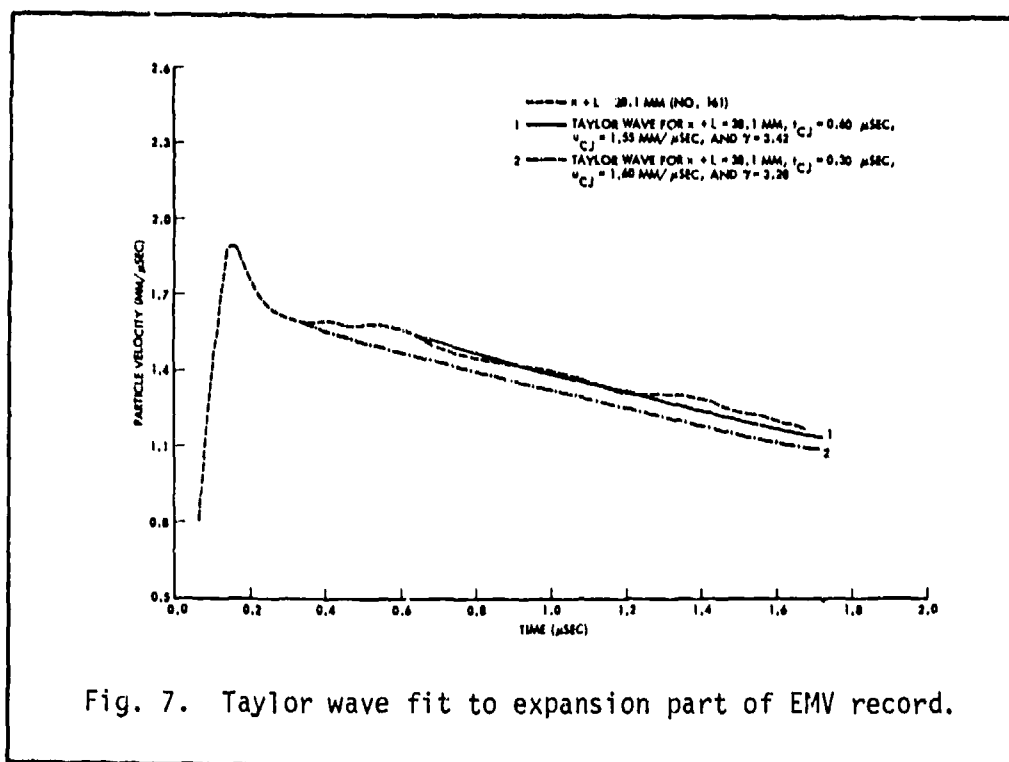


Fig. 7. Taylor wave fit to expansion part of EMV record.

[†]G. Taylor, Proc. Royal Soc. A, 200, 235 (1950)

The two fits shown differ primarily in the value of reaction time assumed in the calculation of the Taylor wave. Figure 8 is a sample record for pressed TNT. When there was only a single record, an estimate of the CJ point could be made by using the intersection of the two tangents as shown in the figure. Figure 9 shows a similar record for pressed tetryl.

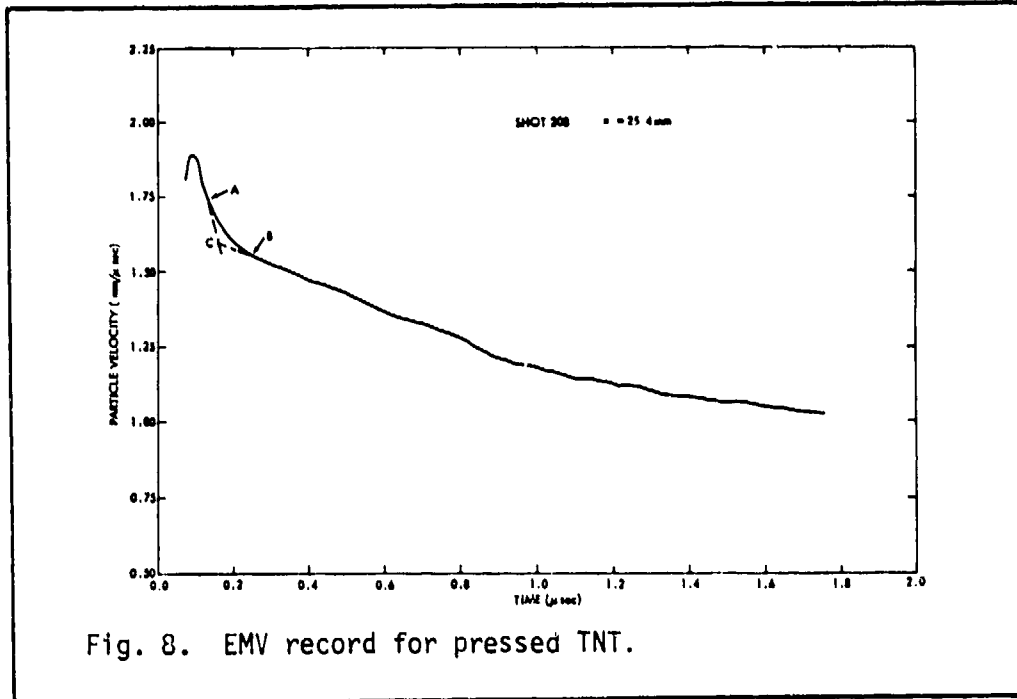


Fig. 8. EMV record for pressed TNT.

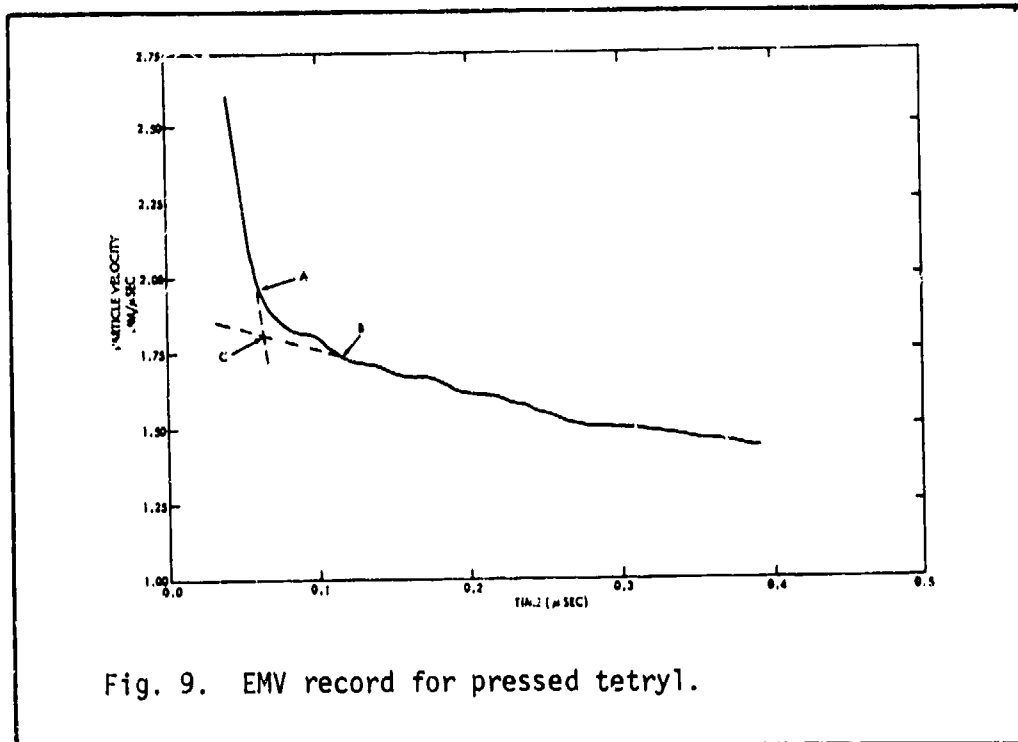


Fig. 9. EMV record for pressed tetryl.

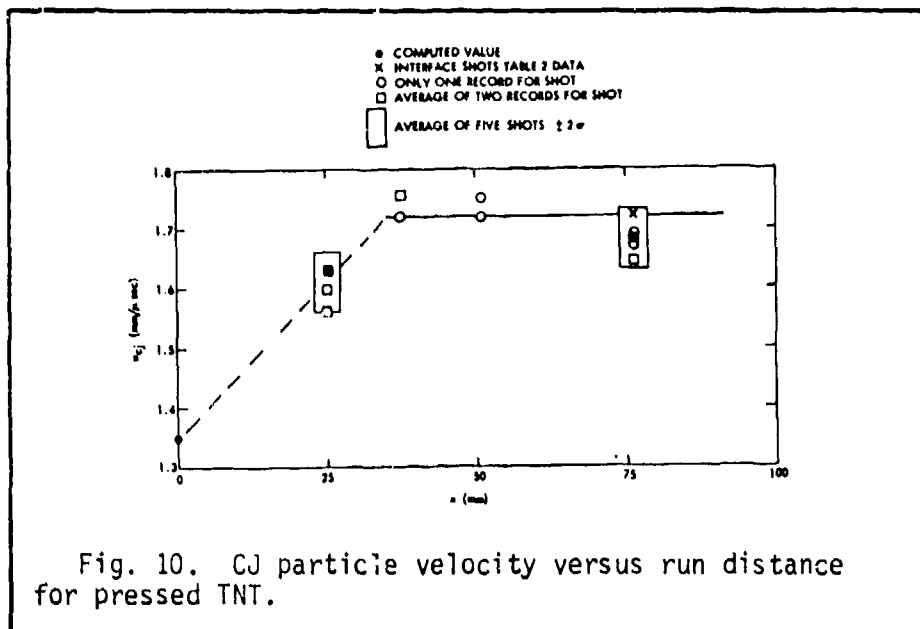


Figure 10 shows the variation of particle velocity with run distance in pressed TNT. The initial point at zero run distance is computed from the known pressure produced by the plane wave booster and the Hugoniot for the pressed TNT. The figure shows the build up in velocity to the steady state value.

This was the state of affairs until 1965 when Craig[†] measured free surface velocity versus plate thickness and obtained the results shown schematically in

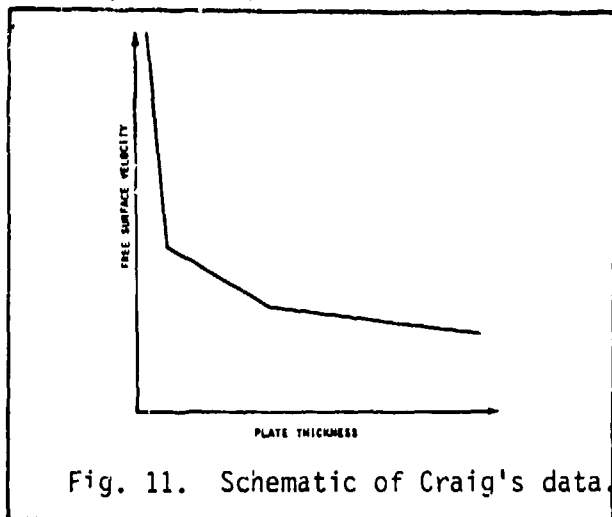


Figure 11 for pressed TNT and several other explosives. He believed that the first break represents the CJ point and the second break represents the beginning of the expansion of the detonation products he could not explain the interval between the breaks but called it the "decay zone". Petrone^{††} here and Dremine^{†††} in Russia

[†]B. G. Craig, "Measurements of the Detonation-Front Structure in Condensed-Phase Explosives", Tenth Symposium (Int.) on Combustion, the Combustion Inst., 1965: pp. 863-867.

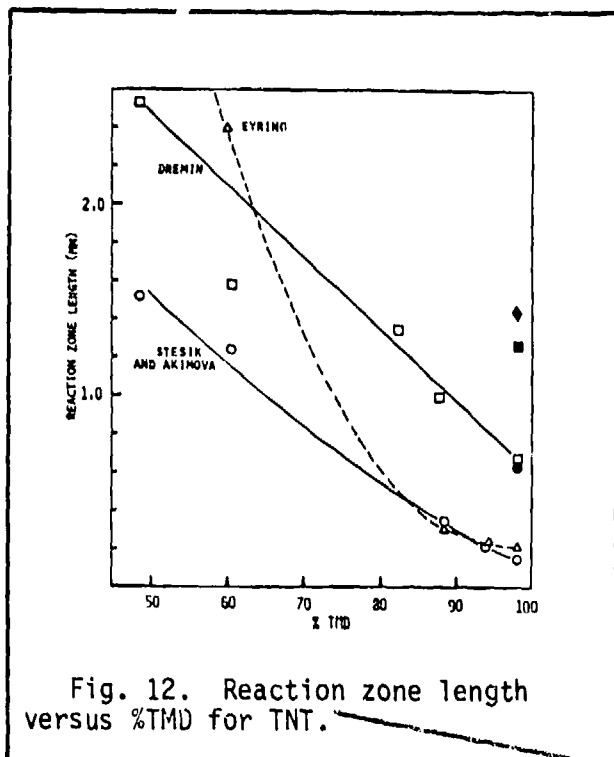
^{††}F. J. Petrone, Phys. Fluids 11 (7), 1473-78 (1968).

^{†††}A.N. Dremine and K.K. Shvedov, PMFT No. 2, 154-159 (1964)(English Translation), V. A. Veretennikov, A. N. Dremine, and K.K. Shvedov, Comb. Explo. and Shock Waves 1, (3), (1965).

first claimed that it was the effect of shock reflection from the metal plate back into the reaction zone. However, Dremin later showed that aluminum plates about 8 mm thick, shock loaded by the explosive charge, would spall off an outer layer about 1 mm thick. The first break in Craig's curve occurs at 1 mm. Dremin also showed, using a series of pre-cut plates, that a smooth free surface velocity versus plate thickness curve could be obtained with a single break at the location of the second break in Craig's curve. Dremin noted that the second break is at 7 mm which is the maximum plate thickness which Duff and Houston used so that they would not have seen the second break. He also re-plotted Deal's data and showed that they too showed two breaks at 1 mm and at 7 mm plate thickness.

Summary

Figure 12 shows reaction zone length as a function of % TMD for TNT. The dashed curve is Eyring's formula, Eq. (1). The box data points are Dremin's EMV data and



the circles are the Stesik-Akimova plate velocity data. The open points are for pressed charges and the closed points are for cast charges. The diamond point at 98% TMD is NOL EMV gage data. The normal trend is that pressed charges exhibit a shorter reaction zone length than cast charges (whatever the measurement method). Figure 13 shows the corresponding reaction times as functions of % TMD. In addition, in Figure 13, the Russian data for pressed RDX are shown. Differences for different explosives tend

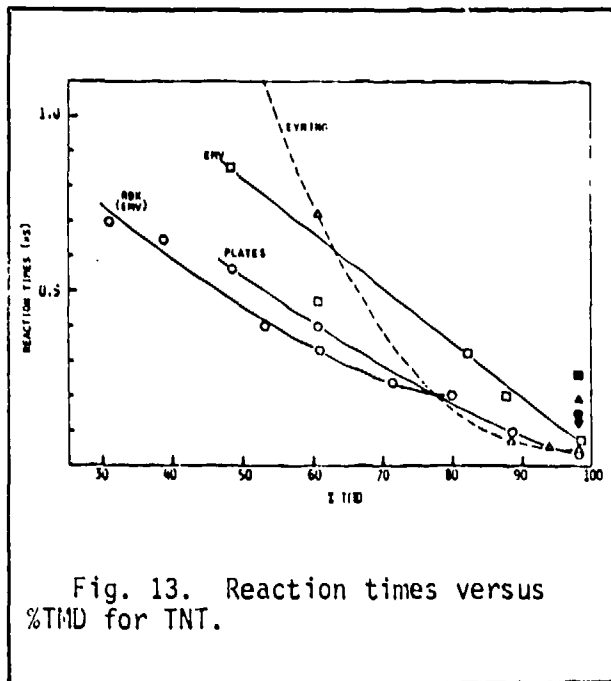


Fig. 13. Reaction times versus %TMD for TNT.

to diminish as 100% TMD is approached. The reaction zone length and reaction time of cast materials are significantly larger than those of pressed materials.

The magnitude of the reaction zone lengths measured by the different methods do not agree but, at least, the direction of the trends is the same; that is, the reaction zone length increases as the porosity increases.

The current majority opinion is that direct measurements using an EMV method is the most promising way to determine reaction times and zone lengths. In our set-up, a rise time of 125 ns presents a severe handicap especially for voidless and/or rapidly reacting explosives. McGuire[†] reported that investigators at LLNL have improved the EMV method to obtain rise times of the order of 3-5 ns. McGuire said that Hayes has used the improved method to measure the reaction times for PBX 9404 and plastic bonded TATB obtaining 12 ns and 50 ns, respectively (corresponding reaction zone lengths are 0.07 mm and 0.26 mm, respectively). A reaction time of 1000 to 1500 ns was obtained for a mixture of 80% TNT and 20% ammonium nitrate. This is the order of magnitude of the apparent reaction time observed at NSWC in an exploratory shot on ammonium perchlorate at 1 g/cm³.

The most hopeful development for measuring detonation reaction time and reaction zone length is the recent EMV gage refinements made by Hayes.^{††}

[†]R. McGuire, at NSWC Energetic Materials Division Colloquium, May 1981.

^{††}B. Hayes and C. M. Tarver, "Interpolation of Detonation Parameters from Experimental Particle Velocity Records", Preprints 7th Symposium (Int.) on Detonation, Vol 2, 800-807, June 1981.

He believes that the end of the reaction is marked by the time at which the function $(d \ln P/d \ln V)$ becomes constant. On this basis, he reports τ values c° less than 50 ns, over 100 ns, and 3500 ns for PBX-9404, 20 μ TATB, and a non-ideal aluminized explosive, respectively. The first two measurements were made at very low porosities. Many more explosives will have to be investigated and the range of porosity extended before a good comparison can be made with the results of other measurements.

DISTRIBUTION

	<u>Copies</u>
Commander Naval Sea Systems Command Attn: Technical Library SEA-62R3, G. Edwards SEA-62R, W. Blaine SEA-64E, R. L. Beauregard Washington, DC 20362	1 1 1 1
Commander Naval Air Systems Command Attn: Technical Library Washington, DC 20361	1
Office of Naval Research Attn: Code 473, R. Miller 800 N. Quincy Street Arlington, VA 22217	1
Office of Naval Technology Attn: J. Enig, MAT-07B Balstan Towers No. 1 800 N. Quincy Street Arlington, VA 22217	1
Defense Technical Information Center Cameron Station Alexandria, VA 22314	12
Naval Ordnance Station Attn: Code TDEIC, P. Wright Technical Library Indian Head, MD 20640	1 1
Commanding Officer Naval Weapons Station Attn: L. R. Rothstein Technical Library Yorktown, VA 23591	1 1

DISTRIBUTION (Cont.)

	<u>Copies</u>
Commander Naval Weapons Center Attn: T. L. Boggs	1
C. F. Price	1
Technical Library	1
China Lake, CA 93555	
Director Strategic Systems Project Office Attn: John F. Kincaid	1
Leory Throckmorton	1
Washington, DC 20376	
Rohm and Haas Company Huntsville Defense Contract Office Attn: Henry M. Shuey	1
Arthur Murray Building 723-A Arcadia Circle Huntsville, AL 35801	
Air Force Rocket Propulsion Lab Attn: Robert L. Geisler	1
Department of the Air Force Edwards AFB, CA 93523	
Lockheed Palo Alto Research Lab Attn: Henry P. Marshall	1
3251 Hanover Street Dept. 52-35, Building 204 Palo Alto, CA 94304	
Joint Venture of Hercules and Thiokol Attn: J. H. Thacher	1
P. O. Box 98 Magna, UT 84044	
Lockheed Missiles & Space Company Attn: Jack Linsk	1
Org. 83-10, Building 154 P. O. Box 504 Sunnyvale, CA 94088	
Los Alamos National Lab Attn: A. W. Campbell	1
R. L. Rabie	1
P. O. Box 1663 Los Alamos, NM 87544	

NSWC MP 81-399

DISTRIBUTION (Cont.)

Lawrence Livermore National Lab
Attn: E. L. Lee
Ed James
P. O. Box 808
Livermore, CA 94550

Copies

1
1